Experimental and Modelling Studies on the Phase Behaviour of Mutual Solvents and Their Transport Through Porous Media in Oil/Brine/Mutual Solvent Systems in the Context of Scale Inhibitor Squeeze Treatments

Volume 2 of 2

Mohamed Arab
MEng (Hons) in Chemical Engineering

Submitted for the Degree of Doctor of Philosophy

Heriot-Watt University
Flow Assurance and Scale Team
Institute of Petroleum Engineering
School of Energy, Geoscience, Infrastructure and Society
May 2018

Abstract

Oilfield scale is a significant problem in oil production which arises due to temperature and pressure changes and mixing of incompatible brines when a well is produced. The most successful and commonly used strategy for mitigating against oilfield scale is the application of scale inhibitor squeeze treatments. A squeeze treatment is applied to the production well, and involves several stages, which are: pre-flush, main treatment, over-flush, shut-in and back-production. During a treatment, a scale inhibitor adsorbs or precipitates into the formation, and its desorption/dissolution into the produced water when the well is put back into production prevents scale formation. A well must be re-squeezed before the scale inhibitor concentration in the produced water falls below the minimum inhibition concentration (MIC) required to prevent scaling.

This work focuses on the pre-flush stage of a squeeze treatment, in which mutual solvents are applied in order to prepare the well for a treatment. This is the least investigated aspect of squeeze treatments, and the one with the greatest opportunity for potential optimisation. Fundamental to understanding how to best apply mutual solvents (MS) in squeeze treatments, to achieve squeeze lifetime enhancements and to mitigate any formation damage risks, is understanding MS phase behaviour, the transport of MS through the porous medium and MS/mineral surface conditioning effects (e.g. wetting changes).

In this work, the phase behaviour of various mutual solvents is investigated in oil/brine/mutual solvent systems. Effects of salinity and chemistry are determined at field relevant conditions. The influence of scale inhibitors on phase behaviour is also investigated and mutual solvent blend design is examined. The work also develops a quantitative understanding of the phase behaviour of mutual solvents and employs that in the development of semi-empirical and thermodynamic models for describing the phase behaviour. Practical analytical tools are also developed to aid mutual solvent investigations as well as analysis in the presence of mutual solvents. Transport studies of MS in sand packs are used to investigate the transport of mutual solvents in single and multiphase systems. Numerous field solutions can be obtained from this work, but more importantly, this work enables and forms the basis for future mutual solvent investigations in the context of scale inhibitor squeeze treatments.

Dedication

To my mum, Baheya Ahmed Ebrahim, and my uncle, Abbas Ahmed Ebrahim.

Daily, I aspire to fulfil the greatest lesson I learned from you – that:
The best I can do for myself is to work for the sake of learning,
And the best I can do for others is to learn for the sake of working.
To acquire knowledge, and therein lies my joy;
And to dedicate my life to the service of others, and therein lies my purpose.

To my sister, Anwaar Arab.

Trying to describe the warmth and silliness of our friendship,
the best I thought of was:

"I love you, you love me; We're a happy family.
With a great big hug and a kiss from me to you;
Won't you say you love me too?"

To my family in Edinburgh, Oleg Ishkov, Anna Ishkova and Sophia Ishkova.

You taught me, how much you taught,
Forever, to you, I'll be grateful.
You taught me, so much you taught,
Without you, my life so fateful.

And because I am a romantic fool, to a girl I am yet to meet.

But my eyes will drink, when they see you;
But my feelings will flood, in the passing of your soul;
And my vision, in your eventual presence, will be whole;
And I hope, our days to come, will please you.

Acknowledgements

It is suiting to begin my acknowledgements by paying tribute to a remarkable girl. Sweetest Khulood, may you rest in peace. You will always be remembered; *In poems, in songs, in texts and thoughts, my love for you is art. And as you once had carried mine, I'll carry, too, your heart*. In my past, you were joy. In my future, you will be inspiration.

My deeply felt gratitude goes to my mum, Baheya – the strongest woman I know. I cannot begin to imagine all the sacrifices you have made over the years to make life possible, to raise me and my siblings in the harshest of circumstances, and to make us feel normal however abnormal life was. You never discouraged me from any undertaking, any adventure, and I always had your complete trust and support. Thank you. You are the wisdom in my mind and the tenderness in my heart. You are my strength, my patience and my success.

My heartfelt appreciation also goes to my dearest uncle, Abbas. I grew up with a strong sense of morality thanks to your presence in my life. You taught me the value of hard work, determination and responsibility, and you constantly inspire me to be selfless, humble and empathetic. Your kindness and generosity touches on every aspect of my existence. Thank you for being my father figure and my role model.

I would also like to acknowledge my siblings for their support and encouragement. Life has taken us in very different directions, and somehow we all made it. We have always been good alone – each and every one of us, but we are better together. It pains me therefore that my life is far away from you all. However, I feel your presence in my daily life as you feel mine in yours. In particular, I would like to mention my sister Anwaar. You are part of every story, the good and the bad, the happy and the sad, from the very beginning to this day. Without you, I am lost, very lost. The last several years have been exceptionally hard at times – I would not have survived them without you. Thank you.

My wholehearted thanks goes to my family in my home away from home, the Ishkov family. I came to Edinburgh with nothing, and in few years I was fortune to have found myself a place I can call home, and best friends I can call family. Oleg, you bring joy and excitement to my life, and you constantly teach me to dream big. This PhD was very entertaining thanks to you, and the support I have received from you throughout this venture is unparalleled, thank you. Anna, you redefined my existence in all ways beautiful and

simple. Without your friendship and support, I would not be where I am today. You are a wonderful addition to my life, a remarkable role model, and my very favourite superhuman. To you both I owe my happiness, my optimism and my life. Thank you for helping me make peace with some of the unfortunate events in my past, for your unending support with this PhD and all aspects of my life, and for your friendship. I feel privileged having you both in my life. I must mention the little one too, Sophia! You are pure joy and love! I love being your "Dadya Mo". You have a very special place in my heart. Thank you for being my little bundle of cheerfulness and motivation.

My sincere gratitude goes to my colleagues and friends in the Flow Assurance and Scale Team (FAST). First and foremost, I would like thank my supervisor Prof. Ken Sorbie. I have been very fortunate and privileged to be your student. Beyond the support, feedback and guidance I received from you, you are an excellent supervisor of character. You give your students the freedom to think, teach them how to ask good questions, and encourage them to test and apply their ideas to solving real problems. Giving me the opportunity to work under your supervision, to me, was a lot more than the opportunity itself; this was also a pivotal turning point in my life – I cannot begin to comprehend what my life would be without it. Thank you for your trust, diligence and commitment to my success.

Secondly, I would like to thank Prof. Eric Mackay. You have been one of the greatest sources of support over the past few years not only on a professional level, but also on a personal level. I feel very fortunate to have been mentored by you and I still have a lot to learn. Thank you for always being so generous with your honest feedback, attention and time, for building my confidence and for being invested in my success. I am humbled by your kindness.

Special thanks goes to Lorraine Boak. You are my mum figure away from home, a great mentor and an incredible friend. You have been an important element in my professional life and my personal life over the last few years. You are the perfect balance of strictness and leniency. Having you supervise my experimental work enabled me to conduct the work methodically and to the highest standards. Cutting me some slack when I was under pressure was also extremely important in enabling me to do this work without feeling overly stressed. You were always there to listen too, and I value your friendship – a key highlight of doing this PhD. Thank you for everything.

I would also like to thank Mike Singleton for his support and feedback, for lending me his time and expertise as I did this work, and for facilitating valuable contacts and opportunities with partners in the industry. This work was enriched by your contributions, encouragement and trust.

Furthermore, I would like to thank Ivan Davis for mentoring me in the lab and sharing his knowledge when I started this work; Wendy McEwan for analysing my samples and explaining the results; Robin Shields and Alan Beteta for helping me work with the sand pack rig and understanding the results; Alexander Graham for being my go to person to ask just about anything, for supporting me on a personal level and for helping me with the ESEM-EDX work; Thomas McGravie and Tom Clark for assisting me with maintenance, repairs and technical support throughout this PhD; and William Thomas for helping me in the lab at the beginning of this PhD. Special thanks to Heather O'Hara for all the help and guidance – nothing can happen without you. I relied on you fully during my time in FAST and I was in very good hands; thank you for everything!

I would also like to thank my friends in FAST. Thank you all; Alsu Valiakhmetova for being a fantastic friend and a great source of support; Khosro Jarrahian for his great friendship and assistance; Suzanny Paiva de Carvalho for being one of the most wonderful souls I had the pleasure of meeting and befriending; Hydra Rodrigues for her friendship, support, and for teaching me things I forgot I am capable of; Giulia Ness for her remarkable care, support and friendship; Ayrton Ribeiro and his lovely wife Alessandra Ribeiro for being amazing friends and a source of inspiration; Duarte Silva for his friendship and his reassurances – particularly at the beginning of this PhD; Nazia Farooqui, Xu Wang and Yaser Alduailej for their friendship. Without you all, doing this PhD would have been a very difficult and lonely task. Thank you for being the music in the background.

Additionally, I would like to thank Koenraad Collart and Brian Hutton for their help with the GC-FID work; Jim Buckman for his help with the ESEM-EDX and allowing me to use it; Buddhika Hewakandamby and Begum Tokay for playing important roles in my success; friends and colleagues in the human rights community for all their help and support; and few of my colleagues at the Warden Team and the Wellbeing Services for their help at various points during this PhD – in particular, Esme Terry for being my rock during the final stages of this PhD; you are an absolute star Esme, thank you.

A huge thank you goes to Alexandra Uhle. Finishing this work would not have been possible without you. You helped me rebuild my confidence, stand on my feet and deliver my best. You have been a wonderful close friend, a source of wisdom and inspiration, a feeling of joy and contentment, and an invaluable asset in my support network and my life. Thank you for emerging into my existence right when I needed you – you are my favourite unicorn! Where would I be today without you?

A very special thank you goes to Heba Shbat. In a life of many variables, you have been the only constant, and one of the only, if not the only, transcendent affair. We have known each other almost all our lives, and yet you continue to enrich my everyday life and I continue to learn from you. You made finishing this work very fun and exciting, you gave my days colour and my life flavour. Thank you for being there for me always and ever, for inspiring hope and optimism, and for making everything pink! I am very fortunate to have you in my life as both, a very close friend and a reliable source of support.

To all the friends cheering for me from all corners of the world, thank you. In particular, I would like to mention Ella Safri (you are one of my most valued encounters, and a very beautiful presence in my life – thank you!), Zita Dieseru (thank you for being an exceptional friend despite how busy you are), Noor Al Wari (your friendship is life – I am so glad I met you), Chevelle Plunkett, Alissa Barbarin, Jenny Wood, Puneeta Mhajan, Trang Chu Minh, Saraswati Patel and Ruzanna Saji Lee. You all played important roles in my life at various points during this PhD. Thank you.

Before ending this, I would like to thank the sponsors of the FAST Joint Industrial Project Phase 5 (Apache, Baker Hughes, BG Group, BP, Cairn, Chevron, Clariant, ConocoPhillips, Equion, Foundation CMG, GALP, Maersk, M-I SWACO, Multi-Chem MWV, Nalco Champion, Nexen, Petrobras, Petronas, REP, Shell, Statoil, Talisman Sinopec, Total and Wintershall) and Phase 6 (ADNOC, Baker Hughes, Clariant, Foundation CMG, Halliburton Multi-Chem, Nalco Champion, Petronas, Repsol Sinopec, Schlumberger, M-I SWACO, Shell, Statoil, Total and Wintershall) for steering this work in the right direction, for their contributions and for their technical and financial support. Without your commitment to advancing research and to the FAST group, achieving this would not be viable. Thank you. I would also like to thank and acknowledge support and services staff at the Institute of Petroleum Engineering, the School of Energy, Geoscience, Infrastructure and Society and Heriot-Watt University in general for all their contributions.

On a final note, I would like to acknowledge my calculator, Lana, whom I lost in mysterious circumstances while I was doing this PhD. It was a beautiful Casio fx-100MS, my most valued possession and was very supportive and dependable. It is the only calculator I owned, and through thick and thin it served me, in seven countries and four continents. I never had to replace the battery – not even once, and it did everything a scientific calculator could do, from doing complex calculations, to spelling simple messages with numbers and symbols in class when I was younger. Thank you, Lana, for all the support with math and numbers however basic (e.g. Hey Lana, what's 1+0; just double-checking it equals 1) or complex, and for being a great companion. Although I have been struggling without a calculator for quite some time now, I find it very difficult to replace you; I don't know if I could. I hope to see you again someday.

Table of Contents

List of Tables

List of Figures

Nomenclature

Chapter 1

$[MIC]$	Minimum inhibitor concentration
$[SI]$	Scale inhibitor concentration

Chapter 2

$P_{o/w}$	Partition coefficient of the mutual solvent in n-octanol to water

Chapter 3

C_0	Initial concentration
D_o	Outside diameter
$P_{o/w}$	Partition coefficient of the mutual solvent in n-octanol to water
$P_{o/w}(MS_i)$	Partition coefficient of mutual solvent (i)
$P_{o/w}(m-MS)$	Theoretical partition coefficient of a mutual solvent blend
S_{or}	Residual oil saturation
c_i	Concentration of ion (i)
x_i	Fraction of mutual solvent (i)
z_i	Charge of ion (i)
$\Delta[TDS]$	Three-phase total dissolved solids interval
ΔT	Three-phase temperature interval
C	Final concentration
I	Ionic strength
L	Length
T	Temperature
TDS	Total dissolved solids
WC	Water cut

Chapter 4

$\left(x_i^k\right)_0$	Volume fraction of component (i) in phase (k) at $(t = 0)$
C_k	The intercept of three-phase analysis for phase (k)
R_{kn}	Phase fraction of phase (k) in sample (n)
$V^{k(n)}$	Volume of phase (k) at iteration (n)

V_k	Phase volume; $k = u, m, l$ for upper, middle and lower phases
$V_k^{k(n)}$	Volume of component (k) in phase (k) at iteration (n)
$V_k^{k(n-1)}$	Volume of component (k) in phase (k) at iteration $(n-1)$
V_{kn}	Volume of phase (k) in sample (n)
V_n	Feed volume in sample (n)
m_k	Slope of three-phase analysis for phase (k)
$x_{i=k}^k$	Volume fraction of component $(i = k)$ in phase (k)
x_i^k	Volume fraction of component (i) in phase (k)
x_{in}^k	Volume fraction of component (i) in phase (k) in sample (n)
z_j	Fixed feed volume of component (j)
ρ_i	Density ($i = o, B, MS$; for oil, brine and mutual solvent)
$\Delta V_{i=k}^{k(n)}$	Disturbance to the feed volume of component $(i = k)$ at iteration (n)
$\Delta V_{i\neq k}^{k(n)}$	Disturbance to the feed volume of component $(i \neq k)$ at iteration (n)
ΔV_k^F	Disturbance to the feed volume of component (k) at $(t = 0)$
C	Number of components
F	Number of degrees of freedom
P	Number of phases
V	Feed volume
X	Three-phase composition vector
t	Time

Chapter 5

(X_{CP}, Y_{CP})	The centroid of the three-phase region in Cartesian coordinates
(X_f, Y_f)	Feed composition in Cartesian coordinates
(X_i, Y_i)	Phase composition in Cartesian coordinates
(X_m, Y_m)	Midpoint composition in Cartesian coordinates
(x_{df}, y_{df})	Feed composition correction in the PDM in Cartesian coordinates*
$(\Delta x_{df}, \Delta y_{df})$	Feed composition correction excess in the PDM in Cartesian coordinates*
*	PDM = Phase Displacement Method
(X, Y)	Composition in Cartesian coordinates
$[TS]_k$	Concentration of the tracer TS in the (k)-rich phase
L_C	Corrected lower phase volume
$P_{o/MS}$	Partition coefficient of a tracer between oil-rich and mutual solvent-rich phases
U_C	Corrected upper phase volume

V_O	Volume of the overall mixture
V_S	Volume of the source sample
V_{i0}^{Z}	Estimated volume of component (i) in phase (Z)
V_i^F	Volume of component (i) in the feed
V_k	Volume of phase (k)
V_t	Volume of the target mixture
Z_C	Corrected feed volume
e_Z^{CE}	Subset of the 2nd convergence parameter for component balance corrections for phase (Z)
e_i^{ZF}	1st convergence parameter for component balance corrections for component (i)
x_{MS}^F	Volume fraction of the mutual solvent in the feed
x_{MS}^{fx}	Volume fraction of the mutual solvent in the phase exhibiting constant composition
x_{i0}^Z	Estimated fraction of component (i) in phase (Z)
x_i^F	Fraction of component (i) in the feed
x_i^O	Volume fraction of component (i) in the overall mixture
x_i^S	Volume fraction of component (i) in the source sample
x_i^Z	Volume fraction of component (i) in phase (Z)
x_i^t	Volume fraction of component (i) in the target mixture
ΔV_i	Volume of component (i) used in the phase displacement
C	Intercept
DP	Decimal point precision for component balance corrections
F	Feed volume
L	Lower phase volume
U	Upper phase volume
Z	Phase volume
dX	Minimisation steps for component balance corrections
dr	Phase separation parameter for estimating phase separation in a two-phase system
ind	The 2nd convergence parameter for component balance corrections
m	Slope
n	Mixing factor (source sample to target mixture) or the number of degrees of freedom

Chapter 6

$\overline{a_0}$	Initial values set for (a_{ji}) used to calculate ($\overline{a}$) for a given system
$\overline{a_{Cm}}$	The (a_{ji}) set in (R'') corresponding the minimum of ($ObjR$)
$\overline{a_{Fm}^z}$	The (a_{ji}) set at stage (z) corresponding the minimum of ($ObjR$)

$\underline{x}^k$	Composition vector of phase (k)
$\emptyset_i$	Volume fraction of component (i)
G_C^{ex}	Combinatorial part of total excess Gibbs free energy
G_R^{ex}	Residual part of total excess Gibbs free energy
G^{ex}	Total excess Gibbs free energy
K_i	Equilibrium constant for component (i)
K_i^{domj}	Equilibrium constant for component (i) in phase rich in dominant component (j)
L^k	Molar flow of phase (k)
N_0	Number of possible (a_{ji}) sets in (R'')
N_z	Number of possible (a_{ji}) sets to test at stage (z)
Q_k	Group area parameter
R'	Range (R) adapted for consistency with (dS_0)
R''	Non-zero containing range (R')
R_0	Start value of range (R)
R'_0	Start value of range (R')
R_G	Universal gas constant
R_{ji}^a	Range of uncertainty around each (a_{ji})
R_k	Group volume parameter
R_n	End value of range (R)
R'_n	End value of range (R')
$\overline{a}$	Final values set for (a_{ji}) used to calculate $(\overline{a})$ for a given system
a_i^k	Activity of component (i) in phase (k)
a_{ji}	UNIQUAC adjustable parameter for the interaction of (j) with (i)
f_i	Feed fraction of component (i)
l_{domi}^k	Molar flow of dominant component (i) in phase (k)
l_i	A term in the UNIQUAC for component (i)
l_i^k	Molar flow of component (i) in phase (k)
p_i	Dominant pair analysis parameter for component (i)
q_i	Surface area parameter of component (i)
r_i	Volume parameter of component (i)
u_{ji}	Average interaction energy for the interaction of (j) with (i)
$v_k^{(i)}$	Number of groups of type (k) in a molecule of component (i)
x_{domi}^k	Fraction of dominant component (i) in phase (k)
x_i	Fraction of component (i)

x_i^{domj}	Fraction of component (i) in phase rich in dominant component (j)
x_{ijk}^{cal}	Calculated fraction of component (i) in phase (j) for sample (k)
x_{ijk}^{exp}	Experimental fraction of component (i) in phase (j) for sample (k)
x_i^k	Fraction of component (i) phase (k)
z_{domi}	Feed fraction of dominant component (i)
γ_i	Activity coefficient of component (i)
γ_i^C	Combinatorial part of the activity coefficient of component (i)
γ_i^R	Residual part of the activity coefficient of component (i)
γ_i^k	Activity coefficient of component (i) in phase (k)
θ_i	Area fraction of component (i)
τ_{ji}	UNIQUAC parameter for the interaction of (j) with (i)
Δg_{mix}	Dimensionless Gibbs free energy for a mixture
$N(R'')$	Number of values in range (R'')
$ObjE$	Squared and weighted nonlinear equilibrium condition
$ObjF$	Objective function
$ObjG$	Squared and weighted dimensionless Gibbs free energy
$ObjR$	Composite objective function for calculating the (a_{ji}) parameters
R	User specified range for (a_{ji}) calculation
S	The number of the values that (a_{ji}) can take within range (R)
T	Temperature
$WF1$	Weighting factor for $(ObjG)$
$WF2$	Weighting factor for $(ObjE)$
dS_0	The step size for expanding range (R')
dS_z	The step size at stage (z)
da_z	The parameter defining the region of uncertainty around all (a_{ji}) at stage (z)
$lb(R_{ji}^a)$	The lower bound on (R_{ji}^a)
$ub(R_{ji}^a)$	The upper bound on (R_{ji}^a)
z	Coordination number
α	The whole number positive multiplier used to define (da_z)
η	Initialisation component-balance parameter

Chapter 7

A'	Ideal area intensity for the analyte
A_i	Area intensity for the analyte for run (i)

A_i'	Ideal area intensity for the analyte for run (i)
A_m	Average area intensity for the analyte
IS'	Ideal area intensity for the internal standard
c_∞	Speed of light
c_m	Average differentiation ratio
f_i	Quantity ratio for run (i)
x_{MS}^{GC}	Fraction of mutual solvents with respect to the organic fraction of the sample
x_{MS}^{S}	Fraction of mutual solvents in the sample
x_b^S	Fraction of brine in the sample
x_o^S	Fraction of oil in the sample
h	Planck's constant
DF	Dilution factor
DP	Number of decimal places
E	Energy
IS_i	Area intensity for the internal standard for run (i)
IS_m	Average area intensity for the internal standard
N	Total number of runs
c	The differentiation ratio
f	The quantity ratio
v	Frequency
λ	Wavelength

Chapter 8

S_{or}	Residual oil saturation
S_{wi}	Initial water saturation
PV	Pore volume

Chapter 9

$P_{o/w}$	Partition coefficient of the mutual solvent in n-octanol to water

Key Abbreviations

A	Analyte
ASOG	Analytical Solution of Groups
BM	Benchmark
D	Diluent

DW	De-ionised Water
EDX	Energy Dispersive X-ray
ESEM	Environmental Scanning Electron Microscopy
FID	Flame Ionisation Detection
GC	Gas Chromatography
ICP	Inductively Coupled Plasma
IS	Internal Standard
KF	Karl-Fischer
LLE	Liquid-Liquid Equilibrium
LLLE	Liquid-Liquid-Liquid Equilibrium
MGFW	Modified Glenelg Formation Water
MH	Multipar H
MS	Mutual Solvent
MSI	Multi-Start Minimisation
MT	Main Treatment
NFFW	Nelson Forties Formation Water
NRTL	Non-Random Two-Liquid
NSSW	North Sea Seawater
OES	Optical Emission Spectroscopy
OM	Overall Mixture
PDM	Phase Displacement Method
RSD	Relative Standard Deviation
SFNSSW	Sulphate-free North Sea Seawater
SFSW	Sulphate-Free Seawater
SI	Scale Inhibitor
SS	Source Sample
SW	Seawater
TM	Target Mixture
TPE	Tetraphenylethylene
TS	Trans-Stilbene
UNIFAC	UNIQUAC Functional Group Activity Coefficient
UNIQUAC	Universal Quasi-Chemical Activity Coefficient
UV	Ultraviolet
Vis	Visible

Publications

ARAB, M. M., SORBIE, K. S., DAVIS, I. & SINGLETON, M. 2017 Published. Simple Qualitative and Quantitative Approaches for Predicting the Phase Behaviour in Oil + Brine + Mutual Solvent Systems. RSC Chemistry in the Oil Industry XV: Enabling Efficient Technologies, 06-08 Nov, Manchester, England, UK: Royal Society of Chemistry.

ARAB, M. M., SORBIE, K. S. & SINGLETON, M. 2016 Published. Mutual Solvent Driven Inorganic Precipitation in the Pre-Flush Stage of Squeeze Treatments. SPE International Conference and Exhibition on Formation Damage Control, 24-26 Feb, Lafayette, Louisiana, USA: Society of Petroleum Engineers.

N.B. This is a list of publications emerging from this work at the time of submitting this thesis. Additional publications based on this work are planned after this submission.

Chapter 6: Using a Thermodynamic Model to Describe the Phase Envelope of Oil/Brine/Mutual Solvent Systems

6.1. OVERALL AIMS AND OBJECTIVES

Capturing the phase diagram of oil/brine/mutual solvent systems using a thermodynamic model will offer significant advantages on the semi-empirical approach. Examples include:

1. The semi-empirical approach requires the input of both three-phase and two-phase separation data to work out the phase regions on the phase diagram. The quasi-ternary phase behaviour of many oil/brine/mutual solvent systems offers opportunities to reduce the reliance on experimental data if the phase diagrams of the systems of interest can be described more rigorously using a thermodynamic model.

2. As described in Chapter 5 section 5.3, a series of error corrections are required to make the raw results of the Phase Displacement Method (PDM) mathematically accurate and physically consistent. This is due to the experimental errors associated with this method. While the errors in mapping the three-phase region can be kept low as demonstrated in Chapter 4, more errors are inevitable in mapping the two-phase region despite the error corrections. Also, the physical consistency of the PDM does not equate to thermodynamic consistency, i.e. conservation equations are satisfied but no equilibrium conditions are considered. Therefore, using a thermodynamic model to map the phase diagram of these systems may result in reduced errors in determining the two-phase compositions.

3. With the semi-empirical approach, interpolation is required on the phase diagram where semi-empirical data are not explicitly available. The interpolation does not ensure thermodynamic equilibrium and only provides a rough estimate of the phase composition data. A thermodynamic model would work out phase compositions whilst ensuring thermodynamic equilibrium.

Assuming quasi-ternary phase behaviour, the aim of the work described in this chapter was to identify and to investigate the ability of existing thermodynamic models to describe the phase behaviour of oil/brine/mutual solvent systems. The work in this section supplements the techniques described in the literature for modelling truly ternary systems, and extends them to allow the modelling of quasi-ternary systems.

6.2. MODELLING CRITERIA

6.2.1. Model Selection

The quantitative thermodynamic modelling of a system of oil/brine/mutual solvent is a complex endeavour. Oil is primarily a mixture of nonpolar compounds (mainly: alkanes, cycloalkanes and aromatics). The brine will contain a wide variety of ions (i.e. electrolytes), and the water itself – unlike the oil constituents – is polar. The brine may also contain scale inhibitors in the form of phosphonates or polymers in squeeze applications. The mutual solvent, in the simplest case, is a single component. However, the use of mutual solvents in blends is of interest and they are often applied in the field in this manner.

As such, a thermodynamic model selected to model this system should be able to cope with multicomponent systems which contain both polar and nonpolar compounds in addition to electrolytes. Furthermore, the model should also be able to cope with the hydrophobicity of the oil constituents, the lipophobicity of the brine components and the amphiphilicity of the mutual solvent. Finally, since the oil, brine and mutual solvent will be in the liquid phase, the model should be able to perform liquid equilibria calculations.

For liquid equilibria modelling, the T-K-Wilson equation, the NRTL and the UNIQUAC models are all useful in representing multicomponent systems (Wilson, 1964; Renon and Prausnitz, 1968; Abrams and Prausnitz, 1975; Tsuboka and Katayama, 1975; Walas, 1985; Rao, 2013). The T-K-Wilson equation is an adaptation of the Wilson equation for liquid-liquid equilibria (Wilson, 1964; Tsuboka and Katayama, 1975). Compared to the NRTL and UNIQUAC equations, it has major drawbacks. The most important of these is the potential for obtaining multiple solutions to the equation with no obvious way for selecting one of the solutions (Walas, 1985). The NRTL equation meets the basic requirements for explicitly modelling the systems described above. However, it cannot independently predict unknown activity coefficients without relying on either the Wilson equation or the UNIQUAC. Note that predictions can be made using group contributions methods such as the Analytical Solutions of Groups method (ASOG) which is based on the Wilson Equation, or the UNIQUAC Functional Group Activity Coefficient method (UNIFAC) which is based on the UNIQUAC model (Wilson and Deal, 1962; Derr and Deal, 1969; Fredenslund, Jones and Prausnitz, 1975; Kojima and Tochigi, 1979). This leaves the UNIQUAC model as the most viable of the discussed options for describing the system of interest explicitly.

However, it is known a priori that the explicit modelling (i.e. each component in the system explicitly defined in the model) of these systems with any success is unlikely. For this to be achieved, interaction parameters must either be available or possible to calculate for all the components. In practice, this is not the case. Interaction parameters for many components and at different conditions are not available due to the huge range of variability associated with the systems of interest. Calculating these values is a very complex and expensive task, and if achieved will only be useful on a case by case basis. It is also unknown if the model would be able to capture three-phase equilibria, and adding complexity to the modelling procedure only makes this less likely.

Therefore, it is imperative to simplify the modelling of oil/brine/mutual solvent systems. In this work, the quasi-ternary phase behaviour of these systems will be used as a basis for this simplification. Similar to the semi-empirical modelling strategies employed in Chapter 4 and Chapter 5, each of the oil, brine and mutual solvent will be treated as single components. In other words, a "black-oil" modelling approach will implemented for describing the phase compositions in the system, in which minimal speciation of the subcomponents (particularly, the constituents of the oil and the brine) is assumed throughout the phase diagram. In the UNIQUAC model, this reduces the primary input requirements to six interaction parameters representing the interactions between the oil and the brine, the oil and the mutual solvent, and the brine and the mutual solvent.

6.2.2. Model Description

The description and the equations provided in this section are provided with reference to: (Abrams and Prausnitz, 1975; Walas, 1985; Lucia, Padmanabhan and Venkataraman, 2000; Denes, Lang and Lang-Lazi, 2006; Rao, 2013). In a non-ideal solution, the excess Gibbs free energy calculates the deviation from ideal behaviour. The Universal Quasi-Chemical Activity Coefficient (UNIQUAC) model describes the excess Gibbs as a combination of two parts: 1) a combinatorial part which factors for the composition, size and shape of the molecules in the system; 2) a residual part which accounts for the intermolecular forces between the molecules. This is given by:

$$G^{ex} = G_C^{ex} + G_R^{ex} = R_G\, T\, \sum_i x_i \ln(\gamma_i) \qquad 6.1$$

Where:

$$\ln(\gamma_i) = \ln\left(\gamma_i^C\right) + \ln(\gamma_i^R) \qquad 6.2$$

$$\ln(\gamma_i^C) = \ln\left(\frac{\emptyset_i}{x_i}\right) + \frac{z}{2}\, q_i\, \ln\left(\frac{\theta_i}{\emptyset_i}\right) + l_i - \frac{\emptyset_i}{x_i} \sum_j x_j\, l_j \qquad 6.3$$

$$\ln(\gamma_i^R) = q_i \left[1 - \ln\left(\sum_j \theta_j\, \tau_{ji}\right) - \sum_{j=1}^{m} \frac{\theta_j\, \tau_{ij}}{\sum_{k=1}^{m} \theta_k\, \tau_{kj}}\right] \qquad 6.4$$

And:

$$\emptyset_i = \frac{x_i\, r_i}{\sum_j x_j\, r_j} \qquad 6.5$$

$$r_i = \sum_k v_k^{(i)}\, R_k \qquad 6.6$$

$$\theta_i = \frac{x_i\, q_i}{\sum_j x_j\, q_j} \qquad 6.7$$

$$q_i = \sum_k v_k^{(i)}\, Q_k \qquad 6.8$$

$$l_i = \frac{z}{2}\,(r_i - q_i) - (r_i - 1) \qquad 6.9$$

$$\tau_{ji} = \exp\left[-\frac{(u_{ji} - u_{ii})}{R\,T}\right] = \exp\left(-\frac{a_{ji}}{T}\right) \qquad 6.10$$

The objective function when modelling the system describes the minimum of the excess Gibbs free energy for the overall mixture and is given by:

$$Min[\Delta g_{mix}] = Min[\ \sum_{k=1}^{p} \sum_{i=1}^{C} l_i^k \left(\ln x_i^k + \ln \gamma_i^k\right)\ ] \qquad 6.11$$

The minimisation in equation 6.11 must be done subject to the following conditions:

1. Positive flows (boundary constraints):

$$l_i^k \geq 0 \qquad 6.12$$

2. Mass conservation (linear constraints):

$$f_i = \sum_{k=1}^{p} l_i^k \qquad 6.13$$

3. Constant activities across all phases at equilibrium (nonlinear constraints):

$$a_i^k\left(l_i^k\right) = x_i^k\left(l_i^k\right)\gamma_i^k\left(l_i^k\right) \qquad 6.14$$

$$a_i^k = constant \text{ for all k} \qquad 6.15$$

6.2.3. Modelling Objectives

One of two scenarios will normally apply. In the first scenario, phase compositions would have been determined from an experiment, and these will be regressed to the model to determine the interaction parameters for the system. In the second scenario, the interaction parameters will be known from the literature, and the model will be used to solve for the phase compositions.

In this work, the first scenario is of interest when the three-phase compositions are available (e.g. via the analytical approach described in Chapter 4 section 4.5). Based on the three-phase compositions, six binary interaction parameters can be calculated for each of the constituents of the ternary system (let: O = Oil, B = Brine, and MS = Mutual Solvent; the interaction parameters (a_{ji}) are: a_{OB}, a_{BO}, a_{OMS}, a_{MSO}, a_{BMS}, and a_{MSB}). Calculating these as part of the modelling procedure allows fitting the thermodynamic model to the experimental data, enabling more accurate calculations for whichever application the model is used for (e.g. transport modelling). Three-phase compositions can be sufficient to perform this regression with excellent accuracy for truly ternary three-phase forming systems (Lin and Chen, 2002; Lin and Chen, 2004). This work will investigate whether this advantage extends to quasi-ternary three-phase forming systems.

The second scenario is unlikely to be encountered for the systems of interest. There are no interaction parameters for oil/brine/mutual solvent systems in the literature as pseudo-components. These are normally available for pure components only. Therefore, for the purposes of this work, the first scenario is the only practical scenario for modelling oil/brine/mutual solvent systems. As part of this work, the second scenario will be implemented to develop the modelling techniques for quasi-ternary systems. These modelling techniques will be investigated for truly ternary systems initially and data in the literature will be relied on.

6.2.4. Solution Criteria

Regardless of the modelling objective, the solution criteria is identical:

1. A modelling algorithm must be employed to assess for liquid equilibria (number of phases at equilibrium). Various algorithms are available in the literature.

2. The model must be initialised. The UNIQUAC model is a highly nonlinear model. Therefore, good initialisation will be required (good estimation of the solution).

The solution to the model involves arriving at the global minimum when minimising the objective function (equation 6.11) subject to the minimisation constraints (equations 6.12-6.15). Poor initialisation will cause the model to arrive at one of many local minima, which would be far from an accurate solution to the minimisation problem.

3. After initialisation, the model must be minimised to achieve the solution. Many minimisation routines/algorithms of varying complexity are available.

6.2.5. Modelling Example of a Three-Phase Forming System

A system of nitromethane, ethylene glycol and lauryl alcohol forms three-phases at 298 K and 1 atm. Around the three-phase region, three two-phase regions exist. This system was successfully modelled using the UNIQUAC model using an algorithm described by Denes, Lang and Lang-Lazi (2006). An illustration of the modelling procedure and the results at each step is provided below:

Step 1

The miscibility of each binary pair is investigated. This is done by studying the dimensionless Gibbs free energy for each pair in the mixture. For the aforementioned system, the results are highlighted in Figure 6.1, Figure 6.2 and Figure 6.3. The structural parameters and the activity coefficients used to arrive at the results are provided in Table 6.1 and Table 6.2 respectively.

In the figures, all curves are concave downward at two locations, which indicates partial immiscibility between all binary pairs (Walas, 1985). The tangent to these concavities gives the range of binary fractions over which the binary pair is deemed to be immiscible. These values are key in initialising the UNIQUAC model in this approach. When the curves have a single concavity, the following applies: 1) a downward concavity implies complete miscibility; 2) an upward concavity implies complete immiscibility (Walas, 1985).

Table 6.1: UNIQUAC structural parameters for Nitromethane, Ethylene Glycol and Lauryl Alcohol (Sørensen and Arlt, 1980; Reddy and Rani, 2012).

Structural Parameters	Compound		
	Nitromethane	Ethylene Glycol	Lauryl Alcohol
r	2.0086	2.4088	8.8495
q	1.8680	2.2480	7.3720

Table 6.2: UNIQUAC interaction parameters for Nitromethane (1), Ethylene Glycol (2) and Lauryl Alcohol (3) at 298 K (Sørensen and Arlt, 1980; Reddy and Rani, 2012).

a_{12}	a_{21}	a_{13}	a_{31}	a_{23}	a_{32}
136.160	490.664	73.442	369.688	87.554	233.251

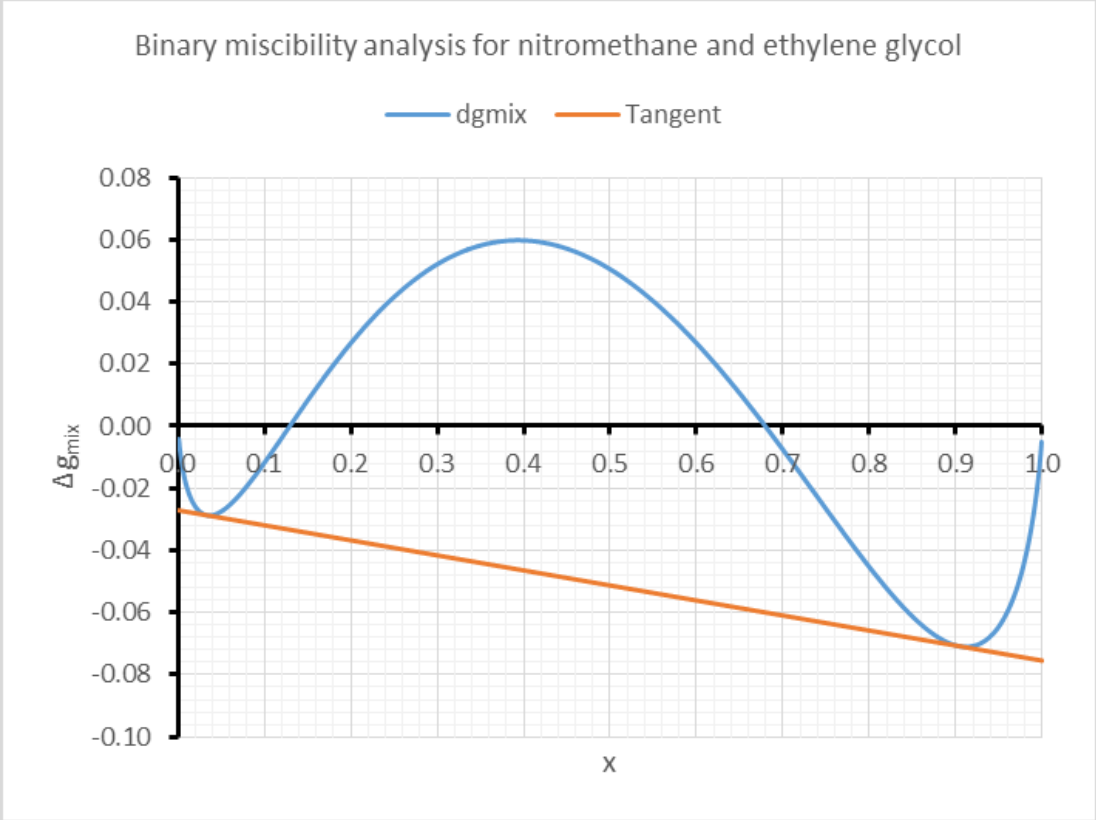

Figure 6.1: Binary pair miscibility analysis for nitromethane (x) and ethylene glycol (1-x).

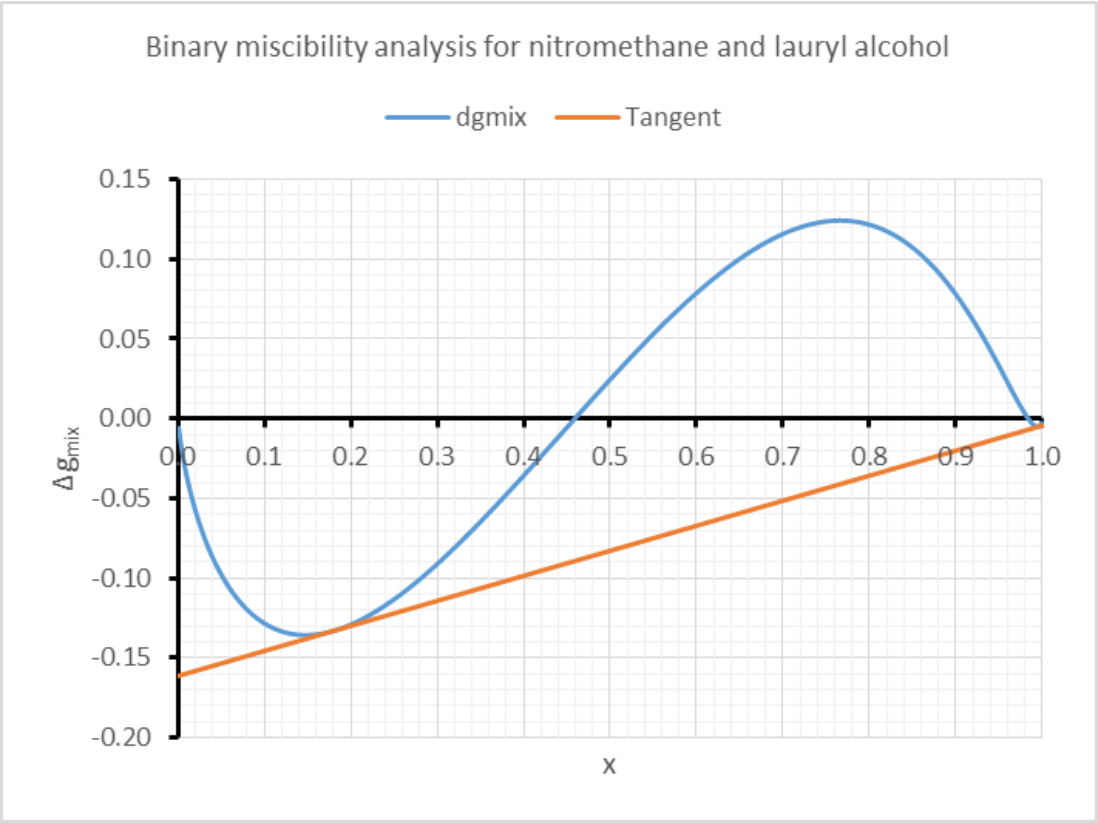

Figure 6.2: Binary pair miscibility analysis for nitromethane (x) and lauryl alcohol (1-x).

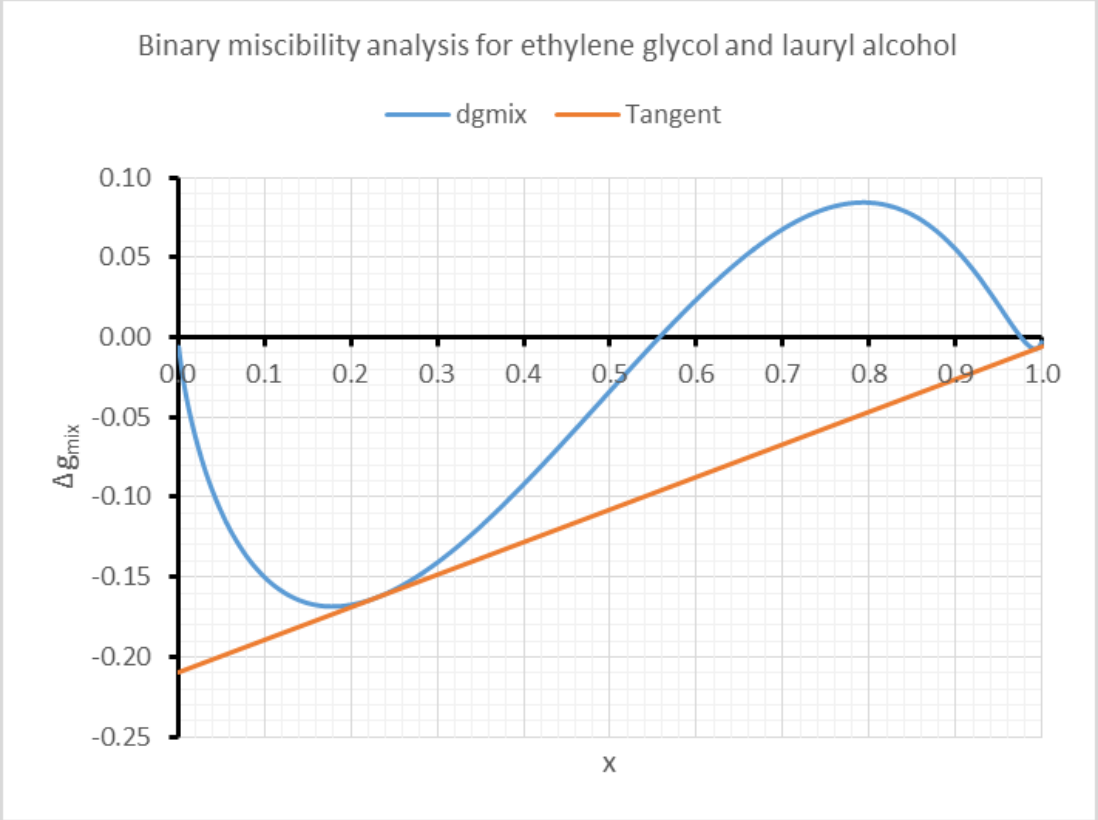

Figure 6.3: Binary pair miscibility analysis for ethylene glycol (x) and lauryl alcohol (1-x).

Step 2

When two or more pairs possess binary immiscibility, as in this example, the dominant immiscible pair must be selected. The procedure for this takes into account both: the relative amounts of each constituent in the feed (i.e. the feed composition), and the mutual solubilities of all components. Equation 6.16 is used to perform this analysis, with the dominant immiscible pair yielding the two highest values.

$$p_i = \frac{ZQ_i}{P_iQ_i} \qquad 6.16$$

Figure 6.4 is a graphical illustration of the dominant pair selection procedure for the system under investigation. The results obtained from equation 6.16 with reference to Figure 6.4 make nitromethane and lauryl alcohol the dominant immiscible pair (p_i = 3.5, 1.9 and 55.3, for nitromethane, ethylene glycol and lauryl alcohol respectively). In initialising the calculations, the remaining component (ethylene glycol) is split between phases rich in each of the dominant pairs (e.g. assuming two phase: nitromethane-rich and lauryl alcohol-rich phases).

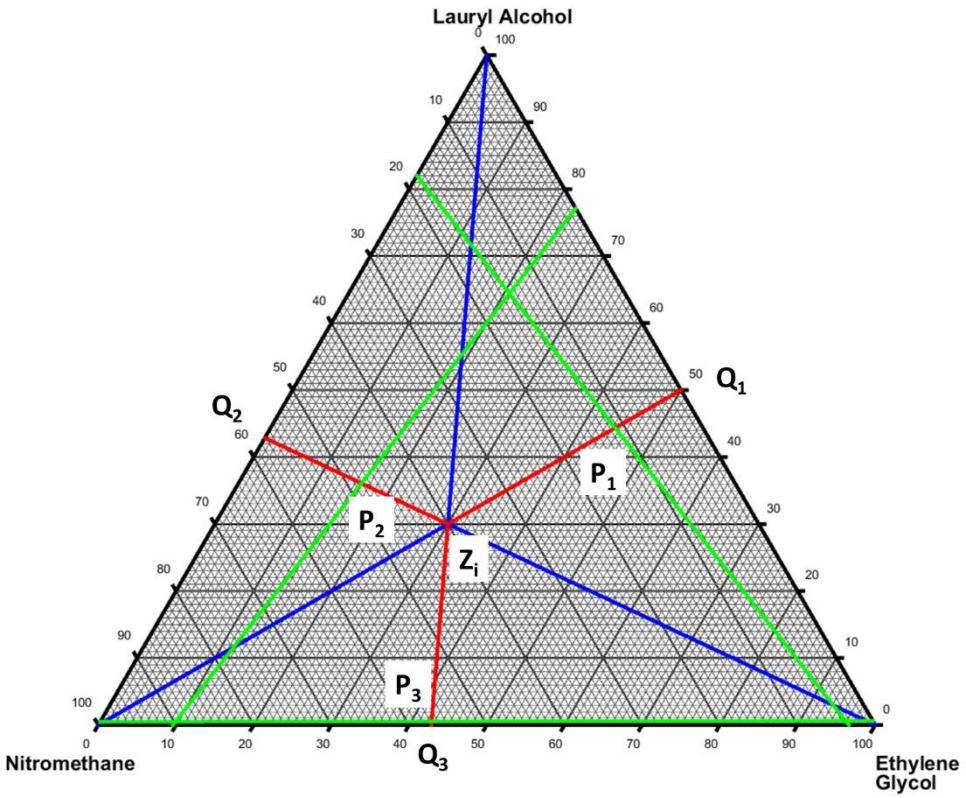

Figure 6.4: Graphical illustration of the dominant immiscible pair selection procedure.

Step 3

Liquid-liquid equilibrium (LLE) is assumed, and the LLE flash calculations are initialised. The full procedure for doing this with detailed explanations is given by Denes, Lang and Lang-Lazi (2006) and Lucia, Padmanabhan and Venkataraman (2000). For illustration purposes, the equations used in the initialisation are provided here. Assume the composition of each phase is:

$$\underline{x}^{I} = \left[\frac{l^{I}_{dom1}}{L^{I}}, \frac{l^{I}_{dom2}}{L^{I}}, \frac{\eta\, f_i}{L^{I}}\right] \tag{6.17}$$

$$\underline{x}^{II} = \left[\frac{l^{II}_{dom1}}{L^{II}}, \frac{l^{II}_{dom2}}{L^{II}}, \frac{(1-\eta)\, f_i}{L^{II}}\right] \tag{6.18}$$

Where:

$$\eta = \frac{z_{dom1} - x^{II}_{dom1}}{x^{I}_{dom1} - x^{II}_{dom1}} \tag{6.19}$$

The above assumptions are necessary to approximate the activity of each phase. Proceeding with the initialisation calculations relies on the solubility of component (i) in the dominant pair. Three types of mixtures are possible:

1. Type (I) mixture: component (i) is completely miscible in both dominant pairs. Given that at equilibrium:

   $$\gamma^{I}_i\, x^{I}_i = \gamma^{II}_i\, x^{II}_i \tag{6.20}$$

   And:

   $$x^{I}_i = \frac{l^{I}_i}{l^{I}_{dom1} + l^{I}_{dom2} + l^{I}_i} \tag{6.21}$$

   $$x^{II}_i = \frac{l^{II}_i}{l^{II}_{dom1} + l^{II}_{dom2} + f_i - l^{I}_i} \tag{6.22}$$

   With reference to equation 6.20, let the equilibrium constant be:

   $$K_i = \frac{y^{II}_i(\underline{x}^{II})}{y^{I}_i(\underline{x}^{I})} = \left(\frac{x^{I}_i}{x^{II}_i}\right)_{new} \tag{6.23}$$

   The new (x^{I}_i) and (x^{II}_i) can be calculated by initially solving equation 6.23 for (K_i) using the UNIQUAC model. This is then used to solve equation 6.24 for (l^{I}_i) subject

to ($0 < l_i^I < f_i$). Once (l_i) is known, the new (x_i^I) and (x_i^{II}) can easily be calculated and the LLE initialisation would be complete.

$$K_i = \frac{\frac{l_i^I}{l_{dom1}^I + l_{dom2}^I + l_i^I}}{\frac{l_i^{II}}{l_{dom1}^{II} + l_{dom2}^{II} + f_i - l_i^I}} \qquad 6.24$$

2. Type (II) mixture: component (i) is partially miscible with one of the dominant pairs. For this kind of mixtures, let:

$$K_i = K_i^{dom1} = \frac{x_i^{dom1}}{x_i^i} \qquad 6.25$$

Once this is calculated, equation 6.24 can be implemented as described before.

3. Type (III) mixture: component (i) is partially miscible with both of the dominant pairs. For this kind of mixtures, let:

$$K_i = \frac{K_i^{dom1}}{K_i^{dom2}} = \frac{x_i^{dom1}}{x_i^{dom2}} \qquad 6.26$$

Once this is calculated, equation 6.24 can be implemented as described before.

Step 4

LLE flash calculations are performed. Here, equation 6.11 is minimised subject to the constraints outlined by equations 6.12-6.15. If a trivial solution is found, only one liquid phase exists at equilibrium. If a nontrivial solution is found, liquid-liquid-liquid equilibrium (LLLE) must be checked.

Step 5

LLLE is assumed, and the LLLE flash calculations are initialised. The same initialisation procedure is followed. The starting point is the results from the LLE calculation. Each of the two-phase pairs obtained are treated separately. The dominant pair for each phase is found using Step 2, and each phase is assumed to split into two phases using Step 3. This yields four phases overall. The two of the four phases that have the closest compositions are combined as a single phase, resulting in three phases overall. This final result is used as the initialisation values for LLLE flash calculations.

Step 6

LLLE flash calculations are performed. Again, equation 6.11 is minimised subject to the constraints outlined by equations 6.12-6.15. If a trivial solution is found, two liquid phase exists at equilibrium and the final result reverts back to the results from Step 4. If a nontrivial solution is found, then three liquid phases exist at equilibrium and the final result is the result obtained from the LLLE flash calculation.

Application

For the example system outlined in this section, several points were investigated throughout the phase diagram subject to the structural parameters and the interaction parameters provided in Table 6.1 and Table 6.2 respectively. The results are presented in Figure 6.5 and they highlight the ability of the UNIQUAC model to resolve the various regions on the phase diagram, including the three-phase region.

Despite the noted success of the modified Lucia, Padmanabhan and Venkataraman (2000) algorithm (Denes, Lang and Lang-Lazi, 2006) in solving this three-phase forming system, and the LLLE systems described in both references, attempts to reproduce results in the literature for simple oil/water/mutual solvent systems – e.g. (Negahban et al., 1986; Lin and Chen, 2002; Lin and Chen, 2004) – were unsuccessful. This is explained by the following points:

1. Interaction parameters provided in the literature for these systems were used. These interaction parameters were produced by minimising the square of the error between an experimental data set and the calculated data using the UNIQUAC model, subject to the following objective function:

$$ObjF = \sum_{k=1}^{N} \sum_{j=1}^{2/3} \sum_{i=1}^{3} \left(\frac{x_{ijk}^{cal} - x_{ijk}^{exp}}{x_{ijk}^{exp}} \right)^2 \qquad 6.27$$

2. The UNIQUAC model's ability to describe these systems was then assessed subject to this objective function, and using experimental data and knowledge regarding the number of phases at equilibrium in initialising the solution.

3. As such, the interaction parameters provided in the literature were not ideal for two reasons. Firstly, if experimental data/knowledge are lacking, the initialisation of the model is not possible, and initialising the model using more accurate data removes the need to model the system all together in any case. Secondly, the

objective function described by equation 6.27 is inherently inconsistent with that describing the equilibrium state of the system (equation 6.11). Solving equation 6.27 shows if the UNIQUAC model can represent the experimental data regardless whether the solution obtained represents thermodynamic equilibrium or not at the specified interaction parameters for the calculation.

Therefore, calculating interaction parameters consistent with equation 6.11 and subject to the constraints described by equations 6.12-6.15 is necessary.

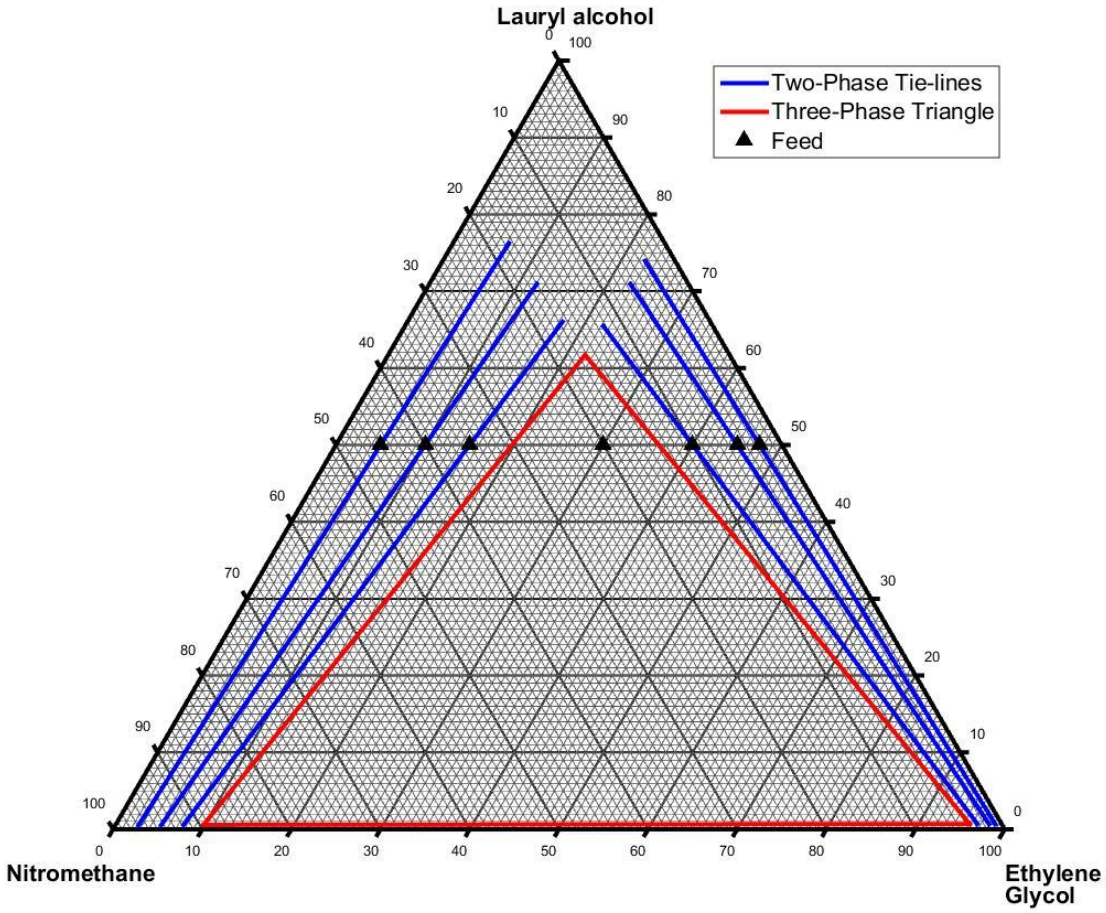

Figure 6.5: The phase diagram of Nitromethane, Ethylene Glycol and Lauryl Alcohol at 298 K obtained from the UNIQUAC model using the modified Lucia, Padmanabhan and Venkataraman (2000) algorithm (Denes, Lang and Lang-Lazi, 2006).

6.3. ADAPTATIONS TO OIL/BRINE/MUTUAL SOLVENT SYSTEMS

6.3.1. Standard Method for Determining the Interaction Parameters

Standard nonlinear constrained minimisation techniques (e.g. interior-point algorithm; the default **fmincon** implementation in MATLAB; (Byrd, Hribar and Nocedal, 1999; Byrd, Gilbert and Nocedal, 2000; Waltz et al., 2006)) can be used to determine the interaction parameters (a_{ji}) of a given system based on:

1. The UNIQUAC structural parameters (r_i and q_i).
2. Experimental data (two- and/or three-phase compositions).
3. The temperature (T).

The objective function given by equation 6.11, and the constraints given by equations 6.12-6.15 may be used. The success of the minimisation of equation 6.11 relies heavily on providing good estimates of (a_{ji}). When dealing with three components/pseudo-components, six interaction parameters must be determined for the interaction of component (j) with component (i). Randomly guessing the initial values for these is difficult and extremely unreliable, and some appreciation of their values is generally required to achieve a successful calculation. Moreover, needing both two- and three-phase compositions to calculate the parameters limits the usefulness of the UNIQUAC model quite significantly.

To overcome these difficulties, a regression approach was developed for determining the interaction parameters (a_{ji}) based on:

1. A technique developed for determining good initial values for the six (a_{ji}) values.
2. Using three-phase compositions only, which can be determined with ease.

Achieving this successfully will largely extend the usefulness of the UNIQUAC model for assessing the phase envelopes of oil/brine/mutual solvent systems.

6.3.2. The Regression Approach: Initialising the Interaction Parameters

The approach for initialising the interaction parameters (a_{ji}) relies on the following:

1. A “composite” objective function.
2. A stepwise evaluation of the composite objective function.

The composite objective function consists of two terms, squared and weighted. The first term is the squared and weighted dimensionless Gibbs free energy of the mixture given by equation 6.28:

$$ObjG = WF1\left[\sum_{k=1}^{p}\sum_{i=1}^{C} l_i^k\left(\ln x_i^k + \ln \gamma_i^k\right)\right]^2 \qquad 6.28$$

The second term is derived from the nonlinear equilibrium condition. This condition requires constant activities (a_i^k) for all the components across all phases as described by equations 6.29-6.31:

$$a_i^k - a_i^m = 0; \qquad 6.29$$

$$k = 1, 2, 3; \qquad \text{(for 3 phases)} \qquad 6.30$$

$$m = \begin{cases} [2,3], & k = 1 \\ [1,3], & k = 2 \\ [1,2], & k = 3 \end{cases} \qquad \text{(for 3 phases)} \qquad 6.31$$

As such, the second term is defined as the squared and weighted sum of the activity differences as described by equations 6.32 and 6.33:

$$ObjE = WF2\left[\sum_{k=1}^{3} a_i^k - a_i^m\right]^2 \qquad \text{(for 3 phases)} \qquad 6.32$$

$$m = \begin{cases} [2,3], & k = 1 \\ [1,3], & k = 2 \\ [1,2], & k = 3 \end{cases} \qquad \text{(for 3 phases)} \qquad 6.33$$

Hence, the composite objective function for initialising (a_{ji}) is given by:

$$ObjR = ObjG + ObjE \qquad 6.34$$

Using this objective function for initialising the interaction parameters removes the complexity of needing to satisfy a nonlinear equilibrium constraint when minimising the objective function. The weighting factors ($WF1$ and $WF2$) allow emphasising the contributions of each term ($ObjG$ and $ObjE$) to the objective function. The term ($ObjE$) should be given a higher weighting. Doing this would result in initial (a_{ji}) values which approximately satisfy the nonlinear equilibrium constraint. This becomes very important when attempting to perform the constrained minimisation using equations 6.11-6.15. In practice, setting ($WF2$) to be an order of magnitude higher than ($WF1$) was found to yield good initial values (i.e. $WF1 = 1; WF2 = 10$).

As for the stepwise evaluation of the objective function, the range (R) within which all (a_{ji}) values exist ($R_0\ to\ R_n$) must be specified. By default, this is set as -3000 to 3000. A very coarse minimisation of the objective function is performed on this range as per the steps listed below:

1. Calculating the step size (dS_0) for searching the range:

$$dS_0 = \frac{R_n - R_0}{S} \tag{6.35}$$

   Where (S) is the number of the values that (a_{ji}) can take within the specified range (R). Once (dS_0) is calculated, the range bounds are re-calculated to conform with (dS_0), i.e. (R_0) is rounded down and (R_n) is rounded up, both to the nearest (dS_0), yielding (R_0') and (R_n'). The resulting range (R') is then expanded at steps of (dS_0). If the range contains a zero, the zero is replaced by two values ($\pm dS_0/S$) since ($a_{ji} \neq 0\ @\ i \neq j$). For the purposes of this discussion, the final range is denoted by (R'').

2. All the possible six combinations of the values in (R'') are determined without repeats. The no repeat condition is based on the idea that interactions between different (i) and (j) pairs must be different. The number of possible (a_{ji}) sets (N_0) is given by:

$$N_0 = \frac{N(R'')!}{(N(R'')-6)!} \tag{6.36}$$

3. Testing all sets against the composite objective function and finding the minimum. The set of (a_{ji}) values which give this minimum is ($\overline{a_{Cm}}$).

Once this coarse minimisation is completed, the results are refined according to the following steps to achieve the initial (a_{ji}) values ($\overline{a_0}$):

4. A range of values (R_{ji}^a) are defined around each (a_{ji}) value in ($\overline{a_{Cm}}$) to yield six independent (R_{ji}^a) ranges. The lower and upper bounds of each range ($lb\left(R_{ji}^a\right)$ and $ub\left(R_{ji}^a\right)$) are determined using:

$$lb\left(R_{ji}^a\right) = a_{ji} - da_z \tag{6.37}$$

$$ub\left(R_{ji}^{a}\right) = a_{ji} + da_z \qquad 6.38$$

Where (da_z) – with (z) denoting the stage number – defines the region of trust around each (a_{ji}) value in $(\overline{a_{Cm}})$.

5. Each (R_{ji}^{a}) range is expanded at steps of (dS_z), where:

$$dS_z = dS_{z-1}/2 \qquad 6.39$$

The value of (dS_z) must be a whole even number. If the result from equation 6.39 does not satisfy this condition, the solution is rounded up to the nearest even number.

6. All the possible six combinations of (a_{ji}) are determined, in which each (a_{ji}) must come from its respective range (R_{ji}^{a}). The number of possible (a_{ji}) sets (N_z) in this case is given by:

$$N_z = \left(\frac{2\,da_z}{dS_z} + 1\right)^6 \qquad 6.40$$

7. The sets are used to evaluate the composite objective function (equation 6.34), and the set that gives the minimum ($\overline{a_{Fm}^{z}}$ with z denoting the stage number) of the function is determined.

8. The steps 4-7 are repeated using $(\overline{a_{Fm}^{z-1}})$ as the starting point for the calculation at each stage (z). This is done until $(dS_z = 1)$ is achieved and assessed.

9. The final $(\overline{a_{Fm}^{z}})$ set at $(dS_z = 1)$ is the initial values set $(\overline{a_0})$ for the interaction parameters. Incorporating this set into an appropriate minimiser (e.g. **fmincon** in MATLAB), and subject to equations 6.11-6.15 allows calculating the interaction parameters for the system under investigation.

When this procedure for calculating $(\overline{a_0})$ is used, a few computational considerations must be highlighted:

1. The selection of (S): As can be seen in equation 6.35, this determines the step size (dS_0) for the coarse minimisation. Given that the termination criteria for the procedure outlined above is $(dS_z = 1)$, the maximum value that (dS_0) can take is $(R_n - R_0)$. This is the setting that will yield the best $(\overline{a_0})$ set since every point in

the range will be investigated. However, this is practically impossible to use due to the prohibitively large number of possible (a_{ji}) sets that will require evaluation as can be deduced from equation 6.36. In fact, due to equation 6.36, a very small value (with respect to $R_n - R_0$) for (S) should be selected to enable a practical calculation as can be seen from Figure 6.6, i.e. a value for (S) on the low end. The smallest value that (S) can take is ($S = 6$) since we need to find a combination of six values without repeats. If the default (R) is selected (-3000 to 3000), ($S = 10$; translating to $dS_0 = 600$) was found to be generally sufficient for a very coarse, but meaningful minimisation. Anything smaller than that for a range (R) containing 6,000 whole number values will result in ($\overline{a_0}$) set of extremely limited usefulness if useful at all.

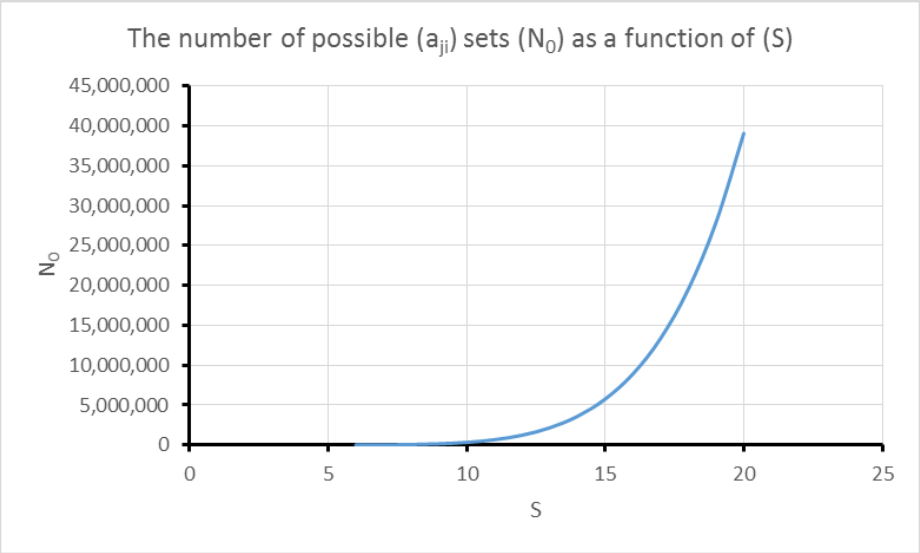

Figure 6.6: The number of possible (a_{ji}) sets (N_0) for the coarse minimisation as a function of (S).

2. The selection of (da_z): As mentioned before, (da_z) defines the region of trust around each (a_{ji}) value at each stage. With a sufficiently small step (dS_z), (a_{ji}) at each stage (z) will reliably default to the value closest to the correct solution in (R_{ji}^a), e.g. if the step size ($dS_{z-1} = 50$) and this is a sufficiently small step size, and (a_{ji}) is calculated as 150, (a_{ji}) in the final correctly calculated ($\overline{a_0}$) must be bigger than ($[150 - dS_{z-1}]/2$) and smaller than ($[150 + dS_z - 1]/2$). Another way to phrase this is: as (S) tends to (S_{max}), (da_z) tends to ($da_z = dS_{z-1}/2$). The need to do a very coarse minimisation (e.g. at $S = 10$) means that ($da_z \neq dS_{z-1}/2$), and a margin of error must be allowed. In fact, given equation 6.39, the smallest (da_z) possible is ($da_z = dS_z$). This produces (R_{ji}^a) ranges for each (a_{ji}) which contain more than one value when expanded as can be deduced from equations 6.37-6.39.

In any case, (da_z) must be defined as a multiple of (dS_z) for all the values in each (R_{ji}^{α}) range to be accessible when expanding them at steps of (dS_z) (equations 6.37 and 6.38). Therefore, (da_z) can be described more generically using equation 6.41:

$$da_z = \alpha\, dS_z \qquad 6.41$$

In the procedure for calculating ($\overline{a_0}$), the value of (dS_z) must reduce by a factor of 2 until ($dS_z = 1$) as per equation 6.39. This defines an upper limit on the value of (α) in equation 6.41 at ($z = 1$). Setting ($\alpha = S$) is the equivalent of defining the region of trust around each (a_{ji}) value to be (R''), i.e. zero trust in the calculated (a_{ji}) value). Therefore, the value of (α) must satisfy the condition:

$$1 \leq \alpha < S \qquad 6.42$$

As with the case of selecting (S), the value of (α) should ideally be on the low end permitted by equation 6.42 to allow a reasonable computation time as illustrated by Figure 6.7. Typically, a value of ($\alpha = 3$) was found to be satisfactory in most cases if the standard minimisation described in section 6.3.1 is to be performed iteratively (i.e. minimising the objective function using ($\overline{a_0}$) as the initial values, recycling the result ($\overline{a}$) by setting ($\overline{a_0} = \overline{a}$), and iterating until a local minimum is found). At ($\alpha = 7$), in almost all cases, there is no need to perform the minimisation described in section 6.3.1 iteratively. However, solving at ($\alpha = 3$) with iterative standard minimisation is far more efficient than solving at ($\alpha = 7$) without iterative standard minimisation (few minutes vs. several hours of computation time respectively).

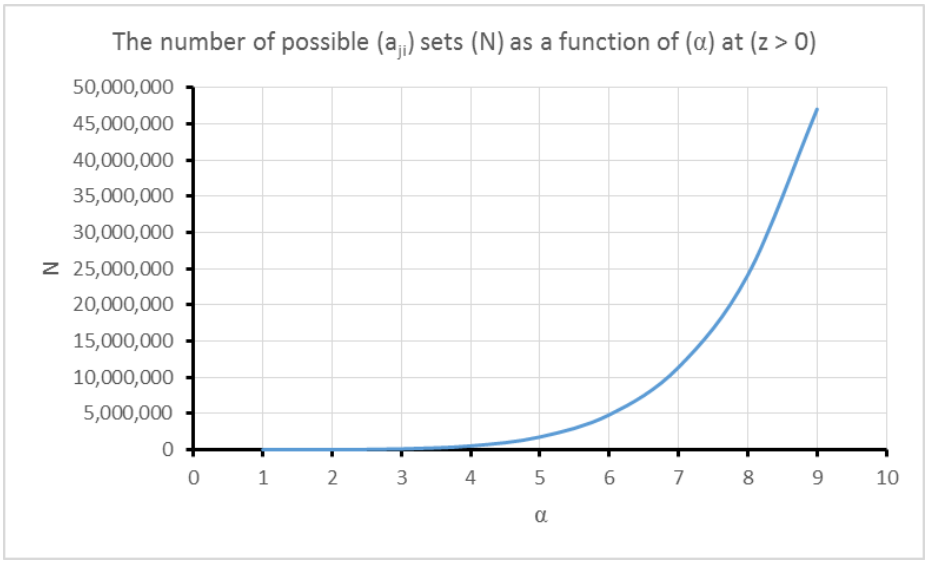

Figure 6.7: The number of possible (a_{ji}) sets (N) as a function of (α) at ($z > 0$).

6.3.3. The Regression Approach: The Three-Phase Compositions

Using only three-phase data to determine the interaction parameters is not a new concept as mentioned in section 6.2.3, and has been shown to yield excellent representation of experimental data with the UNIQUAC model, almost identical to that when additional two-phase data are included for simple oil/water/amphiphile systems (Lin and Chen, 2002; Lin and Chen, 2004). This represents a huge advantage over approaches requiring extensive experimental data to describe the phase envelope of a system.

The three-phase compositions required for determining the interaction parameters can either be obtained from:

1. The literature if available.
2. Determined using simple experiments, e.g. in ternary/quasi-ternary systems using the methods described in Chapter 4.
3. Estimated subject to the availability of qualitative phase behaviour data.
4. Assigned to yield the phase envelope of a hypothetical system with the specified three-phase separations.

Examples will be used to discuss each of the above scenarios in this chapter, section 6.4.

6.3.4. Simplified Model Initialisation

The discussion in section 6.2.5 highlights the complexity of initialising the flash calculations associated with three-phase forming systems. At each calculation point, the dominant pair must be determined, and the remaining component must be split between two phases dominated by one of the dominant components. This is done using both Gibbs free energy analysis and feed compositions as illustrated in section 6.2.5.

In this work, simplifications may be made to avoid complex initialisation. Since three-phase compositions will always be required to calculate the interaction parameters set ($\overline{a}$), the simplest approach is to use the three-phase compositions as a guideline for the initialisation. This is illustrated in Figure 6.8. Any point below the A3B3 line is initialised using a shifted A3B3 line to the feed point. Any point above the A3B3 line is initialised depending on its position with respect to C3. If the point is on the AC side of C3, the calculations are initialised using a shifted A3C3 line to the feed point. Otherwise, the calculations are initialised using a shifted B3C3 line to the feed point. A graphical illustration of this is provided in Figure 6.9.

To ensure that the initialisation is sufficient, a multi-start criterion (i.e. testing several initialisations at regular intervals across the solution domain) is employed when initialising a two-phase calculation. This is done by defining a region of uncertainty around a given tie-line. Two actions are performed:

1. Calculating tie-lines which are a linear contraction/extension of the "base" tie-line.
2. Calculating tie-lines at each linearly contracted/extended tie-lines, at various inclinations.

Figure 6.10 illustrates this by showing the lower and upper bounds on the tie-lines around the base tie-line. A set of initial point tie-lines will exist in between, all of which will be used in the minimisation. A multi-start initialisation of three-phase calculations is also possible as illustrated in Figure 6.11. However, this is not required usually because the model will be based on the supplied three-phase data.

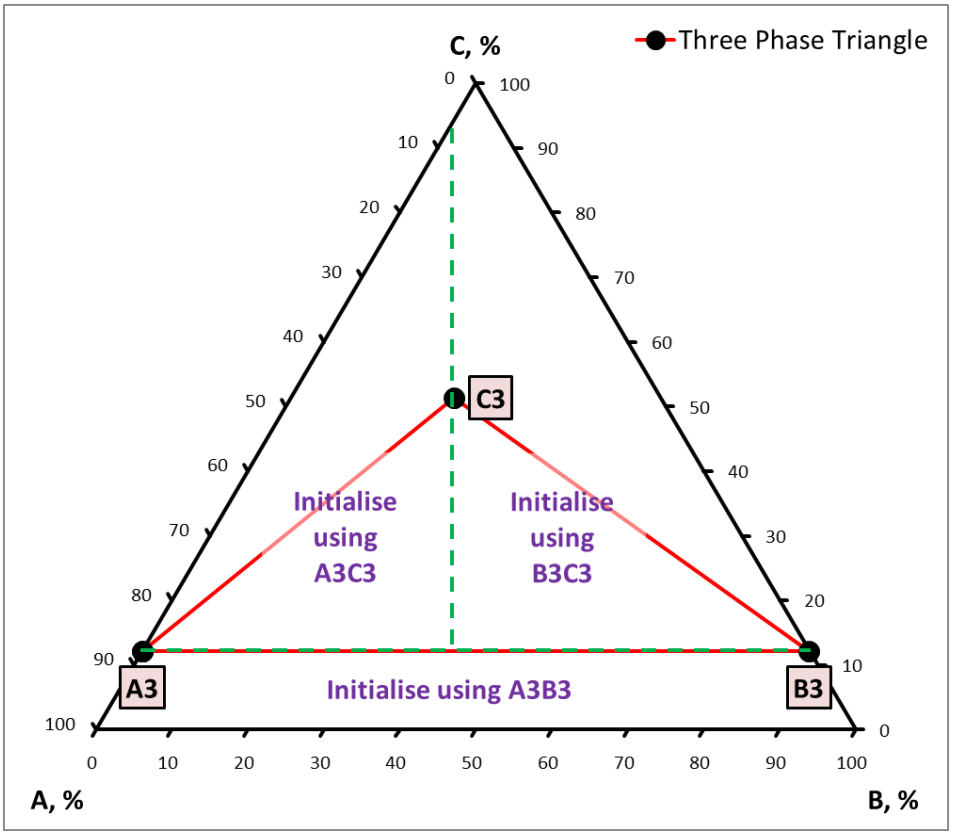

Figure 6.8: The simplified definition of the initialisation regions with respect to the three-phase triangle.

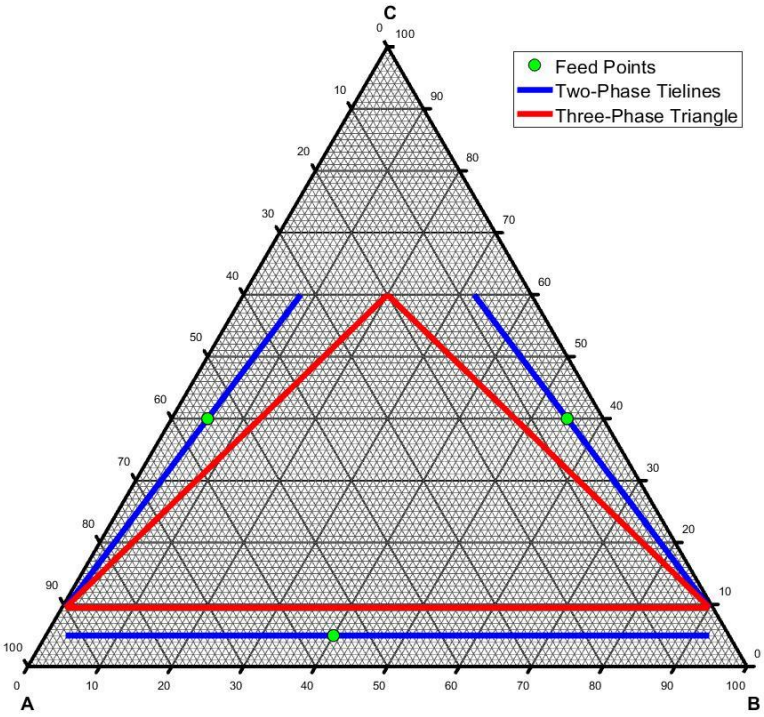

Figure 6.9: The initialisation of feed points at three different locations on the phase diagram.

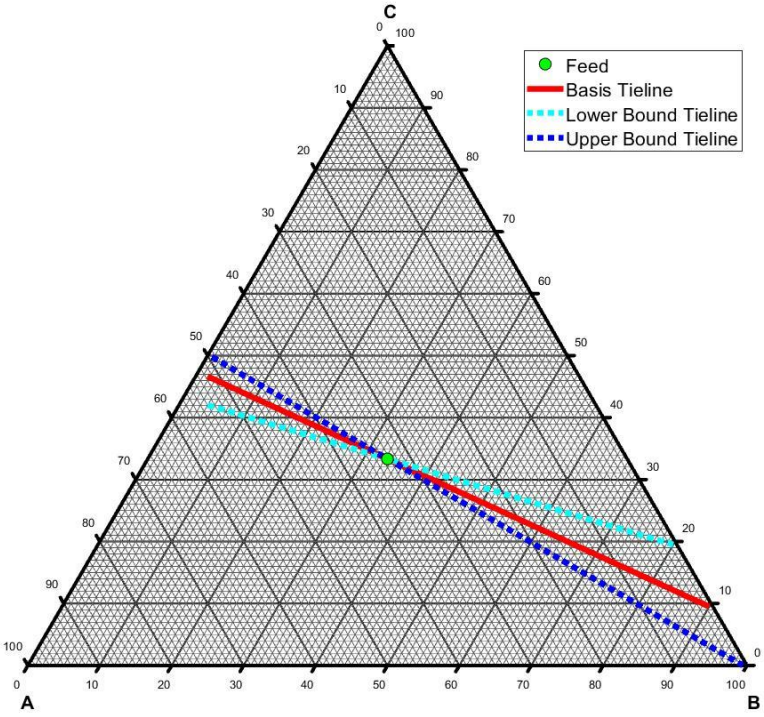

Figure 6.10: The lower and upper bounds on a two-phase multi-start initialisation.

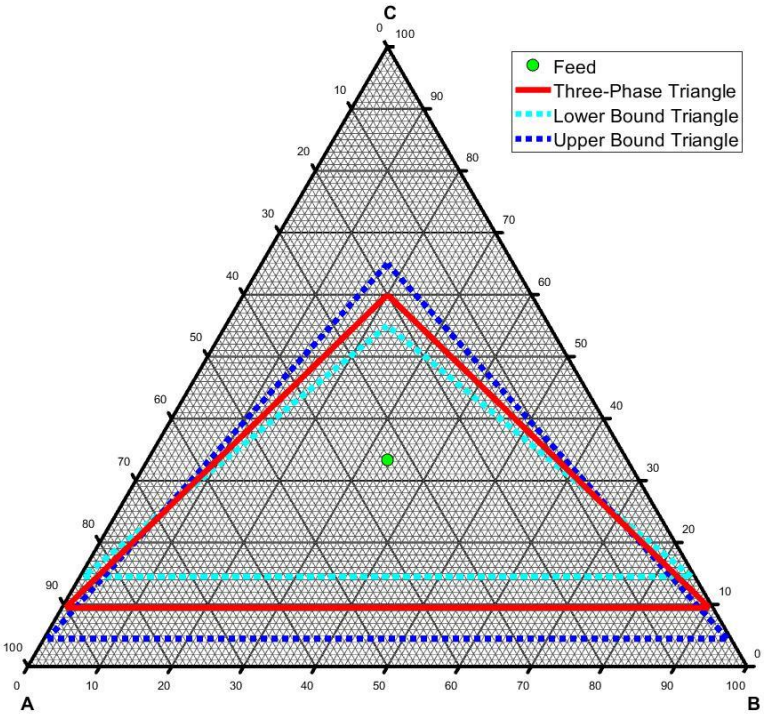

Figure 6.11: The lower and upper bounds on a three-phase multi-start initialisation.

6.3.5. Simplified Modelling Algorithm

The modelling approach used is a simplification of the modelling approach described in section 6.2.5. The following steps are followed:

1. Two liquid phase equilibrium is assumed.
2. A two-phase multi-start initialisation (MSI) is performed.
3. Minimisation of the objective function is performed at all the MSI points. The solution set that gives the minimum of the objective function overall is determined.
4. The solution is checked. If one of the phases default to the feed composition, or both phases have the same composition, there is only one liquid phase and the calculations are terminated. Otherwise, if two unique compositions are calculated, three liquid phase equilibrium is assumed.
5. The three-phase calculations are initialised and the objective function is minimised.
6. The solution is checked. Again, if one of the phases has the feed composition, or if two or more phases have the same composition, the solution is the calculated two-phase compositions in step 4. Otherwise, if three unique compositions are calculated, three phases exist at equilibrium.

These steps are summarised in the logical diagram provided in Figure 6.12 for illustration purposes. Implementing this model for the scenarios described in section 6.3.3 is provided in section 6.4.

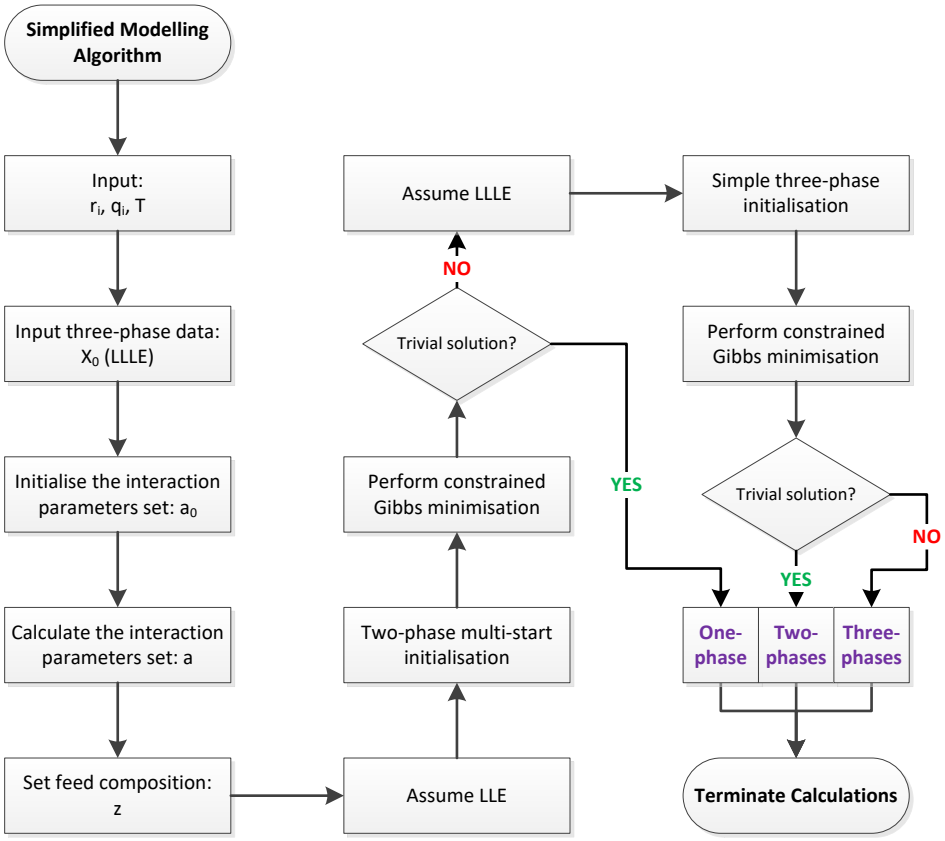

Figure 6.12: Simplified modelling algorithm for three-phase forming systems.

6.4. RESULTS AND DISCUSSION

6.4.1. Calculation of the Interaction Parameters

An example illustrating the calculation of the interaction parameters ($\overline{a}$) is provided here for a system consisting of Dodecane + Water + EGMBE at 35ºC. The three-phase compositions are obtained from the literature and provided in Table 6.3 (Lin and Chen, 2002). The structural parameters (Table 6.4) for the UNIQUAC model (r_i and q_i) are also obtained from the literature (Lin and Chen, 2002).

Table 6.3: Three-phase compositions for Dodecane + Water + EGMBE at 35ºC (Lin and Chen, 2002).

Phase	Mass Fractions		
	Dodecane	**Water**	**EGMBE**
Dodecane-Rich	0.9130	0.0021	0.0849
Water-Rich	0.0001	0.8470	0.1529
EGMBE-Rich	0.0336	0.4697	0.4967

Table 6.4: UNIQUAC structural parameters for Dodecane + Water + EGMBE (Lin and Chen, 2002).

Structural Parameters	Compound		
	Dodecane	**Water**	**EGMBE**
r_i	8.5462	0.9200	5.0558
q_i	7.0600	1.4000	4.3720

For this system, initialising the interaction parameters over the range ($R = -3000:3000$) yields no solution. This could happen when the range is over-defined, i.e. the solution lies within a much smaller range of values. To overcome this issue, the range is reduced to ($R = 0:3000$), then ($R = -1500:1500$), then ($R = 0:1500$), and so on, until a solution is found. For this particular example, a solution is found when initialising the interaction parameters over the range ($R = 0:1500$). Note that for all calculations, ($S = 10$) and ($\alpha = 3$).

For this system, Figure 6.13 shows the evolution of the (a_{ji}) values when calculating the ($\overline{a_0}$) set. All the interaction parameters reach a constant value as the stages proceed to completion at stage 8 where ($dS_8 = 1$). When the ($\overline{a_0}$) set (obtained at stage 8) is substituted into a minimiser, after several iterations, the interaction parameters provided in Table 6.5 are obtained.

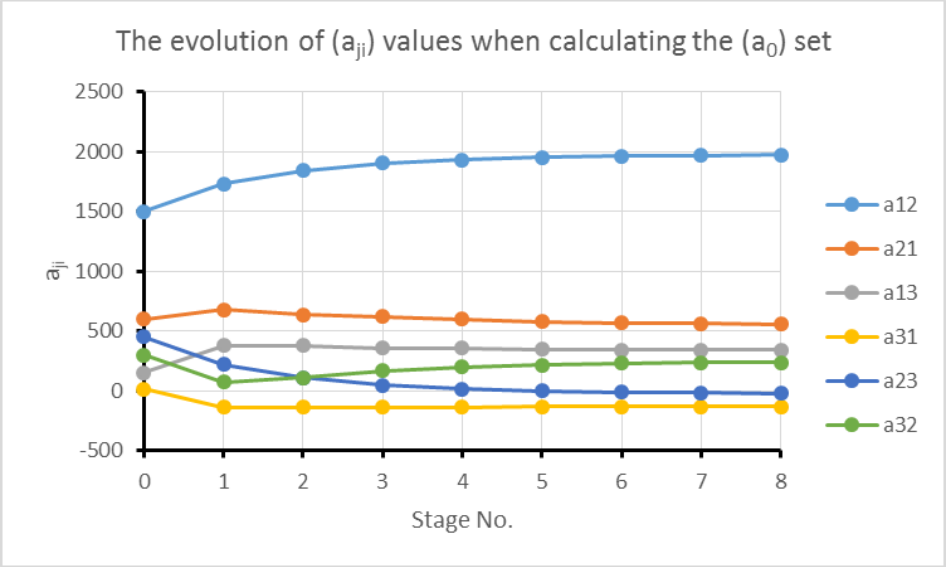

Figure 6.13: The evolution of the (a_{ji}) values when calculating the ($\overline{a_0}$) set.

Table 6.5: The calculated interaction parameters ($\overline{a}$).

T (ºC)	a_{12}	a_{21}	a_{13}	a_{31}	a_{23}	a_{32}
35.0	1602.1716	577.3584	372.3666	-142.8891	-100.9486	418.8297

Figure 6.14 shows the evolution of the (a_{ji}) values when calculating the ($\overline{a}$) set. Most of the (a_{ji}) values remain close to the values in the ($\overline{a_0}$) set. The only value that changes significantly is (a_{12}). However, it converges very quickly after 8 iterations. For this analysis, the region of trust defined around the ($\overline{a_0}$) set values is ±50 when performing the detailed minimisation. Almost instant convergence can be obtained if this is increased up to ±500, without sacrificing the ability to find a solution. The analysis was done at ±50 to illustrate the convergence only.

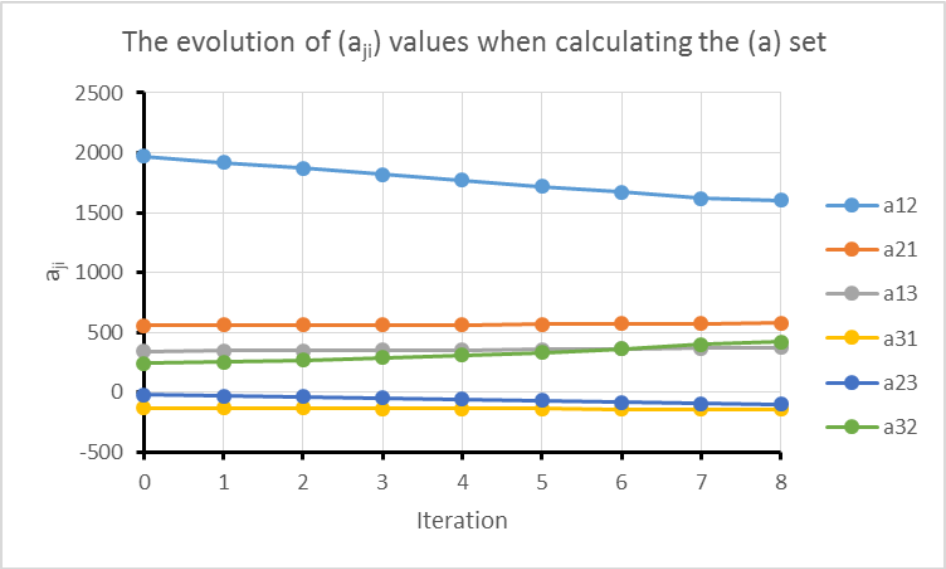

Figure 6.14: The evolution of the (a_{ji}) values when calculating the ($\overline{a}$) set.

The working example provided in section 6.2.5 (Nitromethane + Ethylene Glycol + Lauryl Alcohol at 298 K) represents an ideal case for comparing the interaction parameters provided in the literature with ones calculated using the method described in section 6.3.2. The three-phase compositions for this system are provided in Table 6.6.

Table 6.6: Experimental three-phase compositions for Nitromethane + Ethylene Glycol + Lauryl Alcohol at 298 K and 1 atm (Sørensen and Arlt, 1980; Reddy and Rani, 2012).

Phase	Mass Fractions		
	NM	MEG	LA
NM-Rich	0.8956	0.0986	0.0058
MEG-Rich	0.0359	0.9572	0.0069
LA-Rich	0.1620	0.2209	0.6171

As with the pervious system, a solution is found over the range ($R = 0{:}\,1500; S = 10; \alpha = 3$). Calculation of ($\overline{a_0}$) and ($\overline{a}$), gives the ($a_{ji}$) evolution plots shown in Figure 6.15 and Figure 6.16 respectively (N.B. uncertainty was set at ±20 in calculations post-initialisation for illustration purposes).

The calculated interaction parameters set ($\overline{a}$) is compared with the set found in the literature in Table 6.7 and both sets are in reasonable agreement. It gives a slightly lower value for the Gibbs energy (by less than 0.01%), indicating a marginal improvement on the published data and the reliability of the method used for the calculation.

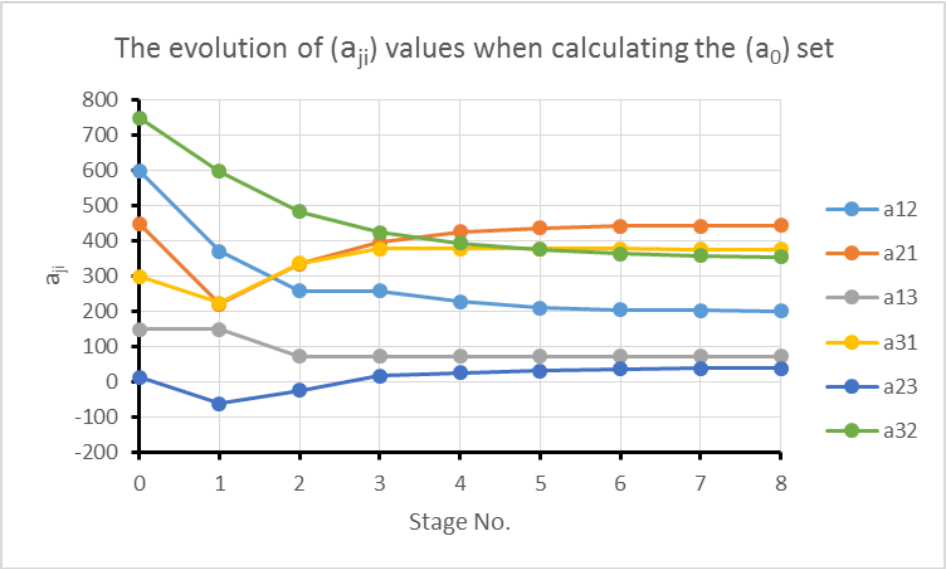

Figure 6.15: The evolution of the (a_{ji}) values when calculating the ($\overline{a_0}$) set.

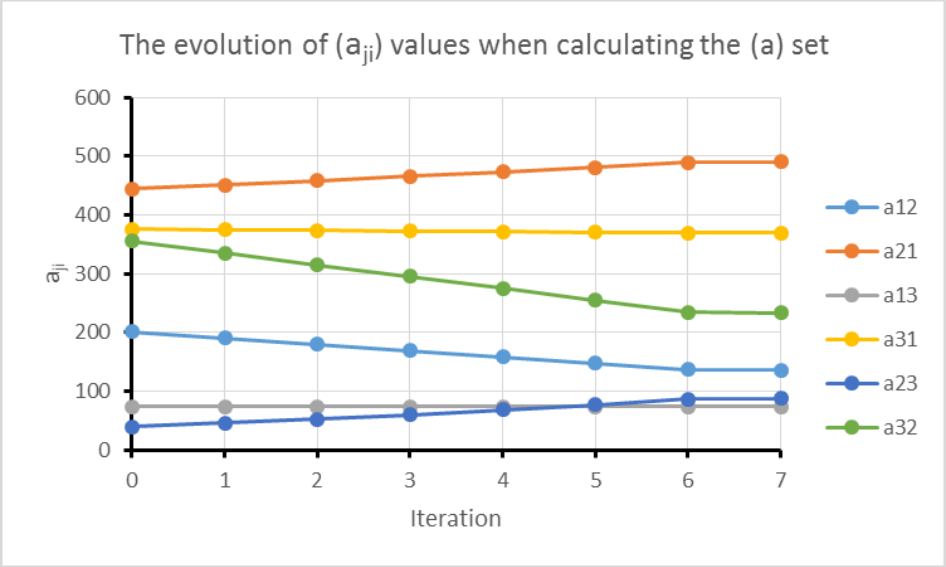

Figure 6.16: The evolution of the (a_{ji}) values when calculating the ($\overline{a}$) set.

Table 6.7: The published vs. the calculated interaction parameters ($\overline{a}$) for Nitromethane + Ethylene Glycol + Lauryl alcohol at 298 K (Sørensen and Arlt, 1980; Reddy and Rani, 2012).

Values	a_{12}	a_{21}	a_{13}	a_{31}	a_{23}	a_{32}
Published	136.1600	490.6643	73.4424	369.6880	87.5541	233.2511
Calculated	136.0892	490.8475	73.5016	369.5845	87.7850	233.0373

As a point of interest, when opting for a finer initialisation of the interaction parameters (e.g. $R = 0{:}\,1500$; $S = 10$; $\alpha = 7$), the calculated ($\overline{a_0}$) set is given in Table 6.8. This is much closer to the solution shown in Table 6.7 than the initialisation at ($R = 0{:}\,1500$; $S = 10$; $\alpha = 3$). However, the coarse grid over several ranges takes few seconds to run, while

the finer and significantly more accurate grid takes several hours to run. Both converge to the same solution for ($\overline{a}$) indicating that **excessive** precision in determining ($\overline{a_0}$) is computationally expensive and is not beneficial for the purposes of obtained a reasonable estimation.

It is noted that the proximity of the solution in Table 6.8 for the finer grid to the final solution illustrates the reliability of the method developed for this work described in section 6.3.2 in effectively initialising the interaction parameters' calculation.

Table 6.8: The initial ($\overline{a_0}$) for a coarse grid vs. a finer grid.

a_0 at	a_{12}	a_{21}	a_{13}	a_{31}	a_{23}	a_{32}
$R = +1500$, $S = 10$, $\alpha = 3$	201	444	74	376	40	355
$R = +1500$, $S = 10$, $\alpha = 7$	136	491	74	369	88	233

6.4.2. Literature Data: Dodecane + Water + EGMBE

The UNIQUAC parameters for this system are provided in Table 6.4. The three-phase data required for calculating the interaction parameters were obtained from Lin and Chen (2002) at various temperatures. A summary of the three-phase data is provided in Table 6.9.

Table 6.9: Experimental three-phase compositions for Dodecane + Water + EGMBE between 35-65ºC (Lin and Chen, 2002).

T	Mass Fractions								
	Oil-Rich			Water-Rich			EGMBE-Rich		
˚C	n-C_{12}	Water	EGMBE	n-C_{12}	Water	EGMBE	n-C_{12}	Water	EGMBE
35.0	0.9130	0.0021	0.0849	0.0001	0.8470	0.1529	0.0336	0.4697	0.4967
40.0	0.8961	0.0026	0.1013	0.0001	0.8872	0.1127	0.0532	0.3730	0.5738
45.0	0.8815	0.0034	0.1151	0.0001	0.8996	0.1003	0.0587	0.3356	0.6057
50.0	0.8528	0.0055	0.1417	0.0001	0.9101	0.0898	0.0704	0.3008	0.6288
55.0	0.8138	0.0091	0.1771	0.0001	0.9169	0.0830	0.0945	0.2596	0.6459
60.0	0.7858	0.0105	0.2037	0.0001	0.9220	0.0779	0.1258	0.2238	0.6504
65.0	0.7278	0.0179	0.2543	0.0001	0.9258	0.0741	0.1509	0.1995	0.6496

The interaction parameters set ($\overline{a}$) calculated for this system at 35˚C – as illustrated in section 6.3.2 – can be used as initial values for calculating the interaction parameters for the same system at the other temperatures listed in Table 6.9. That is, there is no need to repeat the procedure described in section 6.3.2 every time the interaction parameters are

calculated for **the same system**, and minimisation using a robust standard minimiser (e.g. **fmincon** in MATLAB) can be achieved without difficulties. The calculated interaction parameters at all temperatures, with reference to the three-phase compositions in Table 6.9 and using the interaction parameters in Table 6.5 as initial values, are provided in Table 6.10.

Table 6.10: The calculated interaction parameters ($\overline{a}$) for the systems in Table 6.9.

T (°C)	a_{12}	a_{21}	a_{13}	a_{31}	a_{23}	a_{32}
$\overline{a}$ **for** $T = 35$℃, $\overline{a_0}$ **for** $T > 35$℃						
35.0	1602.1716	577.3584	372.3666	-142.8891	-100.9486	418.8297
$\overline{a}$ **for** $T > 35$℃						
40.0	1636.4363	274.1227	321.1460	-110.7691	-118.2594	527.5621
45.0	1572.8996	225.0964	296.7747	-95.2257	-122.3973	569.7082
50.0	1466.0672	195.1649	276.1081	-85.3163	-124.4076	591.0557
55.0	1362.4030	181.9294	266.3382	-83.6272	-126.5767	603.3932
60.0	1424.1176	173.8132	273.0588	-91.1096	-128.5416	608.5667
65.0	1296.3048	166.6937	256.5096	-84.3699	-130.1278	617.9040

Full experimental phase envelope data for Dodecane + Water + EGMBE are available in the paper by Lin and Chen (2002) at 35˚C and 45˚C. Using the interaction parameters in Table 6.10, phase envelopes were calculated for this system at these two temperatures and compared with the experimental data. A good match between the experimental and the calculated tie-lines was observed in both cases (Figure 6.17 and Figure 6.18 respectively).

The errors are fully compared in Table 6.11 and Table 6.12 for both systems, respectively. The errors vary widely, but overall most of the errors are small for both systems (around or well below 2%). The largest errors occur in the alkane/mutual solvent two-phase region where the model has a tendency to overestimate the composition of the mutual solvent-rich phase. In both Table 6.11 and Table 6.12, the three-phase data are calculated perfectly as expected. This will always be the case because the interaction parameters set ($\overline{a}$) are calculated based on these compositions.

For the remaining temperatures in Table 6.10, full experimental phase envelope data are not available for comparison purposes. However, the phase envelopes are produced using the model to demonstrate model functionality. The results are provided in Figure 6.19, Figure 6.20, Figure 6.21, Figure 6.22 and Figure 6.23 for the temperatures 40˚C, 50˚C, 55˚C, 60˚C and 65˚C respectively.

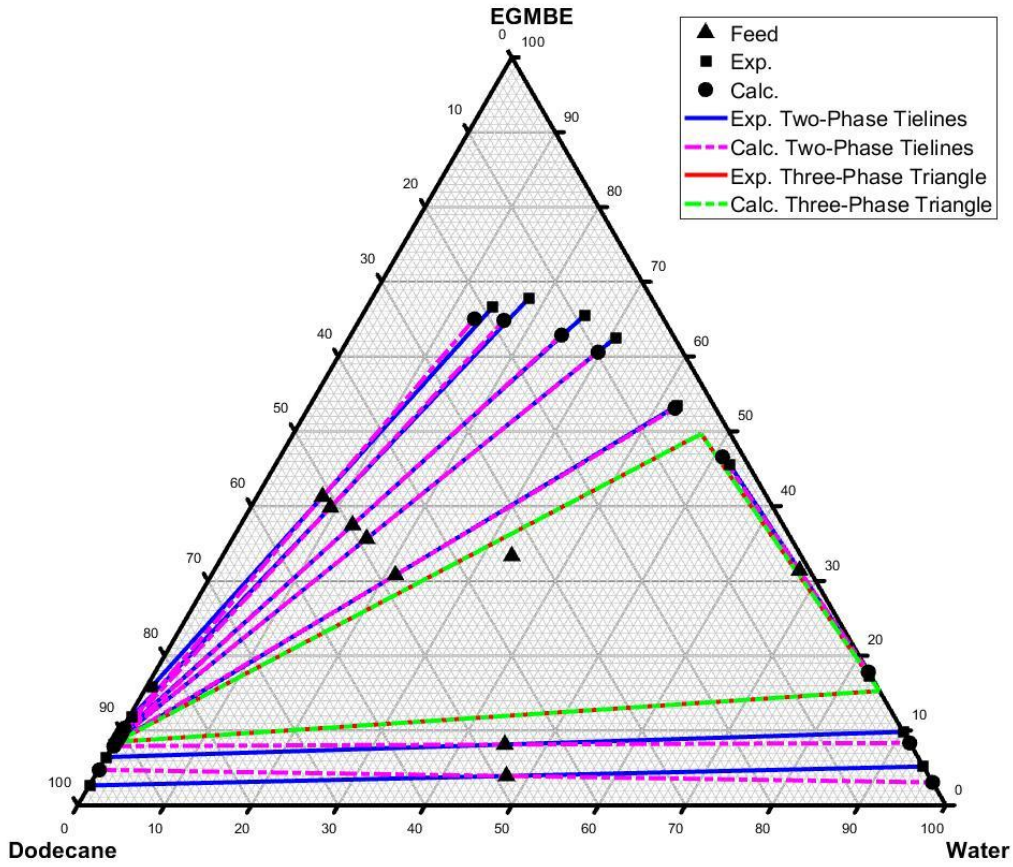

Figure 6.17: Experimental vs. calculated phase envelope for Dodecane + Water + EGMBE at 35˚C.

Table 6.11: The absolute differences between the experimental and the calculated tie-lines for the system Dodecane + Water + EGMBE at 35˚C.

Absolute Difference Between Experimental and Calculated Data								
Dodecane-Rich			**Water-Rich**			**EGMBE-Rich**		
n-C_{12}	**Water**	**EGMBE**	**n-C_{12}**	**Water**	**EGMBE**	**n-C_{12}**	**Water**	**EGMBE**
Three-Phase Region								
0.0000	0.0000	0.0000	0.0000	0.0000	0.0000	0.0000	0.0000	0.0000
AB Two-Phase Region								
0.0215	-0.0007	-0.0208	0.0000	-0.0212	0.0212			
0.0160	-0.0012	-0.0148	0.0000	-0.0148	0.0148			
AC Two-Phase Region								
0.0049	-0.0011	-0.0038				-0.0038	0.0005	0.0033
0.0012	-0.0002	-0.0011				-0.0299	0.0105	0.0194
-0.0022	-0.0002	0.0024				-0.0401	0.0133	0.0268
-0.0210	0.0008	0.0202				-0.0440	0.0141	0.0299
-0.0599	0.0038	0.0561				-0.0294	0.0133	0.0161
BC Two-Phase Region								
			0.0017	0.0037	-0.0054	-0.0030	0.0137	-0.0107

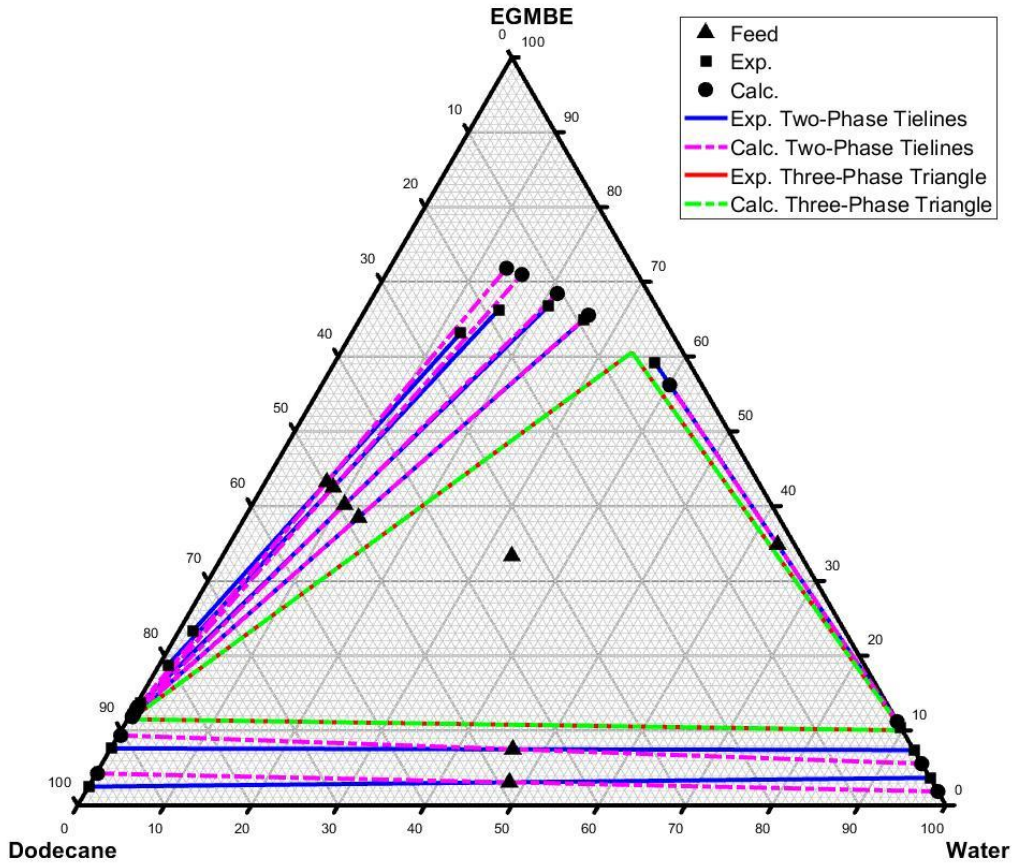

Figure 6.18: Experimental vs. calculated phase envelope for Dodecane + Water + EGMBE at 45˚C.

Table 6.12: The absolute differences between the experimental and the calculated tie-lines for the system Dodecane + Water + EGMBE at 45˚C.

Absolute Difference Between Experimental and Calculated Data								
Dodecane-Rich			Water-Rich			EGMBE-Rich		
n-C_{12}	Water	EGMBE	n-C_{12}	Water	EGMBE	n-C_{12}	Water	EGMBE
Three-Phase Region								
0.0000	0.0000	0.0000	0.0000	0.0000	0.0000	0.0000	0.0000	0.0000
AB Two-Phase Region								
0.0189	-0.0014	-0.0175	0.0000	-0.0182	0.0182			
0.0189	-0.0012	-0.0177	0.0000	-0.0182	0.0182			
AC Two-Phase Region								
-0.0023	0.0003	0.0020				0.0084	-0.0023	-0.0062
-0.0152	0.0011	0.0141				0.0184	-0.0019	-0.0164
-0.0659	0.0066	0.0593				0.0502	-0.0033	-0.0469
-0.1139	0.0128	0.1011				0.0958	-0.0095	-0.0863
BC Two-Phase Region								
			-0.0001	0.0076	-0.0074	0.0020	-0.0322	0.0302

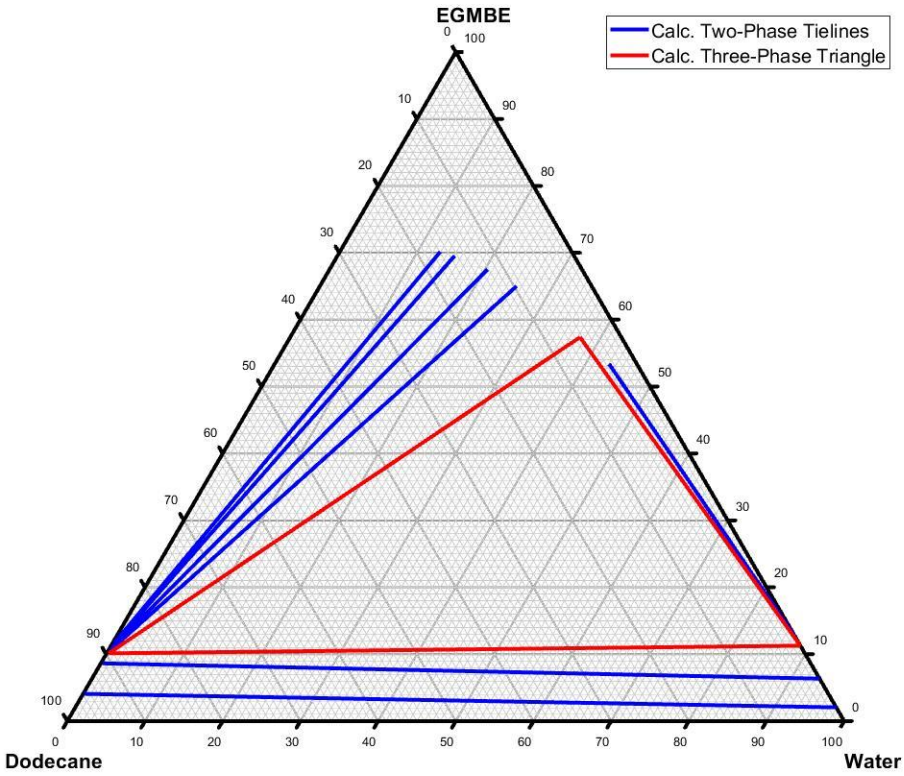

Figure 6.19: Calculated phase envelope for Dodecane + Water + EGMBE at 40˚C.

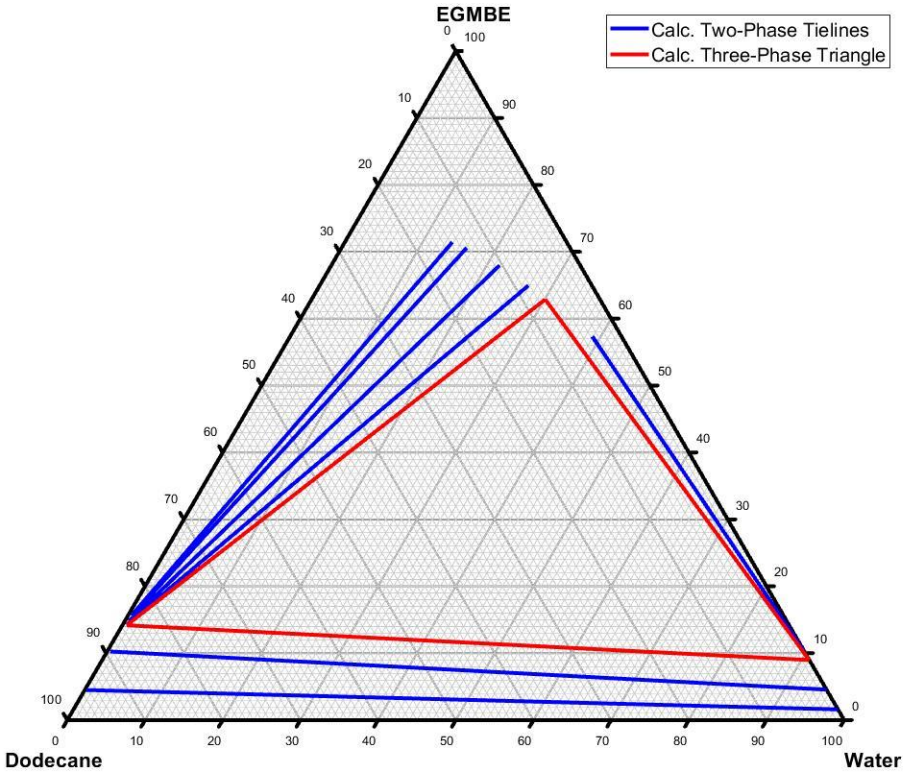

Figure 6.20: Calculated phase envelope for Dodecane + Water + EGMBE at 50˚C.

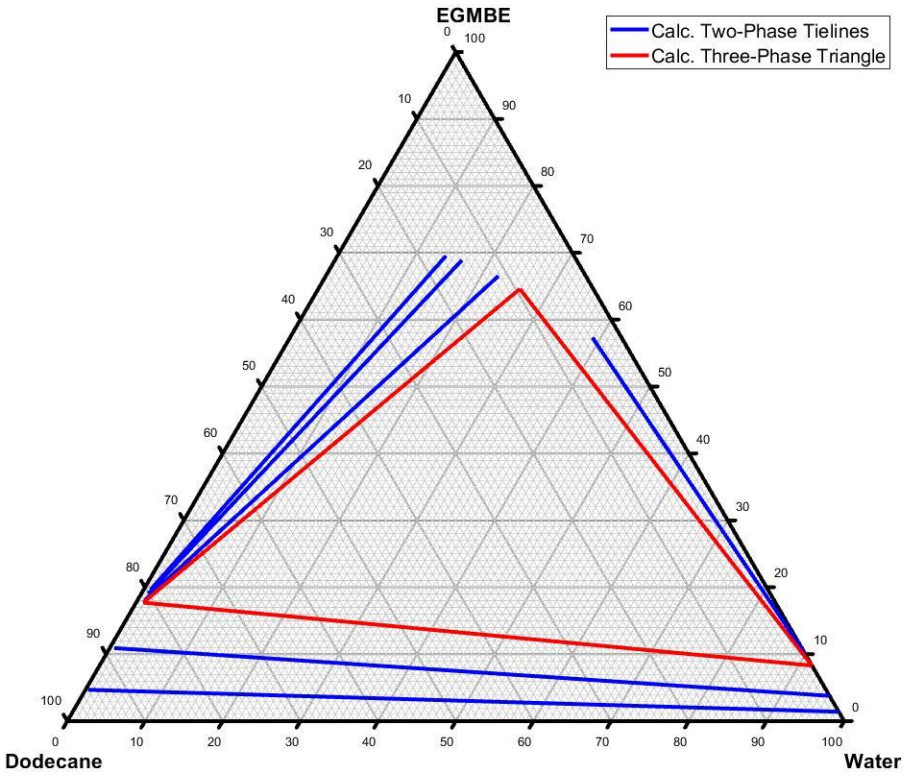

Figure 6.21: Calculated phase envelope for Dodecane + Water + EGMBE at 55˚C.

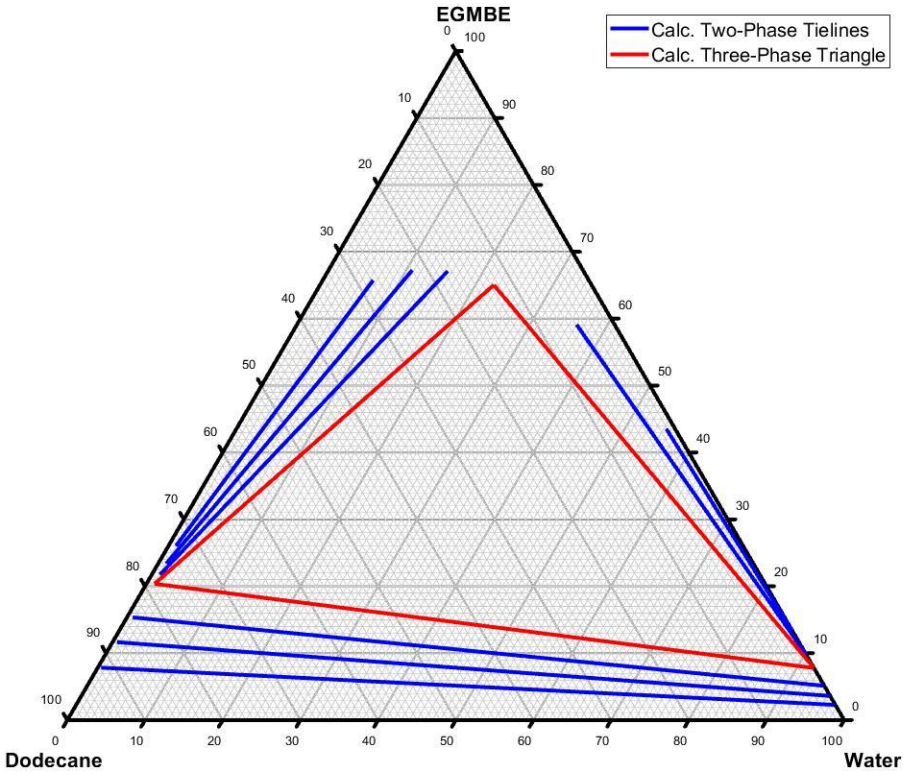

Figure 6.22: Calculated phase envelope for Dodecane + Water + EGMBE at 60˚C.

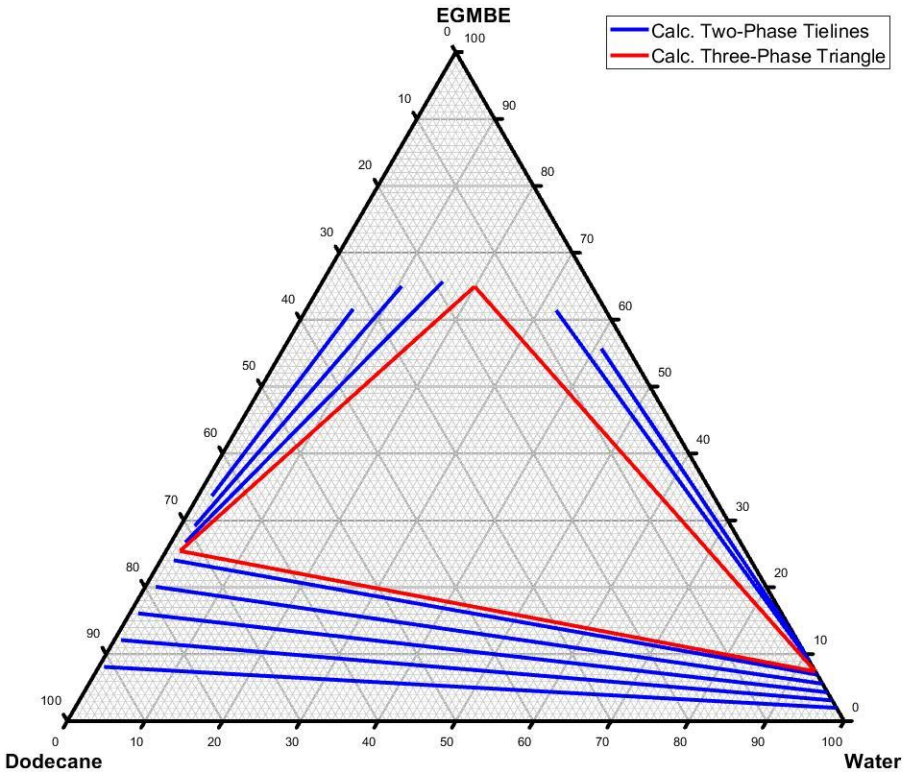

Figure 6.23: Calculated phase envelope for Dodecane + Water + EGMBE at 65˚C.

6.4.3. Experimental Data: Quasi-Ternary Systems

The systems implemented (Table 5.7) in this investigation are the same systems discussed in Chapter 4 and Chapter 5. These systems were mapped semi-empirically using the Phase Displacement Method (PDM). The results from the UNIQUAC model for these systems is compared with the results from the PDM in this section.

Table 6.13: Quasi-ternary systems investigated using the UNIQUAC model (22.5℃ and 1 atm).

System	Designation	Highlight
Multipar H/NSSW/EGMBE	System A	Low salinity (~36,000 ppm)
Multipar H/MGFW/DGBE	System B	High salinity (~264,000 ppm)
Multipar H/(NSSW+5% active DETPMP)/EGMBE	System C	Phosphonate scale inhibitor
Multipar H/(NSSW+5% active PPCA)/EGMBE	System D	Polymeric scale inhibitor
Multipar H/NSSW/(80:20% v/v EGMBE:MEG)	System E	Mutual solvent blend
Medium Crude Oil/NSSW/EGMBE	System F	Crude system

The three-phase compositions calculated for these systems in Chapter 4 (provided in Table 6.14) were used to initialise and calculate the interaction parameters for the systems. The results are provided in Table 6.15.

Table 6.14: Experimental three-phase compositions for the systems listed in Table 5.7.

System	Mass Fractions								
	Oil-Rich			Brine-Rich			Mutual Solvent-Rich		
#	Oil	Brine	MS	Oil	Brine	MS	Oil	Brine	MS
A	0.8932	0.0084	0.0984	0.0000	0.9039	0.0961	0.1979	0.1932	0.6089
B	0.9482	0.0041	0.0476	0.0000	0.9851	0.0149	0.1729	0.1280	0.6991
C	0.8296	0.0088	0.1616	0.0119	0.9342	0.0538	0.2957	0.1264	0.5779
D	0.8807	0.0000	0.1193	0.0000	0.9351	0.0649	0.2261	0.1739	0.6000
E	0.9050	0.0045	0.0904	0.0110	0.8206	0.1684	0.1016	0.1795	0.7189
F	0.9015	0.0000	0.0985	0.0014	0.9075	0.0911	0.0699	0.2789	0.6512

Table 6.15: The calculated interaction parameters ($\overline{a}$) for the systems in Table 6.14.

System	a_{12}	a_{21}	a_{13}	a_{31}	a_{23}	a_{32}
A	1059.6661	251.6037	361.6055	-138.3794	-124.4468	530.1998
B	1295.1035	42.0164	287.4828	-98.7286	-115.3487	709.4147
C	1717.3851	-122.4595	296.7677	-105.0897	-114.1710	731.2749
D	3754.7796	142.9926	344.8622	-134.0827	-115.8924	522.29
E	1445.3011	-52.2872	264.8747	-64.1343	-130.0179	756.3174
F	2889.1791	1.0936	248.2212	-58.6874	-121.8854	650.6492

Subject to the interaction parameters in Table 6.15, the results from the UNIQUAC are compared with the results from the PDM in Figure 6.24, Figure 6.25, Figure 6.26, Figure 6.27, Figure 6.28, Figure 6.29 and Figure 6.30 for System A (standard initialisation), System A (alternative initialisation), System B, System C, System D, System E and System F respectively. The absolute differences between the PDM and the UNIQUAC results are provided in Table 6.16, Table 6.17, Table 6.18, Table 6.19, Table 6.20, Table 6.21 and Table 6.22 respectively.

With System A, the standard initialisation described in section 6.3.4 fails to capture the results in the oil/mutual solvent region of the phase diagram. As discussed in Chapter 5 section 5.4.2, the tie-lines obtained in this region are unlikely to be physical (Figure 6.24), and are more likely to be the case due to experimental limitations. Therefore, the standard initialisation gives a very poor match in this region with the PDM results (Figure 6.24; Table 6.16). However, for the purposes of matching the results of the PDM using the UNIQUAC, an alternative initialisation may be applied, dictating that the lower phase must always be brine-rich. When this is performed, an excellent match between the PDM and the UNIQUAC is obtained (Figure 6.25; Table 6.17). The maximum absolute difference between the results obtained from the two methods is less than 4%.

Overall, an excellent match is observed for all the quasi-ternary systems listed in Table 6.14. The errors vary widely, but are generally low, and the tie-lines calculated are generally in very good agreement. It is unknown whether if the quality of results from the UNIQUAC is higher than those obtained from the PDM due to the semi-empirical nature of the PDM. However, the good agreement between the UNIQUAC and the PDM indicates the ability to use both for the purposes of describing the phase envelopes of quasi-ternary oil/brine/mutual solvent systems.

The ability of the UNIQUAC model to capture these phase envelopes of quasi-ternary systems very well provide enormous opportunities to predict/extrapolate the entire phase envelope from the three-phase compositions. These predictions require inexpensive and readily available three-phase experimental data, which can be obtained as described in Chapter 4. The calculation of the interaction parameters is then possible with ease, and the UNIQUAC model can be applied successfully. The PDM on the other hand requires more phase separation data in the two-phase region to map out the phase diagram as described in Chapter 5. This makes the use of the UNIQUAC model favourable. The UNIQUAC model may even be more favourable than the expensive GC-FID analytical approach described in Chapter 7, which offers additional precision unnecessary for most transport applications. A further discussion of this will be provided in Chapter 7.

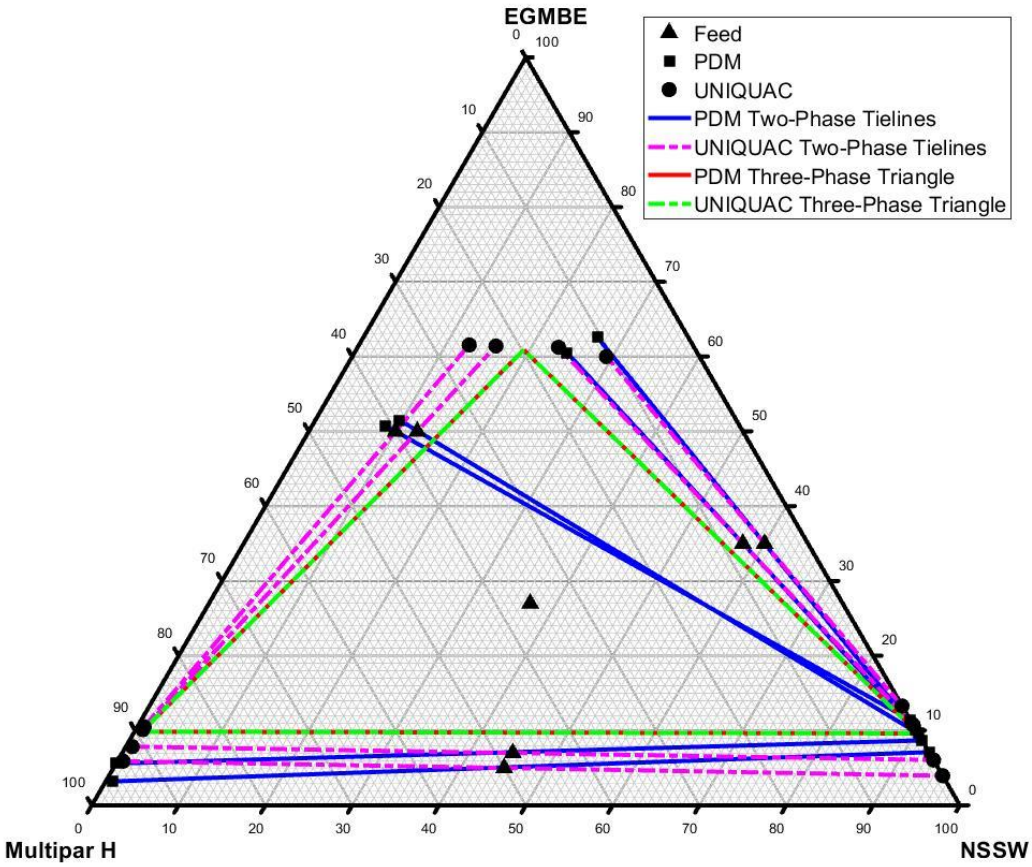

Figure 6.24: PDM vs. UNIQUAC phase envelope for System A (standard UNIQUAC initialisation).

Table 6.16: The absolute differences between the semi-empirical (PDM) and the calculated (UNIQUAC) tie-lines for the system Multipar H + NSSW + EGMBE at 22.5˚C.

Absolute Difference Between Experimental and Calculated Data								
Multipar H-Rich			NSSW-Rich			EGMBE-Rich		
MH	NSSW	EGMBE	MH	NSSW	EGMBE	MH	NSSW	EGMBE
Three-Phase Region								
0.0000	0.0000	0.0000	-0.0001	0.0001	0.0000	0.0000	0.0000	0.0000
AB Two-Phase Region								
0.0251	0.0020	-0.0271	0.0000	-0.0316	0.0316			
0.0300	-0.0074	-0.0226	0.0000	-0.0262	0.0262			
AC Two-Phase Region								
-0.4794	0.0770	0.4025				-0.2574	0.7589	-0.5015
-0.5027	0.0890	0.4137				-0.2274	0.7454	-0.5181
BC Two-Phase Region								
			0.0002	0.0322	-0.0324	-0.0025	-0.0233	0.0258
			-0.0001	0.0120	-0.0118	-0.0061	0.0133	-0.0071

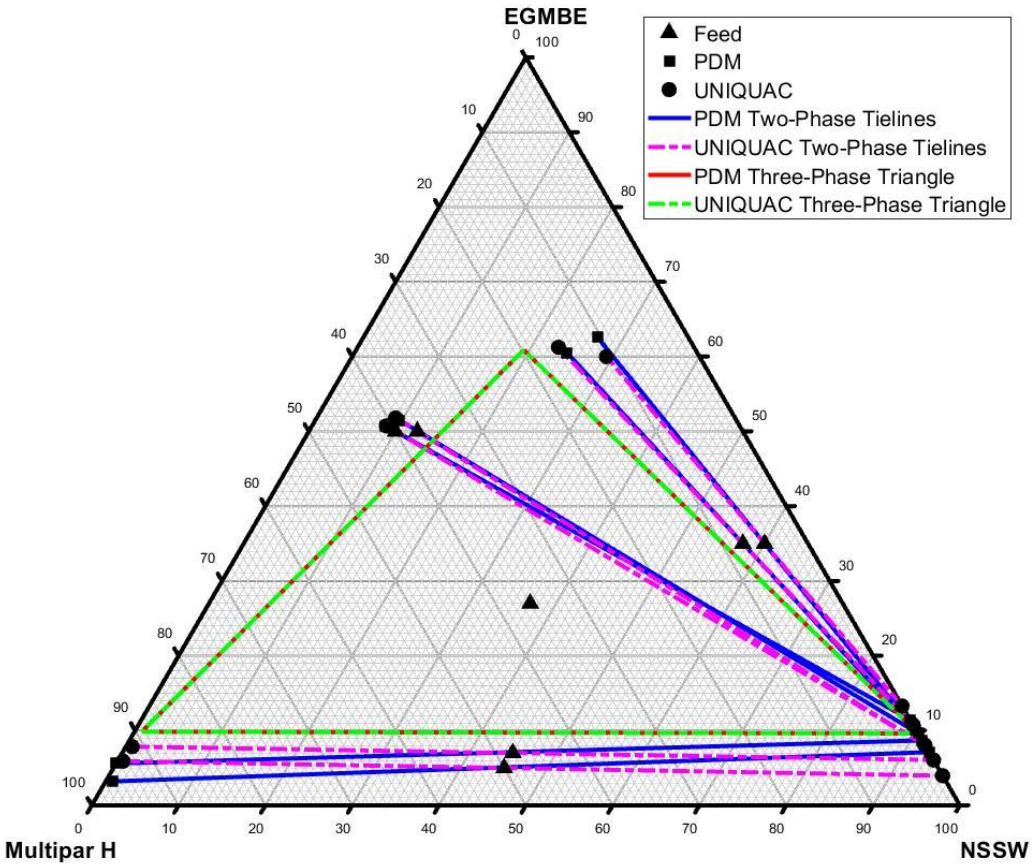

Figure 6.25: PDM vs. UNIQUAC phase envelope for System A (alternative UNIQUAC initialisation).

Table 6.17: The absolute differences between the semi-empirical (PDM) and the calculated (UNIQUAC) tie-lines for the system Multipar H + NSSW + EGMBE at 22.5˚C.

Absolute Difference Between Experimental and Calculated Data								
Multipar H-Rich			NSSW-Rich			EGMBE-Rich		
MH	NSSW	EGMBE	MH	NSSW	EGMBE	MH	NSSW	EGMBE
Three-Phase Region								
0.0000	0.0000	0.0000	-0.0001	0.0001	0.0000	0.0000	0.0000	0.0000
AB Two-Phase Region								
0.0251	0.0020	-0.0271	0.0000	-0.0316	0.0316			
0.0300	-0.0074	-0.0226	0.0000	-0.0262	0.0262			
AC Two-Phase Region								
0.0007	-0.0008	0.0001				-0.0001	-0.0334	0.0335
-0.0032	0.0063	-0.0030				-0.0001	-0.0159	0.0159
BC Two-Phase Region								
			0.0002	0.0322	-0.0324	-0.0025	-0.0233	0.0258
			-0.0001	0.0120	-0.0118	-0.0061	0.0133	-0.0071

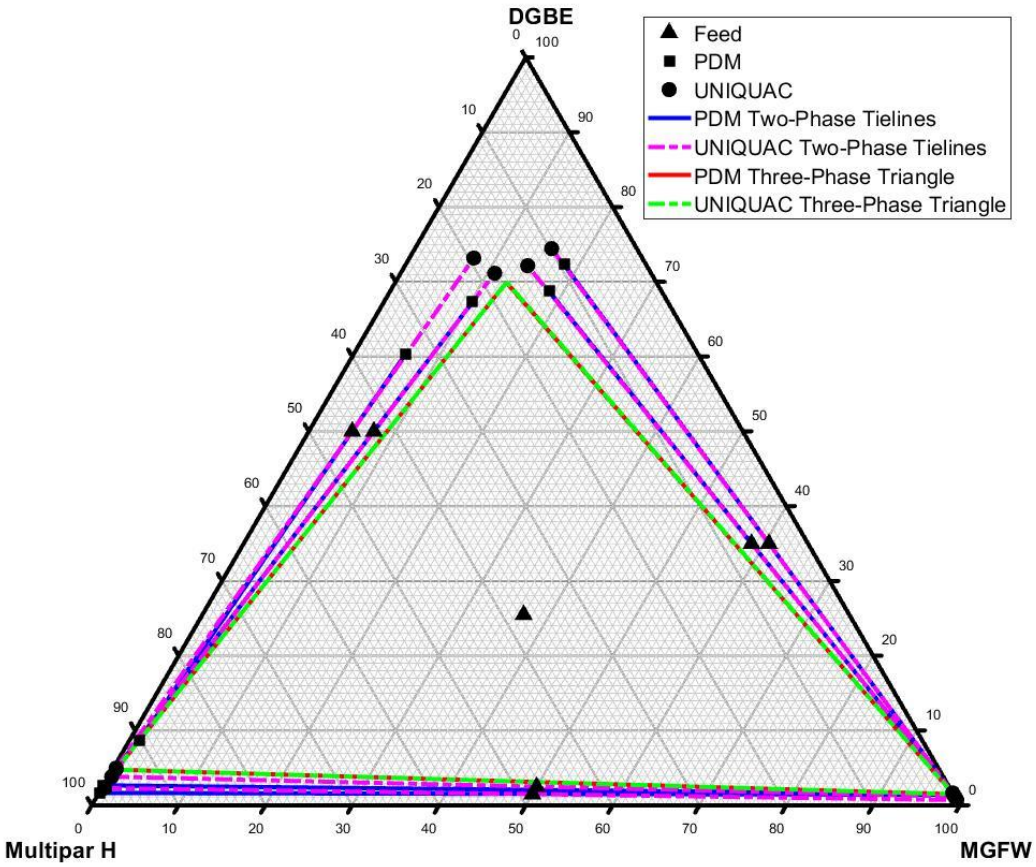

Figure 6.26: PDM vs. UNIQUAC phase envelope for System B.

Table 6.18: The absolute differences between the semi-empirical (PDM) and the calculated (UNIQUAC) tie-lines for the system Multipar H + MGFW + DGBE at 22.5˚C.

Absolute Difference Between Experimental and Calculated Data								
Multipar H-Rich			MGFW-Rich			DGBE-Rich		
MH	MGFW	DGBE	MH	MGFW	DGBE	MH	MGFW	DGBE
Three-Phase Region								
-0.0001	0.0000	0.0000	-0.0001	0.0001	0.0000	0.0006	-0.0001	-0.0005
AB Two-Phase Region								
0.0086	-0.0021	-0.0065	-0.0001	-0.0070	0.0070			
0.0155	-0.0038	-0.0117	-0.0001	-0.0029	0.0030			
AC Two-Phase Region								
-0.0454	0.0084	0.0370				0.1430	-0.0145	-0.1285
0.0011	-0.0004	-0.0007				0.0447	-0.0062	-0.0385
BC Two-Phase Region								
			0.0002	0.0015	-0.0016	-0.0037	0.0248	-0.0211
			0.0002	0.0005	-0.0007	-0.0074	0.0415	-0.0342

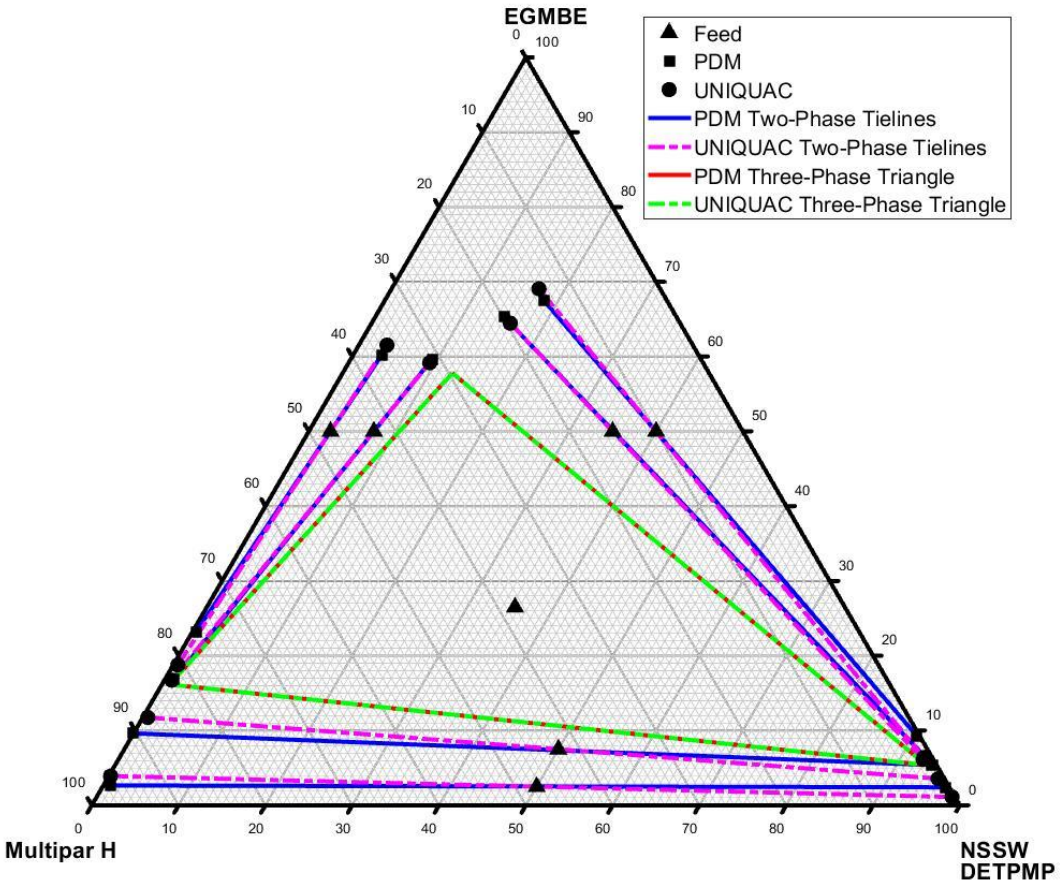

Figure 6.27: PDM vs. UNIQUAC phase envelope for System C.

Table 6.19: The absolute differences between the semi-empirical (PDM) and the calculated (UNIQUAC) tie-lines for the system Multipar H + (NSSW+DETPMP) + EGMBE at 22.5˚C.

Absolute Difference Between Experimental and Calculated Data								
Multipar H-Rich			NSSW-Rich			EGMBE-Rich		
MH	NSSW+SI	EGMBE	MH	NSSW+SI	EGMBE	MH	NSSW+SI	EGMBE
Three-Phase Region								
0.0000	0.0000	0.0000	0.0000	-0.0001	0.0000	0.0000	0.0000	0.0000
AB Two-Phase Region								
0.0061	0.0067	-0.0128	0.0005	-0.0134	0.0129			
0.0271	-0.0057	-0.0213	-0.0013	-0.0168	0.0182			
AC Two-Phase Region								
-0.0427	-0.0012	0.0439				0.0130	0.0006	-0.0137
-0.0027	0.0021	0.0006				-0.0051	0.0004	0.0047
BC Two-Phase Region								
			-0.0064	-0.0223	0.0287	0.0019	0.0142	-0.0161
			-0.0075	0.0150	-0.0075	0.0030	-0.0113	0.0083

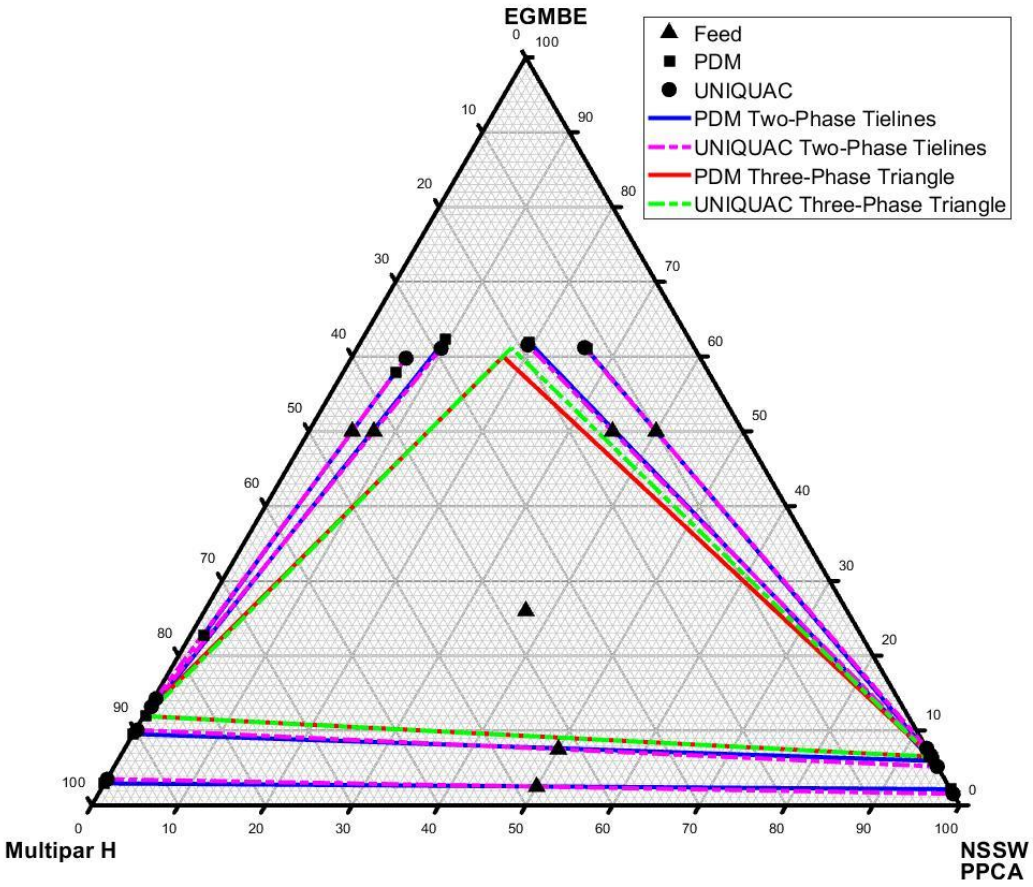

Figure 6.28: PDM vs. UNIQUAC phase envelope for System D.

Table 6.20: The absolute differences between the semi-empirical (PDM) and the calculated (UNIQUAC) tie-lines for the system Multipar H + (NSSW+PPCA) + EGMBE at 22.5˚C.

Absolute Difference Between Experimental and Calculated Data								
Multipar H-Rich			NSSW-Rich			EGMBE-Rich		
MH	NSSW+SI	EGMBE	MH	NSSW+SI	EGMBE	MH	NSSW+SI	EGMBE
Three-Phase Region								
0.0023	-0.0026	0.0003	-0.0001	0.0001	0.0000	0.0152	-0.0035	-0.0117
AB Two-Phase Region								
0.0059	-0.0003	-0.0056	0.0000	-0.0061	0.0061			
0.0073	-0.0019	-0.0053	-0.0001	-0.0073	0.0074			
AC Two-Phase Region								
-0.0969	0.0121	0.0848				0.0215	-0.0028	-0.0188
0.0127	0.0001	-0.0128				-0.0111	-0.0009	0.0120
BC Two-Phase Region								
			-0.0001	0.0116	-0.0115	-0.0014	0.0036	-0.0022
			0.0028	-0.0007	-0.0021	-0.0032	-0.0009	0.0042

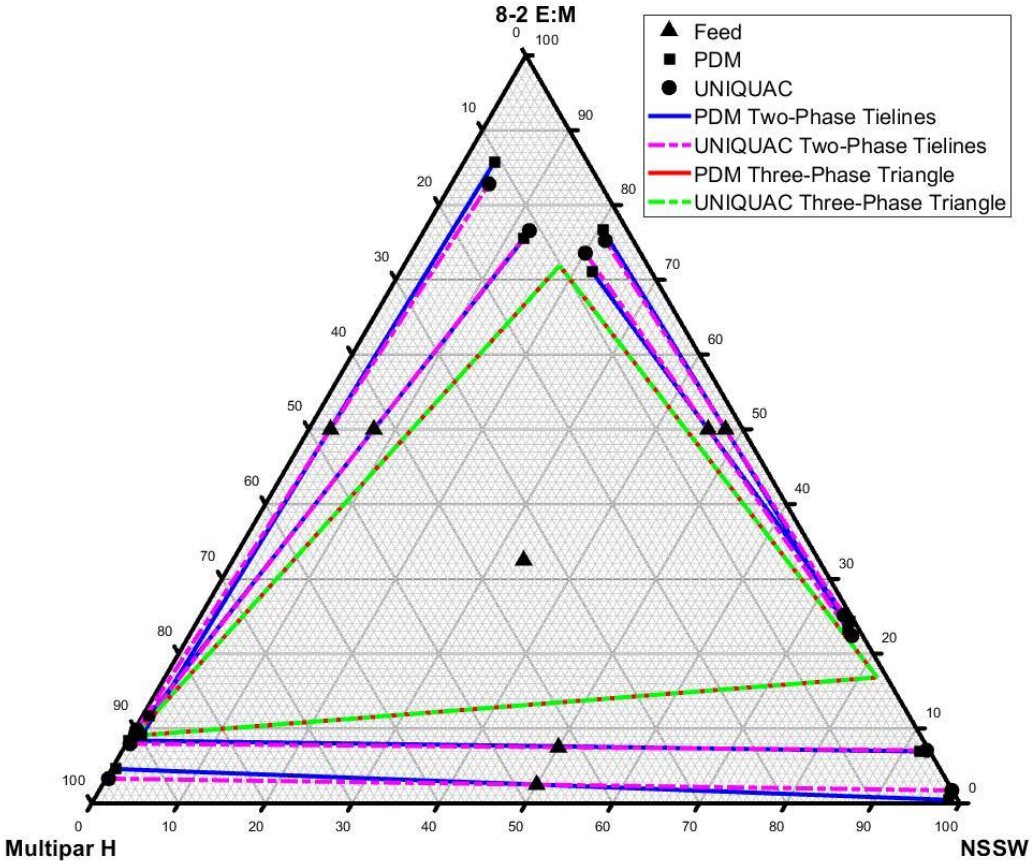

Figure 6.29: PDM vs. UNIQUAC phase envelope for System E.

Table 6.21: The absolute differences between the semi-empirical (PDM) and the calculated (UNIQUAC) tie-lines for the system Multipar H + NSSW + (8-2 E:M) at 22.5°C.

Absolute Difference Between Experimental and Calculated Data								
Multipar H-Rich			NSSW-Rich			Mutual Solvent-Rich		
MH	NSSW	MS	MH	NSSW	MS	MH	NSSW	MS
Three-Phase Region								
-0.0001	0.0000	0.0000	0.0000	0.0000	0.0000	0.0000	0.0000	0.0000
AB Two-Phase Region								
-0.0146	0.0017	0.0129	0.0102	0.0024	-0.0126			
-0.0001	-0.0042	0.0043	0.0081	-0.0067	-0.0014			
AC Two-Phase Region								
-0.0020	0.0098	-0.0078				-0.0210	-0.0083	0.0292
-0.0282	0.0032	0.0250				0.0119	-0.0011	-0.0108
BC Two-Phase Region								
			-0.0069	-0.0117	0.0186	0.0046	0.0207	-0.0253
			0.0042	0.0145	-0.0188	-0.0044	-0.0104	0.0149

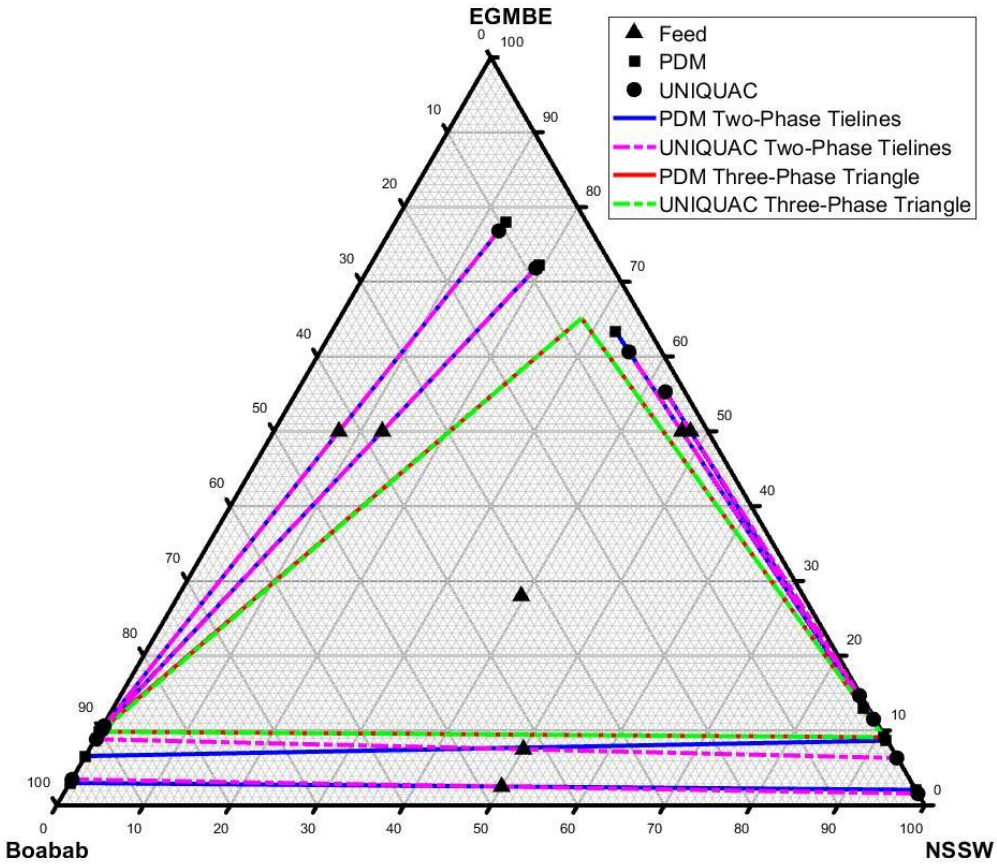

Figure 6.30: PDM vs. UNIQUAC phase envelope for System F.

Table 6.22: The absolute differences between the semi-empirical (PDM) and the calculated (UNIQUAC) tie-lines for the system Boabab + NSSW + EGMBE at 22.5°C.

Absolute Difference Between Experimental and Calculated Data								
Boabab-Rich			NSSW-Rich			EGMBE-Rich		
Oil	Water	EGMBE	Oil	Water	EGMBE	Oil	Water	EGMBE
Three-Phase Region								
0.0015	-0.0016	0.0001	0.0000	0.0000	0.0000	0.0000	0.0000	0.0000
AB Two-Phase Region								
0.0050	-0.0003	-0.0047	-0.0002	-0.0048	0.0050			
0.0240	-0.0013	-0.0226	0.0006	-0.0238	0.0232			
AC Two-Phase Region								
0.0094	-0.0015	-0.0079				-0.0141	0.0022	0.0119
0.0046	-0.0016	-0.0030				-0.0062	0.0017	0.0045
BC Two-Phase Region								
			-0.0002	0.0242	-0.0240	0.0015	-0.0290	0.0275
			0.0041	0.0133	-0.0174	-0.0007	0.0006	0.0001

6.4.4. Qualitative Experimental Data

The scenario described in this section highlights the usability of thermodynamic modelling approach even when quantitative three-phase data are not available. The scenario presented here relies on the availability of qualitative phase behaviour data. Qualitative data for the system Multipar H/MGFW/DGBE are provided in Figure 6.31. Based on the qualitative data, the three-phase composition can be estimated as highlighted on Figure 6.31 assuming quasi-ternary phase behaviour. The estimated phase compositions are provided in Table 6.23. Interaction parameters based on the estimation were calculated, and the results are provided in Table 6.24. The interaction parameters based on quantitative three-phase compositions are also provided in Table 6.24 for comparison purposes.

As a first point of interest, the two sets of interaction parameters ($\overline{a}$) are in close agreement indicating the proximity between the estimated (qualitative) and the actual (quantitative) three-phase data. As such, both sets of interaction parameters should give very similar phase envelopes when implemented in the UNIQUAC model. This is the case as can be seen clearly in Figure 6.32. Table 6.25 compares the results quantitatively. The maximum absolute difference between the two sets of results is less than 3%.

This analysis highlights the ability to perform very rapid phase envelope mapping when knowledge of the phase regions is available, even when quantitative experimental data is lacking. This further highlights the potential applications of the UNIQUAC model for modelling quasi-ternary systems.

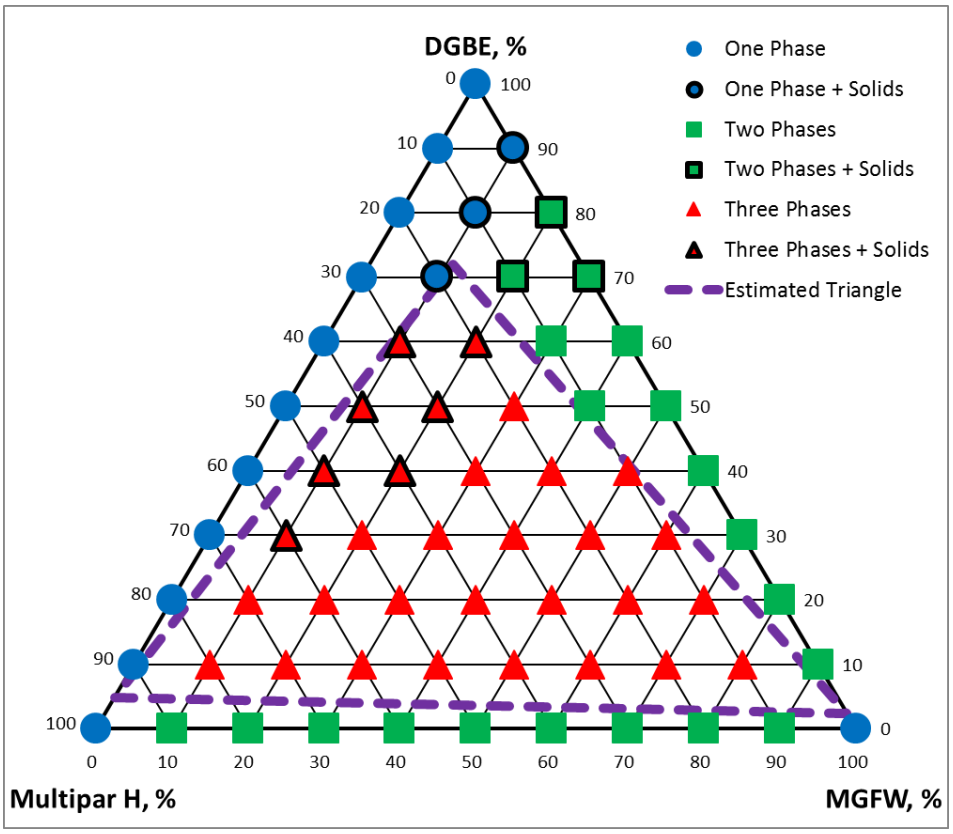

Figure 6.31: Qualitative phase behaviour data for Multipar H + MGFW + DGBE at 22.5˚C

Table 6.23: Estimated three-phase compositions for Multipar H + MGFW + DGBE at 22.5˚C based on qualitative phase behaviour data

Phase	Volume Fractions		
	MH	NSSW	EGMBE
MH-Rich	0.9500	0.0010	0.0490
MGFW-Rich	0.0010	0.9750	0.0240
DGBE-Rich	0.1700	0.1100	0.7200

Table 6.24: Interaction parameters ($\bar{a}$) for Multipar H + MGFW + DGBE at 22.5˚C based on estimated three-phase data with reference to a qualitative phase diagram.

Data	a_{12}	a_{21}	a_{13}	a_{31}	a_{23}	a_{32}
Quantitative (Chapter 4)	1295.1035	42.0164	287.4828	-98.7286	-115.3487	709.4147
Qualitative (Estimated)	1881.3191	-47.8968	277.2146	-91.5639	-132.2680	806.6064

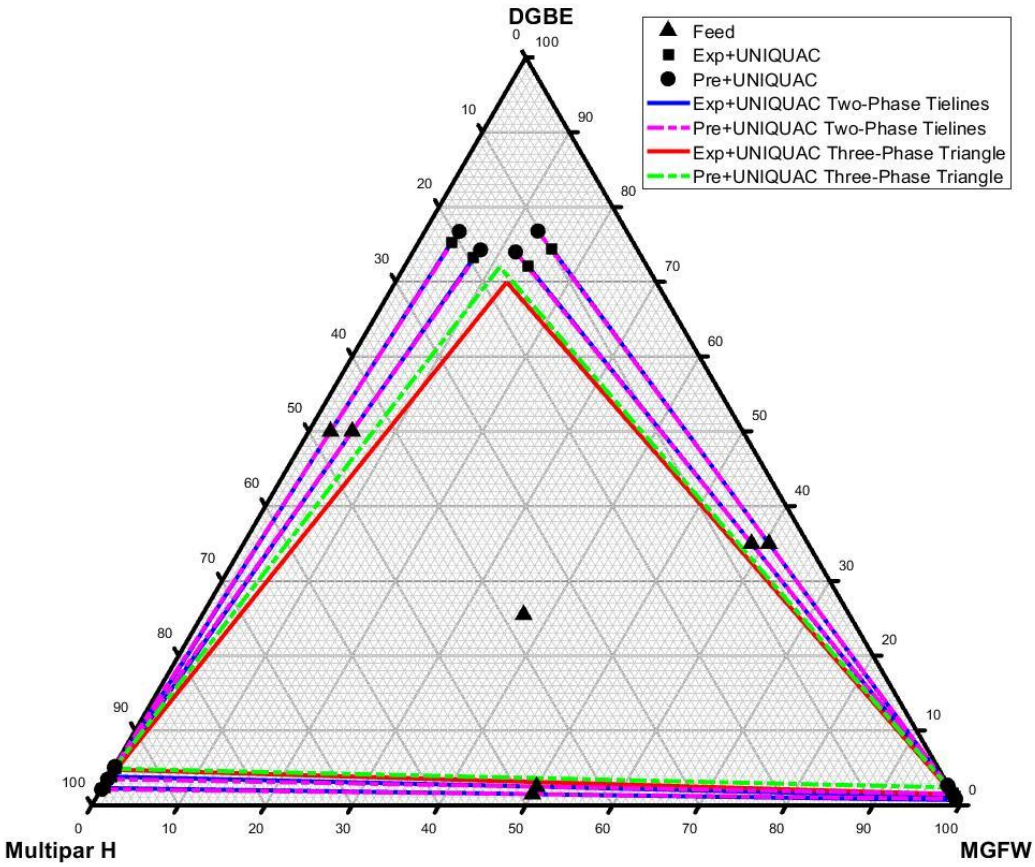

Figure 6.32: UNIQUAC results based on quantitative vs. qualitative experimental data for System B.

Table 6.25: The absolute differences between the UNIQUAC results based on quantitative vs. qualitative experimental data for the system Multipar H + MGFW + DGBE at 22.5˚C.

Absolute Difference Between Experimental and Calculated Data								
Multipar H-Rich			MGFW-Rich			DGBE-Rich		
MH	MGFW	DGBE	MH	MGFW	DGBE	MH	MGFW	DGBE
Three-Phase Region								
-0.0017	0.0031	-0.0014	-0.0009	0.0100	-0.0091	0.0023	0.0181	-0.0204
AB Two-Phase Region								
-0.0043	0.0028	0.0016	-0.0005	0.0021	-0.0016			
-0.0063	0.0030	0.0033	-0.0006	0.0040	-0.0034			
AC Two-Phase Region								
-0.0020	0.0023	-0.0003				0.0133	-0.0024	-0.0109
-0.0012	0.0014	-0.0002				0.0160	-0.0016	-0.0144
BC Two-Phase Region								
			-0.0007	0.0112	-0.0105	-0.0040	0.0275	-0.0235
			-0.0009	0.0104	-0.0095	-0.0048	0.0231	-0.0184

6.4.5. Hypothetical Systems

Because the three-phase triangle is a function of temperature, pressure, salinity and the relative solubility of an amphiphile, using it to calculate the interaction parameters captures all these variables. This provides two opportunities:

1. Qualitative thermodynamic approaches for "guess-estimating" the three-phase compositions for a system at certain conditions – e.g. (Kahlweit, Strey and Busse, 1990) – can be used to roughly predict the phase envelope for the system without needing experimental data. The qualitative approach for gauging the phase envelope based on the partition coefficient discussed in Chapter 3 (in the context of the salinity mapping study) is another example for sourcing information that would enable the implementation of the UNIQUAC model assuming quasi-ternary phase behaviour.

2. Knowledge of how the three-phase region evolves and changes with different parameters can allow phase envelopes for hypothetical systems to be created and numerically studied (e.g. in a transport model for example).

Investigating these opportunities in depth is beyond the scope of this PhD, and this is provided as a high impact suggestion for future work.

6.5. SUMMARY AND RESEARCH SIGNIFICANCE

The findings in this chapter can be summarised in the following points:

- A quasi-ternary implementation of the UNIQUAC model was successfully applied to model quasi-ternary systems.

- Using three-phase data only, the quasi-ternary implementation of the UNIQUAC model described in this chapter can successfully extrapolate the entire phase diagram. This provides substantial opportunities enabling transport modelling of both real and hypothetical systems with minimal or no experimental input. As highlighted in Chapter 3, specific phase behaviour can be targeted using mutual solvent blends (i.e. designing the three-phase region). Implementing this work in transport models for various phase diagrams can allow estimating the phase behaviour that yields most benefits, e.g. highest oil displacement.

- The results from the UNIQUAC model and experimental data from the literature are in close agreement for pure alkane/water/mutual solvent systems.

- The results from the UNIQUAC model are in very good agreement with the results obtained from the PDM for all the investigated complex quasi-ternary systems. This favours the use of the UNIQUAC model over the PDM. The PDM remains useful for verification purposes, and for determining the compositions of samples outside the context of phase behaviour modelling as discussed in Chapter 5.

- Essential to this work was the development of a numerical method for the calculation of interaction parameters based on three-phase data only for the UNIQUAC model. The method developed was demonstrated with success with reference to the literature, and implemented successfully in all the investigated cases.

- Also essential to this work was simplifying the initialisation and modelling algorithms implemented to capture the phase behaviour in these systems. This was achieved successfully as demonstrated by the results discussed in this chapter. The simplifications are sufficient for describing the systems of interest in this work and replaces the complex methods in the literature which are more useful for more generic cases.

Chapter 7: Analytical Methods for Analysing for Mutual Solvents and Analysis in the Presence of Mutual Solvents

7.1. OVERALL AIMS AND OBJECTIVES

The availability of analytical methods is paramount for mutual solvent research. Analysis of mutual solvents in systems of oil/brine/mutual solvents is a complex exercise due to the multicomponent nature of the oil and the brine. However, in the context of the work outlined in this thesis, it is essential for the following reasons:

1. It can be used to provide further confirmation to the quasi-ternary phase behaviour highlighted in Chapter 4.
2. It can be used to verify the semi-empirical model discussed in Chapter 5.
3. It can be used to illustrate the value of the thermodynamic approach outlined in Chapter 6.
4. It would be extremely valuable for field applications where knowledge of the concentration of a mutual solvent in a sample is required.
5. It forms the foundation for future work enabling research on mutual solvent adsorption and the effect of that on scale inhibitor adsorption in squeeze treatments.

Analysis in the presence of mutual solvents is also essential. This is important to allow the development of propagation studies which adequately track the propagation/displacement of the oil, the brine and/or the mutual solvent.

The work described in this section aims to provide a practical analytical approach for determining mutual solvent concentration in samples containing oil and brine. It also aims to investigate the feasibility of analysis in the presence of mutual solvents, with a focus on Ultraviolet/Visible (UV-Vis) Spectrophotometry analysis.

7.2. ANALYSIS FOR MUTUAL SOLVENTS

7.2.1. Gas Chromatography Basics

A Gas Chromatography (GC) system will consist of three main parts: an injector, a column and a detector. A schematic of a generic GC system is shown in Figure 7.1. The sample is introduced through the injector; automatic or manual injection may be involved. Automatic injection via an auto-sampler ensures the introduction of a volume of sample to the column in a consistent fashion. However, it is limited by the cost and the inability of retrofitting auto-sampling devices to an existing GC system. In the case of manual injection, a precise syringe is used to introduce the sample to the column by an operator. Any inconsistencies in sample injections must be accounted for in this case.

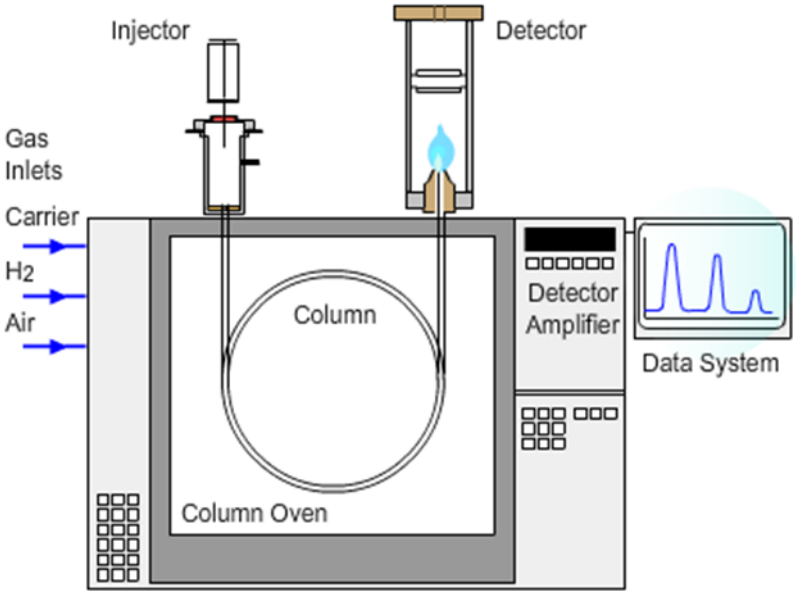

Figure 7.1: Schematic of a GC system (Crawford-Scientific, 2018).

Once injected, the sample will be carried by a carrier gas (N_2, He or H_2) through the column, all the way to the detector. The column has a stationary phase which aids in separating the sample into its constituents by interacting with the different components to varying degrees. Most importantly, the analyte (the component of interest for the analysis) must be resolved effectively from the remaining components in a sample. The chemistry of the stationary phase is of central importance for this process, and it gives rise to the different types of columns. The interaction of the stationary phase with the components of the sample can be described in terms of solubility. Components more soluble in the stationary phase will flow slower through the column, and vice versa. As such, when the chemistry of the

stationary phase is appropriate, the components would arrive at the detector at different times. This is illustrated by Figure 7.2.

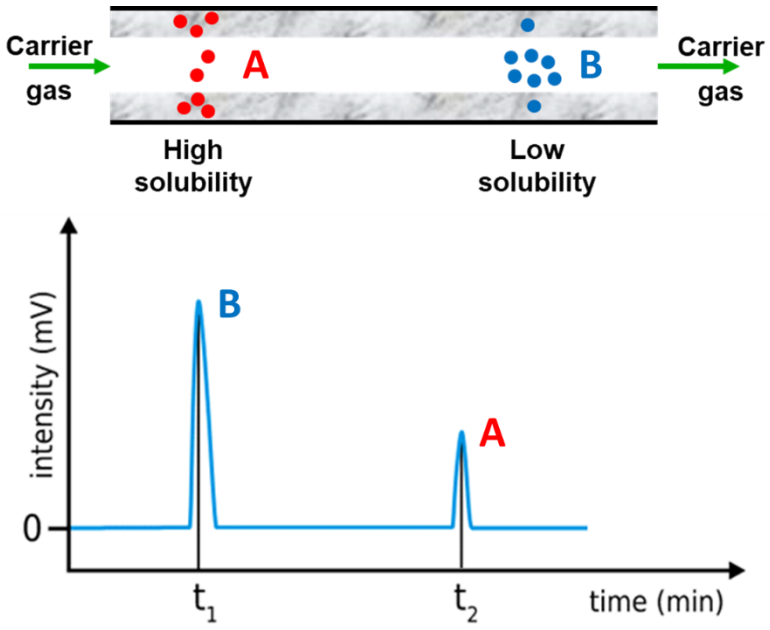

Figure 7.2: The role of the stationary phase in the separation of the constituents of a sample.

Additional parameters affecting the performance of the column in resolving the analyte include: the thickness of the stationary phase, the diameter of the column and the length of the column. The column may be preceded by a retention gap (i.e. guard column) if the sample is "unclean", i.e. samples containing salts or heavy organic components. The column may be housed in an oven to allow temperature control during the analysis.

The detector receives the constituents of the sample once they have travelled through the entire length of the column. Various types of detectors exist depending on the application, with the most common one being flame ionisation detection (FID) (Hinshaw, 2006). The FID detector responds to most organic compounds, making it an ideal choice in most organic applications. The detector is serviced by hydrogen and air, which aid in the combustion of organic compounds, thereby producing a response which is recorded by the detector.

All in all, GC systems are quite complex, and a thorough description of GC theory, components and techniques is beyond the scope of this work. The above description is sufficient for the purposes of the work.

7.2.2. Reference Method

The reference method for analysing samples containing mutual solvents was developed by an external contractor (Butterworth-Laboratories-Ltd, 2014) for analysing samples in **clean** alkane/water/mutual solvent systems. Several modifications were applied to this method to adapt it to the GC system available for this work (PerkinElmer Clarus 500; (PerkinElmer, 2010)). A summary of the key method parameters is provided in Table 7.1.

In the contractor's method, the injector temperature was 180˚C. This was changed to 250˚C to improve sample evaporation and hence minimise sample discrimination (i.e. the whole sample must evaporate instantaneously when introduced into the injector; sample discrimination occurs when the heaviest components in the sample do not evaporate instantaneously, in which case the sample received by the column is not representative of the sample injected into the injector).

Moreover, the column used for the analysis was the Agilent's equivalent of Sigma-Aldrich's SUPELCOWAX 10 due to availability issues. The chemistry of both columns are very similar (Agilent, 2018; Sigma-Aldrich, 2018), and hence they should give a comparable performance to that of the original design.

In addition, the addition of a retention gap to the method should facilitate analysis in **unclean** (brine/crude oil) systems. Investigating the feasibility of this method for this kind of analysis is part of this work.

To ensure system reliability, a "benchmark" sample is analysed via the GC before and after any day's analysis. This is a sample of two or more components at fixed concentrations. The retention times and the peak areas for the benchmark sample are known. As such, analysing the benchmark "BM" before the analysis ensures that the system is operating without any problems. Analysing the BM after the analysis provides certainty that no changes occurred within the system throughout the day's analysis.

The method employed for checking the benchmark sample was identical to the method for the main analysis, with the exception of the temperature programme and the run time.

Table 7.1: The key parameters of the reference method.

Injector	Technique	Split at 300 ml/min	
	Mode	Manual	
	Temperature	250˚C	
	Sample Volume	0.5 µl	
	Liner	Split, straight, restriction, wool, ultra-inert, 1100 µl, 4 mm	
Column	Chemistry	Agilent DB-WAX	
	Stationary Phase Thickness	1 µm	
	Length	60 m	
	Diameter	0.32 mm	
	Retention Gap	Yes if using SW/Crudes At 1 m	
	Oven Temperature Programme	Set	At 40˚C for 2 min
		Ramp	At 10˚C/min
		Set	At 150˚C for 15 min
Detector	Type	FID	
	Temperature	250˚C	
	Utilities	Air and H_2	
Carrier Gas	Gas	He at 1.2 ml/min	
	Pressure	app. 19 psi	
Run Time	Method	2 + 11 + 15 = 28 min	
	Cooling and equilibration	10 + 1 = 11 min	
	Total	28 + 11 = 39 min	
Benchmark	Oven Temperature Programme	Set	At 135˚C for 10 min
	Solution	BM_1	Methanol at 90% v/v
		BM_2	Isoamyl Acetate at 10% v/v
	Retention Times	BM_1	5.2 min
		BM_2	7.3 min
	Peak Intensities	BM_1	App. 83% of total area
		BM_2	App. 17% of total area
	Method Run time	10 min	
	Transition and equilibration	10 min	
	Total	10 + 10 = 20 min	

7.2.2.1. Internal Standard

For analysing samples in oil/brine/mutual solvent systems, the following definitions are made for the constituents of the sample:

1. The analyte (A): the component of interest for the analysis, i.e. the mutual solvent.
2. The internal standard (IS): a component added at a constant concentration to all samples/calibration standards.

3. The diluent (D): If the concentration of the analyte is high, the sample is diluted in a diluent – the diluent must accommodate all the constituents of the sample without any phase separation. Moreover, the diluent must not interfere with the analysis.
4. The remaining components, i.e. oil and the brine.

Due to its common use in the field, EGMBE was the mutual solvent of choice (analyte) for all studies. Due to the manual mode of injection, internal standards were added to all calibration standards to correct for any human errors. The method for this is explained in section 7.2.2.2. Several internal standards were investigated for this purpose, namely: Acetone, IPA, Ethanol, EGPE and EGBEA. The chromatogram for all of these internal standards are overlapped with the chromatogram of a sample containing the oil (Multipar H) and the analyte (EGMBE) in Figure 7.3. Based on this chromatogram, IPA and Ethanol can be ruled out as suitable internal standards due to the inability to resolve their peaks using the method, away from the peaks for the mineral oil.

For the remaining internal standards (Acetone "IS_1", EGPE "IS_2" and EGBEA "IS_3"), a Relative Standard Deviation (RSD) study was conducted to investigate the repeatability of the results for the analyte when the corrections are applied. The RSD study results are provided in Table 7.2. Before corrections, the RSD of the area of the analyte is identical to that of IS_2 (0.0% difference). This indicates that the analyte and IS_2 are subject to the same level of differentiation at the injector (N.B. differentiation is defined as the introduction of the constituents of a sample to the column at different times rather than instantaneously all together, i.e. same separation occurs without the help of the stationary phase within the column). IS_1 gives the highest level of differentiation at the injector (0.4% difference). After correcting the areas (see section 7.2.2.2), the RSDs of the analyte w.r.t. IS_2 and IS_3 were the lowest (0.2%). The RSD for the analyte w.r.t. IS_1 is 0.5%, which is still acceptable.

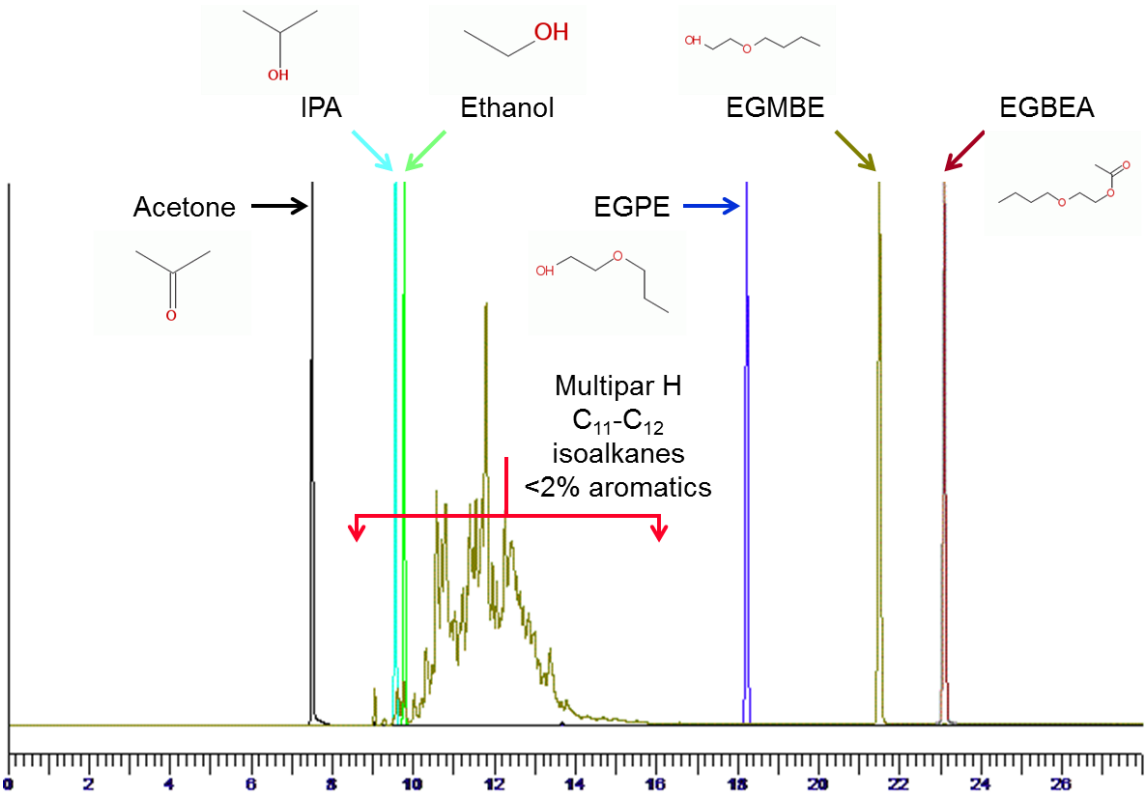

Figure 7.3: Chromatogram of a sample containing mineral oil + NSSW (sample constituents), EGMBE (the analyte), and several internal standards, namely: Acetone, IPA, Ethanol, EGPE and EGBEA.

Table 7.2: The results of an RSD study for the analyte EGMBE "A". Three internal standards were investigated for area corrections, namely: Acetone "IS_1", EGPE "IS_2" and EGBEA "IS_3".

Injection	Uncorrected Area				Corrected Area		
	A	IS_1	IS_2	IS_3	A w.r.t. IS_1	A w.r.t. IS_2	A w.r.t. IS_3
#	µV·s	µV·s	µV·s	µV·s	µV·s	µV·s	µV·s
1	50610.2	40798.0	47598.3	48402.8	51777.1	55744.5	56173.8
2	51724.1	41753.6	48778.6	49393.7	51812.8	55814.3	56135.2
3	50964.4	40213.9	47689.0	49045.3	51225.2	55614.6	56332.7
4	52506.9	42217.4	49287.5	49899.1	51710.3	55695.4	56011.3
5	52109.0	41406.7	48693.3	49733.5	51406.3	55579.4	56121.0
Sum	257914.5	206389.6	242046.7	246474.3	257931.6	278448.3	280773.9
Mean	51582.9	41277.9	48409.3	49294.9	51586.3	55689.7	56154.8
Std Dev	787.3	788.7	735.7	596.9	257.8	95.4	116.3
% RSD	**1.5**	**1.9**	**1.5**	**1.2**	**0.5**	**0.2**	**0.2**

The variability of the differentiation ratio (c) – see section 7.2.2.2 – about its mean value (c_m) is another important parameter. The lower this value is, the more consistent is the analysis. The results for the three internal standards are provided in Figure 7.4. IS_2 and IS_3 give the lowest variability (0.0001), while IS_1 gives a higher variability by a factor of 6 (0.0006). This is understandable given the large structural and physical differences

between IS_1 and the analyte. These are illustrated in Table 7.3. All in all, IS_2 delivers the best performance as an internal standard, followed by IS_3 and finally IS_1. This is also explained by the data in Table 7.3, where IS_2 is the most similar chemical to the analyte, and IS_1 is the least similar one. Without any additional considerations, IS_2 would be the ideal selection.

Despite that, when taking into account the toxicity of IS_2 and IS_3, and their much higher costs as well, and since corrections can be achieved using the much safer and cheaper IS_1 (acetone) to below 1% RSD (high repeatability), IS_1 was deemed to be a more appropriate internal standard for routine GC analysis, and was used in all subsequent work. Choosing IS_1 also offers the added advantage of possible optimisations to the reference method, as it leaves the column very quickly due to its limited interaction with the stationary phase used in the method.

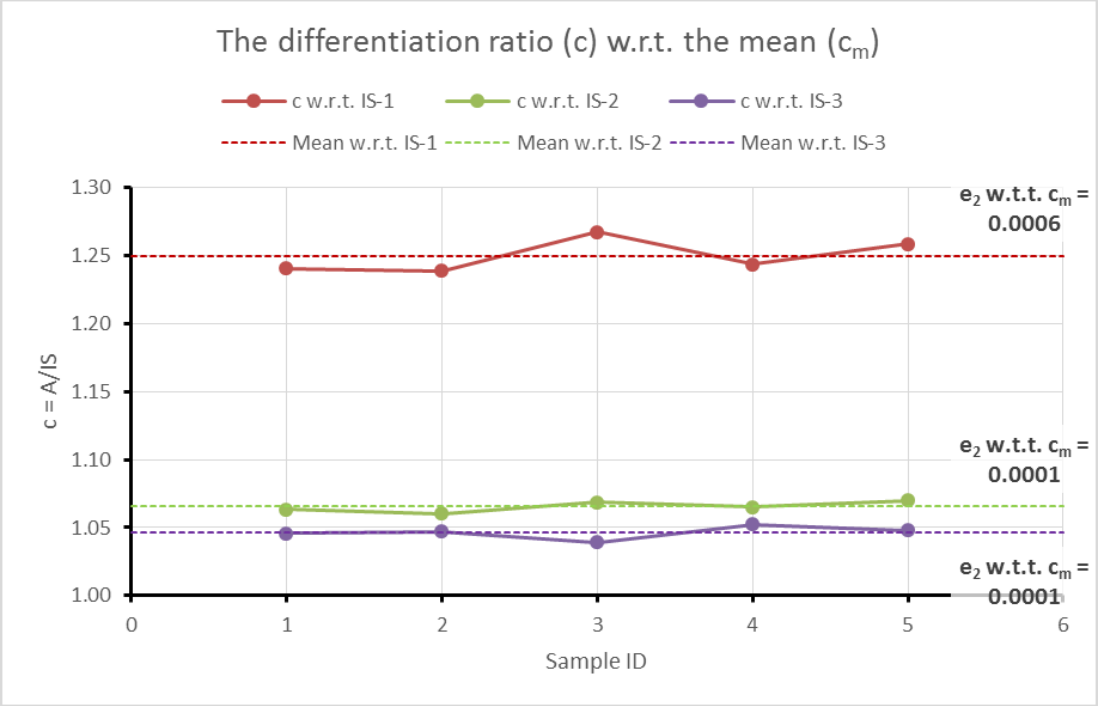

Figure 7.4: The variability of the differentiation ratio (c) about its mean value (c_m) for three internal standards, namely: Acetone "IS_1", EGPE "IS_2" and EGBEA "IS_3". The analyte is EGMBE "A".

Table 7.3: The structure and the boiling points of the analyte EGMBE "A" and three internal standards, namely: Acetone "IS_1", EGPE "IS_2" and EGBEA "IS_3".

Chemical	Designation	Structure	Boiling Point (˚C) At 1013 hPa
EGMBE	Analyte	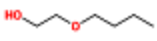	171-173
Acetone	Internal Standard No. 1 – IS_1		56.2
EGPE	Internal Standard No. 2 – IS_2	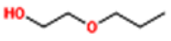	151-153
EGBEA	Internal Standard No. 3 – IS_3	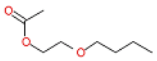	194-196

7.2.2.2. Analysis of GC Data

The correction using an internal standard allows an inspection for two things:

1. If any differentiation takes place at the injector (i.e. failing to deliver the entire sample to the column in a homogeneous fashion; some analyte or internal standard does not reach the column either due to poor evaporation or problems with the injection). This is undesirable and can only be corrected for, if multiple injections are performed.

2. If the amount of sample reaching the column is higher or lower than the volume of sample that should reach the column w.r.t. the method. A higher volume is not encountered usually. A lower volume is possible if the operator does not inject the sample fully. Both scenarios are undesirable and could lead to operator dependent variability in the results. An internal standard can aid in correcting for these errors. Multiple injections are not necessary.

Differentiation can be analysed for by looking at the ratio of the intensities (on an area basis) between the analyte and the internal standard. When a sample is injected perfectly, the constant is given by:

$$c = \frac{A'}{IS'} \qquad 7.1$$

If an injection is performed without any differentiation, then:

$$c = c_i = \frac{A_i}{IS_i} \quad 7.2$$

From equations 7.1 and 7.2, the following equation can be obtained:

$$f_i = \frac{IS_i}{IS'} = \frac{A_i}{A'} \quad 7.3$$

The quantity ratio (f) indicates whether the actual amount of sample injected is higher (> 1) or lower than the ideal amount (< 1). From equation 7.3:

$$A'_i = \frac{A_i}{fi} \quad 7.4$$

The ratio (c) is estimated by running several samples (≥ 2) and calculating the ratio between the intensities of the analyte and the internal standard. The values obtained should ideally be within 1% RSD for the calculation:

$$c_m = \frac{1}{N} \sum_{i=1}^{N} c_i = \frac{1}{N\, IS'} \sum_{i=1}^{N} A'_i \quad 7.5$$

Where (IS') is estimated using:

$$IS' = IS_m = \frac{1}{N} \sum_{i=1}^{N} IS_i \quad 7.6$$

To perform a correction, the following equation is used:

$$A_i = c_m\, IS' \quad 7.7$$

Applying equation 7.5 to equation 7.7:

$$A_i = \frac{1}{N} \sum_{i=1}^{N} A'_i \quad 7.8$$

7.2.2.3. Calibrations

Using the reference method, the feasibility of calibrations in different matrices was investigated. The calibrations sought were the following:

1. EGMBE in distilled water "DW".
2. EGMBE in mineral oil (i.e. Multipar H "MH" supplied by Brenntag; C_{11}-C_{12}, isoalkanes, <2% aromatics).
3. EGMBE in seawater "SW" (app. 36,000 ppm TDS).

Successful calibrations indicate the feasibility of analysing samples containing oil/brine/mutual solvent. The calibrations in DW and MH were carried out using a column without a retention gap. A retention gap was fitted to another column for analysis involving SW. Because the same column is used for DW and MH calibrations, the EGMBE calibrations were predicted to be identical. A quick EGMBE calibration without repeats or an internal standard was produced in DW and MH to investigate this. The results are shown in Figure 7.5, and are consistent with the prediction.

Following on from this, detailed calibration with internal standards and repeats were performed in MH (no need to perform detailed calibrations in DW as the results will be identical). Successful low-end (0.00, 0.10, 0.25, 0.50, 0.75 and 1.00% v/v EGMBE), high-end (0.00, 1.00, 2.50, 5.00, 7.50 and 10.00% v/v EGMBE) and full calibrations (low-end + high-end combined) were achieved as shown in Figure 7.6, Figure 7.7 and Figure 7.8 respectively. All calibrations had excellent correlation coefficients (R^2 = at least 0.999).

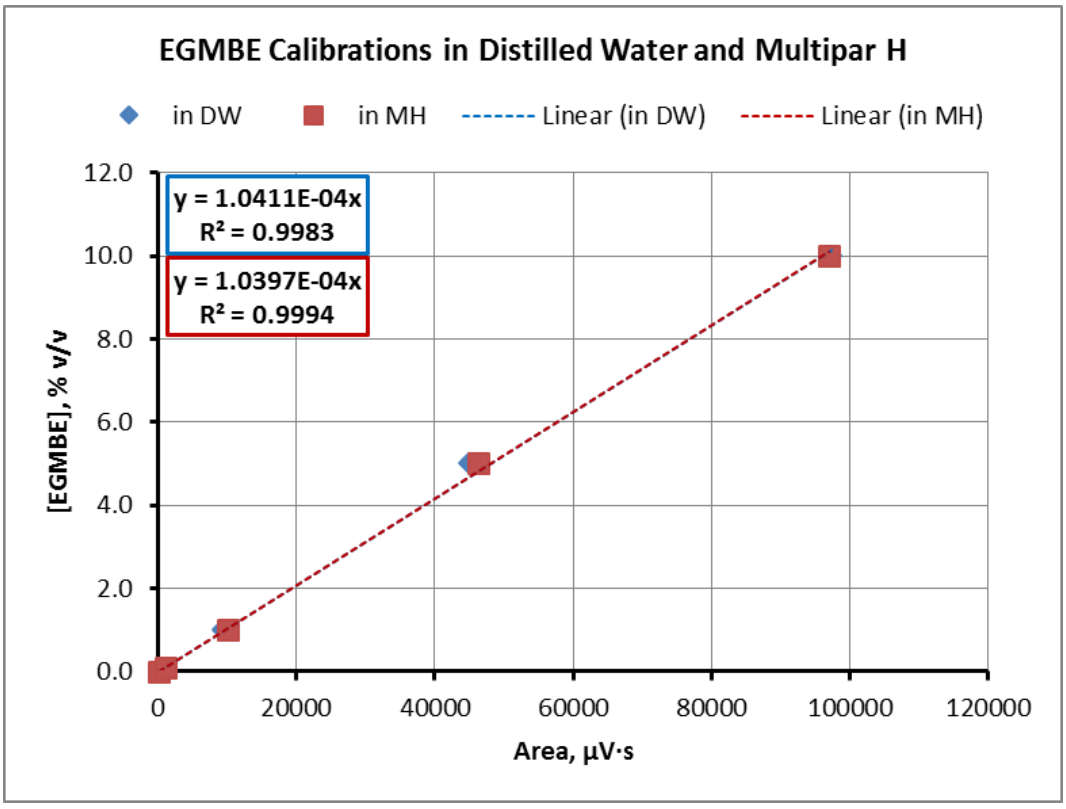

Figure 7.5: Simple EGMBE calibrations in DW and MH without corrections, i.e. no IS or repeats.

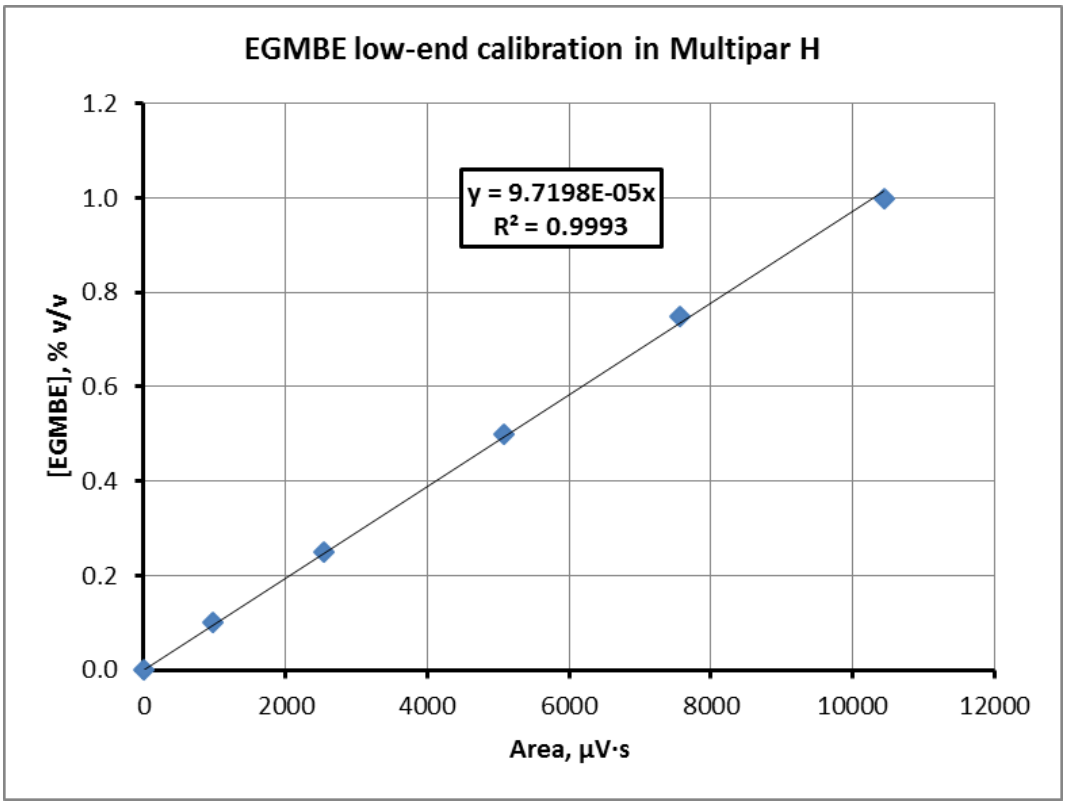

Figure 7.6: Detailed low-end EGMBE calibration in MH with corrections, i.e. with IS and ×3 repeats.

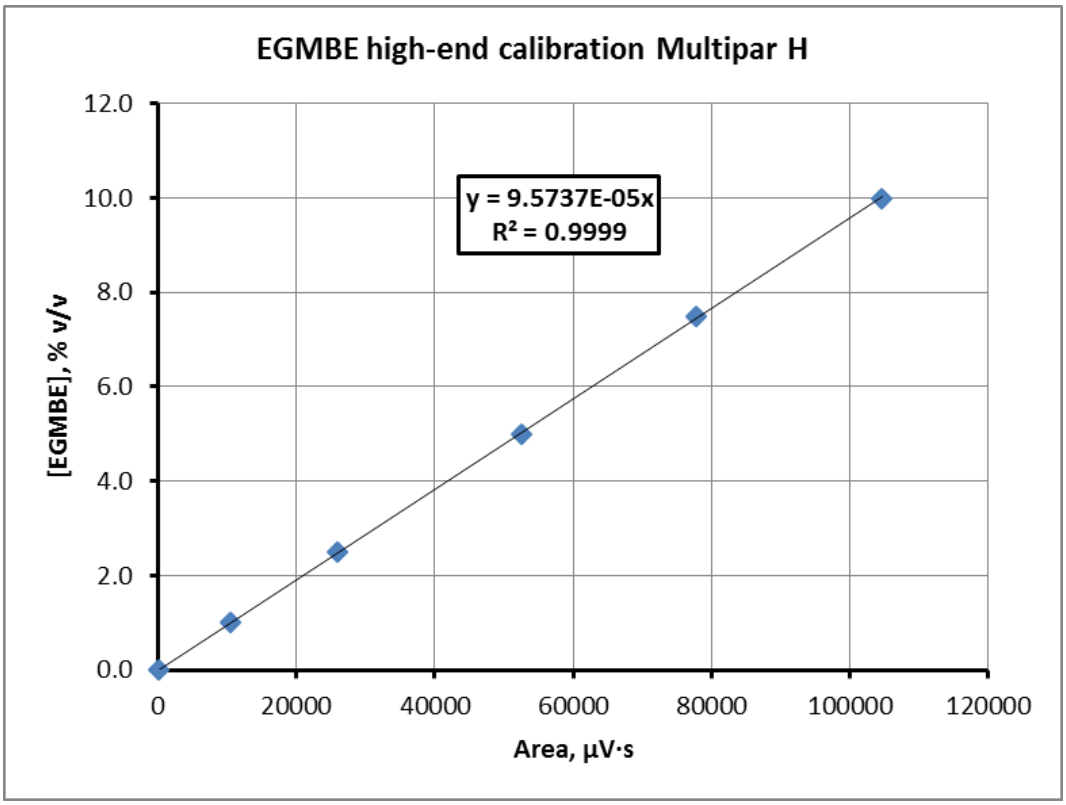

Figure 7.7: Detailed high-end EGMBE calibration in MH with corrections, i.e. with IS and ×3 repeats.

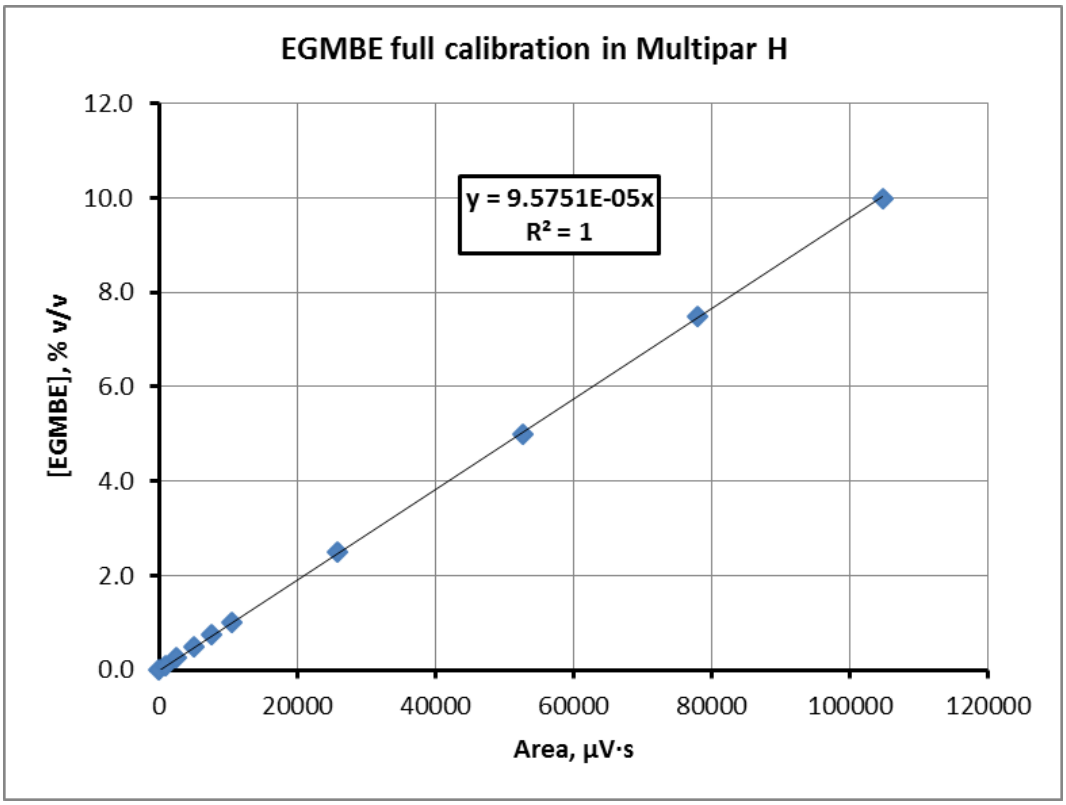

Figure 7.8: Detailed full EGMBE calibration in MH with corrections, i.e. with IS and ×3 repeats.

The SW calibrations which use a different column fitted with a retention gap were also excellent as shown in Figure 7.9, Figure 7.10 and Figure 7.11 for the detailed low-end, high-end and full calibrations respectively (R^2 = at least 0.996).

The difference between the DW/MH and SW calibrations is demonstrated in Figure 7.12 and is solely due to the use of different column setups for producing these calibrations. Otherwise, the same concentrations injected into the column would always give the same area response. In practice, a calibration should be produced prior to any analysis. This is an extensive piece of work due to the long time required to analyse a single sample (39 min/sample; a calibration with 3 concentrations ×3 repeats would take 5.85 hours to produce). Hence, despite the demonstrated effectivity of the reference method, in practice it is very time consuming, making it expensive for operational uses.

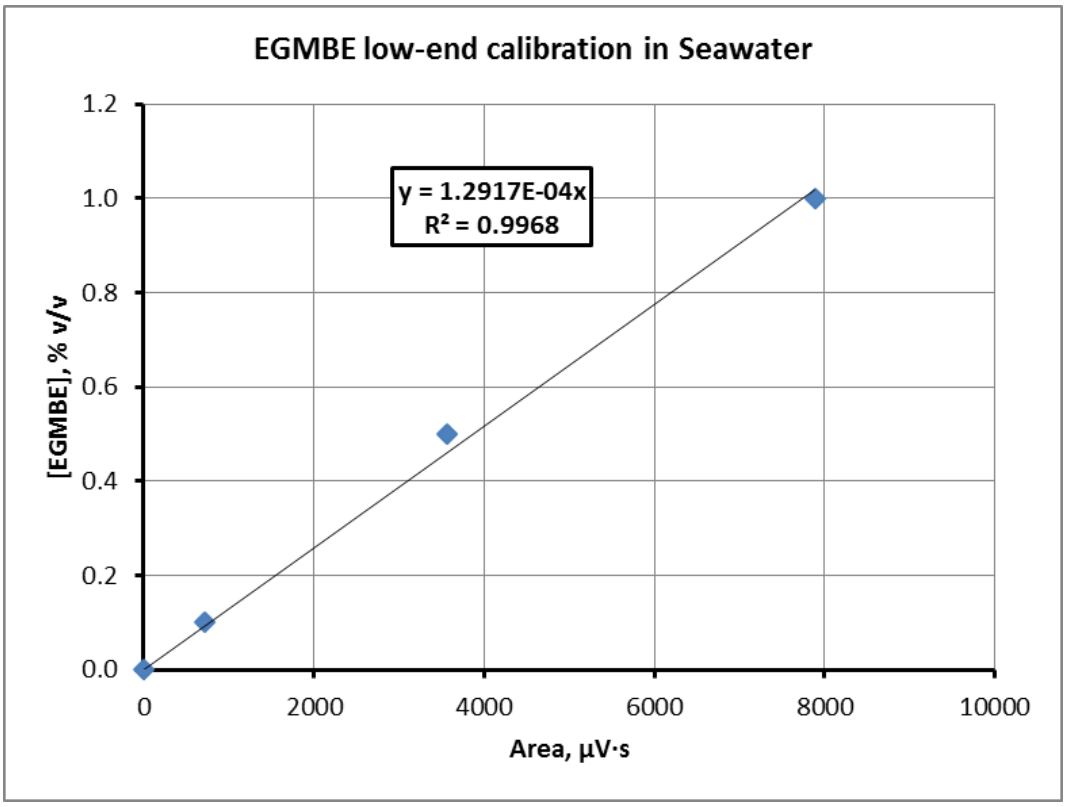

Figure 7.9: Detailed low-EGMBE calibration in SW with corrections, i.e. with IS and ×3 repeats.

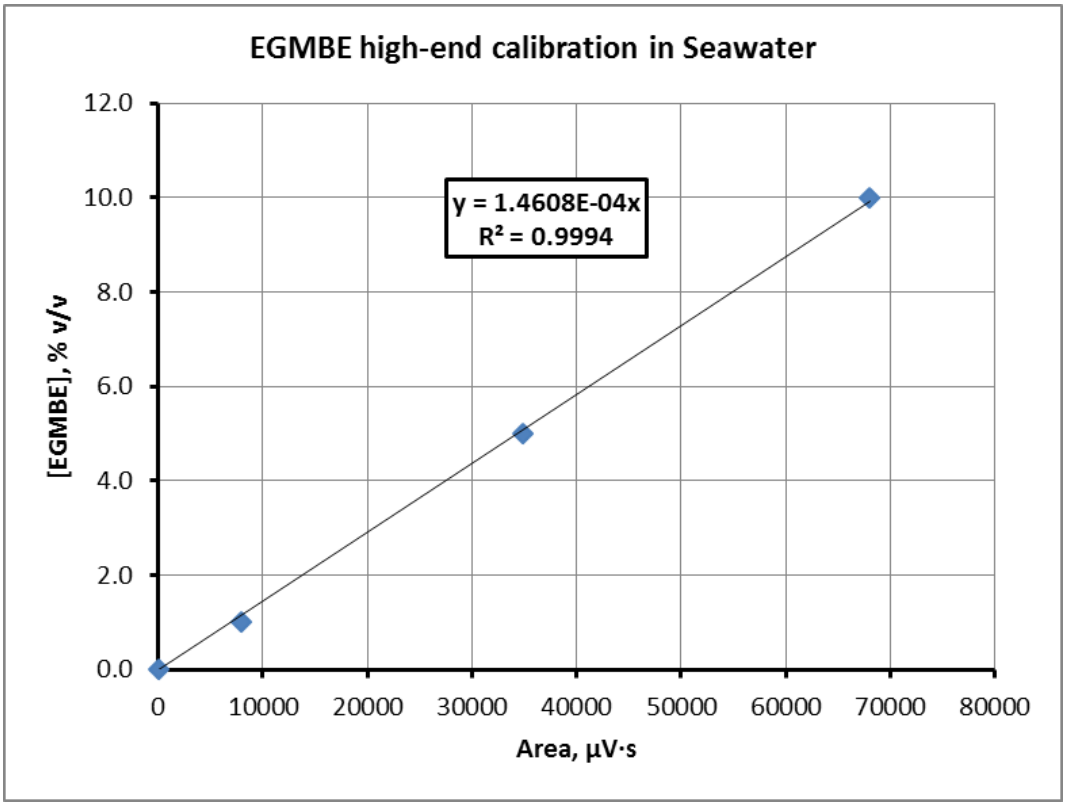

Figure 7.10: Detailed high-end EGMBE calibration in SW with corrections, i.e. with IS and ×3 repeats.

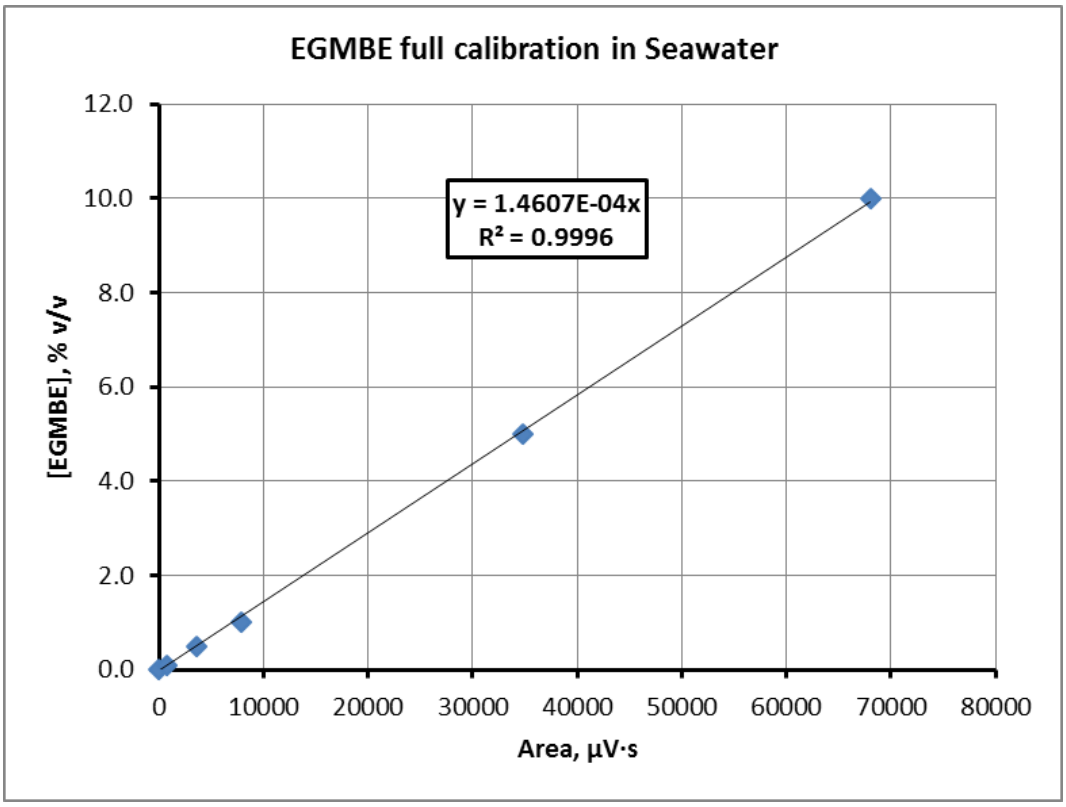

Figure 7.11: Detailed full EGMBE calibration in SW with corrections, i.e. with IS and ×3 repeats.

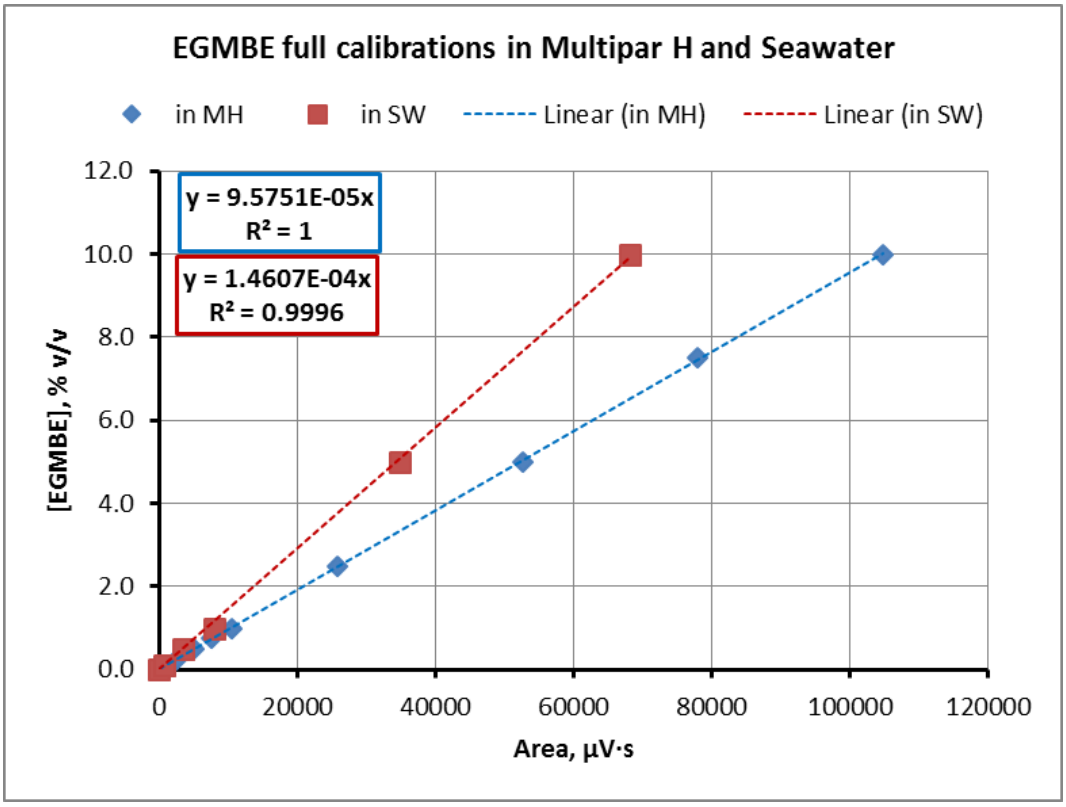

Figure 7.12: Detailed full EGMBE calibration in MH and SW.

7.2.2.4. Limitations

As an overall summary, the reference method is limited by several factors, including:

1. The very long time required to analyse a single sample (39 min/sample). Therefore, for research and field applications, the method – while feasible – is impractical and time consuming.

2. The benchmark method is inherently incompatible with the main method for the analysis due to the differences in the temperature programme. This makes the transition time between the benchmark method and the analysis method unnecessarily long (10 min).

3. Using acetone (IS_1) as the internal standard offers advantages in terms of safety, costs and possible improvements to the method. However, due to its high volatility, samples containing acetone cannot be stored for re-analysis with high reliability. The concentration of acetone will drop below the initial known concentration every time the sample is exposed to air. Alternatives to acetone which are physically more similar to EGMBE would provide higher repeatability if re-analysis is required.

4. As it is, the method cannot provide a measure of the amount of oil or water/brine in a sample. For phase behaviour studies, these additional measurements will be required. An ability to analyse samples of unknown concentrations must be developed.

While the method is only developed for a single mutual solvent, in theory, this is not a problem; it would be possible to adapt the method easily to analyse for other mutual solvents.

7.2.3. Optimised Method

A series of trial runs were conducted in an effort to optimise the reference method to a more practical version. The parameters altered in this optimisation effort were the carrier gas pressure and the temperature programme. The trial runs attempted are included in Table 7.4. The resulting changes to the retention times are provided in Table 7.5.

Table 7.4: Method optimisation runs – changes.

Method	Description		
Basis	Reference Method		
Trial Run 1	Carrier Gas Pressure	App. 19 psi	
	Temperature Programme	Set	At 150˚C for 28 min
Trial Run 2	Carrier Gas Pressure	App. 19 psi	
	Temperature Programme	Set	At 105˚C for 1 min
		Ramp	At 45˚C/min
		Set	At 150˚C for 12 min
Trial Run 3	Carrier Gas Pressure	App. 25 psi	
	Temperature Programme	Set	At 105˚C for 1 min
		Ramp	At 45˚C/min
		Set	At 150˚C for 12 min
Trial Run 4	Carrier Gas Pressure	App. 30 psi	
	Temperature Programme	Set	At 105˚C for 1 min
		Ramp	At 45˚C/min
		Set	At 150˚C for 12 min
Trial Run 5	Carrier Gas Pressure	App. 30 psi	
	Temperature Programme	Set	At 110˚C for 1 min
		Ramp	At 45˚C/min
		Set	At 155˚C for 2 min
		Ramp	At 45˚C/min
		Set	At 200˚C for 3 min
Trial Run 6	Carrier Gas Pressure	App. 30 psi	
	Temperature Programme	Set	At 90˚C for 1 min
		Ramp	At 45˚C/min
		Set	At 135˚C for 2 min
		Ramp	At 45˚C/min
		Set	At 180˚C for 4 min

Table 7.5: Method optimisation runs – retention times.

Method	Retention Times (min)			Method Time (≥ min)
	Acetone	Multipar H	EGMBE	
Basis	7.5	9.0-15.5	21.5	22.0
Trial Run 1	5.0	5.2-7.8	12.2	13.0
Trial Run 2	5.3	5.5-8.7	13.4	14.0
Trial Run 3	4.1	4.2-6.9	10.5	11.0
Trial Run 4	3.4	3.5-5.9	9.0	10.0
Trial Run 5	3.4	3.5-5.9	7.0	8.0
Trial Run 6	3.5	3.7-5.8	8.3	9.0

The logical progression for the optimisation effort is described below with respect to each trial run:

1. Trial Run 1: The temperature programme was simplified to a fixed temperature programme at the maximum temperature of the reference method. This resulted in reducing the total method time by at least 9 minutes with respect to the original method.

2. Trial Run 2: A high-rate temperature programme was introduced for acetone to reduce the time at which the column operates at a high temperature (which depletes the stationary phase overtime). This was found feasible with only 1 min increase in the overall method time w.r.t. the previous trial run.

3. Trial Run 3: The carrier gas pressure was increased to promote faster analysis. This was achieved with the method time reducing by 3 min w.r.t. the previous trial run. However, the separation between acetone and the oil became very close (within 0.1 min). This issue was put on hold to continue investigating increases to the carrier gas pressure.

4. Trial Run 4: The carrier gas pressure was increased to a maximum of 30 psi. This reduced the method run time by another minute w.r.t. the previous run. A separation of 3.6 min continued to exist between the oil and the EGMBE, offering further opportunities to reduce the total analysis time.

5. Trial Run 5: A high-rate temperature programme was introduced just after the acetone leaves the column in an attempt to drive lower retention of the oil and the mutual solvent. This was successful, reducing the method run time by another 2 minutes w.r.t. the previous trial run.

6. Trial Run 6: The starting temperature for the method was lowered to aid better separation between the acetone and the oil. The trial run for this was successful, and this final run was deemed a practical method, with a total run time of 9 min/sample.

The optimised method is described in full in Table 7.6.

Table 7.6: The key parameters of the optimised method.

Injector	Technique	Split at 300 ml/min	
	Mode	Manual	
	Temperature	250˚C	
	Sample Volume	0.5 µl	
	Liner	Split, straight, restriction, wool, ultra-inert, 1100 µl, 4 mm	
Column	Chemistry	Agilent DB-WAX	
	Stationary Phase Thickness	1 µm	
	Length	60 m	
	Diameter	0.32 mm	
	Retention Gap	Yes if using SW/Crudes At 1 m	
	Oven Temperature Programme	Set	At 90˚C for 1 min
		Ramp	At 45˚C/min
		Set	At 135˚C for 2 min
		Ramp	At 45˚C/min
		Set	At 180˚C for 4 min
Detector	Type	FID	
	Temperature	250˚C	
	Utilities	Air and H_2	
Carrier Gas	Gas	He at 1.2 ml/min	
	Pressure	app. 30 psi	
Run Time	Method	1 + 1 + 2 + 1 + 4 = 9 min	
	Cooling and equilibration	1 + 1 = 2 min	
	Total	9 + 2 = 11 min	
Benchmark	Oven Temperature Programme	Same as analysis method	
	Solution	BM_1	Methanol at 90% v/v
		BM_2	Isoamyl Acetate at 10% v/v
	Retention Times	BM_1	3.8 min
		BM_2	5.3 min
	Peak Intensities	BM_1	App. 83% of total area
		BM_2	App. 17% of total area
	Method Run time	9 min	
	Transition and equilibration	2 min	
	Total	9 + 2 = 11 min	

The optimised method also has the added benefits of faster cooling due to higher operation temperature. The benchmark method was also adjusted to be fully consistent with the analysis method. Overall, the optimised method takes 72% less time to analyse the same number of samples as the original method, with a total run time of 11 min/sample (cf. 39 min/sample) when the cooling and equilibration times are taken into account.

7.2.3.1. Calibrations

Calibrations in seawater were checked with the optimised method and were found to be successful. The results are shown in Figure 7.13, Figure 7.14 and Figure 7.15 for the corrected detailed low-end, high-end and full calibrations.

These calibrations compare very closely with the calibrations obtained using the original method as illustrated in Figure 7.16. The slight differences may be due to the much higher carrier gas pressure in the optimised method (by app. 58%). In any case, the much lower run time for the optimised method makes it practical to run a calibration prior to any planned analysis. Therefore, any variations in the calibrations across different runs should not impact the analysis.

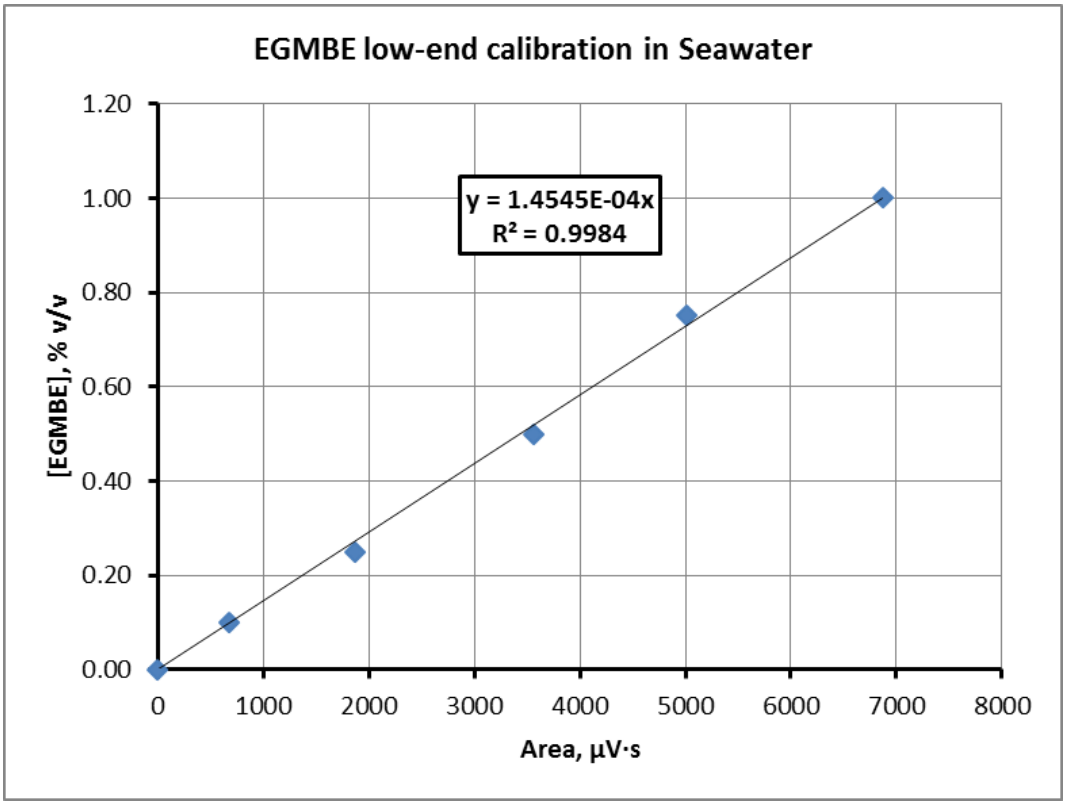

Figure 7.13: Corrected low-end EGMBE calibration in SW using the optimised method (2 repeats).

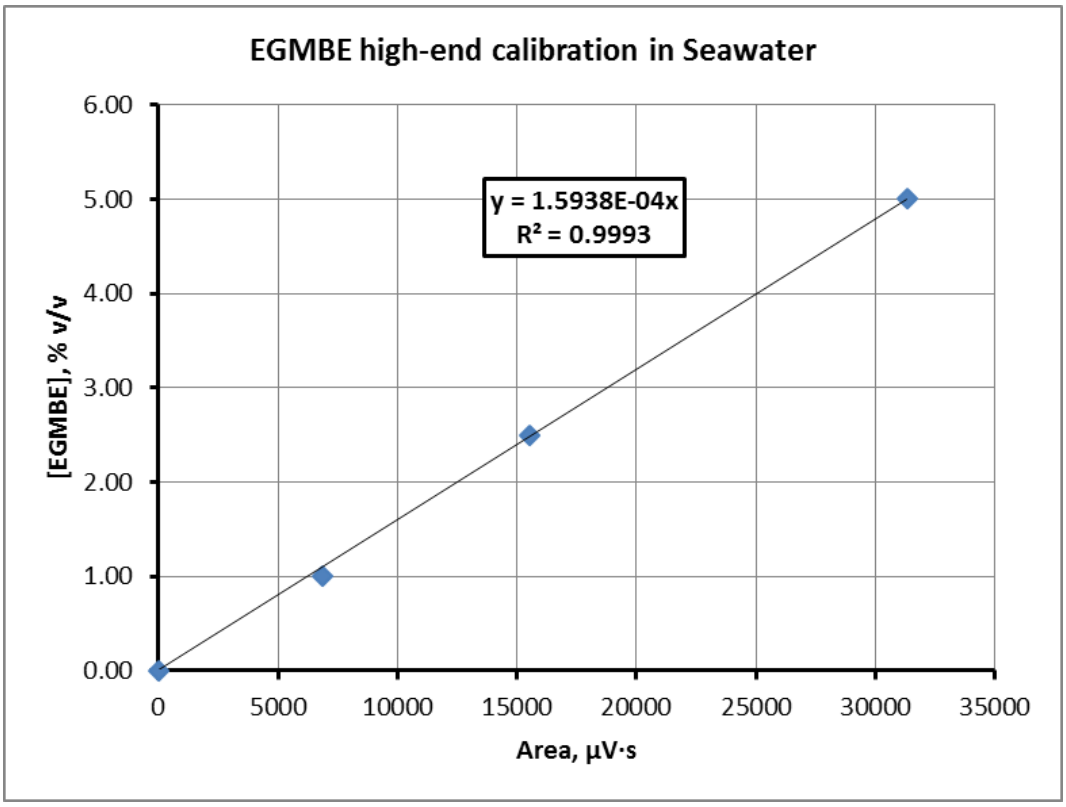

Figure 7.14: Corrected high- end EGMBE calibration in SW using the optimised method (2 repeats).

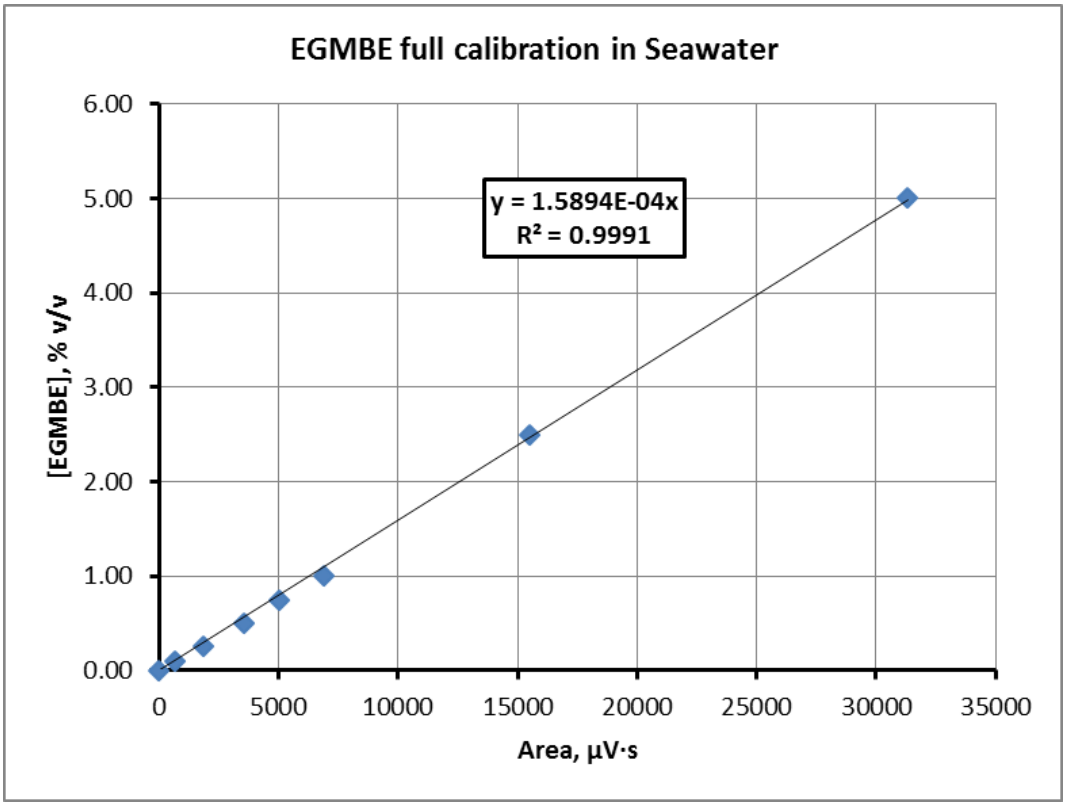

Figure 7.15: Corrected full EGMBE calibration in SW using the optimised method (2 repeats).

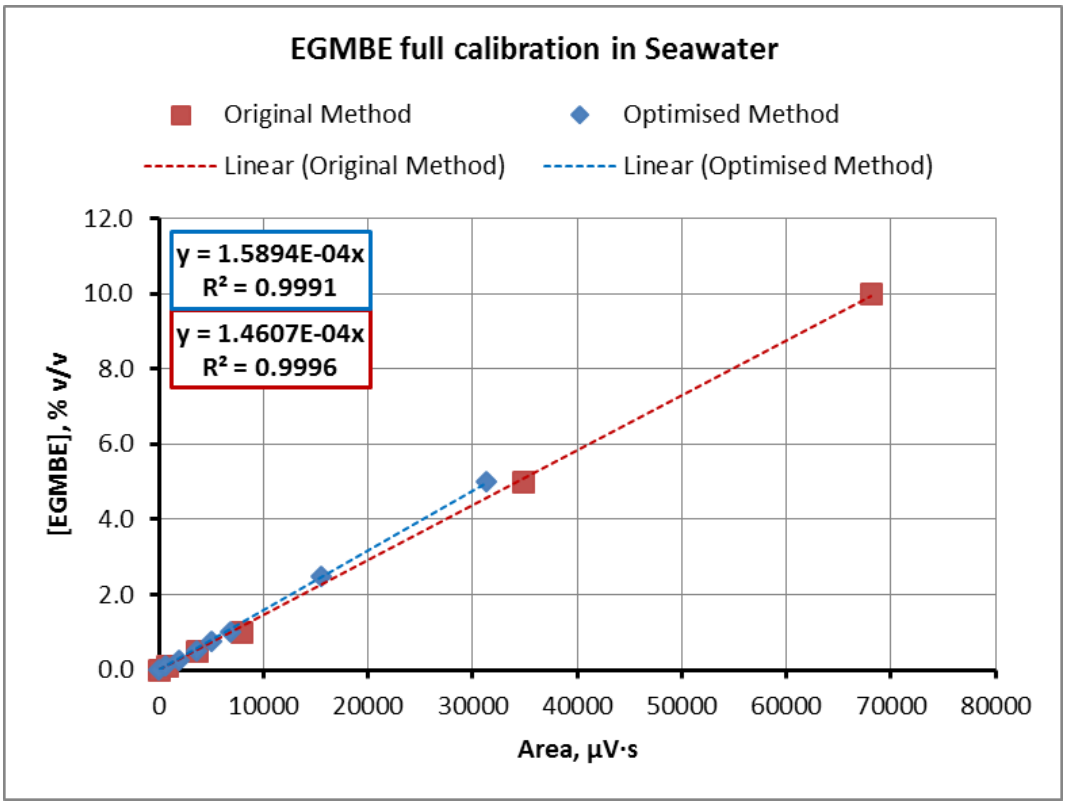

Figure 7.16: Corrected full EGMBE calibration in SW: the original vs. the optimised methods.

7.2.3.2. Phase Behaviour Analysis: Sample Preparation

When oil/brine/mutual solvent are mixed at known proportions, and phase separation occurs, the concentration of the mutual solvent in the resulting phases is unknown. To analyse the resulting phases, they must be diluted to fit within a calibration range. Moreover, the dilution should not result in further phase separation.

For this purpose, a suitable diluent must be selected, and the dilution factor selected should not compromise the integrity of the analysis. All of this makes devising suitable criteria for sample preparation rather complex. However, phase behaviour modelling combined with a sensitivity analysis should aid this objective.

The mass balance model described in Chapter 5 was employed for this purpose. The system of choice for this analysis was a system of Multipar H/NSSW/EGMBE at laboratory conditions (22.5˚C and 1 atm). For the feed samples in Table 7.7, the mass balance model predicts the phase compositions provided in Table 7.8.

Table 7.7: Selected feed samples.

Feed Sample	Region	Feed, % v/v		
		Oil	Brine	MS
1	Three Phase	30.0	30.0	40.0
2	Three Phase	60.0	20.0	20.0
3	Three Phase	20.0	60.0	20.0
4	Two Phase	50.0	45.0	5.0
5	Two Phase	48.0	45.0	7.0
6	Two Phase	40.0	10.0	50.0
7	Two Phase	37.5	12.5	50.0
8	Two Phase	5.0	60.0	35.0
9	Two Phase	7.5	57.5	35.0

Table 7.8: Predicted phase compositions for the feed samples in Table 7.7.

Feed Sample	Region	Enrichment Status	Phase Sample #	Predicted Composition, % v/v		
				Oil	Brine	MS
1	Three Phase	Oil-Rich	1o	89.32	0.84	9.84
1		Brine-Rich	1b	0.00	90.39	9.61
1		MS-Rich	1m	19.79	19.32	60.89
2	Three Phase	Oil-Rich	2o	89.32	0.84	9.84
2		Brine-Rich	2b	0.00	90.39	9.61
2		MS-Rich	2m	19.79	19.32	60.89
3	Three Phase	Oil-Rich	3o	89.32	0.84	9.84
3		Brine-Rich	3b	0.00	90.39	9.61
3		MS-Rich	3m	19.79	19.32	60.89
4	Two Phase	Oil-Rich	4o	95.96	0.84	3.20
4		Brine-Rich	4b	0.00	92.89	7.11
5	Two Phase	Oil-Rich	5o	94.41	0.00	5.59
5		Brine-Rich	5b	0.00	91.32	8.68
6	Two Phase	Oil/MS-Rich	6om	40.78	8.48	50.75
6		Brine-Rich	6b	0.00	88.59	11.41
7	Two Phase	Oil/MS-Rich	7om	38.78	9.72	51.50
7		Brine-Rich	7b	0.00	90.39	9.61
8	Two Phase	MS-Rich	8m	10.47	26.94	62.58
8		Brine-Rich	8b	0.05	89.91	10.05
9	Two Phase	MS-Rich	9m	15.00	24.46	60.54
9		Brine-Rich	9b	0.00	90.39	9.61

For several dilution factors (DF), an error analysis can be performed which assumes that the results from the GC will be accurate to a given number of decimal places (DP), e.g. 0, 1, 2 and 3 decimal places accuracy. Based on this, the absolute errors when determining the mutual solvent concentration via the GC can be estimated by applying equations 7.9-

7.11. The results for this are provided in Table 7.9. The maximum absolute error at various (DF) can also be estimated using real GC data. The results for this are provided in Table 7.10.

$$[MS]_{measured} = Round\left(\frac{[MS]_{model}}{DF}, DP\right) \quad 7.9$$

$$[MS]_{sample} = [MS]_{measured} \times DF \quad 7.10$$

$$Estimated\ Abs\ Error = [MS]_{sample} - [MS]_{model} \quad 7.11$$

Table 7.9: Estimated maximum absolute errors in the determined MS concentration at various DF based on rounding analysis.

Dilution Factor	Maximum Error Absolute Error at D.P. =			
	0	1	2	3
5	2.42	0.25	0.02	0.00
10	4.41	0.50	0.05	0.01
15	7.11	0.66	0.06	0.01
20	9.96	0.89	0.10	0.01
25	12.42	1.18	0.11	0.01
30	11.41	1.11	0.14	0.01
35	16.50	1.75	0.16	0.01
40	19.46	1.96	0.19	0.02
45	17.58	2.11	0.21	0.02
50	12.58	2.42	0.25	0.02
Maximum Abs Error for all DF	19.46	2.42	0.25	0.02

Table 7.10: Estimated maximum absolute errors in the determined MS concentration at various DF based on GC analysis.

Theoretical [MS], % v/v	Area (GC), µV·s	DF w.r.t 5% v/v MS	Amplified Area, µV·s	Measured [MS], % v/v	Absolute Error
0.10	668.3	50.0	33414.9	5.31	0.31
0.25	1872.9	20.0	37458.5	5.95	0.95
0.50	3561.8	10.0	35618.1	5.66	0.66
0.75	5017.8	6.7	33451.9	5.32	0.32
1.00	6871.6	5.0	34358.0	5.46	0.46
2.50	15506.5	2.0	31013.1	4.93	-0.07
5.00	31328.6	1.0	31328.6	4.98	-0.02
Maximum Abs Error for all DF					0.95

Based on the results in Table 7.9 and Table 7.10, the accuracy of the GC results fits between 1 and 2 decimal places rounding. Based on this, an error range can be set up for the various dilution factors, and a linear interpolation with reference to the GC results can aid in calculating a weighted average error at each dilution factor. The results for this are provided in Table 7.11. This sensitivity analysis suggests that the dilution errors (w.r.t. the mutual solvent) can be kept below 1% up to a dilution factor of 50.

Table 7.11: Estimated weighted average error in the determined MS concentration at various DF based on GC analysis.

Dilution Factor	Absolute Error Range, % v/v		Weighted Average Error, % v/v
	Min	Max	
5	0.02	0.25	0.09
10	0.05	0.50	0.19
15	0.06	0.66	0.26
20	0.10	0.89	0.35
25	0.11	1.18	0.46
30	0.14	1.11	0.46
35	0.16	1.75	0.68
40	0.19	1.96	0.77
45	0.21	2.11	0.83
50	0.25	2.42	0.95

As for the calibration range, based on the modelling results in Table 7.8, this can be estimated at various dilution factors. The results are provided in Table 7.12. From this table, a dilution factor of 25 is found to be ideal. This keeps the dilution errors at a low value while giving a practical calibration range, a small enough sample volume and a MS content in the sample that would prevent phase separation post-dilution. As for the diluent, from compatibility experiments (w.r.t. MH/SW), IPA was found to be an idea choice.

Table 7.12: Estimated calibration range and MS content of the samples at various dilution factors.

Dilution Factor	Error at Perfect Dil., % v/v	Calibration Range, % v/v		Sample per 10ml, ml	[MS], % v/v
		Min	Max		
10	0.19	0.10	7.50	1.000	> 90%
25	0.46	0.10	5.00	0.400	> 96%
50	0.95	0.01	1.50	0.200	> 98%

Therefore, to perform sample preparation, a 25 dilution factor should be applied in IPA, and in the presence of an internal standard (acetone at 5% v/v). To prepare a 10 ml sample

for GC analysis, this would equate to 0.4 ml of the phase that requires analysis, 0.5 ml IS and 9.1 ml diluent. The calibration range for this analysis is between 0.10-5.00% v/v mutual solvent, and all calibration standards should be corrected with respect to an internal standard (acetone at 5% v/v). A summary of the sample preparation criteria for phase behaviour analysis is provided in Table 7.13.

Table 7.13: Sample preparation criteria.

Sample Type	Runs	Volume, ml			
		Sample	Acetone	IPA	Total
Phase	At least ×2	0.4	0.5	9.1	10.0

A chromatogram for a sample prepared as prescribed in Table 7.13 is shown in Figure 7.17.

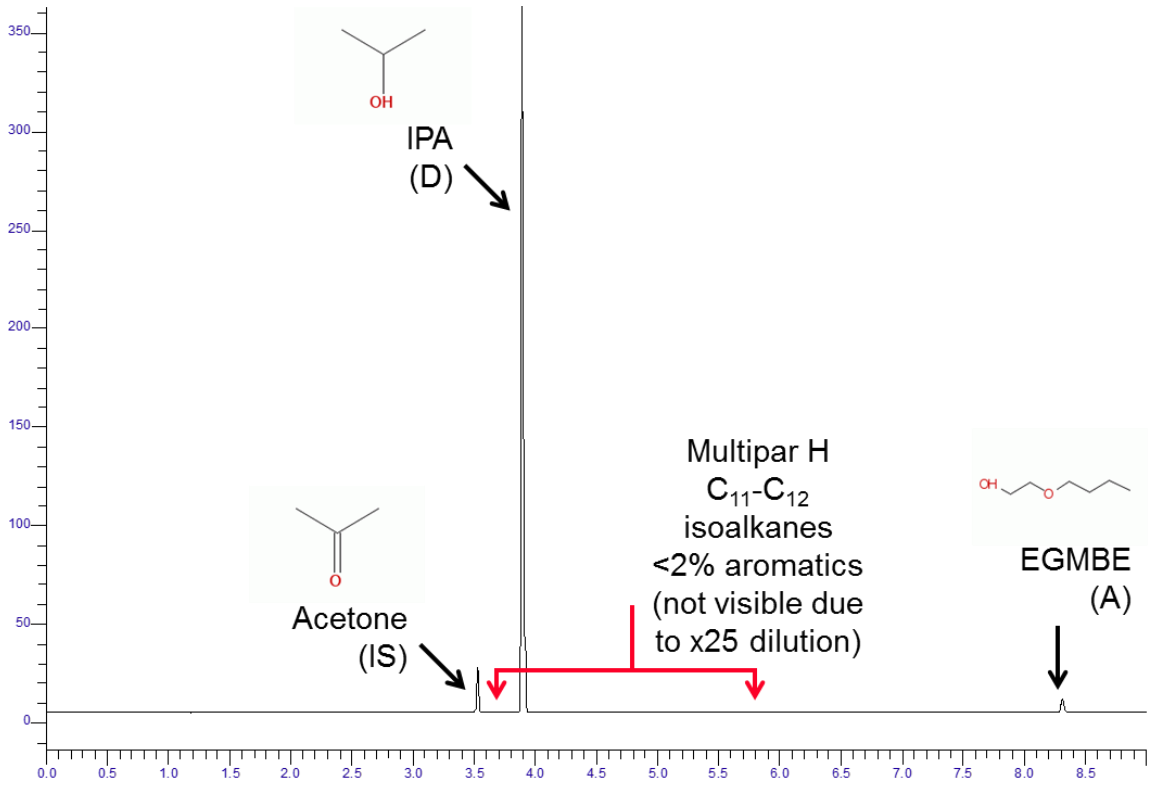

Figure 7.17: Chromatogram of a sample prepared as per the instructions in Table 7.13.

7.2.3.3. Application

For the system Multipar H/NSSW/EGMBE at laboratory conditions (22.5˚C and 1 atm), GC analysis was conducted for several samples and the mutual solvent concentration was determined. The results for the two-phase region are provided in Table 7.14, and compared with the modelling results from Chapter 5 (obtained via the Phase Displacement Method – PDM). Most of the absolute differences were within 1%. These results are plotted in Figure

7.18. The equation ($y = x$) represents the data very well with almost a perfect correlation coefficient. This highlights the excellent agreement between the GC results and the modelling results.

Table 7.14: Two-phase samples – GC vs. modelling (PDM) results.

Sample	[MS]		Absolute Difference
	GC	Model	
#	% v/v	% v/v	% v/v
4o	3.0	3.2	0.2
4b	7.0	7.1	0.1
5o	5.4	5.6	0.2
5b	8.1	8.7	0.6
6om	50.4	50.7	0.3
6b	9.3	11.4	2.1
8m	63.3	62.6	-0.7
8b	10.2	10.0	-0.1
9m	60.0	60.5	0.5
9b	9.8	9.6	-0.2

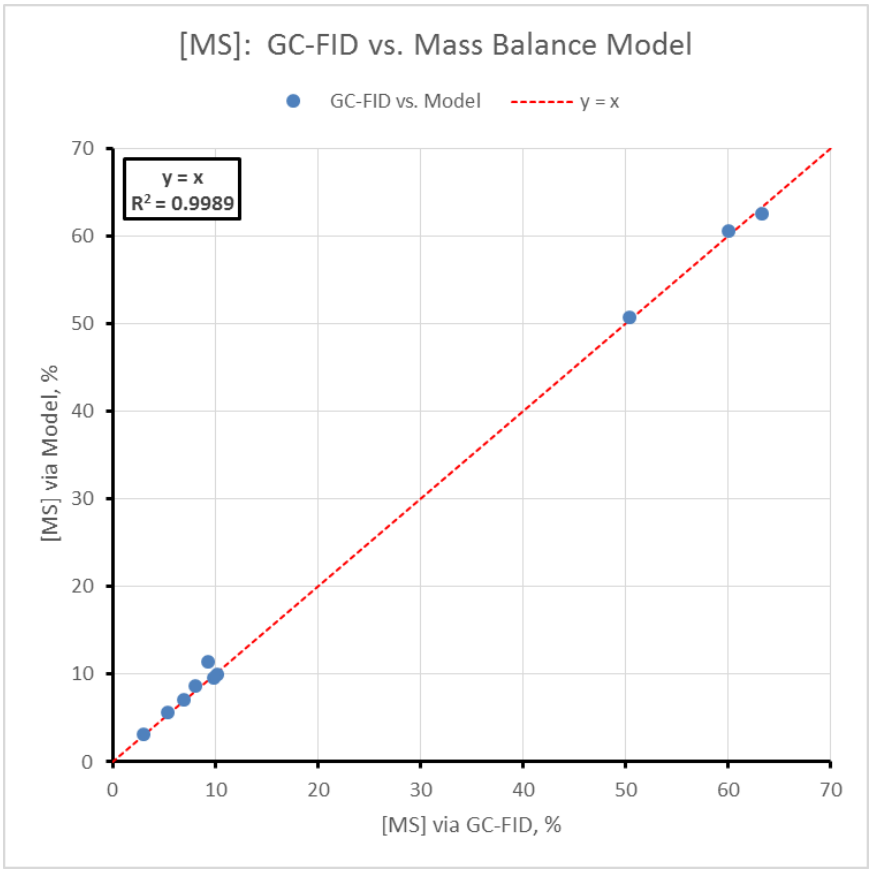

Figure 7.18: Two-phase samples – GC vs. modelling (PDM) results; ($y = x$) fitted to the data.

Likewise, with three-phase samples, low absolute differences between the GC and the PDM modelling data were achieved (Table 7.15), and the results can be represented very well by the equation ($y = x$) as seen in Figure 7.19. Since the PDM (Chapter 5) was in good agreement with the quasi-ternary implementation of the UNIQUAC model (Chapter 6), the results for this system validate both modelling approaches.

Another outcome of this analysis is further confirmation to the quasi-ternary phase behaviour of the Multipar H/NSSW/EGMBE system as seen in Table 7.15. The ×3 three-phase samples taken at different parts of the three-phase region (Table 7.7) have relatively the same mutual solvent content. This is vividly clear for the mutual solvent-rich phase, where all samples are found to contain exactly the same amount of mutual solvent. Variability within roughly 1% are observed for the oil-rich and the brine-rich phases. However, this is well within experimental errors.

Table 7.15: Three-phase samples – GC vs. modelling (PDM) results.

Sample	[MS]		Absolute Difference
	GC	Model	
#	% v/v	% v/v	% v/v
1o	10.5	9.8	-0.6
2o	10.1	9.8	-0.3
3o	9.3	9.8	0.5
1b	9.3	9.6	0.3
2b	8.7	9.6	1.0
3b	8.4	9.6	1.2
1m	60.0	60.9	0.9
2m	60.0	60.9	0.9
3m	60.0	60.9	0.9

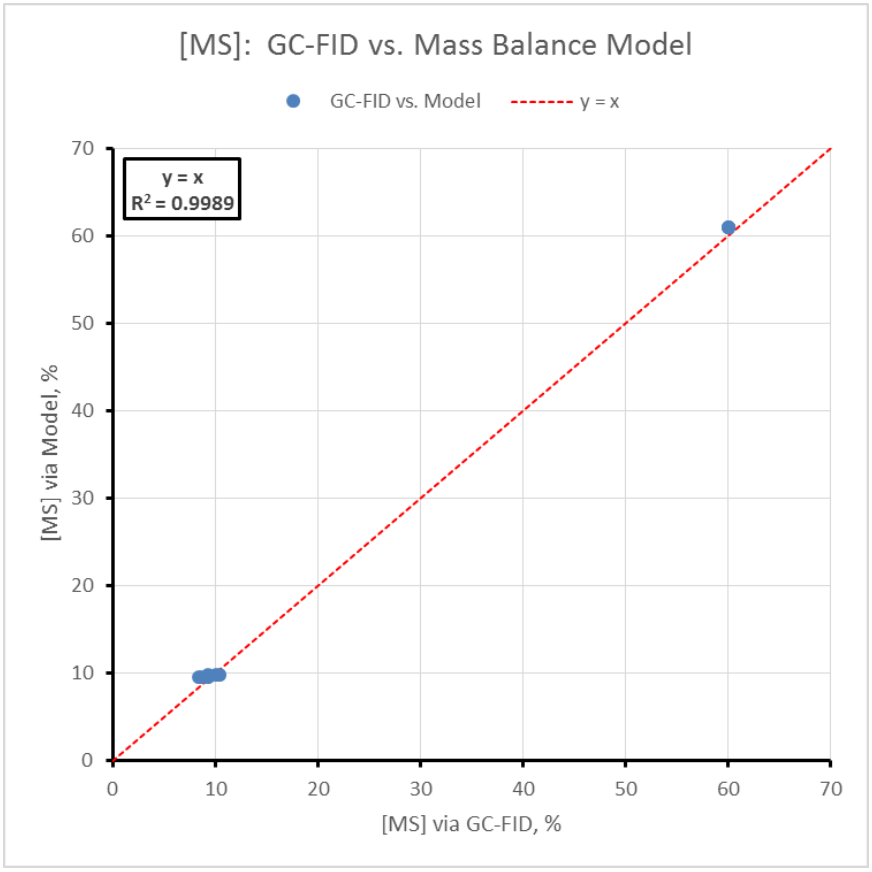

Figure 7.19: Three-phase samples – GC vs. modelling (PDM) results; ($y = x$) fitted to the data.

7.2.3.4. Oil/Water Content of a Sample

Determining the oil and the water content of a sample is desirable for complete sample analysis. However, achieving this is not straightforward because:

1. The oil is a mixture of components, so it cannot be calibrated on the GC, and;
2. The water cannot be detected by an FID detector.

In this work, two approaches were considered for determining the oil and the water contents of a sample. One approach relies on GC data, and the other requires the use of Karl-Fischer (KF) titration. Both are presented below.

The GC Approach to the Oil Content of a Sample

When a sample is injected into the GC, only the oil and the mutual solvent give a signal. The water will not give a signal. The percentage of the total signal (area) due to the mutual solvent can be calibrated. This was attempted and achieved with success. The results are shown in Figure 7.20, Figure 7.21 and Figure 7.22 for the low-end, high-end and full calibrations. The y-axis in these plots is not the theoretical [EGMBE] in a sample (x_{MS}^{S}).

Instead, it is the [EGMBE] in the sample if it were only made up of oil and MS (x_{MS}^{GC}) as shown in 7.12. This is the [EGMBE] that the GC sees w.r.t. the sample as it cannot detect the water.

$$x_{MS}^{GC} = \frac{x_{MS}^{S}}{x_{MS}^{S} + x_{o}^{S}} \quad 7.12$$

When the sample contains no brine, then:

$$x_{MS}^{S} = x_{MS}^{GC} \quad 7.13$$

This means that the % area calibrations can be produced using the same data from the calibrations in the oil, without any additional work required in order to implement this approach.

With this in hand, the determination of the oil content in a sample using this approach is simple. We determine (x_{MS}^{S}) from normal area calibrations and (x_{MS}^{GC}) from % area calibrations. Then, we can calculate the oil content of the sample (x_{o}^{S}) by re-arranging 7.12 to obtain:

$$x_{o}^{S} = x_{MS}^{S} \left(\frac{1 - x_{MS}^{GC}}{x_{MS}^{GC}} \right) \quad 7.14$$

Applying equation 7.14 allows the calculation of the oil content of the sample. The water content of the sample (x_{b}^{S}) will then simply be:

$$x_{b}^{S} = 1 - x_{MS}^{S} - x_{b}^{S} \quad 7.15$$

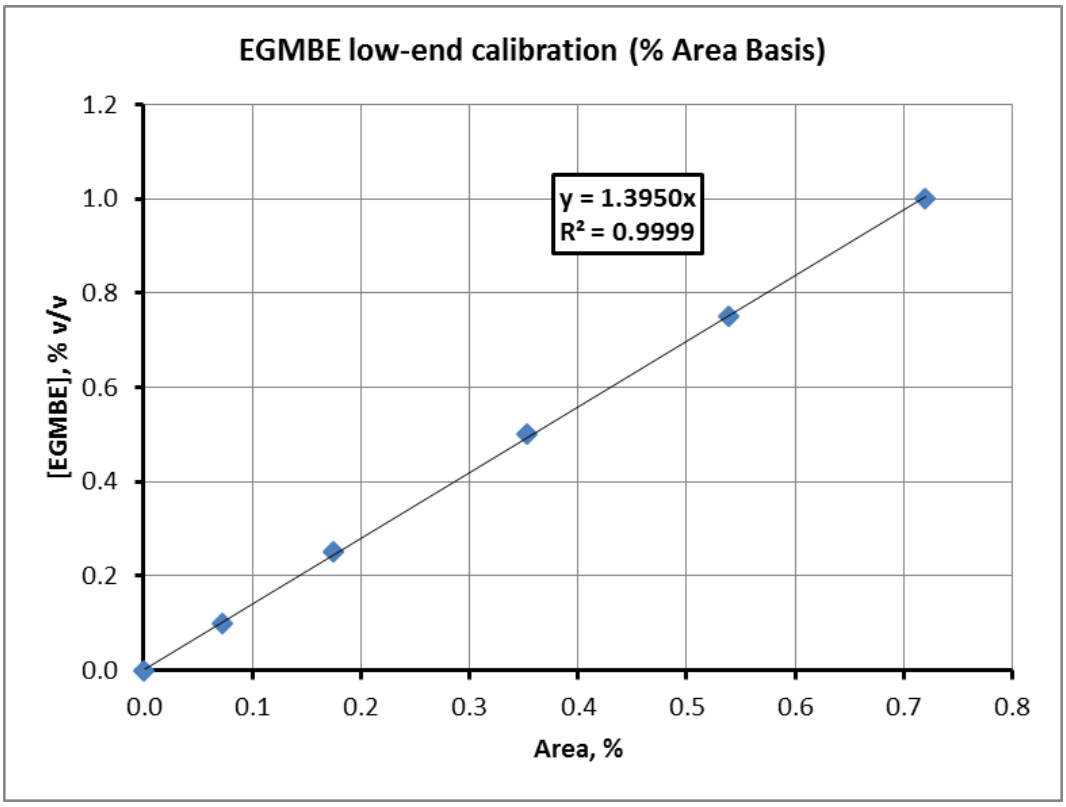

Figure 7.20: Corrected low-end EGMBE calibration on % area basis.

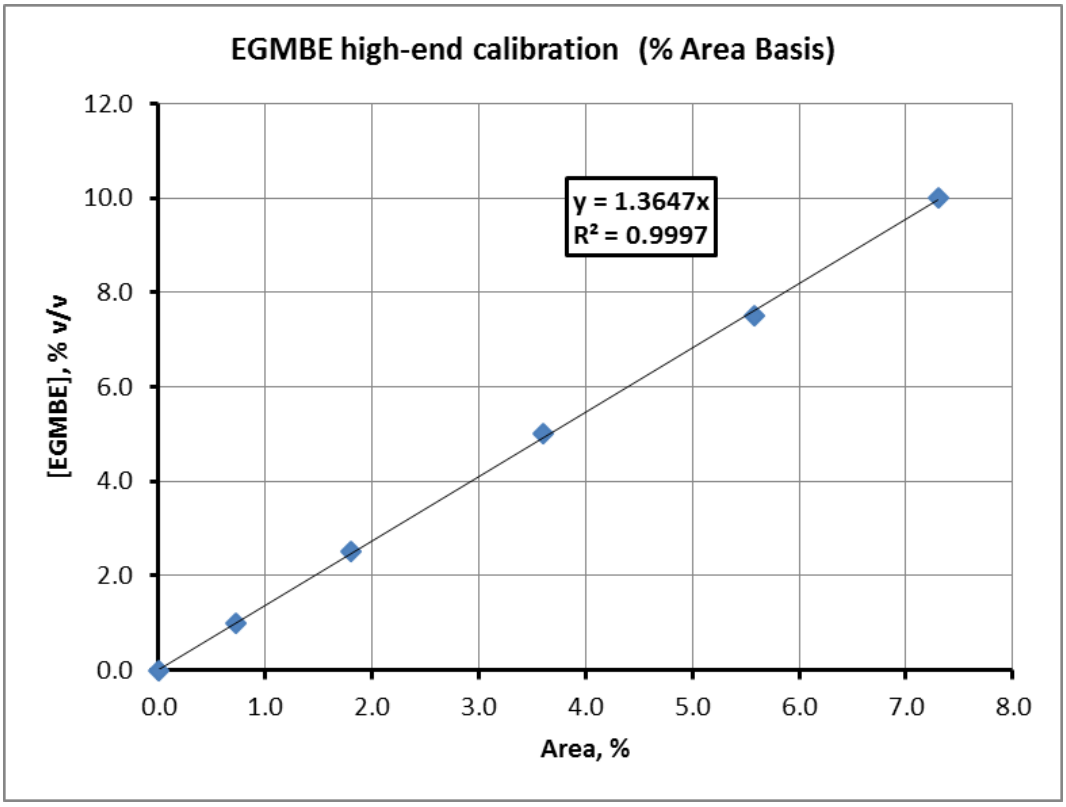

Figure 7.21: Corrected high-end EGMBE calibration on % area basis.

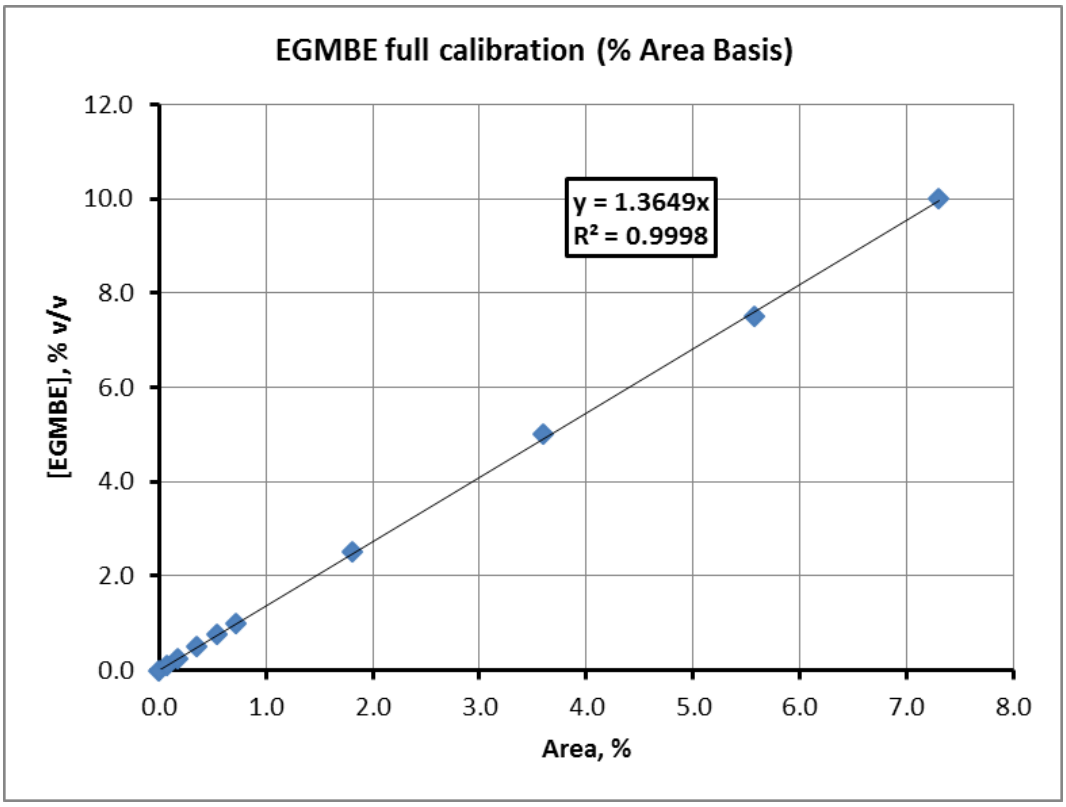

Figure 7.22: Corrected full EGMBE calibration on % area basis.

The approach above was tested for the same samples in section 7.2.3.3. The results are provided in Table 7.16 and Table 7.17 for the two-phase and three-phase samples respectively.

A good agreement is only obtained for brine-rich samples. Otherwise, this approach fails in calculating the oil and the water content of the sample. The application of equation 7.14 amplifies dilution errors massively due to the high dilution factor. Therefore, when the oil content of the sample is high, it becomes impossible to estimate its value using this approach. On the other hand, when the oil content of the sample is low, equation 7.14 defaults to zero (or close to zero) and the brine content of the sample is estimated correctly. For this reason, this approach will only work for brine-rich samples.

A workaround the dilution errors is possible by injecting a neat sample, i.e. without any dilutions, and using the % areas from that injection to determine the oil content of the sample. However, this was not tested due to time constraints on the availability of the GC facilities, and could be the subject of future developments of this work.

Table 7.16: Two-phase samples – calculated vs. modelling results.

Sample	[Multipar H]		Absolute Difference	[NSSW]		Absolute Difference
	Calculated	Model		Calculated	Model	
#	% v/v	% v/v	% v/v	% v/v	% v/v	% v/v
4o	73.3	96.0	22.7	23.7	0.8	-22.8
5o	57.0	94.4	37.4	37.6	0.0	-37.6
4b	0.0	0.0	0.0	93.0	92.9	-0.1
5b	0.0	0.0	0.0	91.9	91.3	-0.6
6b	0.0	0.0	0.0	90.7	88.6	-2.1
8b	0.0	0.0	0.0	89.8	89.9	0.1
9b	0.0	0.0	0.0	90.2	90.4	0.2
6om	8.2	40.8	32.6	41.4	8.5	-32.9
8m	0.0	10.5	10.5	36.7	26.9	-9.7
9m	0.0	15.0	15.0	40.0	24.5	-15.5

Table 7.17: Three-phase samples – calculated vs. modelling results.

Sample	[Multipar H]		Absolute Difference	[NSSW]		Absolute Difference
	Calculated	Model		Calculated	Model	
#	% v/v	% v/v	% v/v	% v/v	% v/v	% v/v
1o	60.8	89.3	28.6	28.8	0.8	-27.9
2o	65.1	89.3	24.2	24.8	0.8	-23.9
3o	59.9	89.3	29.5	30.8	0.8	-30.0
1b	0.0	0.0	0.0	90.7	90.4	-0.3
2b	0.0	0.0	0.0	91.3	90.4	-1.0
3b	0.0	0.0	0.0	91.6	90.4	-1.2
1m	0.0	19.8	19.8	40.0	19.3	-20.7
2m	0.0	19.8	19.8	40.0	19.3	-20.7
3m	0.0	19.8	19.8	40.0	19.3	-20.7

The Karl-Fischer (KF) Approach to the Water Content in a Sample

To analyse a sample using the KF method, the water content of the sample must be at or below 1,000 ppm roughly. This demands a very high dilution of any sample with high water content. The consequences of this is the opposite of what was observed in the GC Approach. Here, it will not be possible to analyse brine-rich samples accurately. This is despite the high precision of the KF method. KF results highlighting this are presented in Table 7.18. For the mutual solvent-rich phase, smaller errors were obtained when using the KF Approach w.r.t. the GC Approach by at least 12%.

Table 7.18: Three-phase samples – calculated vs. modelling results.

Sample	[Multipar H]		Absolute Difference	[NSSW]		Absolute Difference
	KF	Model		KF	Model	
#	% v/v	% v/v	% v/v	% v/v	% v/v	% v/v
Oil-Rich	91.0	89.3	-1.7	0.0	0.8	0.8
Brine-Rich	17.9	0.0	-17.9	73.2	90.4	17.2
MS-Rich	32.9	19.8	-13.1	12.5	19.3	6.8

Note that for KF analysis, it was determined that analysing samples containing mutual solvent is only possible when the concentration of the mutual solvent in the sample is kept below approximately 10% (see Figure 7.23).

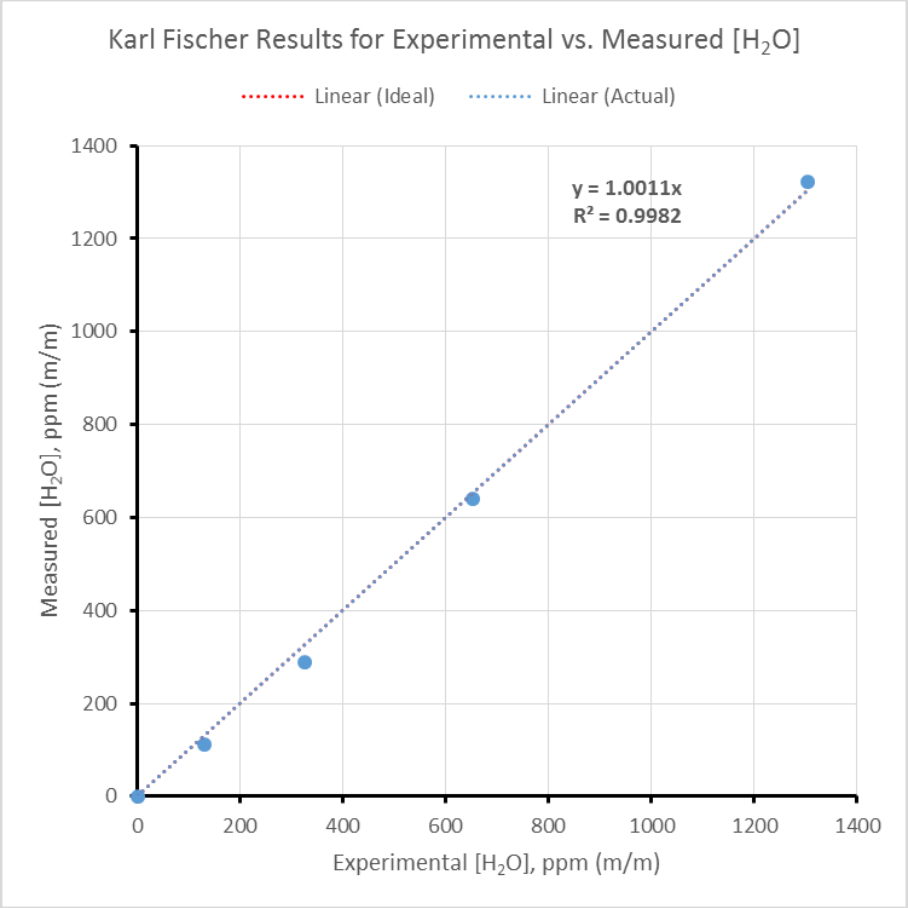

Figure 7.23: Water calibration via the KF in Multipar H (EGMBE ≤10% v/v).

When the mutual solvent concentration is high (see Figure 7.24), a linear calibration cannot be achieved reliably. The reason proposed for this is explained below:

1. The general two-step reaction proposed for the KF (Scholz, 1984) is given by:

$$ROH + SO_2 + R'N \leftrightarrow [R'NH]SO_3R \qquad 7.16$$

$$H_2O + I_2 + [R'NH]SO_3R + 2\,R'N \rightarrow [R'NH]SO_4R + 2\,[R'NH]I$$

2. When Hydranal is used to provide the reagents for this reaction, the group (R) is (CH_3) (Scholz, 1984; Honeywell, 2017).

3. In the presence of EGMBE ($C_4H_9OC_2H_4OH$), the first part of the reaction described by equation 7.16 is affected due to the following reaction taking place:

$$C_4H_9OC_2H_4OH + SO_2 + R'N \leftrightarrow [R'NH]SO_3C_4H_9OC_2H_4 \qquad 7.17$$

4. The reaction above (equation 7.17) has to be slower than the reaction involving methanol (equation 7.16a) due to the long ($C_4H_9OC_2H_4$) chain interfering with the reaction. Therefore, limiting the concentration of EGMBE in a sample is sufficient to allow the KF analysis to be performed without significantly impacting on the results (Figure 7.23 vs. Figure 7.24).

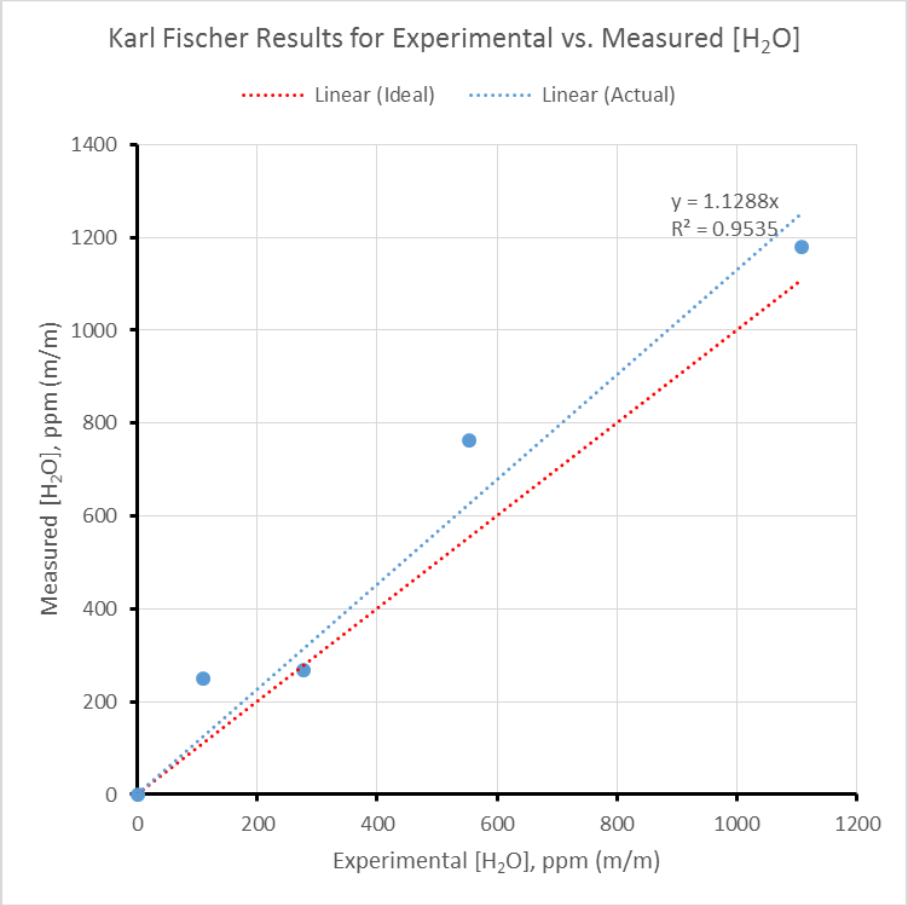

Figure 7.24: Water calibration via the KF in EGMBE.

7.2.3.5. Limitations

Despite the optimisation steps taken here, several limitations remain in the optimised method. The main limitations are:

1. The optimisation only looked at the carrier gas pressure and the temperature programme as adjustable parameters. Other operational parameters such as the carrier gas flowrate, the sample volume and the split ratio were not considered. As such, a further optimisation of the operational parameters may be possible, making the method more attractive for high throughput analysis.

2. Further investigations are required to establish better ways to capture the oil and the water content of a sample for comprehensive sample analysis. Working with the GC Approach without dilutions would be a good starting point for these investigations.

3. The sensitivity of the GC method at low and high concentrations must be further investigated.

4. As it is, this GC method is not suitable for full phase diagram mapping due to the inability to determine the oil/brine concentrations reliably.

7.2.3.6. Comparison of Methods

Table 7.19 compares the three main methods developed as part of this work with the intention of mapping the phase behaviour of oil/brine/mutual solvent systems. The quasi-ternary implementation of the UNIQUAC model (Chapter 6), is the least experimentally demanding of these, and is most suitable for mapping the phase behaviour of these systems for modelling applications. The PDM (Chapter 5) is also suitable for mapping the phase region, but more experimentally intensive due to the requirement of two-phase separation data. This makes it more suitable for sample analysis, e.g. the effluent from a sand-pack/coreflood experiment. The GC-FID method is not suitable for mapping the phase diagram due to difficulties in resolving the oil and brine compositions, and requires further development. However, it is thought to be the most accurate for determining the mutual solvent concentration in a sample and the most sensitive method available. Further developments of this method should make it useful for more advanced application, e.g. effects of mutual solvent adsorption on squeeze treatments. For simple applications (e.g. effluent analysis), the PDM is simpler, reliable and cost effective.

Table 7.19: Comparison of methods for phase behaviour mapping.

Parameter	PDM	UNIQUAC	GC-FID
Key Requirements	- Three-phase separation data - Two-phase separation data	- Three-phase separation data - Two-phase separation data	- Calibrations - Samples in all phase regions - Sample preparation
Type	- Semi-empirical in all phase-regions	- Semi-empirical in the three-phase region only	- Analytical
Mathematical Basis	- Mass-balance model	- Equation of state	- Corrections w.r.t. an internal standard
Output	- Unknown sample analysis - Phase-mapping	- Phase-mapping	- Unknown sample analysis
Estimated Accuracy	- Within 5% accuracy for most phase-mapping applications	- Within 5-10% accuracy for most phase-mapping applications	- Within 1-2% accuracy for MS analysis

7.3. ANALYSIS IN THE PRESENCE OF MUTUAL SOLVENTS

7.3.1. Scope of Work

Analysis of other components in the presence of mutual solvents is essential for transport studies, e.g. sand-packs and core-floods. In this context, two analytical methods are important: Inductively Coupled Plasma – Optical Emission Spectroscopy (ICP-OES) and Ultraviolet/Visible (UV-Vis) Spectrophotometry. Analysis using ICP-OES can use an internal standard to correct for any errors in the measurement, e.g. Yttrium (Y) or Rhodium (Rh). This, coupled with high dilution of the sample or matrix matching is generally sufficient for analysing the ionic content of a sample, e.g. Li^+ tracers used to calculate pore volumes or to track the propagation.

UV-Vis tracers are more problematic. Typically, iodide (I^-), analysed at 230 nm, is used as a tracer in transport studies. However, most mutual solvents have a high UV absorbance at 230 nm. Therefore, (I^-) is not a suitable tracer in the presence of mutual solvents; calibration and analysis will not be possible due to background interferences from the mutual solvent. While the use of (Li^+) can continue to track aqueous phases (with analysis conducted using ICP-OES), a suitable UV-Vis tracer must be identified to track oleic phases in propagation.

Trans-Stilbene (TS), analysed at 316 nm, may be used for tracking the propagation of mineral oil for instance as will be highlighted in section 7.3.2. However, background interferences from mutual solvents continue to be an issue. The work described herein aimed to highlight and to resolve some of the difficulties associated with tracking the propagation in transport studies in the presence of mutual solvents.

UV-Vis tracers are only useful for studies involving mineral oil. When crude oil is used, the crude oil will always constitute background interferences which will prevent any UV-Vis analysis. Therefore, this work will only look at systems in which the oil is clean mineral oil (Multipar H).

7.3.2. Oleic Phase Analysis Using Trans-Stilbene

Multi-wavelength scans for Multipar H and several mutual solvents (EGMBE, DGBE, Ethanol and MEG) are presented in Figure 7.25. These UV-Vis scans were performed in the absence of TS (Figure 7.31). Most of the background interferences due to the mineral oil occur below 250 nm, and below 310 nm for the mutual solvents investigated.

Absorbance is observed for the mutual solvents at higher wavelengths too as illustrated in Figure 7.26.

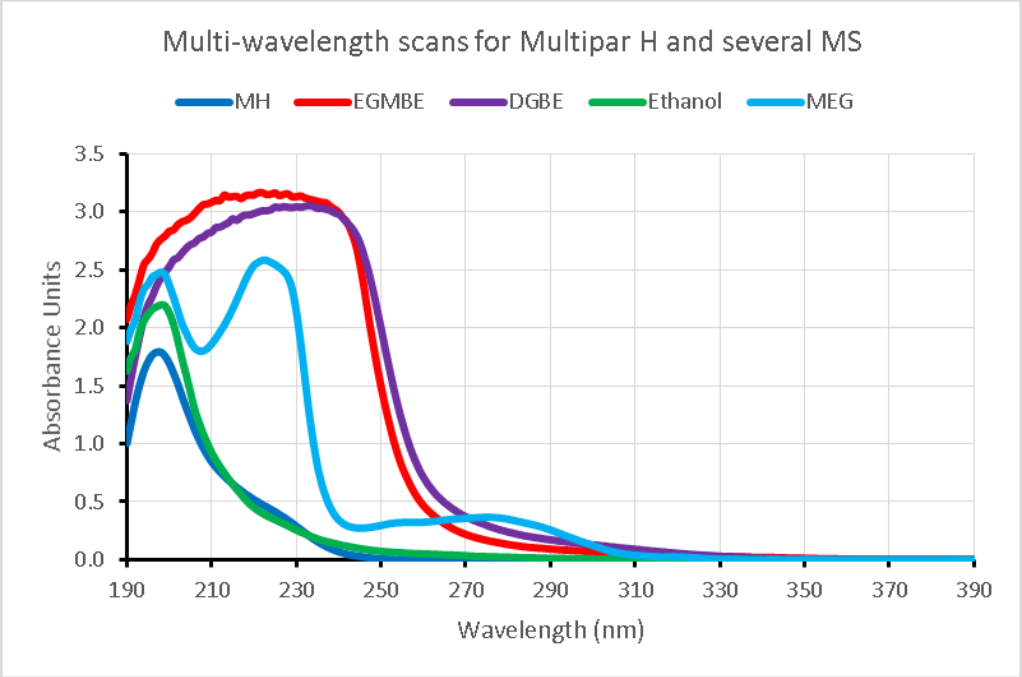

Figure 7.25: Multi-wavelength scans for Multipar H, EGMBE, DGBE, Ethanol and MEG.

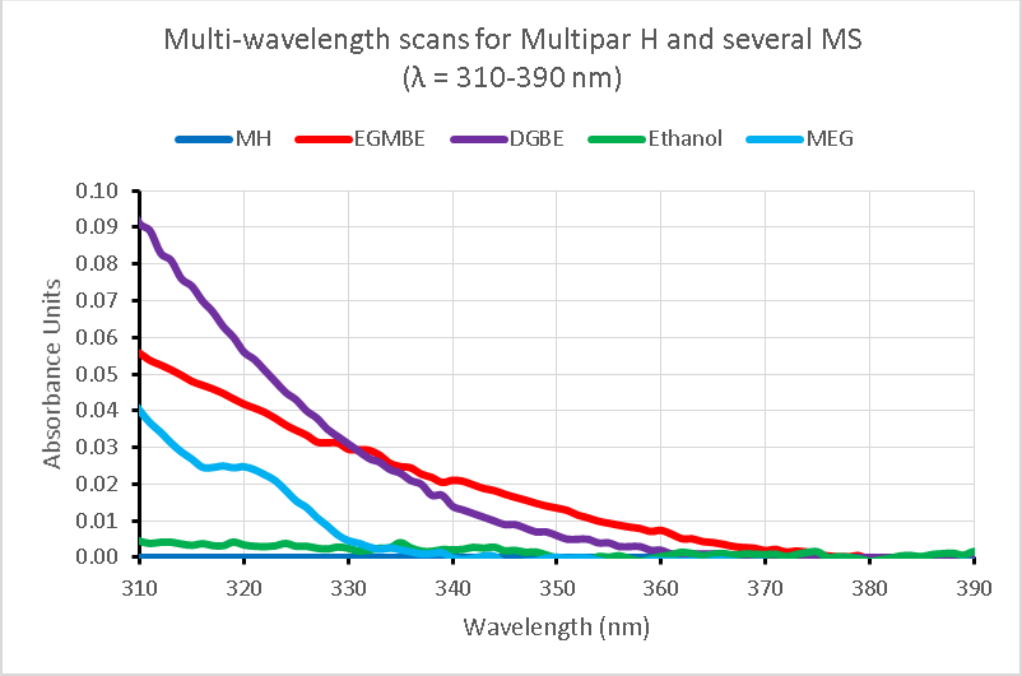

Figure 7.26: Close-up on the wavelength range 310-390 nm in Figure 7.25.

At 316 nm, the wavelength at which TS analysis is performed, measurable background interferences are observed for almost all mutual solvents (Figure 7.26), with EGMBE and DGBE presenting the highest tracer-free absorbance values at 316 nm. The influence of

these background interferences can be illustrated by adding TS to mineral oil and both mutual solvents at 5 ppm. The resulting multi-wavelength scans are provided for EGMBE and DGBE in Figure 7.27 and Figure 7.28 respectively.

Visually, it seems that the curves for the oil and the mutual solvents (both EGMBE and DGBE) overlap at 316 nm in the presence of 5 ppm TS. However, quantitatively, 3.8% and 7.0% differences for EGMBE and DGBE respectively exist between the measurements at this wavelength as highlighted on the plots (Figure 7.27 and Figure 7.28 respectively).

The above-mentioned differences translate to the calibrations of TS. Three matrices were tested for illustrative purposes, namely: 100% oil, 100% mutual solvent and 50%:50% oil to mutual solvent. All calibrations are linear as seen in Figure 7.29 and Figure 7.30. However, the calibration line varies with respect to the matrices. As such, when the concentration of the mutual solvent is not known in an oleic phase, it is not possible to perform quantitative TS tracer analysis via UV-Vis spectrophotometry at 316 nm.

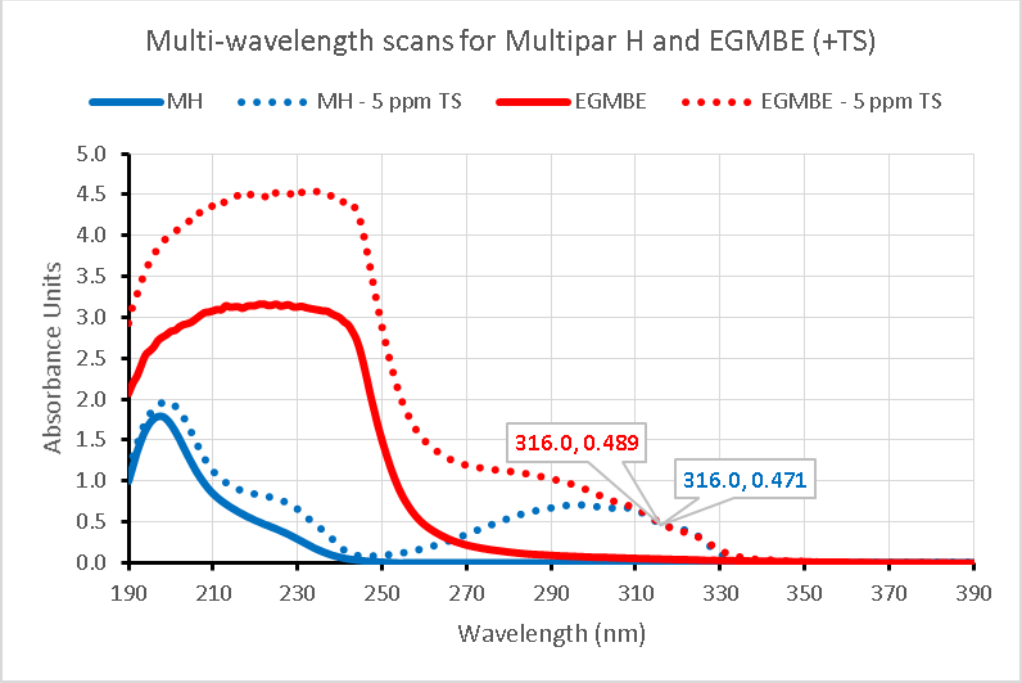

Figure 7.27: Multi-wavelength scans for Multipar H and EGMBE with and without 5 ppm TS.

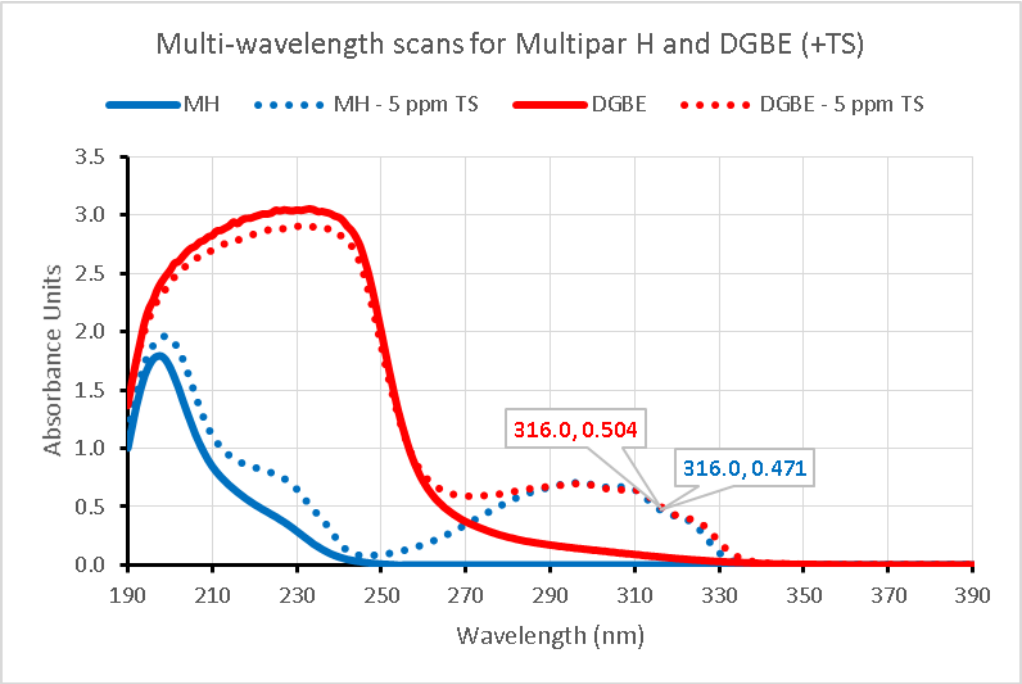

Figure 7.28: Multi-wavelength scans for Multipar H and DGBE with and without 5 ppm TS.

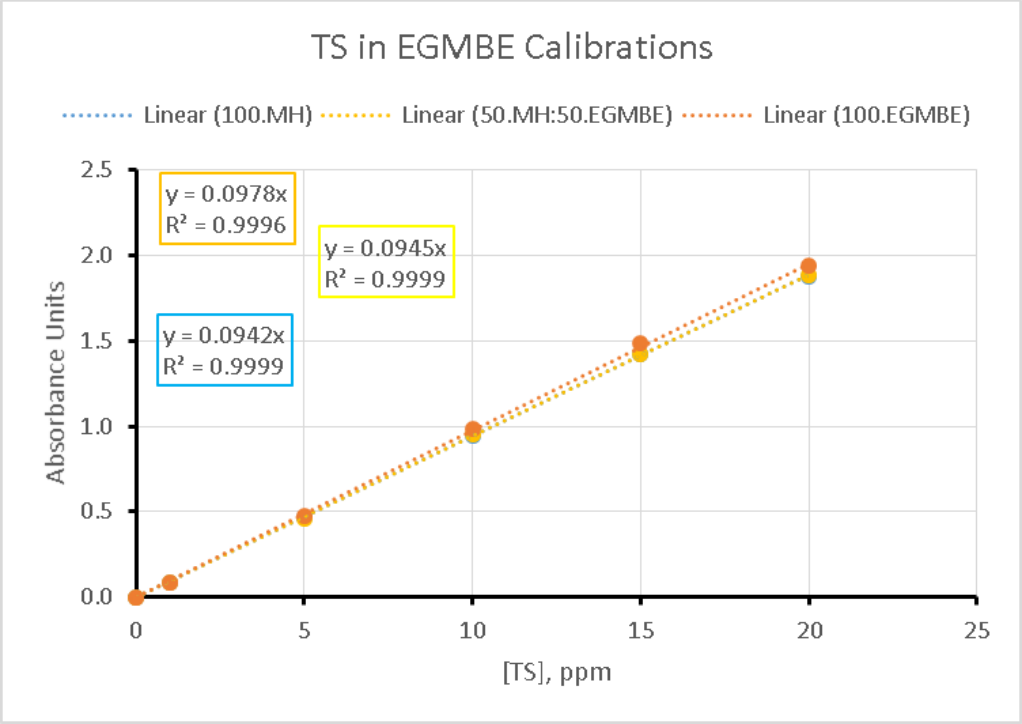

Figure 7.29: TS in EGMBE calibrations for three mixtures.

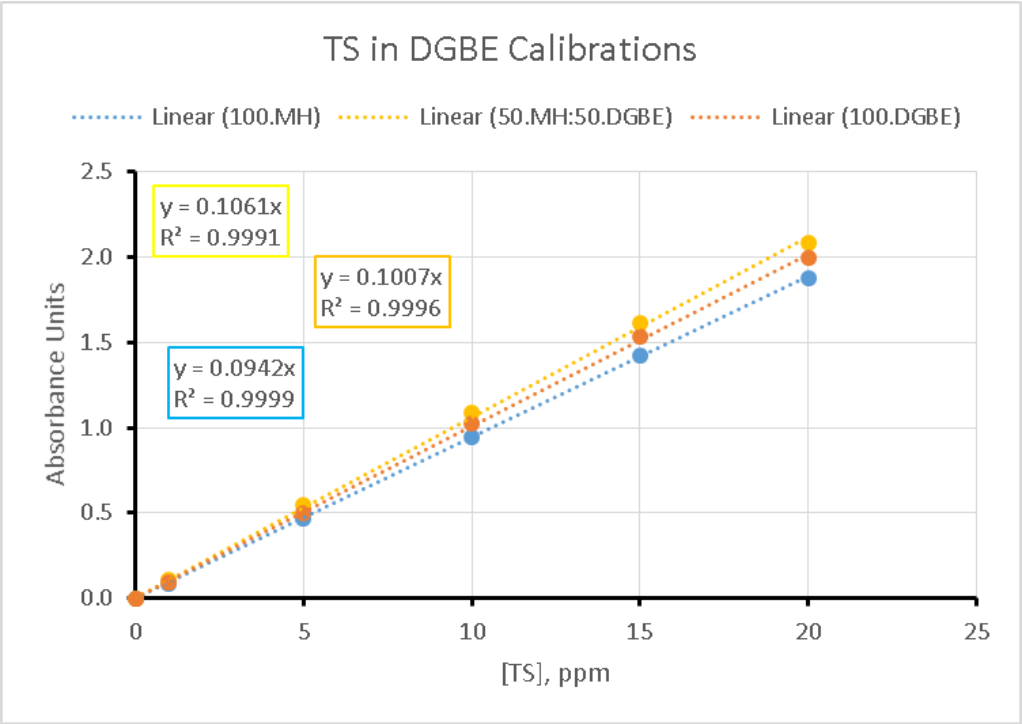

Figure 7.30: TS in DGBE calibrations for three mixtures.

7.3.3. UV-Vis Absorption Theory

The outline of the theory provided in this section is a summary of the detailed explanations provided by: Rao (1974), Skoog, Holler and Grouch (2007) and Harris (2010).

A molecule (M) reaches an excited state (M*) when it absorbs ultraviolet or visible radiation as described by the following reaction:

$$M + E \rightarrow M^* \qquad 7.18$$

Where:

$$E = h\,\upsilon = \frac{h\,c_\infty}{\lambda} \qquad 7.19$$

Absorbance in the near ultraviolet and visible regions (200-800 nm) is primarily due to two different types of electron transitions:

- ($\pi \rightarrow \pi^*$) transition: electrons in a (π) bonding orbital (i.e. in double/triple bonds) are excited to occupy a higher energy antibonding (π^*) orbital.
- ($n \rightarrow \pi^*$) transition: electrons in non-bonded orbitals (i.e. lone pairs) are excited to occupy a higher energy antibonding (π^*) orbital.

($\pi \rightarrow \pi^*$) transition constitutes a bigger energy jump than the ($n \rightarrow \pi^*$) transition. As such, ($\pi \rightarrow \pi^*$) transition will give absorbance at higher wavelengths. By the same logic, increasing delocalisation of electrons reduces the energy required for absorbance, and therefore absorbance occurs at higher wavelengths.

Figure 7.31 presents the molecular structure of TS. The absence of non-bonded electrons means that the absorbance observed in Figure 7.32 is strictly due to ($\pi \rightarrow \pi^*$). With reference to UV-Vis absorption theory, to overcome background interferences due to mutual solvents (e.g. as in Figure 7.27 and Figure 7.28), more absorbance at lower energies and hence higher wavelengths is required. This can be achieved by working with a variant of TS with lone pairs of electrons to achieve ($n \rightarrow \pi^*$) transitions. Alternatively, working with a variant of TS with increased delocalisation of electrons should achieve the same purpose without introducing any ($n \rightarrow \pi^*$) transitions to the absorbance.

The molecule 1,1,2,2-TetraPhenylEthylene (TPE; Figure 7.33) was identified as a suitable candidate. The addition of two phenyl rings to TS allows for absorbance at higher wavelengths than can be obtained with TS (Figure 7.34). TPE has the additional benefits of remaining strictly oleophilic. Moreover, since its structure is comparable to TS, it should be comparably non-adsorbing, making it suitable to be used as a tracer. For this purpose, investigations were conducted to investigate the use of TPE as UV-Vis tracer in the presence of mutual solvents.

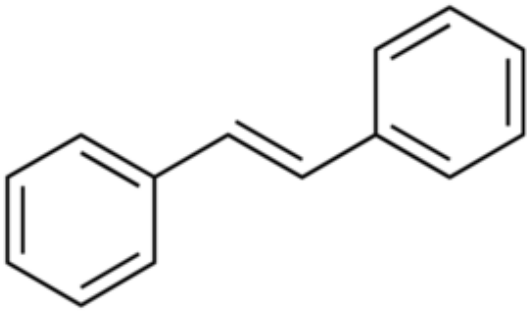

Figure 7.31: Molecular structure of trans-stilbene (TS).

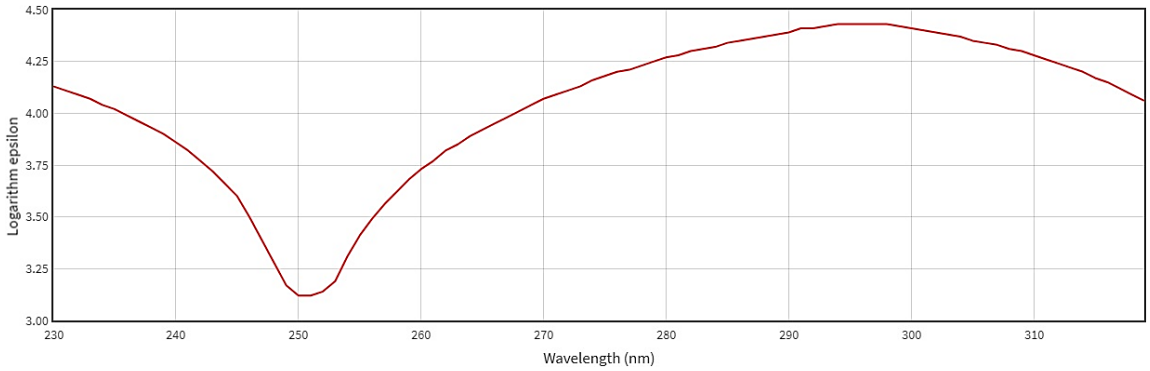

Figure 7.32: UV-Vis spectrum of TS (Rodebush and Feldman, 1946; NIST, 2017).

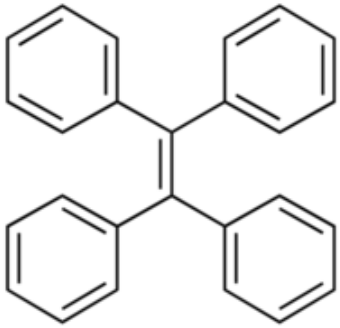

Figure 7.33: Molecular structure of 1,1,2,2-tetraphenylethylene (TPE).

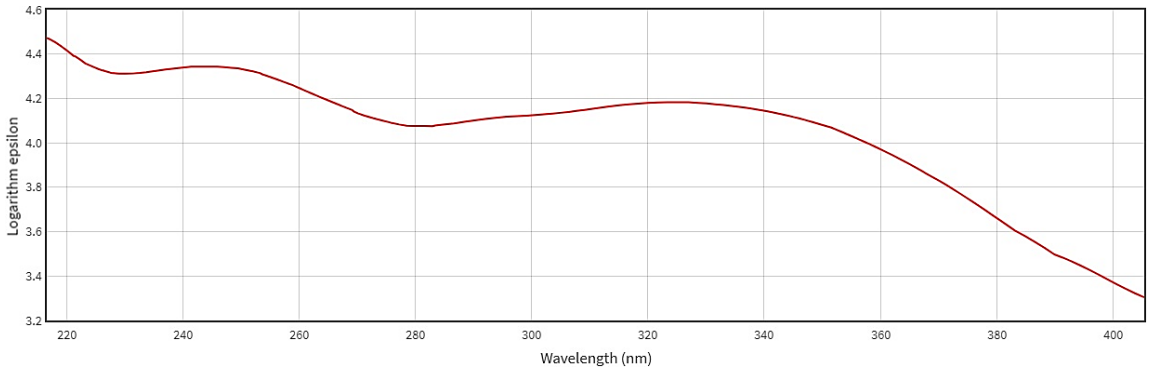

Figure 7.34: UV-Vis spectrum of TPE (Suzuki, 1960; NIST, 2017).

7.3.4. Oleic Phase Analysis Using TetraPhenylEthylene

At 316 nm and 10 ppm, TS gives an absorbance almost three times higher than the absorbance of TPE. The reason for this is the high delocalisation, making it much easier to excite the electrons in the molecule at higher wavelengths instead. Moreover, at this low concentration, the intensity of the absorbance for TPE is undesirably low for the purposes of using it as a tracer.

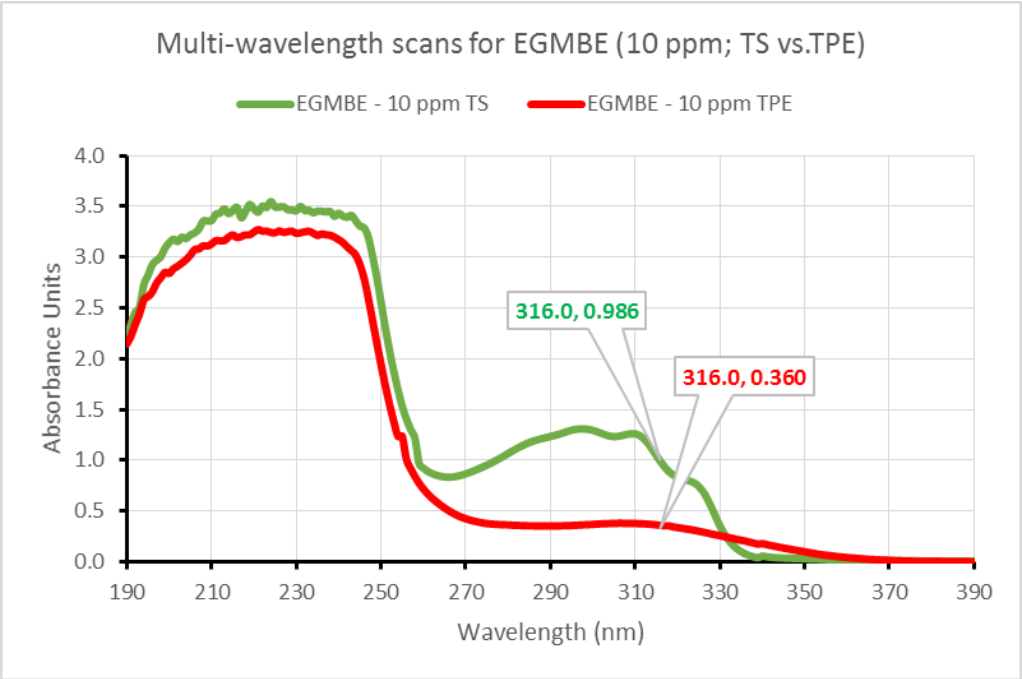

Figure 7.35: Multi-wavelength scans for EGMBE with 10 ppm tracer (TS vs. TPE).

Looking at the absorbance profile for EGMBE with TPE, Figure 7.36 highlights the ability to achieve higher absorbance values at much higher wavelengths at high TPE concentrations. A close up of this plot over the range 370-380 nm (Figure 7.37) indicates distinguishable absorbance values for 1000 ppm TPE; at the same wavelength, the absorbance at 10 ppm TPE is not high enough to allow a propagation curve to be developed (0-10 ppm gives the absorbance range 0-0.008), i.e. at this concentration, TPE will not be useful as an oil phase tracer for transport studies.

TPE cannot be loaded into Multipar H at 1000 ppm (supersaturated solution at room temperature). A saturated solution of Multipar H was found to give the absorbance 0.676 at 375 nm. Assuming no background interferences from the oil/mutual solvent at 375 nm, and with reference to the TPE calibration in EGMBE (Figure 7.38), this equates to roughly 903 ppm saturated TPE concentration in Multipar H at room temperature. Note that the TPE in EGMBE calibrations (low-end, high-end and full range) were all found to be perfectly linear as seen in Figure 7.38.

For the purposes of keeping the TPE concentration in EGMBE low but useful, the TPE concentration can be set at 400 ppm for analytical purposes in the context of propagation studies. The absorbance profile of TPE in Multipar H and EGMBE over the range 350-390 nm is provided in Figure 7.39. Both profiles are identical, and at 375 nm, Multipar H and EGMBE give identical readings as expected. All of this indicates no background

interferences at high wavelengths, and also indicate the suitability of TPE as an oil phase UV-Vis tracer at 400 ppm when the analysis is carried out at 375 nm.

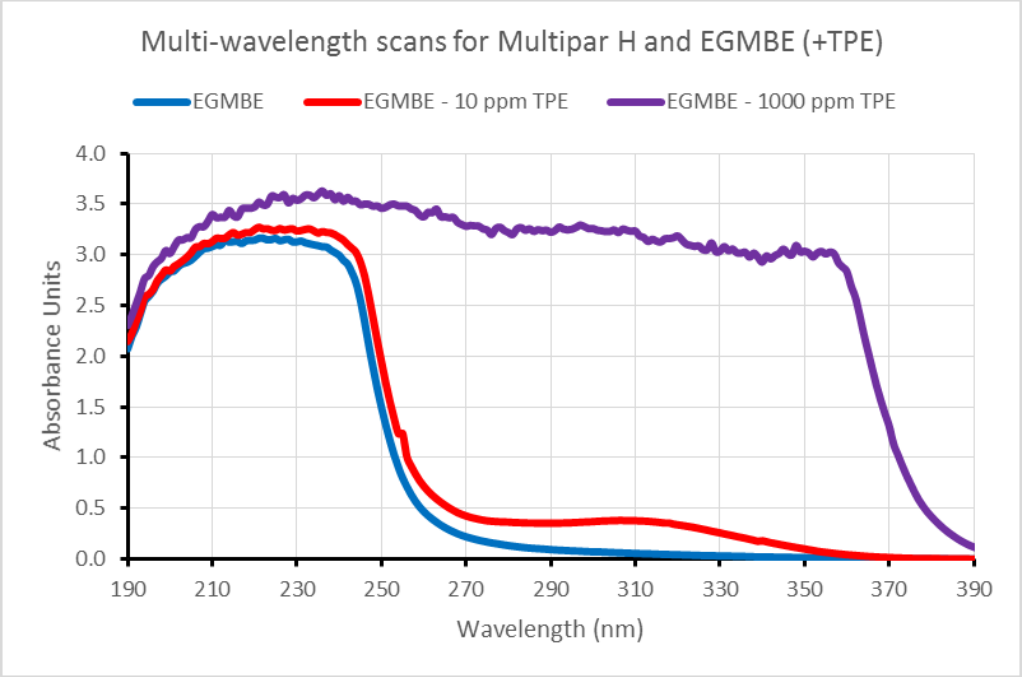

Figure 7.36: Multi-wavelength scans for EGMBE with and without TPE.

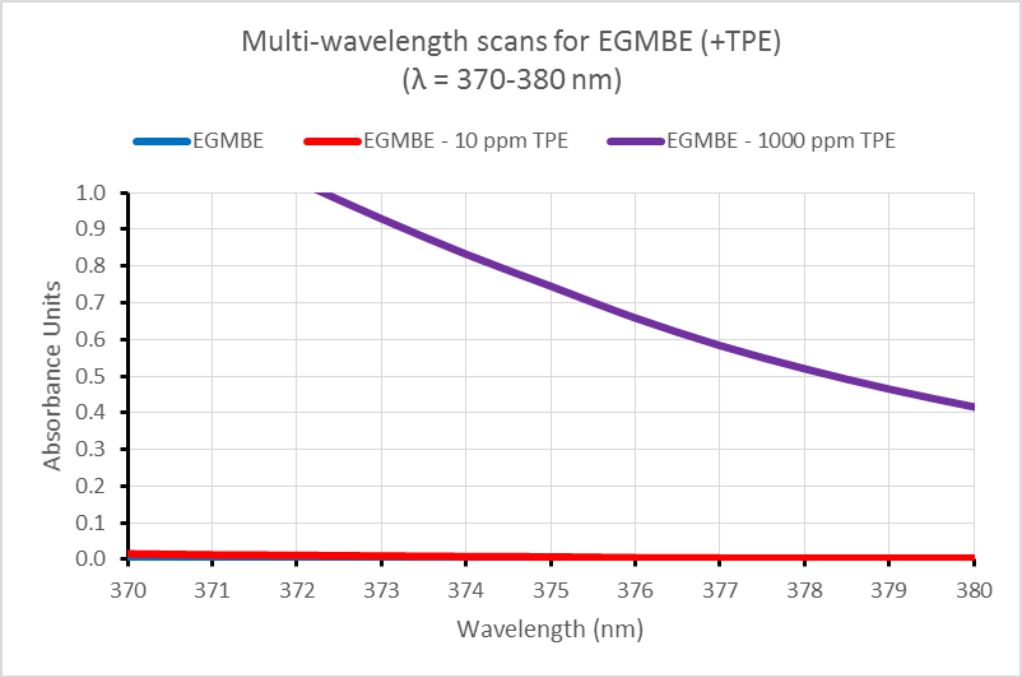

Figure 7.37: Close-up on the wavelength range 370-380 nm in Figure 7.36.

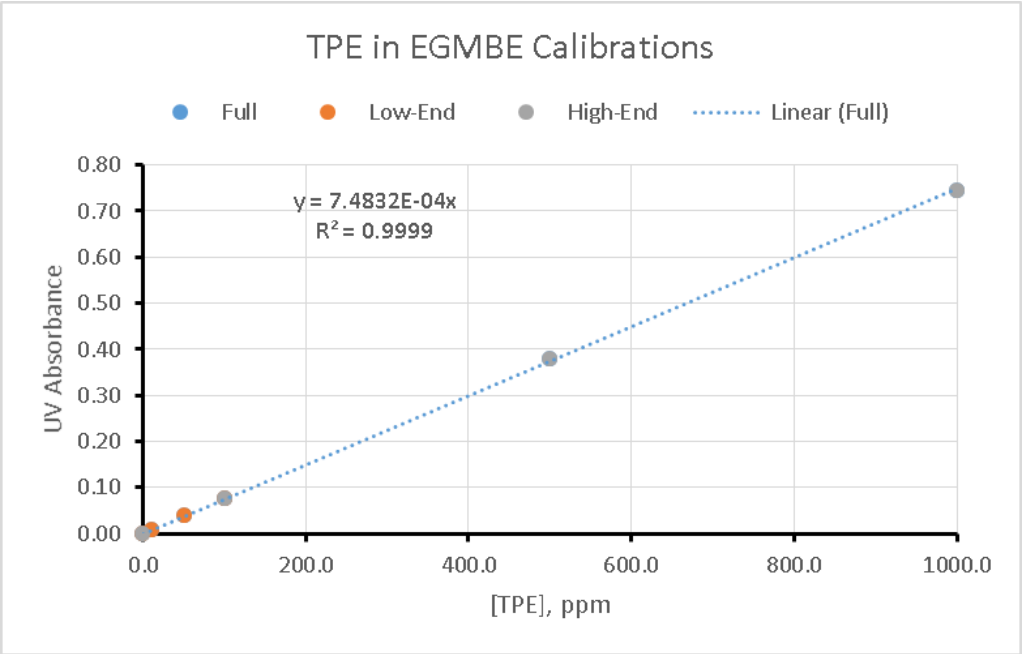

Figure 7.38: TPE in EGMBE calibrations (low-end, high-end and full).

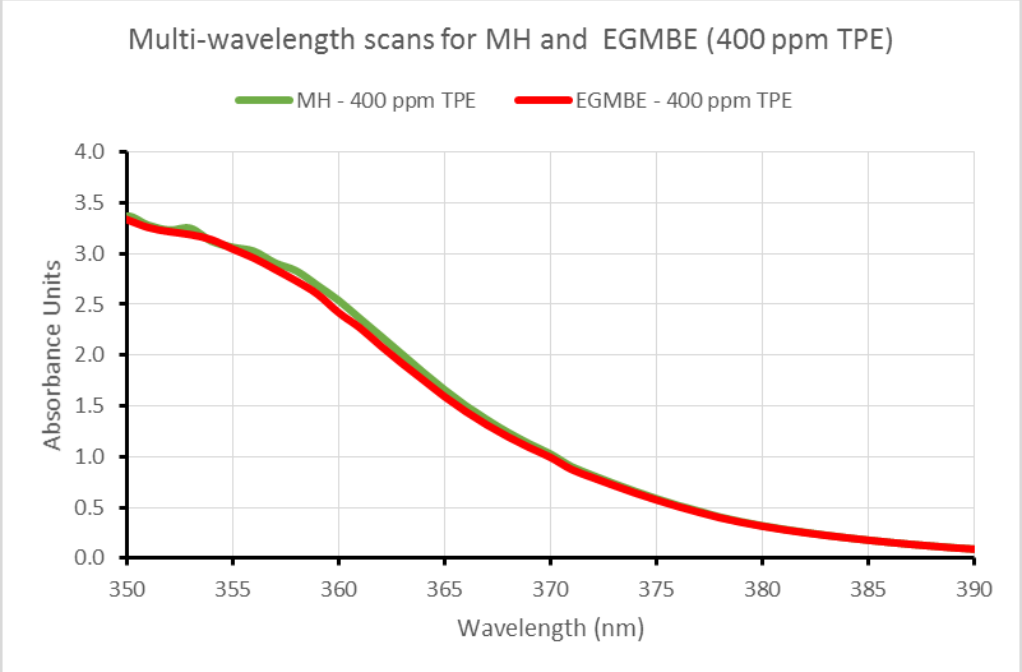

Figure 7.39: Multi-wavelength scans for Multipar H and EGMBE with 400 ppm TPE.

7.4. SUMMARY AND RESEARCH SIGNIFICANCE

The findings in this chapter can be summarised in the following points:

- A GC-FID method for analysing the mutual solvent concentration in a sample was investigated and optimised successfully. The optimised version of this method is suitable for practical application, whereas the original version was impractical.

- The GC-FID method cannot be extended reliably to analyse for the oil/brine content of a sample due to the FID detector used in this work. Workarounds are possible as demonstrated in this work. However, further method development is required.

- The results from the GC-FID method is in excellent match with the results from the PDM (Chapter 5) for the system Multipar H/NSSW/EGMBE. By extension, the quasi-ternary implementation of the UNIQUAC model (Chapter 6) will also compare very well to the GC-FID results.

- Trans-stilbene cannot be used as a UV-Vis tracer for analysis involving MS. An alternative tracer (Tetraphenylethylene) was identified and demonstrated as a suitable alternative through successful application of UV-Vis absorption theory.

Chapter 8: Propagation of Mutual Solvents in Single and Multi-Phase Systems

8.1. OVERALL AIMS AND OBJECTIVES

The aim of the studies outlined in this section is to provide a preliminary understanding for how the phase interactions in oil/brine/mutual solvent systems influence their transport. Thorough transport investigations are beyond the scope of this work due to the grand nature of such endeavour. However, such investigations have been enabled by the developments in mutual solvent research as part of this work, and should be the focus of any future studies.

The transport studies outlined here will apply the techniques in the previous chapters to shed some light on mutual solvent transport in oil/brine systems. Two questions will be considered:

1. What is the observed effect of the partition coefficient of a mutual solvent on the oil/brine displacement?

2. What is the influence of three-phase flow on oil displacement as opposed to two-phase flow alone?

To answer these questions, a baseline will be provided for the transport of the mutual solvents in the absence of oil. Once this is achieved, two- and three-phase displacements will be investigated.

As mentioned earlier, this chapter will incorporate applications from previous chapters of this work. Examples include: the analytical approach from Chapter 4, the Phase Displacement Method from Chapter 5, the quasi-ternary implementation of the UNIQUAC model from chapter 6, and the tetraphenylethylene oil phase tracer from Chapter 7. The value of these implementations will be demonstrated on phase behaviour plots illustrating the propagation of the mutual solvent and the displacement of the oil and brine.

8.2. SINGLE-PHASE DISPLACEMENT TESTS

8.2.1. Experimental Method

The single-phase displacement tests involve three mutual solvents. Ethanol which partitions with intermediate affinity to water ($\log_{10} P_{o/w} = -0.30$) is the base case mutual solvent. EGMBE ($\log_{10} P_{o/w} = 0.80$) was used to study the influence of increased oil affinity of the mutual solvent on the transport, and MEG ($\log_{10} P_{o/w} = -1.40$) was used to study the influence of increased water affinity of the mutual solvent on the transport.

To achieve single-phase systems, all single-phase displacements were strictly binary, i.e. no oil used to avoid oil/water immiscibility. Moreover, the North Sea Seawater brine used was sulphate-free (SFSW) to prevent any brine/mutual solvent immiscibility (Chapter 3). Therefore, any mixtures forming within a sand-pack as the brine displaces the mutual solvent and vice versa should be single phase mixtures.

Additional physical properties of the mutual solvents and the brine used are provided in Table 8.1. The wide variations in densities/viscosities of the mutual solvents with respect to the brine are typically encountered and constitute an additional parameter that will influence the displacements.

Table 8.1: Physical properties of the solutions/solvents used in the experiments at 20°C and 1 atm.

Constituent	Density, kg/m^3	Viscosity, cP
SFNSSW	1024.6	1.074
Ethanol	789.5	1.200
EGMBE	902.0	5.310
MEG	1115.0	21.000

The flooding plan in single-phase displacement tests is outlined in Figure 8.1. It involves three stages during which the permeability of the sand-pack is evaluated: the pre-MS stage (step 2), the MS stage (step 7) and the post-MS stage (step 10). Ultraviolet-Visible (UV-Vis) spectrophotometry was incorporated in the work. Iodide was used to track the brine propagation/displacement at 230 nm, and Trans-Stilbene (TS) was used to track the mutual solvent propagation/displacement at 316 nm. UV-Vis analysis was done in-line. Lithium was used to track transitions from seawater to mutual solvent and vice versa (step 4 and step 8). Lithium was analysed using Inductively Coupled Plasma – Optical Emission Spectroscopy (ICP-OES) analysis.

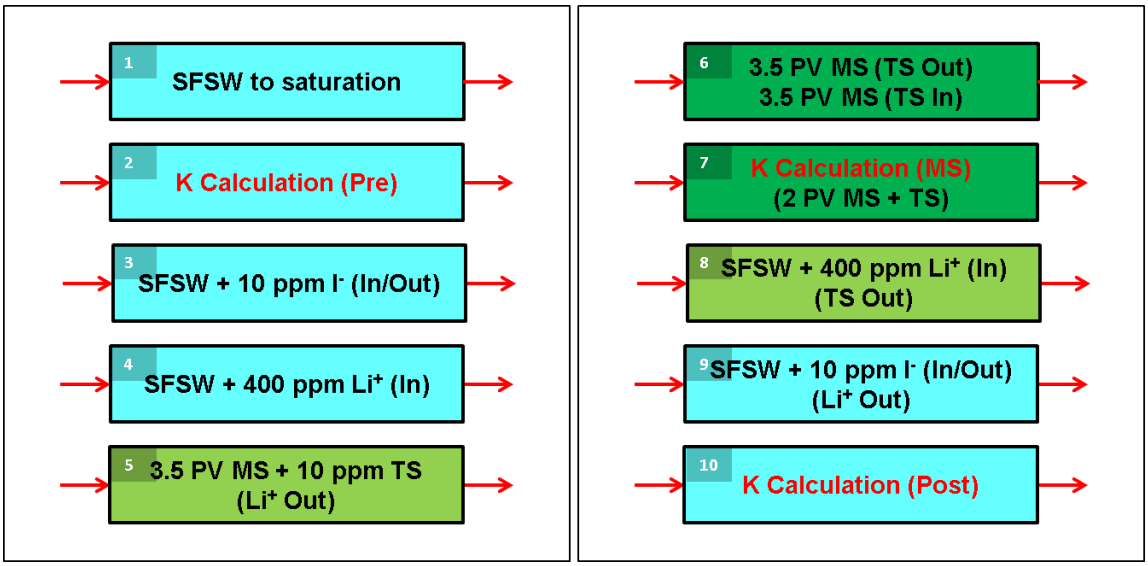

Figure 8.1: Flooding plan for the single-phase displacement tests.

A schematic of the experimental setup is provided in Figure 8.2. Properties of the sand-pack are provided in Table 8.2. Note that the sand-pack has a maximum pressure limit of 50 psi.

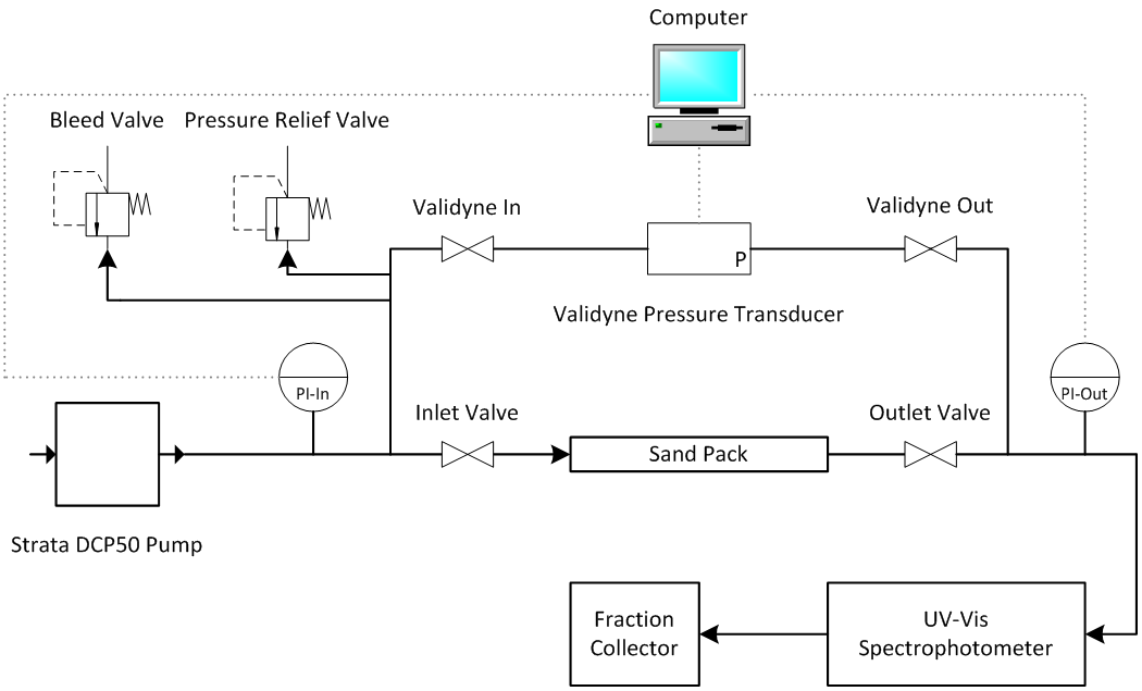

Figure 8.2: Schematic of the experimental setup of the sand-pack.

Table 8.2: Properties of the sand-pack.

Parameter	Details
Material	Fine silica sand; Minerals Marketing Ltd, 120 µm average particle size
Diameter (cm)	1.490
Length (cm)	19.250

The dead volume of the system was calculated at both the UV-Vis Spectrophotometer and the Fraction Collector using both iodide and lithium. The results are provided in Figure 8.3 and Table 8.3. These results will be used as a basis to correct for time delay in all subsequent propagation plots. The tracer in/out profiles are consistent as seen in Figure 8.3.

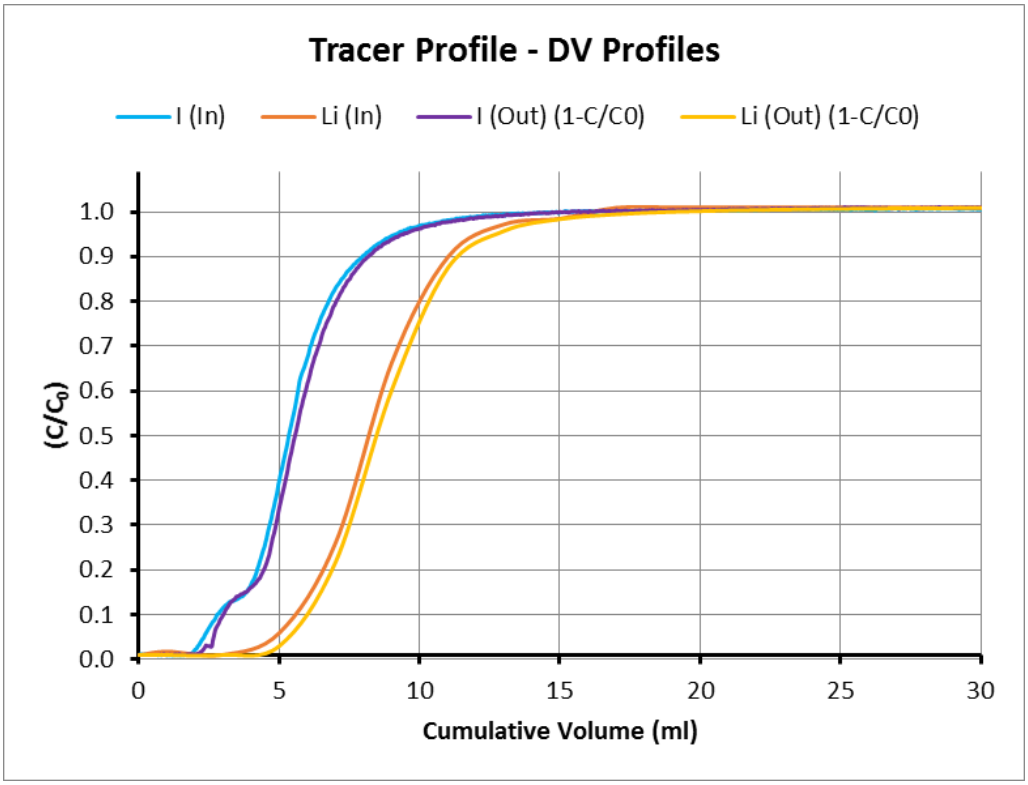

Figure 8.3: Tracer profiles for the calculation of the dead volumes.

Table 8.3: Dead volumes at the UV-Vis and the Fraction Collector.

Data	DV	DV Difference	Average DV	Notes
	ml	ml	ml	
I^- (In)	5.76	0.20	5.69	@ UV-Vis
I^- (Out)	5.96			
Li^+ (In)	8.42	0.47	8.49	@ Fraction Collector
Li^+ (Out)	8.89			

8.2.2. Base Case Mutual Solvent: Ethanol

The base case will be discussed in detail, following the steps outlined in Figure 8.1, in order to illustrate the procedure and the verification steps incorporated within this work. In the other cases, only the key results will be highlighted.

Figure 8.4 shows consistency between the in/out iodide tracer profiles pre-MS injection. This is done to ensure repeatability of the PV calculated at this stage (Figure 8.1; step 3). Figure 8.5 shows the consistency between the iodide and the lithium tracer profiles for the same stage (Figure 8.1; step 4). This provides further confidence in the PV calculated for the pre-MS injection stage, and highlights consistency between the results obtained from UV-Vis analysis and ICP-OES analysis. The PV via the iodide and the lithium at the pre-MS injection stage was found to be 14.05 ml and 14.00 ml respectively. These will be used as the reference PV for the sand-pack for all subsequent analysis for the base case.

The displacement of the SW by the MS (Figure 8.1; step 5) shows a reduction in the PV available to the MS flow by 0.85 ml after 3.5 PV of MS injected, i.e. 6.1% residual SW after 3.5 PV MS injected. The profiles of the calcium and magnesium follow the profile of the lithium (Figure 8.7) indicating no retention of these ions at this stage. The TS tracer injected with the MS in step 5 shows more interesting behaviour (Figure 8.8; TS original). The ($C/C_0 > 1$) are thought to be due to mobilisation of fines. Fine sand particles were observed in the samples collected using the fraction collection during this stage. Furthermore, repeating step 5 at the end of the experiment (Figure 8.8; TS repeat) showed a lower degree of UV-Vis absorbance denoting ($C/C_0 > 1$) values. Incomplete mixing between the MS and the SW as they mix, and thus the formation of pseudo-phases may also contribute to this effect. However, this is thought to be a very small contribution in this case, if at all present, since performing the opposite procedure (i.e. displacing MS by SW; Figure 8.11) does not exhibit the behaviour seen in Figure 8.8 for the TS. Normalising ($C/C_0 > 1$) values and assuming 0.2 PV dispersion to allow PV estimation via the TS, the results obtained are consistent with those obtained from the lithium profile (13.26 ml vs. 13.15 ml respectively).

The tracer profiles during the MS injection stage (Figure 8.1; step 7) shows the stripping of the remaining SW in the sand-pack. This is observed as enhanced dispersion during the MS injection stage (Figure 8.9). Diluting the samples at the tail end of these profiles (1.3-2.7 PV) with mineral oil shows water dropout (Figure 8.10), thereby confirming the enhanced dispersion observed in Figure 8.9. The enhanced dispersion despite the absence of oil in the system (i.e. no competitive oil/water displacement) is likely due to the density differences between the brine and the MS (235.1 kg/m^3 difference; Table 8.1). The brine at the top layer of the horizontal sand-pack is thought to be displaced more efficiently than brine at the bottom layer due to some degree of gravity separation, causing the brine at the lower part of the sand-pack to be stripped more slowly.

The displacement of the MS by the SW (Figure 8.1; step 8) is shown in Figure 8.11. No evidence of mobilisation of fines in this case is observed, which may be related to the viscosity effects. Although there is qualitative agreement between the tracer profiles for lithium and TS, there is roughly 1 ml difference in the PV calculation. The results for the calcium and the magnesium are in agreement with the lithium results (Figure 8.12). Therefore, mixing of ethanol/brine must be interfering with the TS measurement. Moreover, comparing Figure 8.6 and Figure 8.13 reveals more efficient displacement happening when SW displacing MS than the opposite displacement (1.9% residual MS vs. 6.1% residual SW after 3.5 PV injection). This is helped by the density differences and the viscous fingering happening in the unstable displacement in the case of MS and SW (Table 8.1).

The characterisation of the sand-pack post-MS injection (Figure 8.1; step 9) indicates an increase in the final PV by approximately 0.3 ml with respect to the PV pre-MS injection (Figure 8.14; Figure 8.15; 14.38 ml and 14.31 ml via iodide and lithium respectively). While this is within experimental error, part of this PV increase must be due to the fine mobilisation discussed before (Figure 8.1; step 5).

A summary of all PV measurements is provided in Table 8.4. As for the permeabilities, a summary of the results for all pure solvent stages (Figure 8.1; step 2, step 7 and step 10) are provided in Table 8.5. A reduction of permeability by roughly 200 mD is observed overall. This may be due to the fine mobilisation causing smaller pores to block, and it may be indicative of potential formation damage that is independent of the brine chemistry. In any case, these differences are not large enough to warrant any conclusive findings, and studies with cores at higher pressures are more appropriate to investigate this aspect.

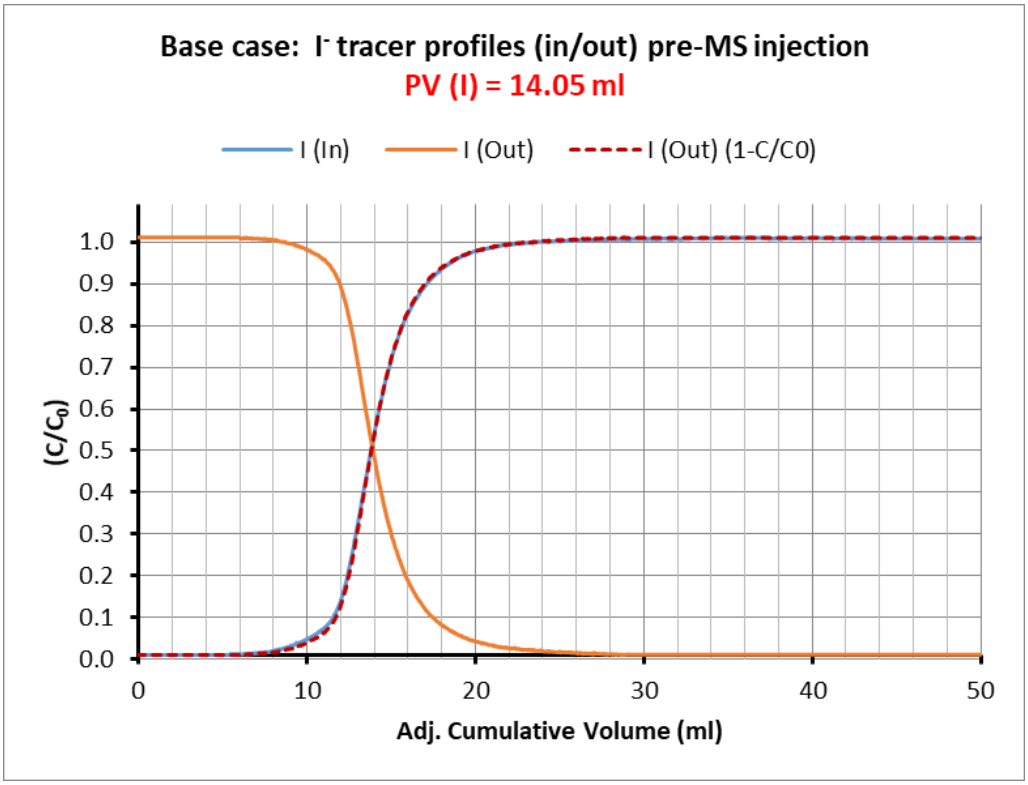

Figure 8.4: Base case iodide tracer profiles (in/out) pre-MS injection.

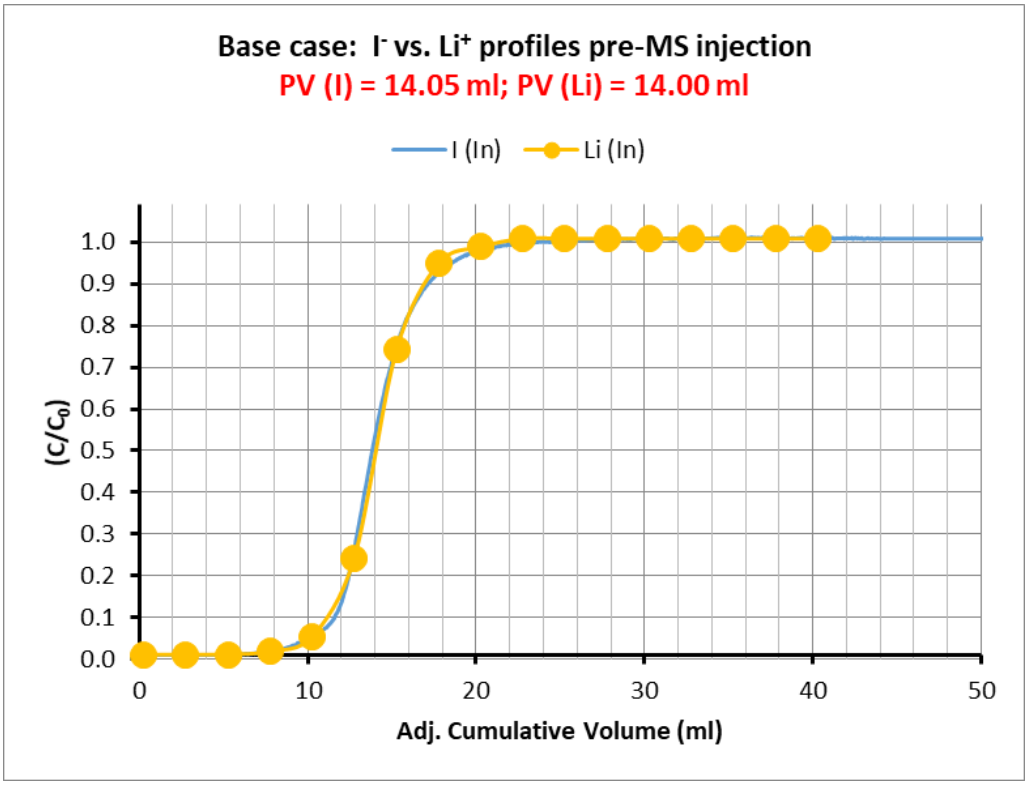

Figure 8.5: Base case iodide vs. lithium profiles pre-MS injection.

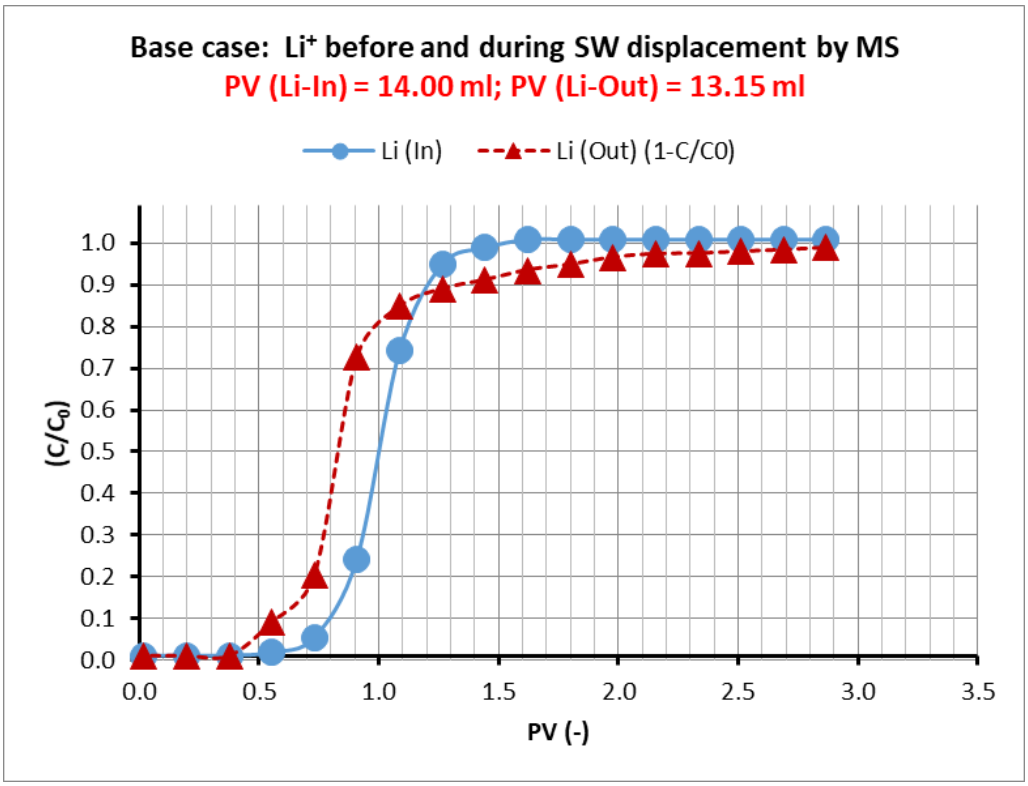

Figure 8.6: Base case lithium profiles pre-MS injection (in) and as MS displaces SW (out).

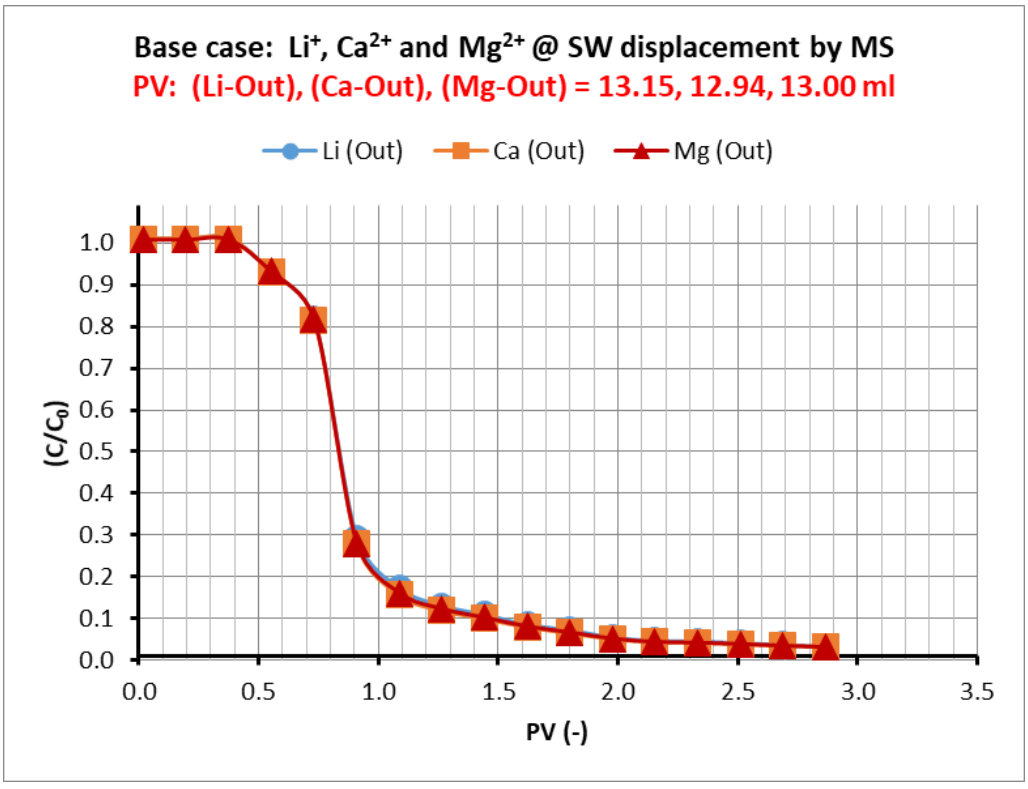

Figure 8.7: Base case lithium/calcium/magnesium as MS displaces SW.

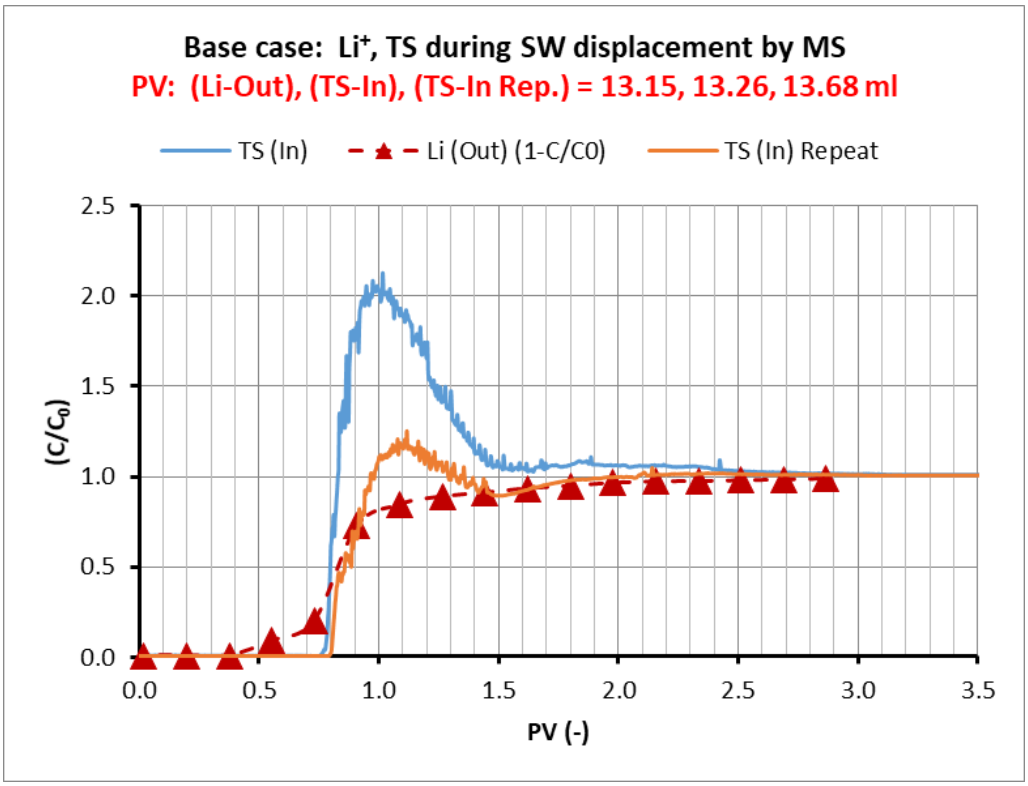

Figure 8.8: Base case lithium and trans-stilbene as MS displaces SW.

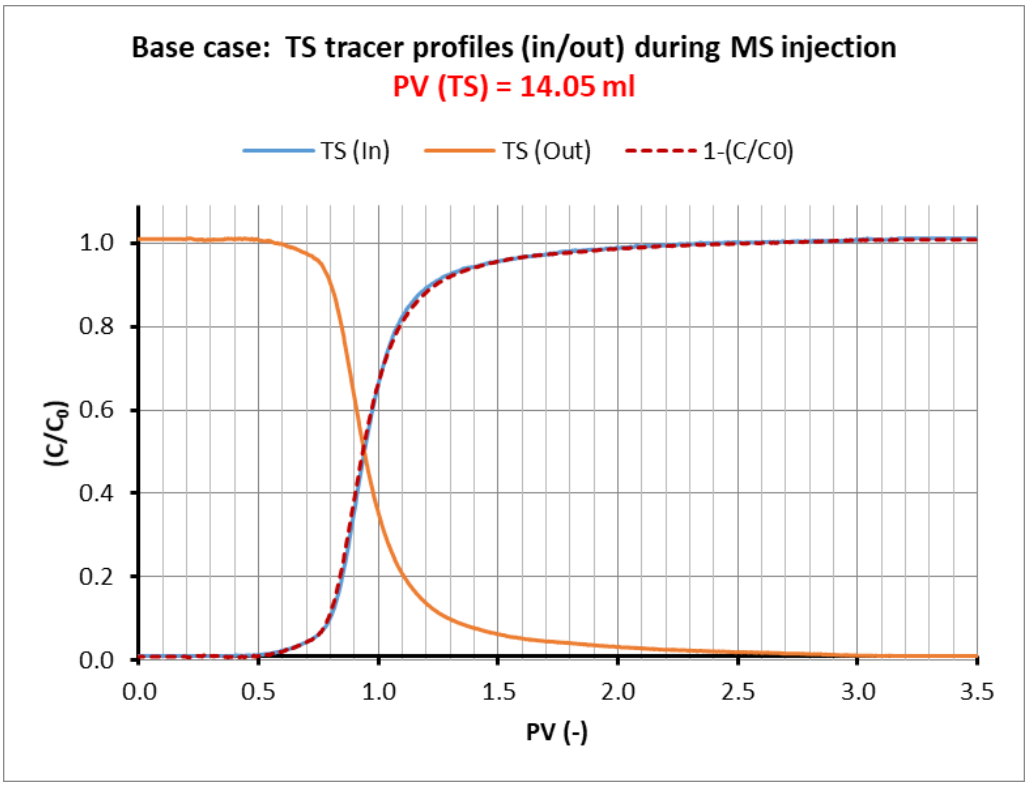

Figure 8.9: Base case trans-stilbene tracer profiles (in/out) during MS injection.

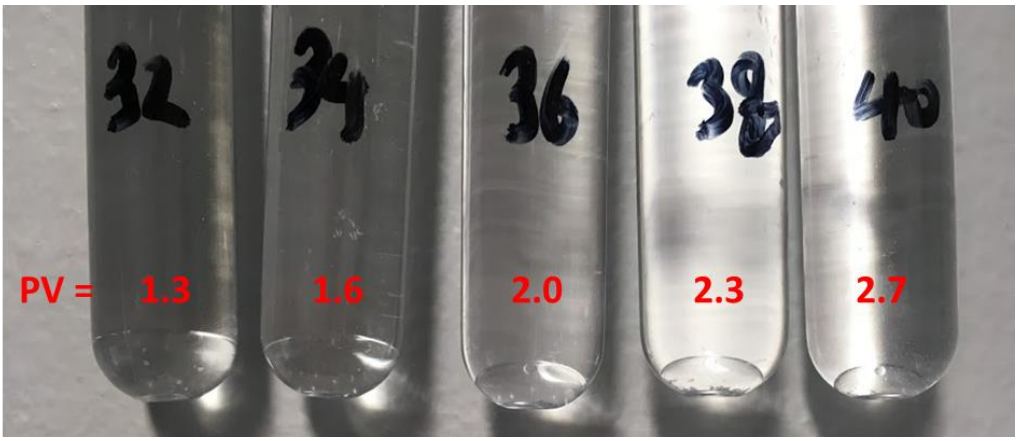

Figure 8.10: Water dropout in selected MS samples diluted × 10 with mineral oil.

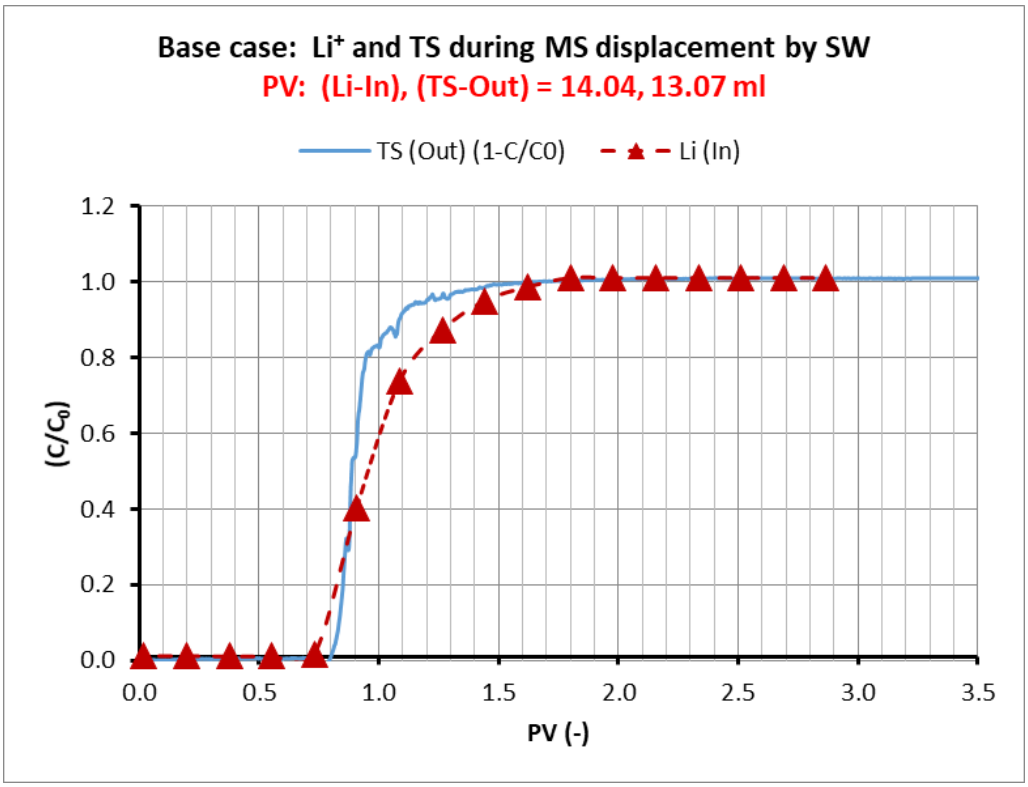

Figure 8.11: Base case lithium and trans-stilbene as SW displaces MS.

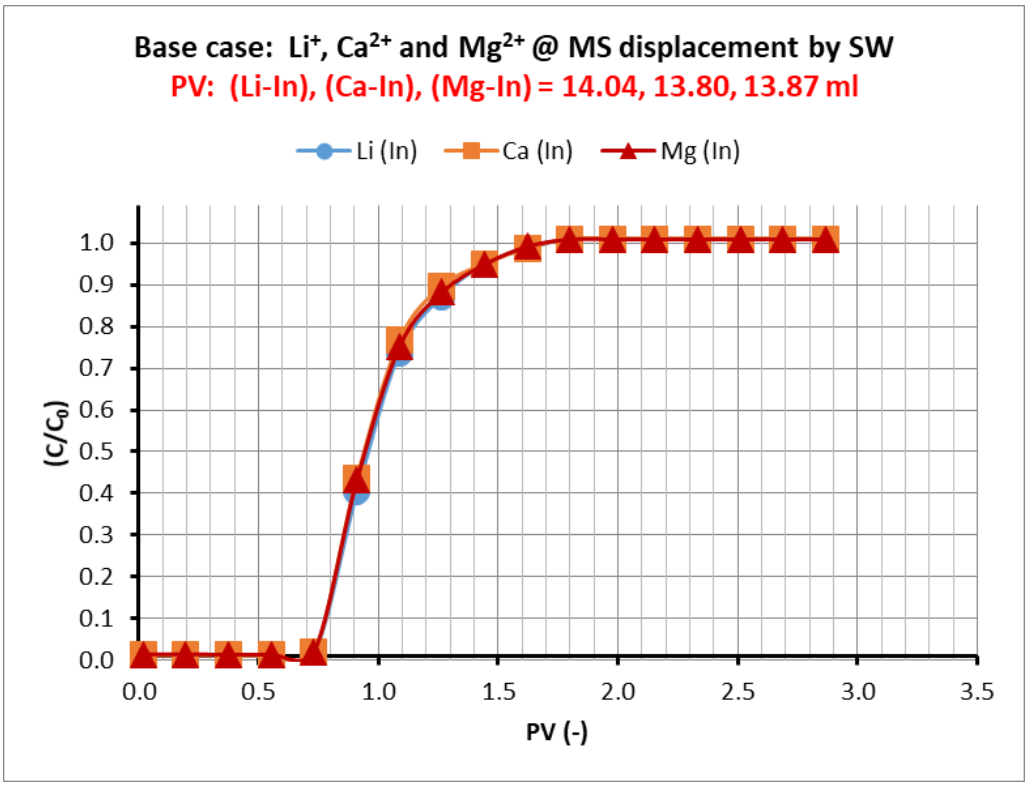

Figure 8.12: Base case lithium/calcium/magnesium as SW displaces MS.

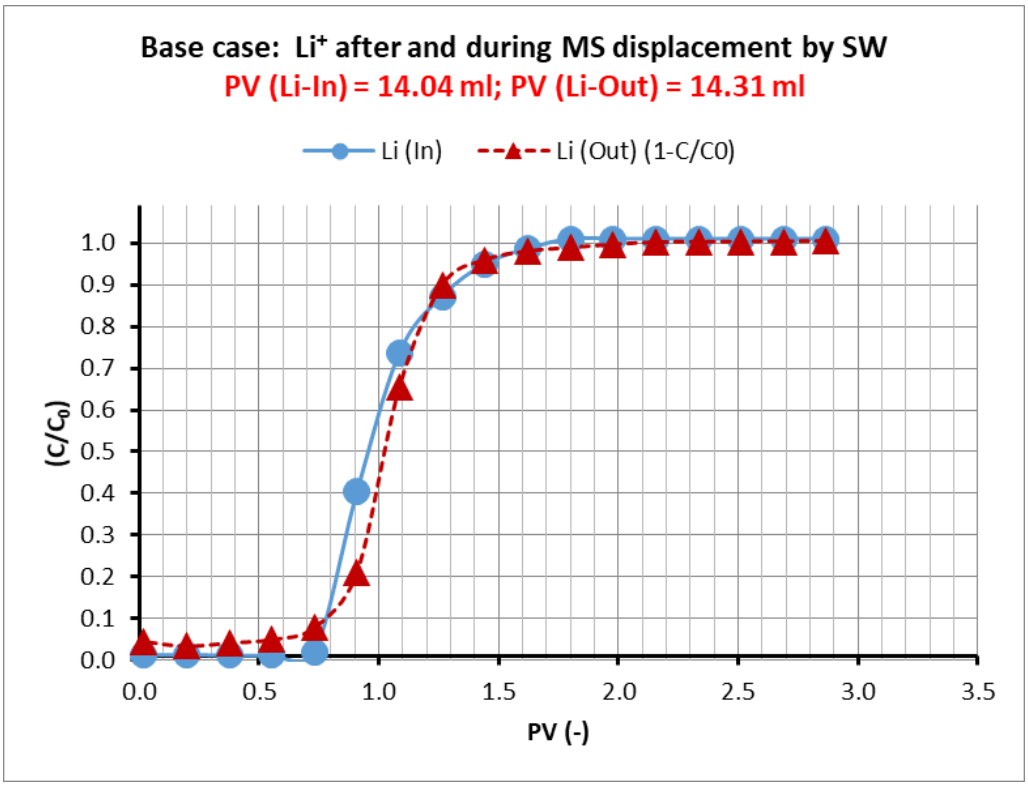

Figure 8.13: Base case lithium profiles post-MS injection (out) and as SW displaces MS (in).

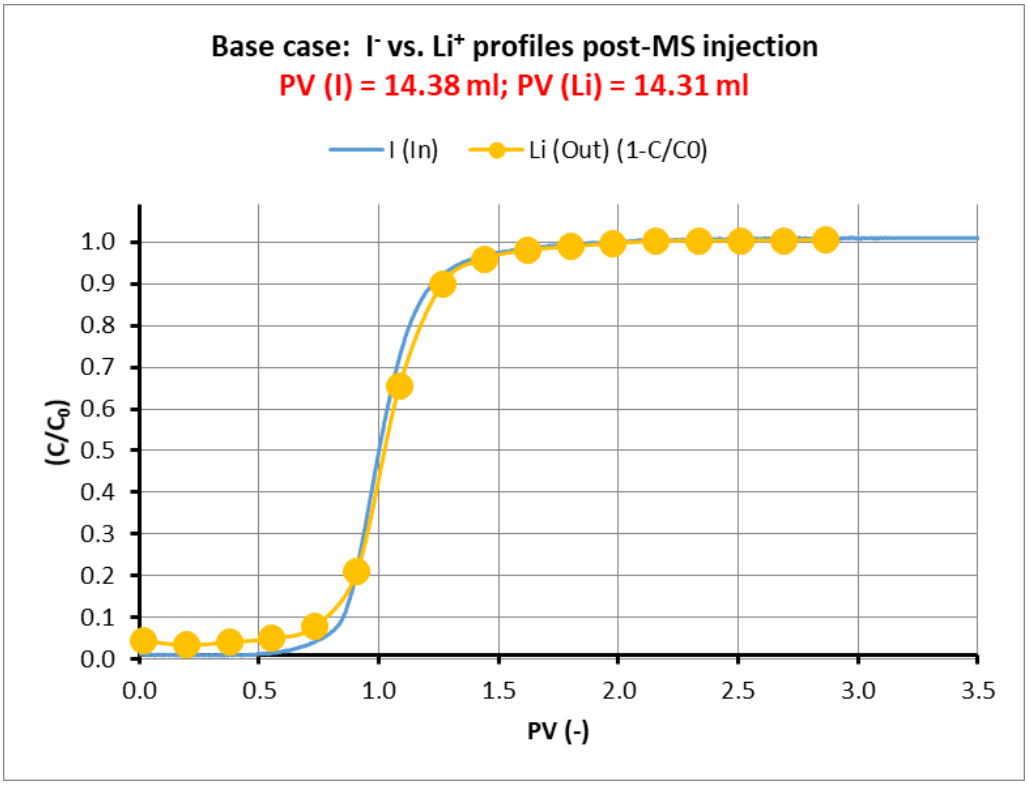

Figure 8.14: Base case iodide vs. lithium profiles post-MS injection.

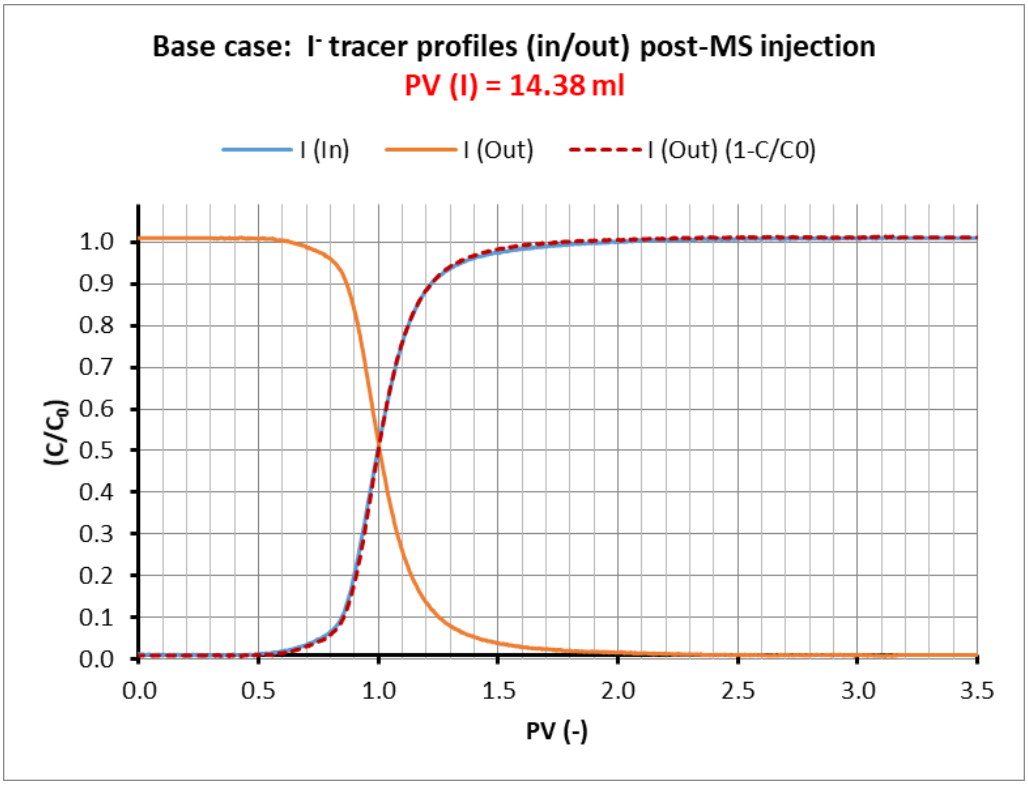

Figure 8.15: Base case iodide tracer profiles (in/out) post-MS injection.

Table 8.4: Summary of PV measurements for the base case.

Stage/Tracer		PV (ml)
Pre-MS	I^-	14.05
	Li^+	14.00
MS displacing SW	Li^+	13.15
	Ca^{2+}	12.94
	Mg^{2+}	13.00
	TS	13.26
MS	TS	14.05
SW displacing MS	Li^+	14.04
	Ca^{2+}	13.80
	Mg^{2+}	13.87
	TS	13.07
Post-MS	I^-	14.38
	Li^+	14.31

Table 8.5: Permeability measurements for the base case.

Stage	Permeability (mD)
Pre-MS	1969.6
MS	1862.5
Post-MS	1780.1

8.2.3. Case A – Increased Preferential Oil Solubility Case: EGMBE

The discussion for Case A will focus on the key stages in Figure 8.1 (step 5 to step 8). A summary of all PV measurements is provided in Table 8.6.

When the MS is displacing SW (Figure 8.1; step 5) a 2.4% residual SW is observed after 3.5 PV injection (Figure 8.16). Therefore, EGMBE (Case A) has a greater efficiency in displacing the SW compared to ethanol (Base Case; 6.1% residual SW) despite the higher affinity of ethanol to SW. This indicates that in single phase systems, the affinity of the MS to the brine will not necessarily translate to a higher efficiency in displacing the brine. Instead, the physical properties of the MS with respect to the brine are more relevant in the absence of other phases. Here, the higher density of EGMBE compared to ethanol (Table 8.1) explains the higher performance of EGMBE (i.e. the smaller degree of gravity separation).

Whereas the residual water is stripped out completely in the case of ethanol upon further ethanol injection (Figure 8.1; step 7), this is not the case with the EGMBE. The residual water remains in the sand-pack during this stage (Figure 8.17). This indicates that while smaller volumes of EGMBE will perform a better displacement of the brine, this does not apply as the volumes grow bigger. Ethanol is helped by a lower viscosity much closer to that of the brine in this case (Table 8.1), enabling it to ultimately overcome viscous imbalances and displace all the brine in the sand-pack.

Figure 8.18 shows the displacement of the MS by the SW (Figure 8.1; step 8). While viscous fingering was expected due to the higher viscosity of EGMBE with respect to the brine (Table 8.1), this is not observed on the lithium profile. However, it can be seen clearly on the TS profile (Figure 8.20). The residual MS after 3.5 PV in Case A is comparable with the base case at 1.7% vs. 1.9%. It remains the case due to the higher density of the brine than the MS in both studied cases.

Two additional results must be highlighted. The same fine mobilisation effect is observed when EGMBE displaces SW (Figure 8.19). This happens to a lesser degree with EGMBE due to its higher viscosity compared to ethanol (Table 8.1). Also, as with the base case, there is no retention of calcium and magnesium at any stage. Their profiles follow the profile of lithium irrespective of whether the MS is displacing SW or vice versa (Figure 8.21 and Figure 8.22 respectively). Permeability results are provided in Table 8.7. It is unclear why the permeability increases significantly during the MS stage. However, this is more likely to be an erroneous result due to uncertainties in the viscosity of EMGBE which varies considerably over the temperature range 20-25ºC.

Table 8.6: Summary of PV measurements for Case A.

Stage/Tracer		PV (ml)
Pre-MS	I^-	14.37
	Li^+	14.52
MS displacing SW	Li^+	14.18
	Ca^{2+}	13.85
	Mg^{2+}	13.85
	TS	13.72
MS	TS	14.10
SW displacing MS	Li^+	14.57
	Ca^{2+}	14.53
	Mg^{2+}	14.35
	TS	14.31
Post-MS	I^-	14.35
	Li^+	14.33

Table 8.7: Permeability measurements for the Case A.

Stage	Permeability (mD)
Pre-MS	1233.1
MS	2603.4
Post-MS	1522.3

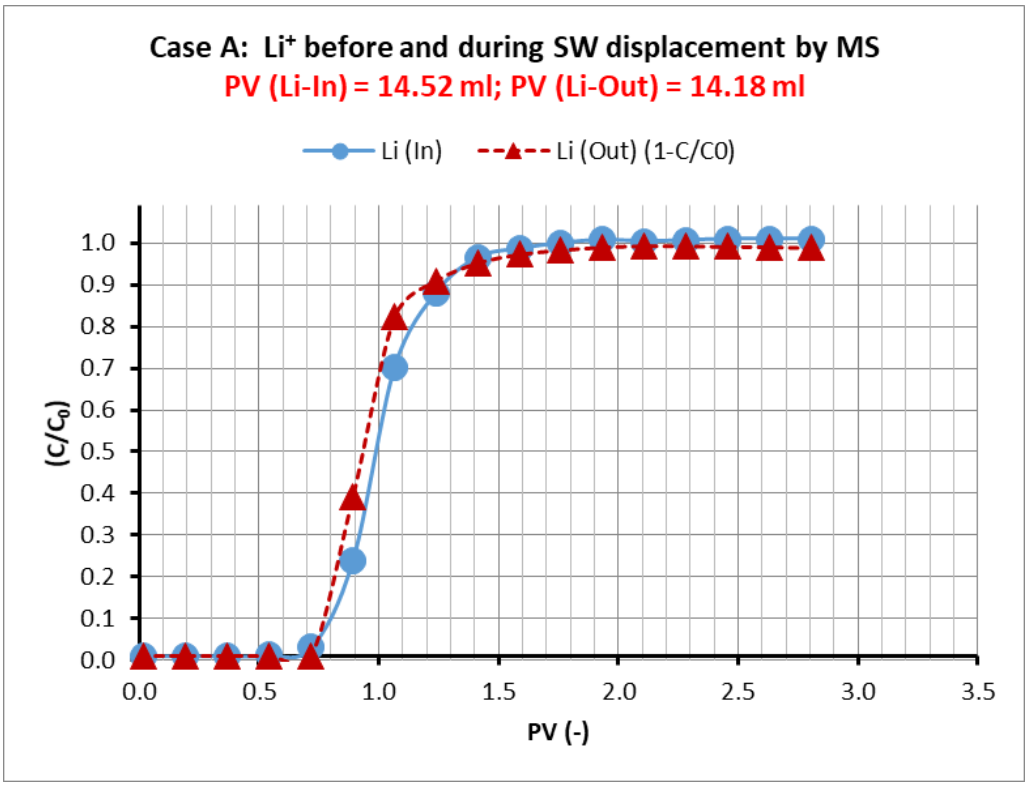

Figure 8.16: Case A lithium profiles pre-MS injection (in) and as MS displaces SW (out).

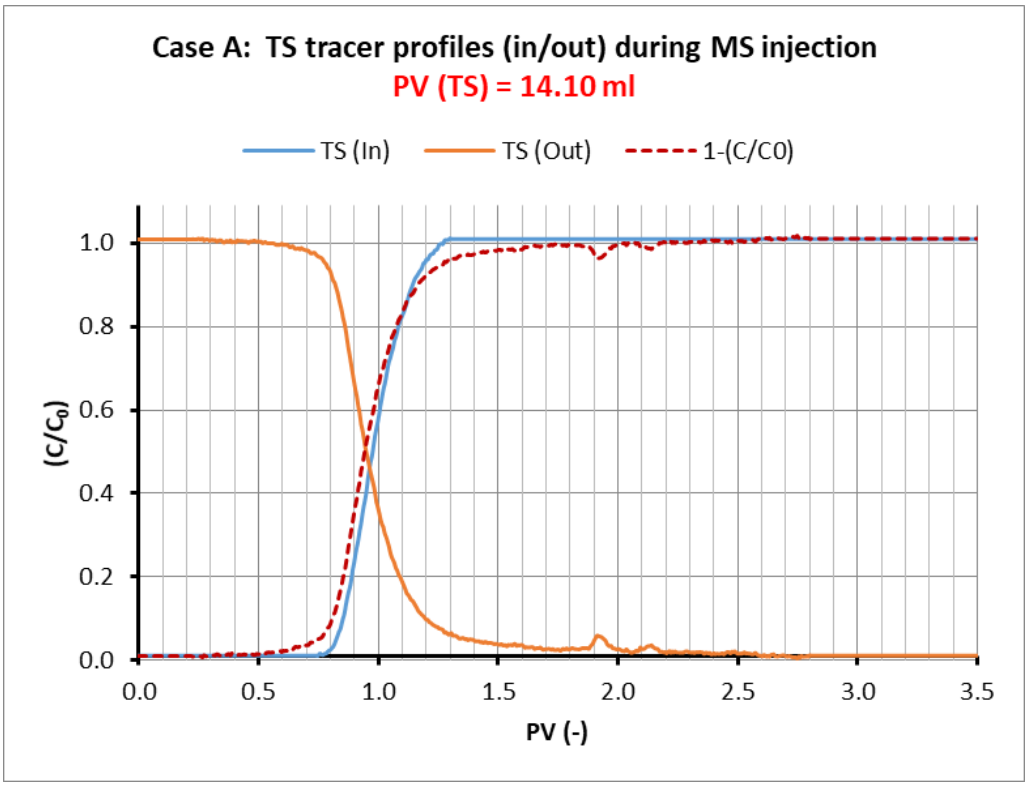

Figure 8.17: Case A trans-stilbene tracer profiles (in/out) during MS injection.

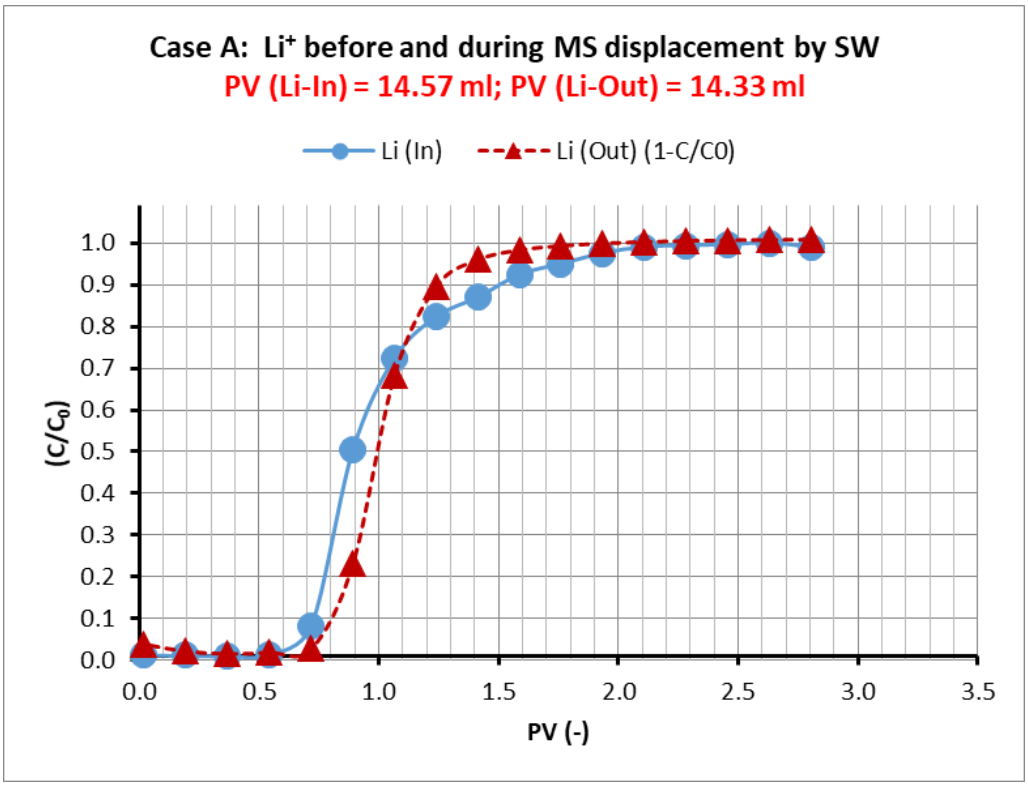

Figure 8.18: Case A lithium profiles post-MS injection (out) and as SW displaces MS (in).

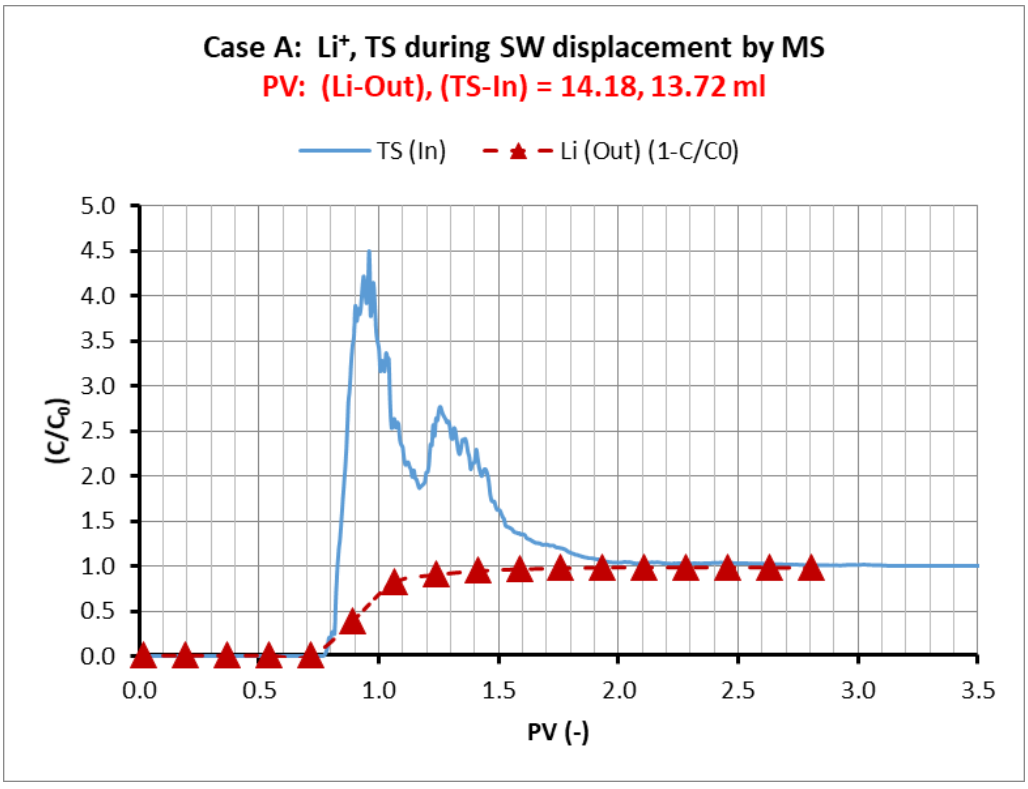

Figure 8.19: Case A lithium and trans-stilbene as MS displaces SW.

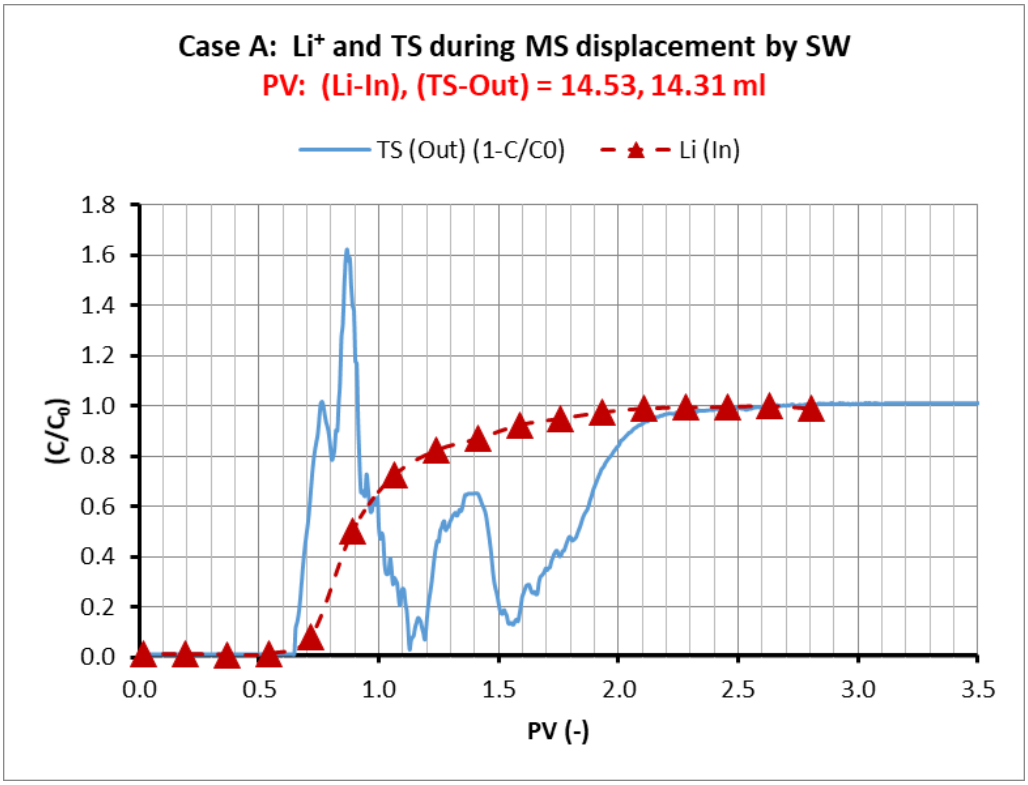

Figure 8.20: Case A lithium and trans-stilbene as SW displaces MS.

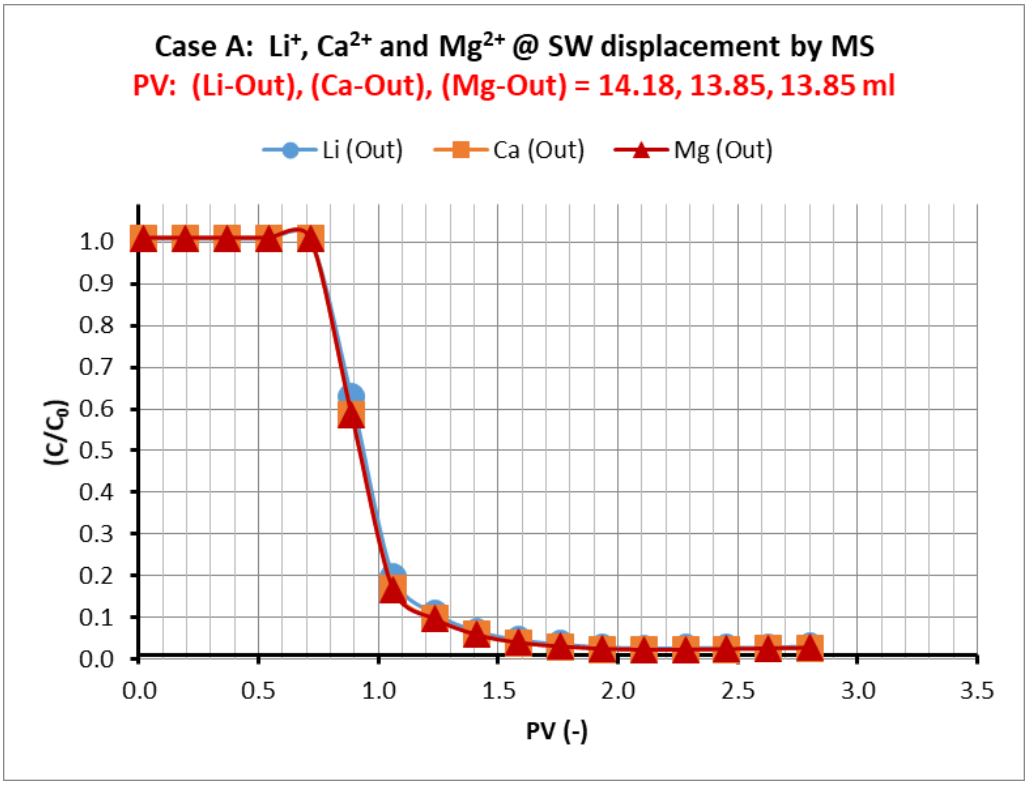

Figure 8.21: Case A lithium/calcium/magnesium as MS displaces SW.

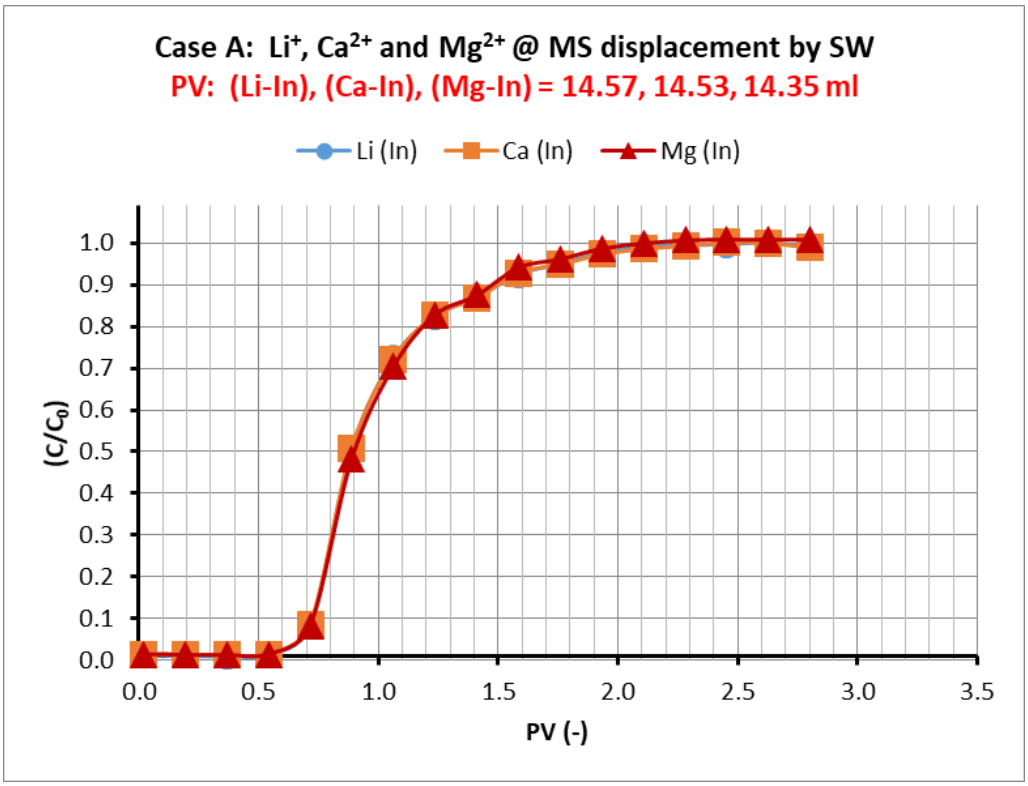

Figure 8.22: Case A lithium/calcium/magnesium as SW displaces MS.

8.2.4. Case B – Increased Preferential Water Solubility Case: MEG

A summary of all PV and permeability measurements are provided in Table 8.8 and Table 8.9. The plots for Case B corresponding to those for Case A are also provided (Figure 8.23 to Figure 8.29).

All findings are consistent with the explanations for Case A. As expected, the efficiency of the SW displacement by the mutual solvent is found to be a function of density in single phase systems. MEG (Case B) performs the highest compared to all MS tested with 0% residual SW saturation after 3.5 PV injection (Figure 8.23). Therefore, the MS stage gives a PV identical to the initial PV (Figure 8.24). Viscous fingering is severe with MEG displacement by SW (Figure 8.25 and Figure 8.27). This is due to the very high viscosity of MEG compared to SW (Table 8.1). Fines mobilisation is lowest for MEG which has the highest viscosity of the tested MS (Figure 8.26), thereby confirming this to be a function of viscosity in single phase systems. Furthermore, calcium and magnesium profiles continue to follow the lithium profile regardless of the nature of the displacement (MS displacing SW or SW displacing MS; Figure 8.28 and Figure 8.29 respectively). Finally, there is an overall reduction of permeability. However, as mentioned in the discussion for the base case, this may be within experimental uncertainty and further investigations are required.

Table 8.8: Summary of PV measurements for Case B.

Stage/Tracer		PV (ml)
Pre-MS	I^-	14.50
	Li^+	14.58
MS displacing SW	Li^+	14.51
	Ca^{2+}	14.51
	Mg^{2+}	14.51
	TS	14.51
MS	TS	14.53
SW displacing MS	Li^+	13.39
	Ca^{2+}	13.24
	Mg^{2+}	13.27
	TS	13.46
Post-MS	I^-	14.41
	Li^+	14.41

Table 8.9: Permeability measurements for the Case B.

Stage	Permeability (mD)
Pre-MS	1563.8
MS	1547.2
Post-MS	1458.8

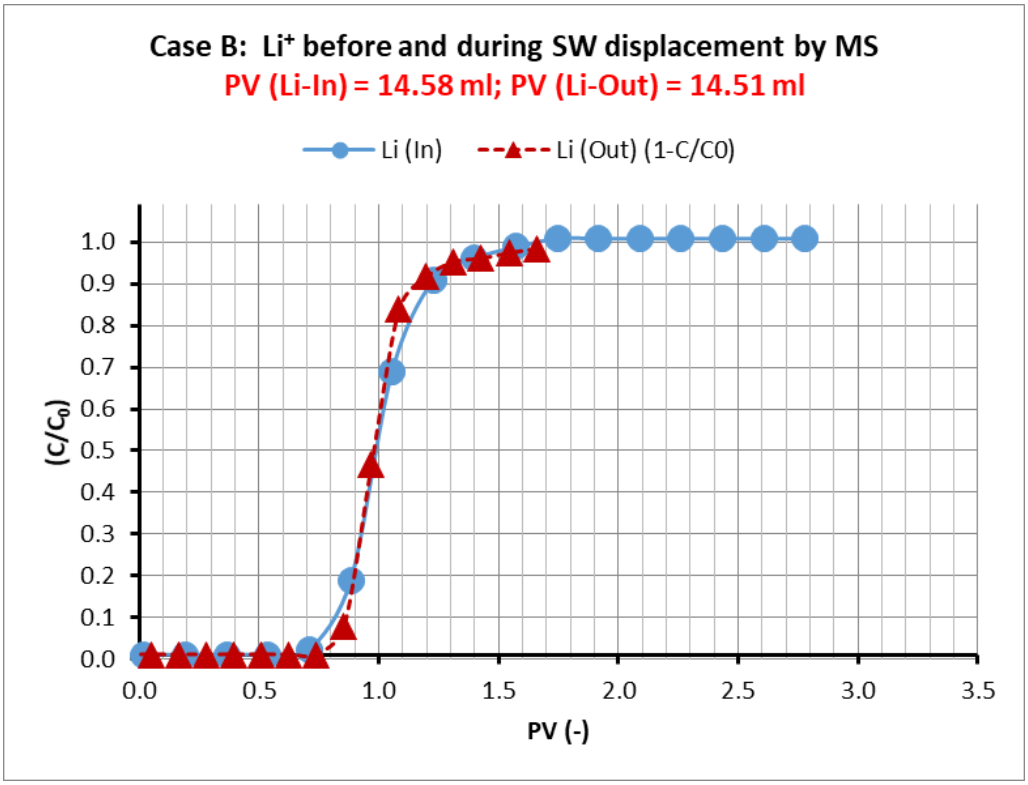

Figure 8.23: Case B lithium profiles pre-MS injection (in) and as MS displaces SW (out).

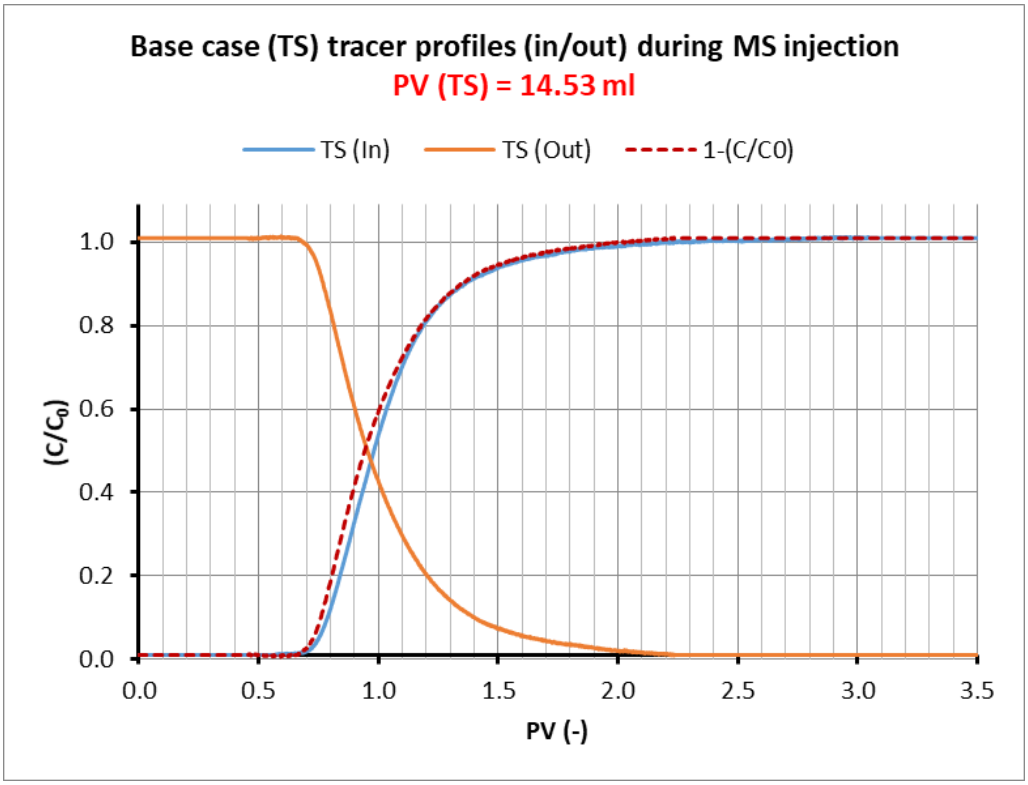

Figure 8.24: Case B trans-stilbene tracer profiles (in/out) during MS injection.

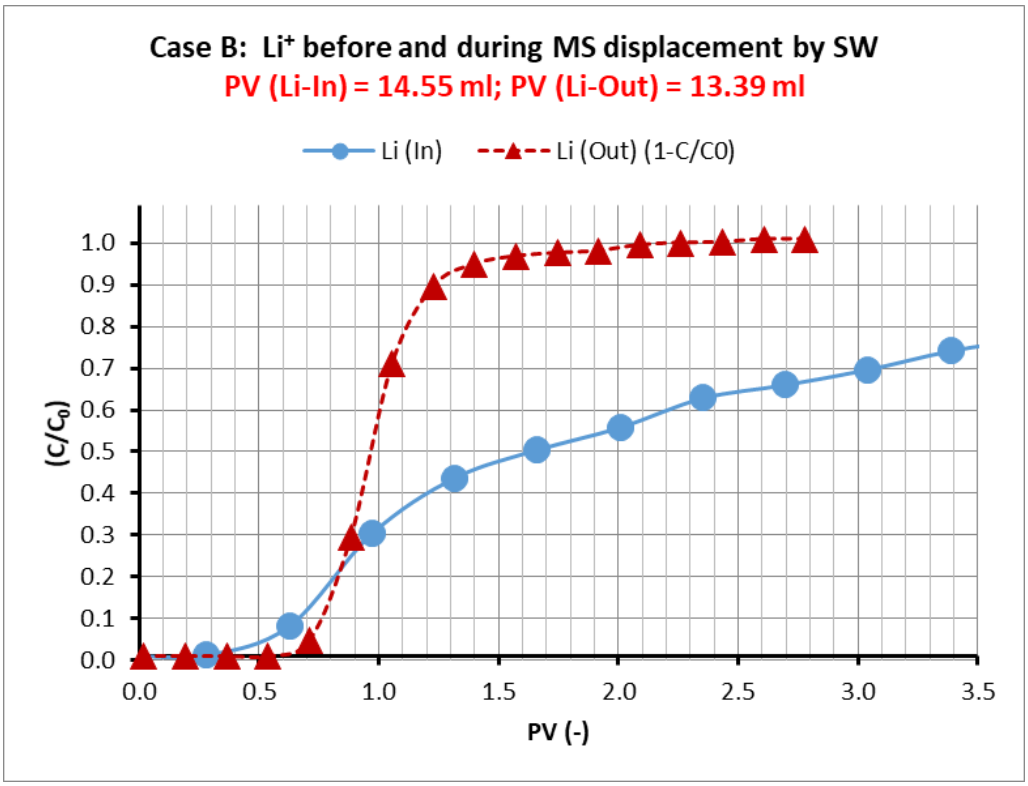

Figure 8.25: Case B lithium profiles post-MS injection (out) and as SW displaces MS (in).

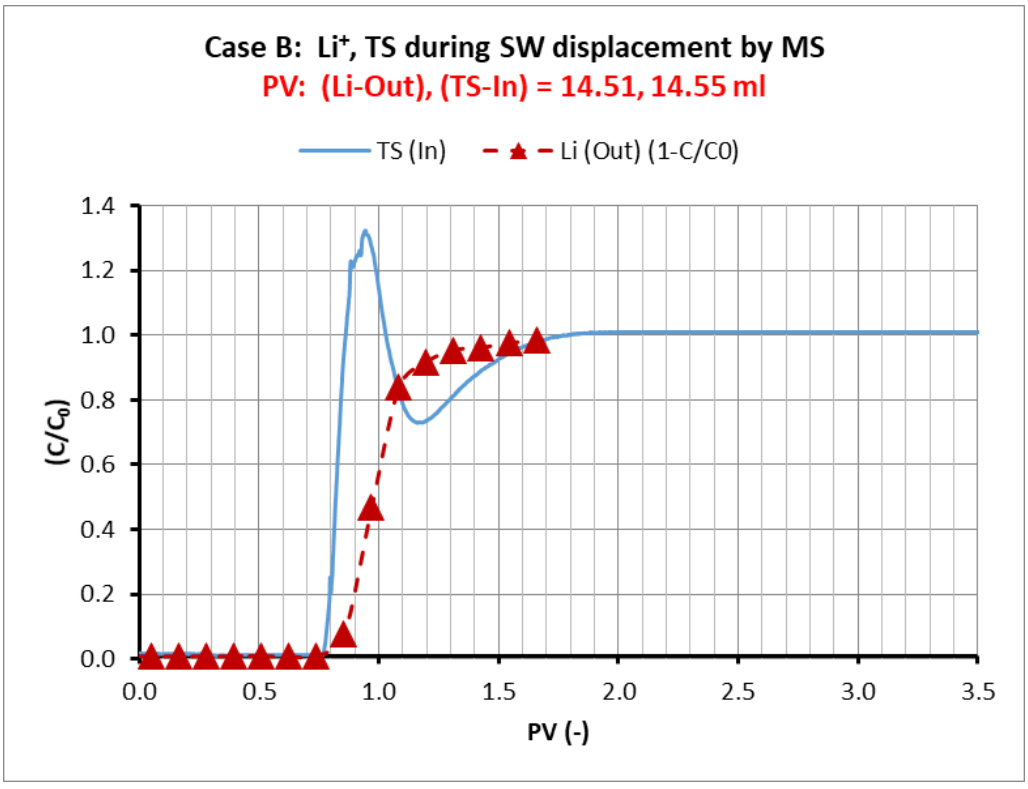

Figure 8.26: Case B lithium and trans-stilbene as MS displaces SW.

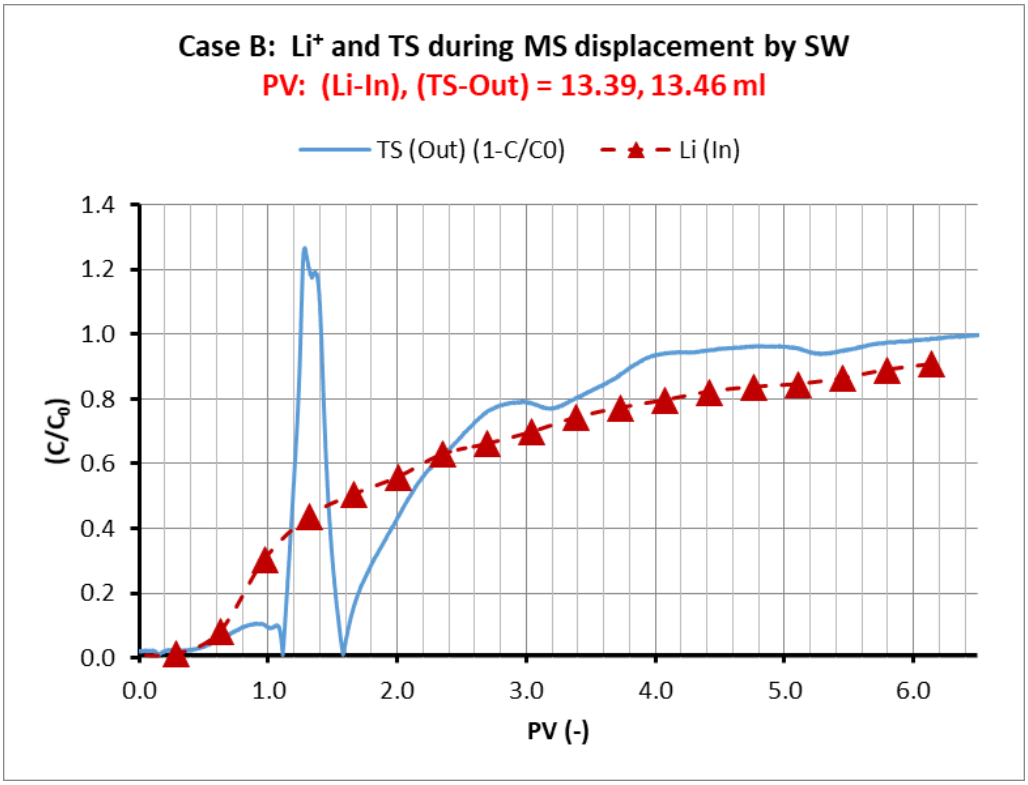

Figure 8.27: Case B lithium and trans-stilbene as SW displaces MS.

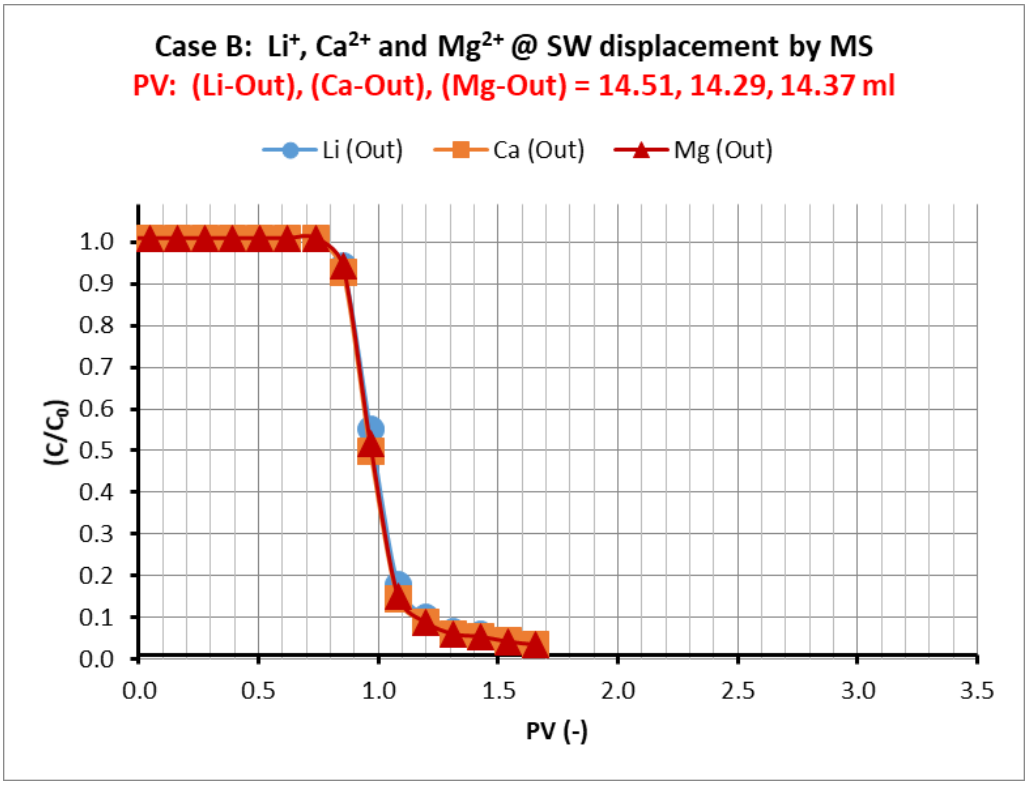

Figure 8.28: Case B lithium/calcium/magnesium as MS displaces SW.

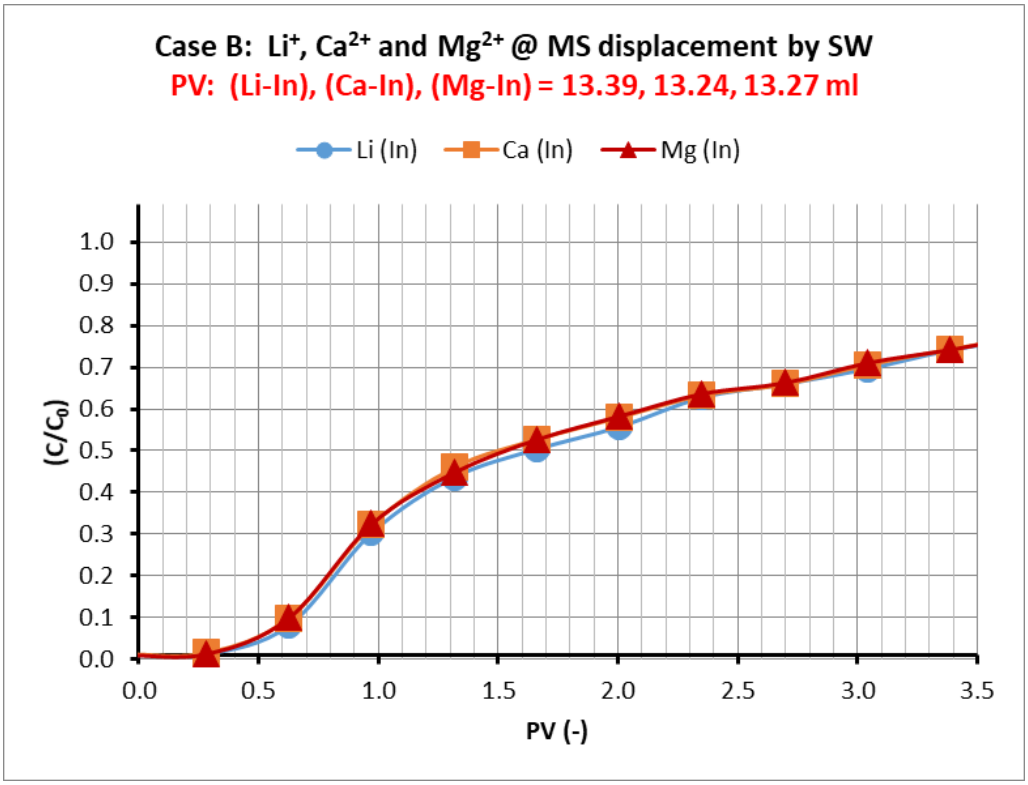

Figure 8.29: Case B lithium/calcium/magnesium as SW displaces MS.

8.2.5. Key Findings

The single-phase displacement studies provide understanding for the effects that may arise as MS displaces SW and vice versa in the absence of complex phase interactions. This understanding will be used to inform observations in multi-phase displacement studies. The highlights are:

1. Preferential affinity of the MS to oil or water seem to have no effects in single-phase systems. Therefore, in the presence of multiple phases, the role of this parameter will be more evident.

2. The efficiency of SW displacement by the MS is a function of density, with more efficient displacement achieved as the density of the MS increases in a horizontal sand-pack configuration.

3. Mobilisation of fines occurs to increasing degree as the viscosity of the MS decreases, and seems to only occur when a MS is displacing SW.

4. Calcium and magnesium are not reactive in single-phase systems and follow the lithium profiles closely.

8.3. MULTI-PHASE DISPLACEMENT TESTS

8.3.1. Experimental Overview

The flooding plan in multi-phase displacement tests is outlined in Figure 8.30. It is similar to the flooding plan for single-phase displacement tests (Figure 8.1), albeit in the presence of mineral oil (Multipar H). Before injecting the mutual solvent, the sand-pack is brought to residual oil saturation (Figure 8.30; steps 5-6). This gives rise to multiphase flow.

When the mutual solvent is ethanol (Case 2P), only two-phase flow is expected, while three-phase flow is possible with EGMBE (Case 3P). Therefore, studying these cases and combining that with the learnings from the single-phase displacement tests should enable understanding the influence of multiphase flow on the oil/brine displacement.

The experimental setup for the cases investigated in this section is identical to the experimental setup described in section 8.2.

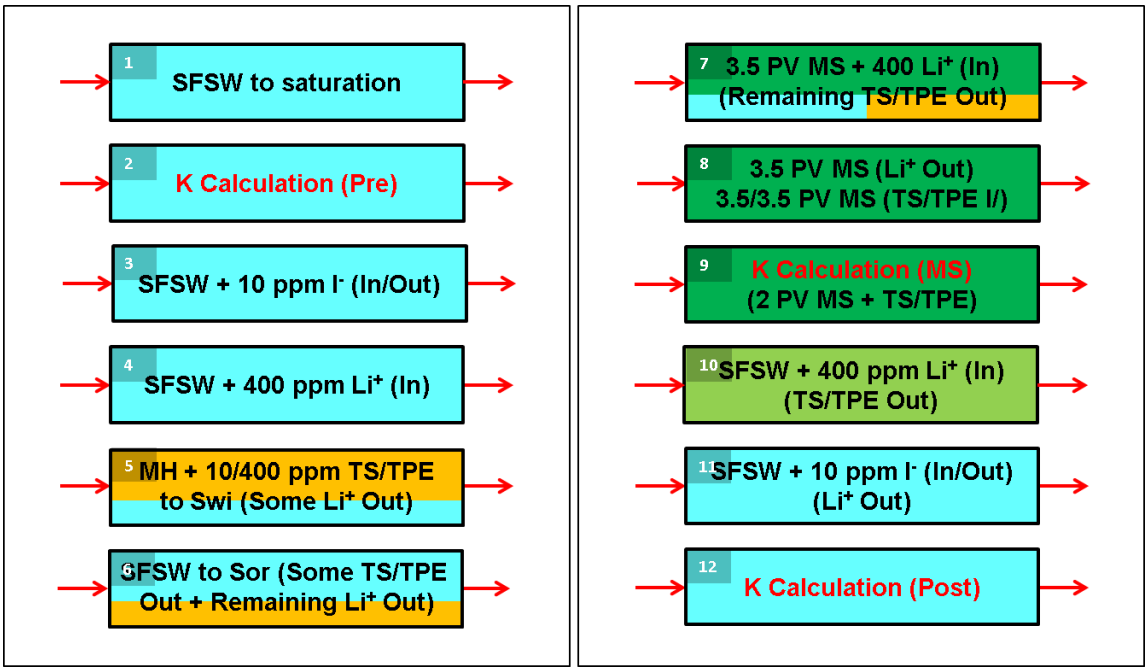

Figure 8.30: Flooding plan for the multi-phase displacement tests.

8.3.2. Results and Discussion

The key step in these experiments is the injection of the mutual solvent after the sand-pack had been brought to residual oil saturation (Figure 8.30; step 7). As such, this step will be the focus of the discussions below.

The residual oil saturation (S_{or}) measurement for Case 2P and Case 3P are illustrated in Figure 8.31 and Figure 8.32 respectively. In Case 3P, (S_{or}) is higher (37.7%) than that in Case 2P (28.4%). Therefore, this will impact the comparability of the cases. However, since the (S_{or}) in Case 3P is higher, this will be an excellent test to evaluate the performance of a preferentially oil soluble mutual solvent (EGMBE) in displacing the oil, and the impact of the three-phase region.

When MS containing (Li^+) is injected (Figure 8.30; step 7), both the oil and the brine will be displaced. Analysing for (Li^+) during the MS injection allowed determining the MS breakthrough and propagation. Analysing for (Ca^{2+}) and (Mg^{2+}) allowed observing the brine displacement. For Case 2P and Case 3P, the results of this analysis are provided in Figure 8.33 and Figure 8.34. Taking into account the phase separation and the densities, all the (Li^+) can be accounted for, i.e. after 3.5 PV, the sand-pack is fully saturated with MS in both cases. However, displacement of the oil and the brine are distinctly different, which can be inferred from these figures.

Using the results in these figures, the oil displacement can be estimated. This is illustrated in Figure 8.35 and Figure 8.36 for Case 2P and Case 3P respectively. The differential pressure is also provided in these figures for both cases. In Case 2P (Figure 8.35), the oil displacement occurs over 1.9 PV after MS (ethanol) breakthrough. In contrast, in Case 3P (Figure 8.36), a much sharper oil displacement is observed, which happens over 0.8 PV after MS (EGMBE) breakthrough. This represents almost 58% more efficient displacement of the oil in Case 3P despite the residual oil saturation being higher by 32.7% compared with Case 2P. This is clear evidence that a more efficient displacement can be achieved with EGMBE than ethanol under the investigated conditions. Taking into account the findings from single-phase displacement tests, the observed oil displacement is thought to be predominantly the result of the preferential partitioning of the mutual solvents, and cannot be accounted for fully by other physical parameters influencing the flow.

In Figure 8.35 and Figure 8.36, the differential pressure profile follows the oil displacements. Moreover, it indicates more complex phase interactions in Case 3P than in Case 2P, highlighting potential three-phase flow (oil-rich, brine-rich and MS-rich phases). To explore this in a greater detail, sample compositions were investigated. For Case 2P which is a strictly two-phase forming system, the one parameter simplified (dr) model described in Chapter 5 (section 5.4.3), and the Karl Fischer analysis in the presence of MS described in Chapter 7 (section 7.2.3.4) were employed to estimate the displacement taking place during ethanol injection. The results are provided in Figure 8.37. For Case 3P which

is a three-phase forming system, the quasi-ternary implementation of the UNIQUAC model described in Chapter 6 based on the three-phase mapping outlined in Chapter 4, and using the phase displacement method described in Chapter 5 was used to calculate the displacement taking place during EGMBE injection. The results are provided in Figure 8.38.

In Case 2P (Figure 8.37), the equal oil/water displacement curve indicates the displacement that would take place at the (S_{or}) value for Case 2P if ethanol was to displace the oil and the brine equally. Displacements on the left hand side of this line indicate higher displacement of oil with respect to water. The opposite applies for displacements on the right hand side of this line. The estimated O/W displacement curve indicates the experimental observations. This is provided as a function of PV of MS injected.

The ethanol is seen to displace more oil than brine at 0.70 PV, which rapidly switches to higher brine displacement above 0.70 PV (30% U-turn with respect to the brine concentration). The brine is then displaced at a higher rate than the oil. Much of the oil is displaced above 1.05 PV. This is in constrast to the findings in Case 3P (Figure 8.38), in which preferential oil displacement is strongly observed. Above 1.05 PV, the EGMBE starts to displace the brine at a greater rate as the remaining oil concentration drops to zero. It is noted that the observed phase separation of the samples is perfectly consistent with phase diagrams in Figure 8.37 and Figure 8.38.

Based on these results, it can be said that with the preferentially water soluble ethanol, much of the oil displacement will happen after initial strong preference to water displacement. With the preferentially oil soluble EGMBE, the opposite applies. This finding is significant because:

1. It preliminarily validates the use of preferentially oil soluble mutual solvents in squeeze treatments at the pre-flush stage. At this stage, one of the objectives is to displace as much oil as possible using the least volume of chemical.

2. It indicates that the preferential solubility does not describe the full process of the displacement. For example, with the preferentially oil soluble EGMBE, the observation is not the displacement of all of the oil, and then the displacement of the remaining brine. Instead, much of the oil will be displaced initially. After that, the brine will be displaced at a greater rate than the oil as the oil concentration drops to zero. Likewise, with the preferentially water soluble ethanol, the observation is

not the displacement of all of the brine, and then the displacement of the remaining oil. Instead, much of the brine will be displaced initially, then the oil will be displaced at a greater rate than the brine as the brine concentration drops to zero.

In Case 3P, much of the oil displacement happens within the three-phase region. This highlights that three-phase formation will not hinder oil displacement, which was thought to be a risk due to three-phase flow and greater degree of slip between the phases in transport compared to two-phase flow. In fact, a sharp and efficient oil displacement is observed despite the three-phase region. However, this result is limited in that it cannot conclusively determine if EGMBE will be more efficient in displacing the oil in the absence of the three-phase region, and further investigations are required.

For the remaining steps of these experiments (Figure 8.30), the results are identical to the results from single-phase displacement tests as expected. A summary of all PV measurements are provided in Table 8.10 and Table 8.11 for Case 2P and Case 3P respectively.

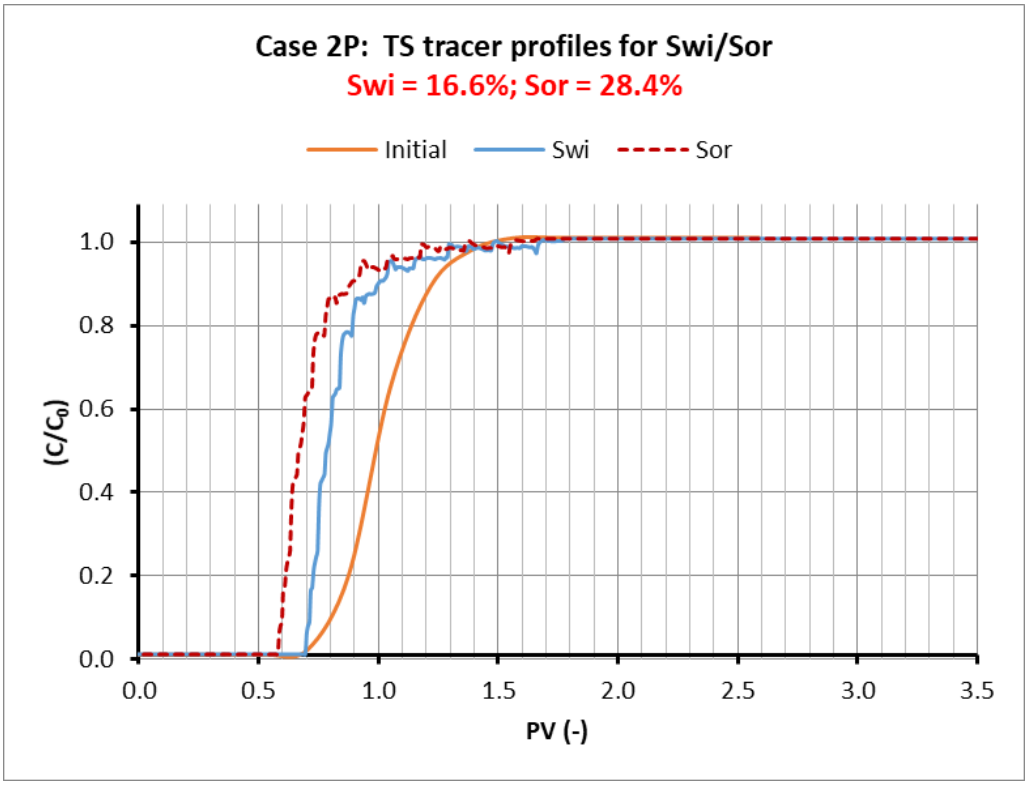

Figure 8.31: Case 2P (S_{wi}) and (S_{or}) before mutual solvent (ethanol) injection.

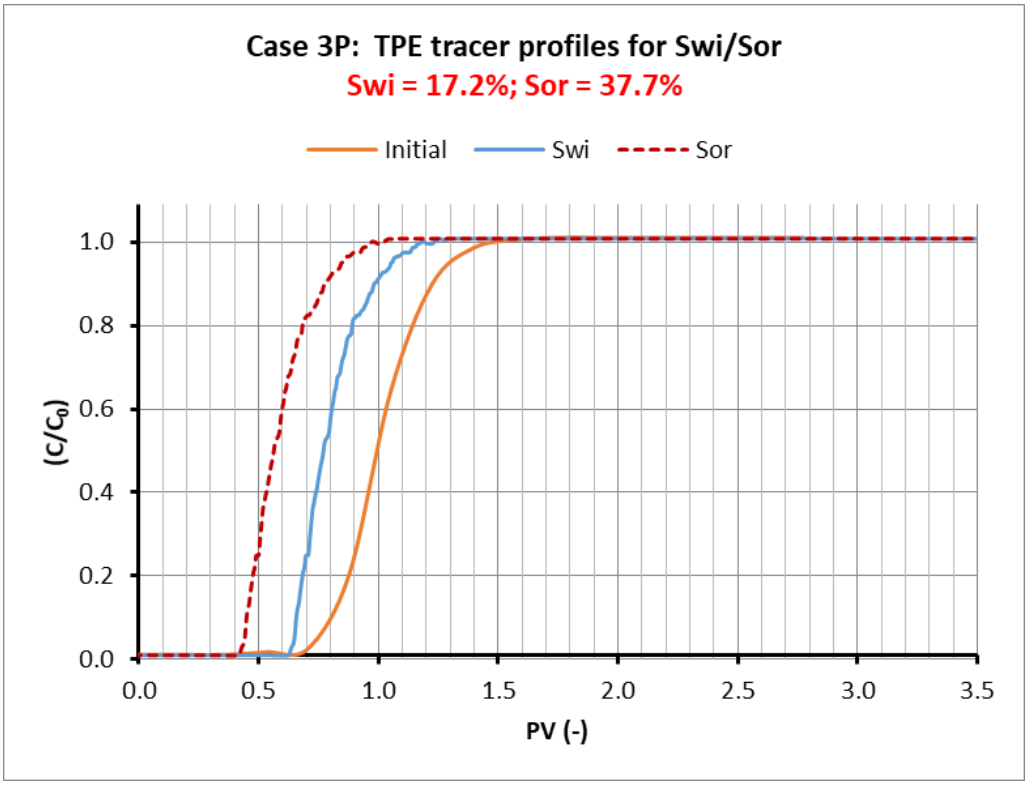

Figure 8.32: Case 3P (S_{wi}) and (S_{or}) before mutual solvent (EGMBE) injection.

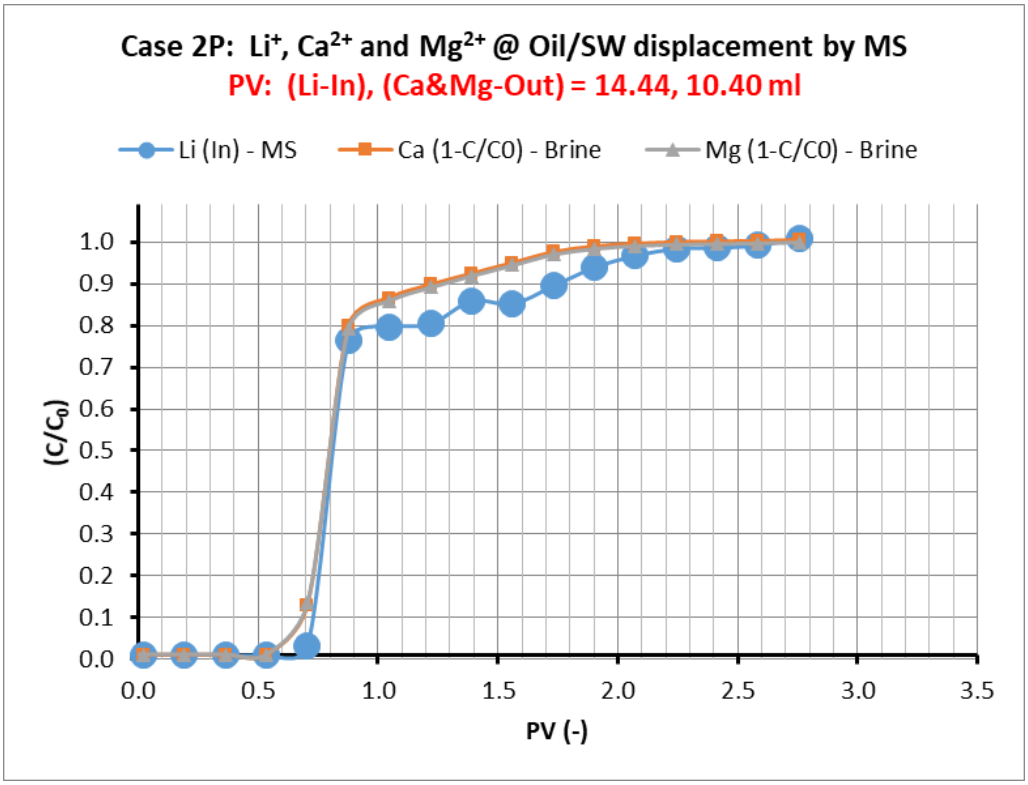

Figure 8.33: Case 2P ions during MS injection (Li^+ in MS, Ca^{2+} and Mg^{2+} in brine).

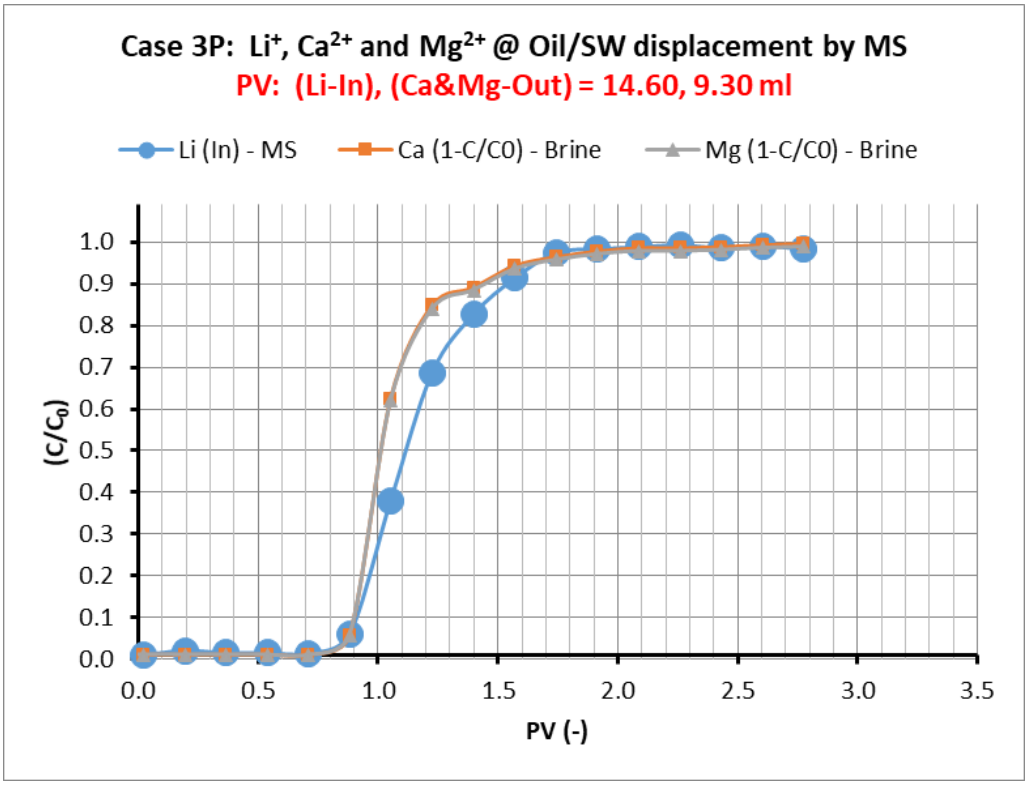

Figure 8.34: Case 3P ions during MS injection (Li^+ in MS, Ca^{2+} and Mg^{2+} in brine).

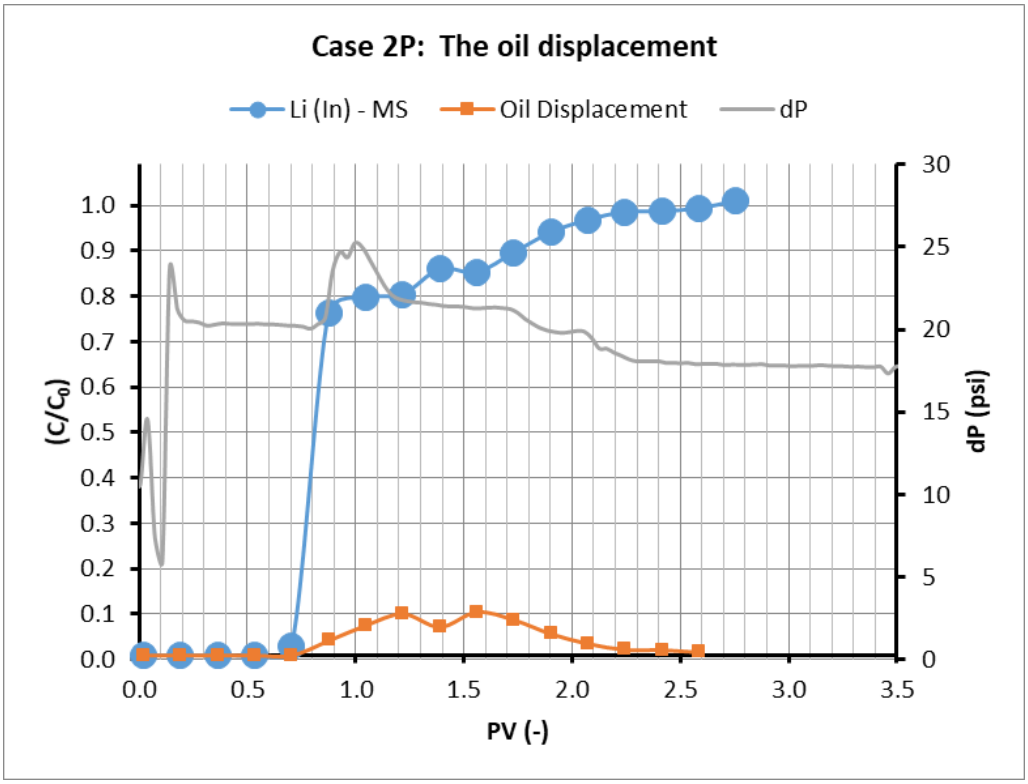

Figure 8.35: Case 2P oil displacement (ethanol).

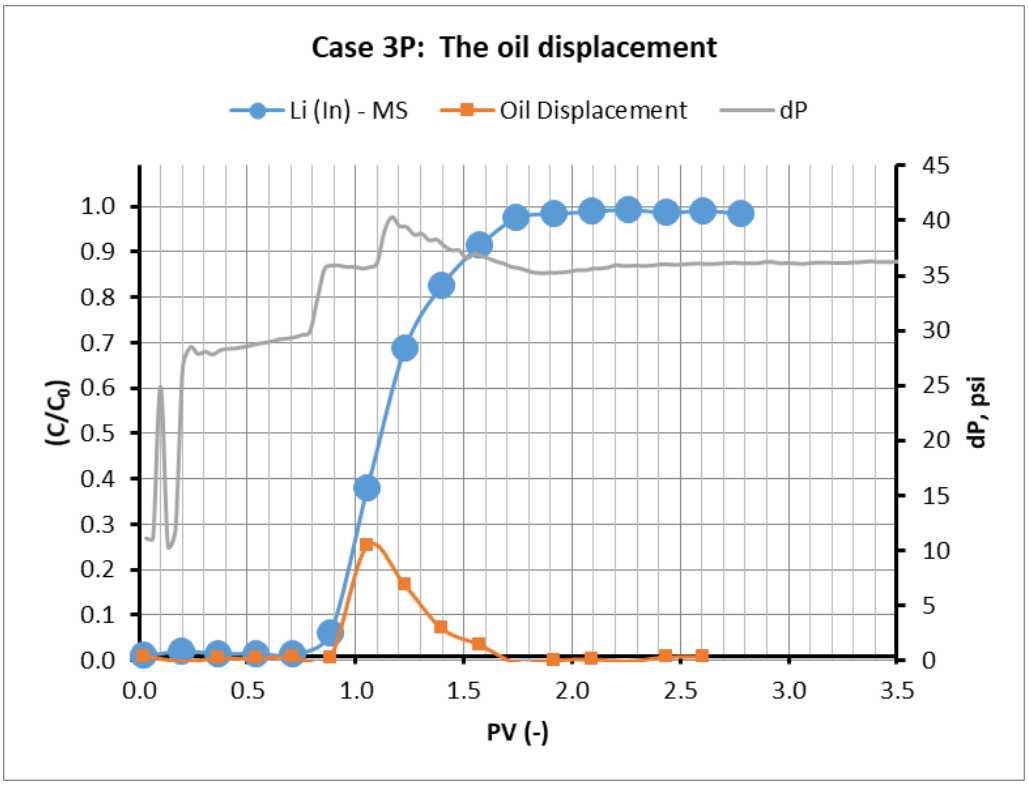

Figure 8.36: Case 3P oil displacement (EGMBE).

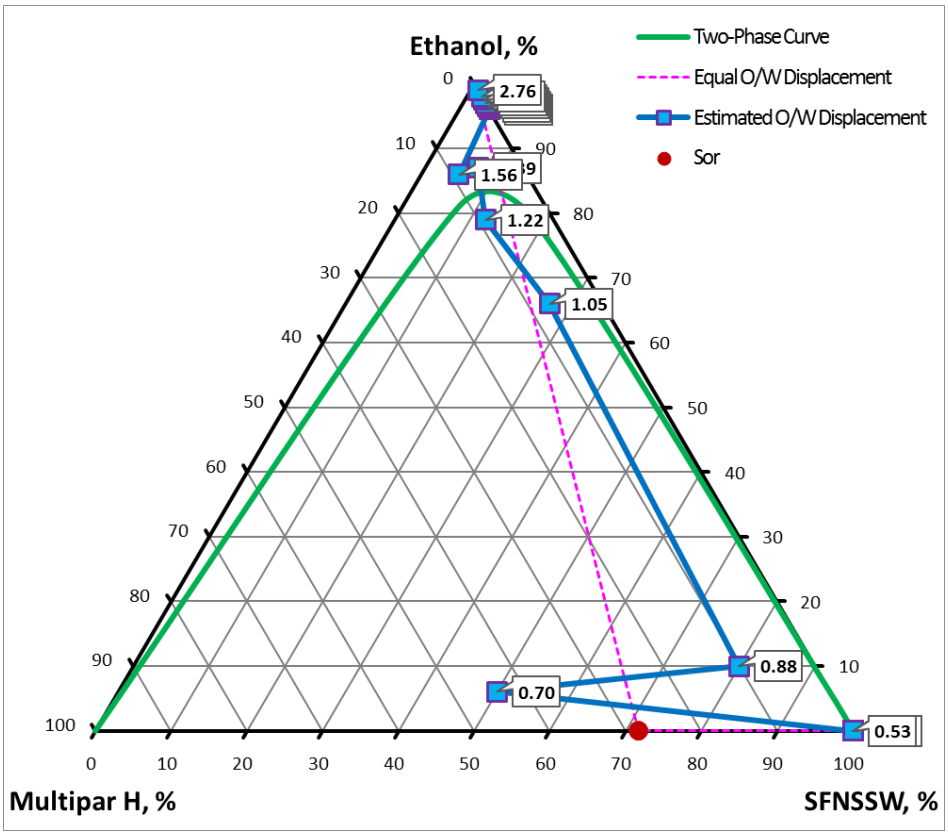

Figure 8.37: Case 2P full displacement as a function of PV (ethanol).

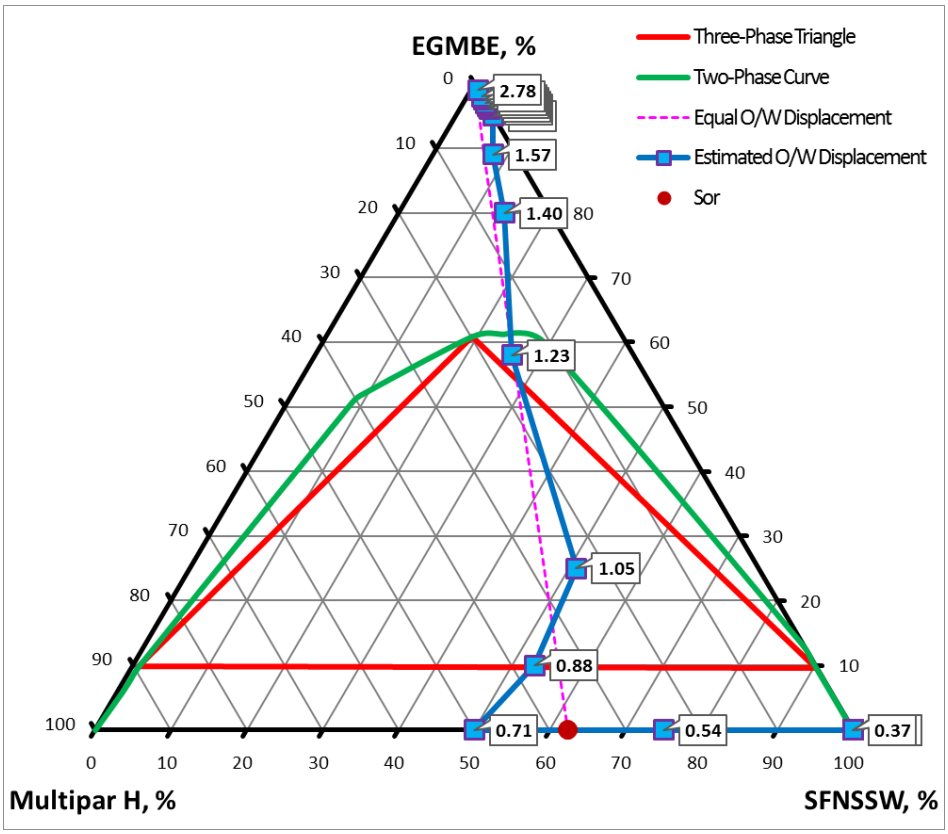

Figure 8.38: Case 3P full displacement as a function of PV (EGMBE).

Table 8.10: Summary of PV measurements for Case 2P.

Stage/Tracer		PV (ml)
Pre-MS	I^-	14.61
	Li^+	14.61
S_{wi}	TS	12.18
	PV-Li^+	12.16
S_{or}	PV-TS	10.47
	Ca^{2+}/Mg^{2+}	10.40
MS displacing oil/brine	Li^+	14.44
MS	Li^+	14.55
MS	TS	14.51
SW displacing MS	Li^+	14.14
	Ca^{2+}	14.17
	Mg^{2+}	14.23
	TS	14.10
Post-MS	I^-	14.51
	Li^+	14.61

Table 8.11: Summary of PV measurements for Case 3P.

Stage/Tracer		PV (ml)
Pre-MS	I^-	14.51
	Li^+	14.58
S_{wi}	TS	12.02
	PV-Li^+	12.07
S_{or}	PV-TS	9.04
	Ca^{2+}/Mg^{2+}	9.30
MS displacing oil/brine	Li^+	14.60
MS	Li^+	14.52
MS	TS	14.48
SW displacing MS	Li^+	14.31
	Ca^{2+}	14.30
	Mg^{2+}	14.35
	TS	14.39
Post-MS	I^-	14.47
	Li^+	14.53

8.4. SUMMARY AND RESEARCH SIGNIFICANCE

The findings in this chapter can be summarised in the following points:

- A neat application of a mutual solvent shows fines displacement in sand-pack tests. This is an observed feature all investigated cases from both, UV absorbance analysis and small particles of sand in the samples collected. A smaller degree of this is observed as the mutual solvent viscosity drops.

- In single phase systems, it seems that the brine displacement by a mutual solvent is independent of the partition coefficient of the mutual solvent. Differences in displacements can be explained by the physical properties of the mutual solvent in these cases.

- In multi-phase systems, the preferentially oil soluble EGMBE showed a more sharp oil displacement than the preferentially water soluble ethanol. This is despite three-phase flow with the EGMBE. It is unknown if a better oil displacement can be achieved in the absence of three-phase flow and further investigations are required.

- With the preferentially oil soluble EGMBE, much of the oil displacement happens initially, after which the brine is displaced at a greater rate as the oil concentration drops to zero. The opposite effect applies with the preferentially water soluble ethanol.

- All (Ca^{2+}) and (Mg^{2+}) profile closely follow the lithium profile in all cases involving the mutual solvent. This indicates their non-reactivity (i.e. they behave as natural tracers) in the absence of inorganic precipitation or other reactions.

- The key findings in these preliminary investigations have been enabled by the developments in the previous chapters. More thorough investigations are possible and are highlighted as the most important suggestions for future work.

Chapter 9: Conclusions and Recommendations

9.1. CONCLUSIONS

We present the conclusions of this doctoral study, organising them by chapter:

Chapter 3: Qualitative Experimental Studies on the Phase Behaviour of Mutual Solvents

On a qualitative basis, the phase behaviour of mutual solvents in systems of oil/brine/MS is largely predictable. A general appreciation for the expected phase behaviour of a mutual solvent can be made with reference to the partition coefficient ($P_{o/w}$) and some knowledge of the system. This is very useful in preliminary selection of mutual solvents for field applications or mutual solvent blend design. It will also enable quick evaluation of potential downhole and downstream issues arising from the mutual solvent application.

Salinity was found to be detrimental to the solubility of the mutual solvent in the aqueous phase in all field scenarios. Therefore, a mutual solvent selection can take this into account to optimise the displacement required prior to a treatment. For example, in high salinity fields, a mutual solvent with high affinity to the water may be selected to overcome salinity effects on the phase behaviour. Moreover, risks associated with inorganic precipitation due to the mutual solvent use are known and can be prevented either through mutual solvent selection or blends involving scale inhibitors. This represents the key effect of using scale inhibitors in mutual solvent blends; the liquid phase behaviour will only be affected at very high concentrations of the scale inhibitor. Inorganic precipitation in the presence of mutual solvent comprises of sulphate salts. Non-sulphate salts (primarily NaCl) are only observed at very high salinity or for highly polar mutual solvents.

Another aspect of mutual solvent blend design, aside from the effect of scale inhibitors, is the effect of blending multiple mutual solvents. This does not affect the inorganic precipitation resulting from the primary mutual solvent in the blend. However, it enabled the targeting of specific phase behaviour, and this includes designing the three-phase region on the phase diagram. This is immensely important for both downhole and downstream considerations, and forms the basis for future mutual solvent blend design work.

Chapter 4: Quantitative Experimental Studies on the Phase Behaviour of Mutual Solvents

The phase behaviour in systems of oil/brine/MS is quasi-ternary, i.e. it resembles the phase behaviour in truly ternary systems. This phase behaviour property extends to cover systems

with high levels of complexity, e.g. high salinity systems, systems with phosphonates and polymers, crude oil systems and systems involving mutual solvent blends. This makes it useful for squeeze treatment applications.

The low speciation of the detailed compositions of the oil and the brine has profoundly useful implications in terms of modelling the phase behaviour. Where a quasi-ternary system is a three-phase forming system, graphical, numerical and analytical methods can be used to work out the three-phase compositions inexpensively and with ease. The experimental input for these methods is relatively minor, making this accessible for all applications.

The quasi-ternary phase behaviour does not only cover simple oil/brine/MS systems, it is also useful in enabling huge simplifications to the modelling of the phase behaviour in oil/brine/MS systems. In transport, it will also influence oil displacement and potentially wettability changes in three-phase forming system within which the MS-rich phase is immune to dilution effects within the boundaries of the three-phase region. This may make three-phase formation a desirable property in mutual solvent blend design.

Chapter 5: Semi-Empirical Methods for Resolving the Phase Envelope of Oil/Brine/Mutual Solvent Systems

The quasi-ternary property of mutual solvent systems can be exploited for simple semi-empirical quantitative mapping of the phase behaviour. This was achieved successfully using a mass balance model aided with simple experimental and mathematical procedures devised specifically for these systems. The applicability of this procedure was demonstrated with success for systems of varying levels of complexity. The experimental procedure developed as part of this work may also be used to analyse the contents of a sample, which enables applications in propagation studies, as well as field applications.

It was also observed as part of this work that in strictly two-phase forming systems, one of the phases will exhibit a relatively constant phase composition. The impact of this on MS speciation, oil displacement and scale inhibitor adsorption must therefore be integral in the selection of the mutual solvent. This may also be useful in limiting the mutual solvent concentration in the aqueous phase, while keeping its concentration high in the oleic phase when required, e.g. for displacement of heavier oils or mitigation of inorganic precipitation, or vice versa, e.g. to remove water-block. This finding also enables further simplification to the modelling of the phase behaviour in MS systems as demonstrated by this work.

Chapter 6: Using a Thermodynamic Model to Describe the Phase Envelope of Oil/Brine/Mutual Solvent Systems

A successful quasi-ternary implementation of the UNIQUAC model was achieved. The outcome of this is the ability to perform transport modelling investigations of both real and hypothetical systems with minimal or no experimental input. The results of this implementation of the UNIQUAC model were in good agreement with both data in the literature and semi-empirical data produced in Chapter 5. This highlights the value of this work, and this development may evolve to be an integral part in mutual solvent blend design for field applications.

A numerical method was developed to enable successful calculation of the interaction parameters for quasi-ternary systems, and was applied with success. Moreover, this work simplifies the initialisation and modelling algorithms required to capture the phase behaviour in three-phase forming systems.

Chapter 7: Analytical Methods for Analysing for Mutual Solvents and Analysis in the Presence of Mutual Solvents

The development of a practical GC-FID method for analysis of mutual solvents in oil/brine/MS systems was achieved. This method was used to verify the semi-empirical model and the quasi-ternary implementation of the UNIQUAC model for the system Multipar H/NSSW/EGMBE. Further optimisations are possible. However, this method remains unfavourable compared with the alternatives in Chapter 5 and Chapter 6 due to: 1) the level of experimental work required for the analysis; 2) the inability to resolve the oil/brine compositions reliably. In this work, in addition to trans-stilbene, tetraphenylethylene was identified as a suitable UV-Vis tracer for transport applications.

Chapter 8: Propagation of Mutual Solvents in Single and Multi-Phase Systems

The results in all previous chapters were applied to study the propagation of mutual solvents in multiphase systems, with studies of mutual solvent transport based on the partition coefficient in single phase systems used as a baseline.

Greater fine displacement with neat applications of MS were observed with increasing viscosity. Moreover, in the absence of oil, the relative partitioning of the mutual solvent was not an important factor in the displacement of the brine. However, in multiphase systems, this is not the case. Preliminary observations highlight more efficient oil

displacement in mutual solvents with affinity to the oil. There is no negative impact of three-phase flow on the oil displacement, and it may be helped by it. Preliminary investigations also indicate that the displacement of the oil and the brine tie in well with the partition coefficient of the mutual solvent. The detailed composition of the brine remained unchanged in all investigations.

With further development of this work, and taking into account all the tools made available by this PhD, further investigations can be performed to determine desirable phase behaviour features, and to start investigating the precise influence of the mutual solvent on the performance of squeeze treatments.

9.2. RECOMMENDATIONS

The following recommendations are made for researchers working on expanding this topic:

- Carry out detailed quantitative assessments on mutual solvent blend design with blends involving multiple mutual solvents and scale inhibitors.

- Perform quantitative assessments to establish conditions under which mutual solvent concentration can be limited in either the oleic or the aqueous phase in strictly two-phase forming systems.

- Investigate the effect of MS presence on PPCA and DETPMP adsorption and performance in static bottle tests.

- Perform transport modelling investigations using the quasi-ternary implementation of the UNIQUAC model on hypothetical three-phase forming systems. This work could identify which mutual solvent blends to design for various applications.

- Further developments to the GC method in Chapter 7 to enable analysis at concentrations lower than 0.1%. This would be required to investigate MS adsorption on different substrates.

- Perform multiphase transport investigations for preferentially oil soluble mutual solvents in the absence of the three-phase region to establish the precise influence of three-phase formation on oil displacement.

- Expand the work on the multiphase transport investigations of the mutual solvent to cover a wider range of mutual solvents.

- Incorporate scale inhibitors in the transport investigations, and use the semi-empirical work in Chapter 5 to design an experiment in which the effects of the mutual solvent flow back on a squeeze lifetime is appropriately represented.

- Perform transport investigations using sand packs with different substrates and different scale inhibitors. Moreover, it would be advisable in advance of any field application to investigating the influence of the temperature, the mutual solvent volumes and the mutual solvent concentrations on the observed effects. The investigations should be extended by working with crudes instead of mineral oil.

- Performing investigation on cores once some of the mutual solvent effects have been understood and established in simpler systems.

References

ABRAMS, D. S. & PRAUSNITZ, J. M. 1975. Statistical Thermodynamics of Liquid-Mixtures - New Expression for Excess Gibbs Energy of Partly or Completely Miscible Systems. *Aiche Journal*, 21, 116-128.

AGILENT. 2018. *GC Columns for Accurate, Reliable Performance* [Online]. Available: https://www.agilent.com/en/products/gas-chromatography/gc-columns [Accessed April 2018].

ATKINSON, G. & MECIK, M. 1997. The Chemistry of Scale Prediction. *Journal of Petroleum Science and Engineering*, 17, 113-121.

BALDWIN, R. L. 1996. How Hofmeister Ion Interactions Affect Protein Stability. *Biophysical Journal*, 71, 2056-2063.

BANTIGNIES, J. L., MOULIN, C. C. D. & DEXPERT, H. 1997. Wettability Contrasts in Kaolinite and Illite Clays: Characterization by Infrared and X-Ray Absorption Spectroscopies. *Le Journal de Physique IV*, 7, C2-867-C2-869.

BENNION, D. B., THOMAS, F. B. & BIETZ, R. F. 1996 Published. Low Permeability Gas Reservoirs: Problems, Opportunities and Solutions for Drilling, Completion, Stimulation and Production. *SPE Gas Technology Symposium*, 28 Apr-01 May, Calgary, Alberta, Canada: Society of Petroleum Engineers.

BOGAERT, P., BERREDO, M. C., TOSCHI, C., BRYSON, B., JORDAN, M. M., FRIGO, D. M. & AFONSO, M. 2008. Managing Formation-Damage Risk from Scale-Inhibitor Squeeze Treatments in Deepwater, Subsea Fields in the Campos Basin. *SPE Production & Operations*, 23, 468-477.

BOGAERT, P. J., BERREDO, M. C., TOSCHI, C., JORDAN, M. M., FRIGO, D. M., MORGENTHALER, L. N. & AFONSO, M. 2006 Published. Scale Inhibitor Squeeze Treatments Deployed from an FPSO in a Deepwater, Subsea Field in the Campos Basin. *SPE Annual Technical Conference and Exhibition*, 24-27 Sep, San Antonio, Texas, USA: Society of Petroleum Engineers.

BOGAERT, P. J., BERREDO, M. C., TOSCHI, C., JORDAN, M. M., FRIGO, D. M., MORGENTHALER, L. N. & AFONSO, M. 2007 Published. Scale Inhibitor Squeeze Treatments Deployed from an FPSO in a Deepwater, Subsea Field in the Campos Basin. *SPE International Oilfield Scale Conference and Exhibition*, 11-12 May, Aberdeen, Scotland, UK: Society of Petroleum Engineers.

BOURNE, H. M., BOOTH, S., BRUNGER, A., TAYLOR, R. & WILLIAMS, G. 1998 Published. Combining Innovative Technologies to Maximise Scale Squeeze Cost Reduction – a Laboratory and Field Study. *9th NIF International Oilfield Chemical Symposium*, 22-25 Mar, Fagernes, Norway: Norske Sivilingeniørers Forening.

BOURNE, H. M., BOOTH, S. L. & BRUNGER, A. 1999 Published. Combining Innovative Technologies to Maximize Scale Squeeze Cost Reduction. *SPE International Symposium on Oilfield Chemistry*, 16-19 Feb, Houston, Texas, USA: Society of Petroleum Engineers.

BOURNE, H. M., BUCKLEY, A. S., SPARK, I., PATEY, I., FLEMING, N., CARBONNE, L. & STOTT, L. 1999 Published. A Mechanistic Investigation of the Dunbar Scale Challenge-the Use of Cryogenic Sem to Determine Wettability Alteration. *1st SPE Symposium Oilfield Scale: Field Applications and Novel Solutions*, 27-28 Jan, Aberdeen, Scotland, UK: Society of Petroleum Engineers.

BRADY, J. E., RUSSELL, J. W. & HOLUM, J. R. 2000. *Chemistry : Matter and Its Changes,* New York, USA, Wiley.

BROWN, M. 1998. Full Scale Attack. *REview: The BP Technology Magazine*, 30, 30-32.

BURAUER, S., SACHERT, T., SOTTMANN, T. & STREY, R. 1999. On Microemulsion Phase Behavior and the Monomeric Solubility of Surfactant. *Physical Chemistry Chemical Physics*, 1, 4299-4306.

BUTTERWORTH-LABORATORIES-LTD 2014. Development for the Determination of Ethylene Glycol Mono Butyl Ether (Egmbe) in Water and Multipar H (C6-C10 Branched Alkane Distillate). Prepared for Heriot-Watt University.

BYRD, R. H., GILBERT, J. C. & NOCEDAL, J. 2000. A Trust Region Method Based on Interior Point Techniques for Nonlinear Programming. *Mathematical Programming*, 89, 149-185.

BYRD, R. H., HRIBAR, M. E. & NOCEDAL, J. 1999. An Interior Point Algorithm for Large-Scale Nonlinear Programming. *Siam Journal on Optimization*, 9, 877-900.

CARVALHO, S., PALERMO, L., BOAK, L., SORBIE, K. & LUCAS, E. F. 2017. Influence of Terpolymer Based on Amide, Carboxylic, and Sulfonic Groups on the Barium Sulfate Inhibition. *Energy & Fuels*, 31, 10648-10654.

CHA, M., SHIN, K., KIM, J., CHANG, D., SEO, Y., LEE, H. & KANG, S. P. 2013. Thermodynamic and Kinetic Hydrate Inhibition Performance of Aqueous Ethylene Glycol Solutions for Natural Gas. *Chemical Engineering Science*, 99, 184-190.

CHAPMAN, R. G., COLLINS, I. R., GOODWIN, S. P., LUCY, A. R. & STEWART, N. J. 1997. *Oil and Gas Field Chemicals*. USA patent application US5690174A. 25/11/1997.

CHARLESTON, J. 1970. Scale Removal in the Virden, Manitoba, Area. *Journal of Petroleum Technology*, 22, 701-704.

COLLINS, I., WILLIAMS, G. & BOURNE, H. 1998 Published. The Removal of Trapped Water and the Stimulation of Oil Production by the Application of a Water-Soluble Additive. *9th NIF International Symposium on Oil Field Chemicals*, 22-25 Mar, Fagernes, Norway: Norske Sivilingeniørers Forening.

COLLINS, I. R. 1998. *A Process and a Formulation to Inhibit Scale in Oil Field Production*. UK patent application PCT/GB1997/003553. 16/07/1998.

COLLINS, I. R. 2005. *Process for Treating an Oil Well*. USA patent application US6939832B2. 06/09/2005.

COLLINS, I. R., COWIE, L. G., NICOL, M. & STEWART, N. J. 1997a Published. The Field Application of a Scale Inhibitor Squeeze Enhancing Additive. *SPE Annual Technical Conference and Exhibition*, 05-08 Oct, San Antonio, Texas, USA: Society of Petroleum Engineers.

COLLINS, I. R., COWIE, L. G., NICOL, M. & STEWART, N. J. 1999. Field Application of a Scale Inhibitor Squeeze Enhancing Additive. *SPE Production & Facilities*, 14, 21-29.

COLLINS, I. R., GOODWIN, S. P., MORGAN, J. C. & STEWART, N. J. 2001a. *Use of Oil and Gas Field Chemicals*. USA patent application US6225263B1. 01/05/2001.

COLLINS, I. R. & HEWARTSON, J. A. 2002 Published. Extending Squeeze Lifetimes Using Miscible Displacement. *International Symposium on Oilfield Scale*, 30-31 Jan, Aberdeen, Scotland, UK: Society of Petroleum Engineers.

COLLINS, I. R., JORDAN, M. M., FEASEY, N. & WILLIAMS, G. D. 2001b Published. The Development of Emulsion-Based Production Chemical Deployment Systems. *SPE International Symposium on Oilfield Chemistry*, 13-16 Feb, Houston, Texas, USA: Society of Petroleum Engineers.

COLLINS, I. R., STEWART, N. J., WADE, S. R., GOODWIN, S. G., HEWARTSON, J. A. & DEIGNAN, S. D. 1997b Published. Extending Scale Squeeze Lifetimes Using a Chemical Additive: From the Laboratory to the Field. *3rd International Conference on Solving Oilfield Scaling*, 22-23 Jan, Aberdeen, Scotland, UK: IBC.

COLLINS, I. R. & VERVOORT, I. 2003. *Water-in-Oil Microemulsions Useful for Oil Field or Gas Field Applications and Methods for Using the Same*. USA patent application US6581687B2. 24/06/2003.

COWAN, J. C. & WEINTRITT, D. J. 1976. *Water-Formed Scale Deposits,* Houston, Texas, USA, Gulf Publishing Company.

CRABTREE, M., ESLINGER, D., FLETCHER, P., MILLER, M., JOHNSON, A. & KING, G. 1999. Fighting Scale—Removal and Prevention. *Oilfield Review*, 11, 30-45.

CRAWFORD-SCIENTIFIC. 2018. *Chromacademy: Gas Chromatography* [Online]. Available: https://www.chromacademy.com/gc-training.html [Accessed April 2018].

DALRYMPLE, E. D., EOFF, L. S., REDDY, B. R., BROWN, D. L. & BROWN, P. S. 2002. *Methods of Reducing the Water Permeability of Subterranean Formations*. USA patent application US6364016B1. 02/04/2002.

DAVIS, R., LOMAX, I. & PLUMMER, M. 1996. Membranes Solve North Sea Waterflood Sulfate Problems. *Oil & Gas Journal*, 94, 59-64.

DENES, F., LANG, P. & LANG-LAZI, M. 2006. Liquid-Liquid-Liquid Equilibrium Calculations. *IChemE Symposium Series*, Rugby, England, UK: Institution of Chemical Engineers.

DERR, E. L. & DEAL, C. H. 1969. Analytical Solutions of Groups: Correlation of Activity Coefficients through Structural Group Parameters. *IChemE Symposium Series*, Rugby, England, UK: Institution of Chemical Engineers.

DOW. 2001. *Glycol Ethers* [Online]. Available: http://msdssearch.dow.com/PublishedLiteratureDOWCOM/dh_0032/0901b80380032bc8.pdf [Accessed April 2018].

DOW. 2002. *Dow P-Series/E-Series Glycol Ethers* [Online]. Available: http://msdssearch.dow.com/PublishedLiteratureDOWCOM/dh_012d/0901b8038012d976.pdf [Accessed April 2018].

FEASEY, N. D., JORDAN, M. M., BUDGE, M. & ROBB, M. 2006 Published. Development and Deployment of Improved Performance "Green" Combined Scale/Corrosion Inhibitor for Subsea and Topside Application, North Sea Basin. *CORROSION 2006*, 12-16 Mar, San Diego, California, USA: NACE International.

FENDLER, J. H. 2008. *Nanoparticles and Nanostructured Films: Preparation, Characterization, and Applications*, Weinheim, Germany, Wiley.

FLEMING, N., RAMSTAD, K., NELSON, A. & GRAHAM, G. 2009. Impact of Successive Squeezes on Treatment Lifetime and Well Productivity: Laboratory and Field Evidence. *SPE Production & Operations*, 24, 450-458.

FLEMING, N., RAMSTAD, K., NELSON, A. C. & GRAHAM, G. M. 2008 Published. Impact of Successive Squeezes on Treatment Lifetime and Well Productivity: Laboratory and Field Evidence. *SPE International Oilfield Scale Conference*, 28-29 May, Aberdeen, Scotland, UK: Society of Petroleum Engineers.

FREDENSLUND, A., JONES, R. L. & PRAUSNITZ, J. M. 1975. Group-Contribution Estimation of Activity-Coefficients in Nonideal Liquid-Mixtures. *Aiche Journal*, 21, 1086-1099.

FRIGO, D. M., GRAHAM, G. M., LITTLEHALES, I. J. & JAMES, J. S. 2005 Published. Design and Laboratory Testing of a Hybrid Scale-Inhibitor Package for an Hthp Gas-Condensate Reservoir. *SPE International Symposium on Oilfield Scale*, 11-12 May, Aberdeen, Scotland, UK: Society of Petroleum Engineers.

GARRETT, D. E. 2001. *Sodium Sulfate: Handbook of Deposits, Processing, Properties, and Use*, California, USA, Academic Press.

GIDLEY, J. L. 1971. Stimulation of Sandstone Formations with the Acid-Mutual Solvent Method. *Journal of Petroleum Technology*, 23, 571-578.

GHOSH, B., ALKLIH, M. Y. & LI, X. 2016 Published. Pre-Flush Design for Extended Scale Inhibitor Squeeze Lifetime in Limestone Reservoir – Laboratory Investigations and Cost Benefit Analysis. *Offshore Technology Conference Asia*, 22-25 Mar, Kuala Lumpur, Malaysia: Offshore Technology Conference.

GHOSH, B., LI, X. & ALKLIH, M. Y. 2016. Preflush Design for Oil-Wet Carbonate Formations: Key to Enhance Scale-Inhibitor-Squeeze Lifetime. *SPE Journal,* 21, 776-785.

GIBBS, J. W. 1878. Art. Lii.--on the Equilibrium of Heterogeneous Substances. *American Journal of Science and Arts (1820-1879),* 16, 441.

GRAHAM, G. M., BOAK, L. S. & SORBIE, K. S. 2003. The Influence of Formation Calcium and Magnesium on the Effectiveness of Generically Different Barium Sulphate Oilfield Scale Inhibitors. *SPE Production & Facilities,* 18, 28-44.

GRAHAM, G. M. & COLLINS, I. R. 2004 Published. Assessing Scale Risks and Uncertainties for Subsea Marginal Field Developments. *SPE International Symposium on Oilfield Scale*, 26-27 May, Aberdeen, Scotland, UK: Society of Petroleum Engineers.

GRAHAM, G. M., GYANI, A., JORDAN, M. M., STRACHAN, C., MCCLURE, R., LITTLEHALES, I. J. & FITZGERALD, A. 2002a Published. Selection and Application of a Non-Damaging Scale Inhibitor Package for Pre-Emptive Squeeze in Mungo Production Wells. *International Symposium on Oilfield Scale*, 30-31 Jan, Aberdeen, Scotland, UK: Society of Petroleum Engineers.

GRAHAM, G. M., HILL, P. H., SORBIE, K. S., CARBONNE, L. & STOTT, L. 1999 Published. The Mechanism of Formation Damage and Recovery Following Chemical Squeeze Application in Low Permeability Water Sensitive Reservoirs. *10th NIF International Oilfield Chemical Symposium*, 28 Feb-03 Mar, Fagernes, Norway: Norske Sivilingeniørers Forening.

GRAHAM, G. M., KIDD, S. L., FITZPATRICK, R. & WRIGHT, R. J. 2010 Published. Appropriate Simulation of Field Treatments Using Core Flood Data. *SPE International Conference on Oilfield Scale*, 26-27 May, Aberdeen, Scotland, UK: Society of Petroleum Engineers.

GRAHAM, G. M., KIDD, S. L., STALKER, R. & WRIGHT, R. 2012 Published. Effect of Coreflood Test Methodology on Appropriate Simulation of Field Treatments. *SPE International Symposium and Exhibition on Formation Damage Control*, 15-17 Feb, Lafayette, Louisiana, USA: Society of Petroleum Engineers.

GRAHAM, G. M., MACKAY, E. J., DYER, S. J. & BOURNE, H. M. 2002b Published. The Challenges for Scale Control in Deepwater Production Systems: Chemical Inhibition and Placement. *CORROSION 2002*, 02-11 Apr, Denver, Colorado, USA: NACE International.

GRAHAM, G. M., SORBIE, K. S. & JORDAN, M. M. 1997 Published. How Scale Inhibitors Work and How This Affects Test Methodology. *3rd International Conference on Solving Oilfield Scaling*, 22-23 Jan, Aberdeen, Scotland, UK: IBC.

HALL, B. E. 1975. The Effect of Mutual Solvents on Adsorption in Sandstone Acidizing. *Journal of Petroleum Technology*, 27, 1439-1442.

HALL, B. E. & DILL, W. R. 1988. Iron Control Additives for Limestone and Sandstone Acidizing of Sweet and Sour Wells. *SPE Formation Damage Control Symposium*, 08-09 Feb, Bakersfield, California, USA: Society of Petroleum Engineers.

HARDY, J. A. & SIMM, I. 1996. Low Sulfate Seawater Mitigates Barite Scale. *Oil & Gas Journal*, 94, 64-67.

HARRIS, D. C. 2010. *Quantitative Chemical Analysis*, New York, USA, W. H. Freeman.

HELLSTEN, M. & HARWIGSSON, I. 1999. *Use of Alkoxylated Alkanolamide Together with Alkoxylated Alcohol as a Friction-Reducing Agent*. USA patent application US5979479A. 09/11/1999.

HINSHAW, J. V. 2006. The Flame Ionization Detector. *LC GC Europe*, 19, 206-216.

HOFMEISTER, F. 1888. Zur Lehre Von Der Wirkung Der Salze. *Archiv für Experimentelle Pathologie und Pharmakologie*, 24, 247-260.

HONEYWELL. 2017. *Hydranal: Product Overview Guide* [Online]. Available: https://www.lab-honeywell.com/wp-content/uploads/2018/01/Direct-Hydranal-Product-Line-Overview-Brochure_A4_v14_EN_DIGITAL.pdf [Accessed April 2018].

HOUSE, J. E. 2013. *Inorganic Chemistry*, Massachusetts, USA, Elsevier/Academic Press.

IHS-MARKIT 2017. *Chemical Economics Handbook: Glycol Ethers*, London, England, UK, IHS Markit Ltd.

IHS-MARKIT 2018. *Chemical Economics Handbook: Ethylene Glycols*, London, England, UK, IHS Markit Ltd.

JELINEK, W. & SCHRAMM, L. L. 2005 Published. Improved Production from Mature Gas Wells by Introducing Surfactants into Wells. *International Petroleum Technology Conference*, 21-23 Nov, Doha, Qatar: International Petroleum Technology Conference.

JONES, C. R. & TALBOT, R. E. 2004. *Biocidal Compositions and Treatments*. USA patent application US6784168B1. 31/08/2004.

JORDAN, M. M., ARCHIBALD, I., DONALDSON, L., STEVENS, K. & KEMP, S. 2003 Published. Deployment, Monitoring and Optimisation of a Combined Scale/Corrosion Inhibitor within a Subsea Facility in the North Sea Basin. *International Symposium on Oilfield Chemistry*, 05-07 Feb, Houston, Texas, USA: Society of Petroleum Engineers.

JORDAN, M. M., COLLINS, I. R. & MACKAY, E. J. 2008. Low Sulfate Seawater Injection for Barium Sulfate Scale Control: A Life-of-Field Solution to a Complex Challenge. *SPE Production & Operations*, 23, 192-209.

JORDAN, M. M., FEASEY, N. D., BUDGE, M. & ROBB, M. 2006 Published. Development and Deployment of Improved Performance "Green" Combined Scale/Corrosion Inhibitor for Subsea and Topside Application, North Sea Basin. *SPE International Oilfield Corrosion Symposium*, 30 May, Aberdeen, Scotland, UK: Society of Petroleum Engineers.

JORDAN, M. M., FRIGO, D. M., BOGAERT, P. J., BRYSON, B., TOSCHI, C., AFONSO, M. & BERREDO, M. C. 2007 Published. Managing Formation Damage Risks from Scale-Inhibitor Squeeze Treatments in Deepwater, Subsea Fields in the Campos Basin. *European Formation Damage Conference*, 30 May-01 Jun, Scheveningen, The Netherlands: Society of Petroleum Engineers.

JORDAN, M. M., GRAFF, C. J. & COOPER, K. N. 2000 Published. Development and Deployment of a Scale Squeeze Enhancer and Oil-Soluble Scale Inhibitor to Avoid Deferred Oil Production Losses During Squeezing Low-Water Cut Wells, North Slope, Alaska. *SPE International Symposium on Formation Damage Control*, 23-24 Feb, Lafayette, Louisiana, USA: Society of Petroleum Engineers.

JORDAN, M. M., GRAFF, C. J. & COOPER, K. N. 2001. Deployment of a Scale Squeeze Enhancer and Oil-Soluble Scale Inhibitor to Avoid Oil Production Losses in Low Water-Cut Well. *SPE Production & Facilities*, 16, 267-276.

JORDAN, M. M., HISCOX, I., DALTON, J. F., MACKIE, J. & KEMP, S. 2002 Published. The Design and Deployment of Enhanced Scale Dissolver/Squeeze Treatment in Subsea Horizontal Production Wells, North Sea Basin. *International Symposium and Exhibition on Formation Damage Control*, 20-21 Feb, Lafayette, Louisiana, USA: Society of Petroleum Engineers.

JORDAN, M. M. & MACKAY, E. J. 2009 Published. The Challenge of Modelling and Deploying Divertion for Subsea Scale Squeeze Application. *8th European Formation Damage Conference*, 27-29 May, Scheveningen, The Netherlands: Society of Petroleum Engineers.

JORDAN, M. M., MACKAY, E. J. & VAZQUEZ, O. 2008 Published. The Influence of Overflush Fluid Type on Scale Squeeze Life Time - Field Examples and Placement Simulation Evaluation. *CORROSION 2008*, 16-20 Mar, New Orleans, Louisiana, USA: NACE International.

JORDAN, M. M., SJURAETHER, K., COLLINS, I. R., FEASEY, N. D. & EMMONS, D. 2001 Published. Life Cycle Management of Scale Control within Subsea Fields and Its Impact on Flow Assurance, Gulf of Mexico and the North Sea Basin. *SPE Annual Technical Conference and Exhibition*, 30 Sep-03 Oct, New Orleans, Louisiana, USA: Society of Petroleum Engineers.

JORDAN, M. M., SORBIE, K. S., GRIFFIN, P., HENNESSEY, S., HOURSTON, K. E. & WATERHOUSE, P. 1995a Published. Scale Inhibitor Adsorption/Desorption Vs. Precipitation: The Potential for Extending Squeeze Life While Minimising Formation Damage. *SPE European Formation Damage Conference*, 15-16 May, The Hague, Netherlands: Society of Petroleum Engineers.

JORDAN, M. M., SORBIE, K. S., GRIFFIN, P., ISAAC, K., HILL, P. & HUGHES, C. 1995b Published. The Application of Surfactants to Improve Scale Inhibitor Squeeze Lifetime in Mixed-Wet Reservoirs: A Coreflood Study Using Oil Reconditioned Core from a Large North Sea Field. *6th NIF International Oilfield Chemical Symposium*, 19-22 Mar, Geilo, Norway: Norske Sivilingeniørers Forening.

JORDAN, M. M., SORBIE, K. S., JIANG, P., YUAN, M., TODD, A. C. & TAYLOR, K. 1994 Published. Mineralogical Controls on Inhibitor Adsorption/Desorption in Brent Group Sandstone and Their Importance in Predicting and Extending Field Squeeze Lifetimes. *European Production Operations Conference and Exhibition*, 15-17 Mar, Aberdeen, Scotland, UK: Society of Petroleum Engineers.

KAHLWEIT, M., STREY, R. & BUSSE, G. 1990. Microemulsions: A Qualitative Thermodynamic Approach. *The Journal of Physical Chemistry,* 94, 3881-3894.

KAHLWEIT, M., STREY, R. & BUSSE, G. 1993. Weakly to Strongly Structured Mixtures. *Phys Rev E Stat Phys Plasmas Fluids Relat Interdiscip Topics,* 47, 4197-4209.

KAHLWEIT, M., STREY, R., FIRMAN, P., HAASE, D., JEN, J. & SCHOMACKER, R. 1988a. General Patterns of the Phase-Behavior of Mixtures of H_2O, Nonpolar-Solvents, Amphiphiles, and Electrolytes .1. *Langmuir,* 4, 499-511.

KAHLWEIT, M., STREY, R., HAASE, D. & FIRMAN, P. 1988b. Properties of the 3-Phase Bodies in H_2O-Oil-Nonionic Amphiphile Mixtures. *Langmuir,* 4, 785-790.

KAHLWEIT, M., STREY, R., SCHOMACKER, R. & HAASE, D. 1989. General Patterns of the Phase-Behavior of Mixtures of H_2O, Nonpolar-Solvents, Amphiphiles, and Electrolytes .2. *Langmuir,* 5, 305-315.

KALFAYAN, L. 2000. *Production Enhancement with Acid Stimulation*, Tulsa, Oklahoma, USA, PennWell.

KELLAND, M. A. 2014. *Production Chemicals for the Oil and Gas Industry, Second Edition,* Florida, USA, CRC Press.

KING, G. E. & LEE, R. M. 1988. Adsorption and Chlorination of Mutual Solvents Used in Acidizing. *SPE Production Engineering,* 3, 205-209.

KOJIMA, K. & TOCHIGI, K. 1979. *Prediction of Vapor-Liquid Equilibria by the Asog Method - Volume 3,* Oxford, England, UK, Elsevier Scientific Pub. Co.

LIN, B. J. & CHEN, L. J. 2002. Liquid-Liquid Equilibria for the Ternary System Water Plus Dodecane Plus 2-Butyloxyethanol in the Temperature Range from 25 Degrees C to 65 Degrees C. *Journal of Chemical and Engineering Data,* 47, 992-996.

LIN, B. J. & CHEN, L. J. 2004. Liquid-Liquid Equilibria for the Ternary System Water Plus Tetradecane+2-Butyloxyethanol. *Fluid Phase Equilibria,* 216, 13-20.

LUCIA, A., PADMANABHAN, L. & VENKATARAMAN, S. 2000. Multiphase Equilibrium Flash Calculations. *Computers & Chemical Engineering,* 24, 2557-2569.

LYNN, J. D., NASR-EL-DIN, H. A. & HASHEM, M. K. 2002 Published. Iron Phosphonate Stabilized Emulsion and Formation Damage During an Adsorption Squeeze Treatment for Scale Mitigation. *International Symposium and Exhibition on Formation Damage Control*, 20-21 Feb, Lafayette, Louisiana, USA: Society of Petroleum Engineers.

MACKAY, E. J., JORDAN, M. M., FEASEY, N. D., SHAH, D., KUMAR, P. & ALI, S. A. 2005. Integrated Risk Analysis for Scale Management in Deepwater Developments. *SPE Production & Facilities,* 20, 138-154.

MAHMOUD, M. A. 2014. Evaluating the Damage Caused by Calcium Sulfate Scale Precipitation During Low- and High-Salinity-Water Injection. *Journal of Canadian Petroleum Technology,* 53, 141-150.

MEYERS, K. O., SKILLMAN, H. L. & HERRING, G. D. 1985. Control of Formation Damage at Prudhoe Bay, Alaska, by Inhibitor Squeeze Treatment. *Journal of Petroleum Technology,* 37, 1019-1034.

MILES, A. F., BOURNE, H. M., SMITH, R. G. & COLLINS, I. R. 2003 Published. Development of a Novel Water in Oil Microemulsion Based Scale Inhibitor Delivery System. *International Symposium on Oilfield Scale*, 23-30 Jan, Aberdeen, Scotland, UK: Society of Petroleum Engineers.

MILLER, A. R. 2005. *Iron Sulfide Clean-up Composition and Method*. USA patent application US6887840B2. 03/05/2005.

NASR-EL-DIN, H. A. 2000. Surfactant Use in Acid Stimulation. *In:* SCHRAMM, L. L. (ed.) *Surfactants: Fundamentals and Applications in the Petroleum Industry.* Cambridge, England, UK: Cambridge University Press.

NASR-EL-DIN, H. A. 2003 Published. New Mechanisms of Formation Damage: Lab Studies and Case Histories. *SPE European Formation Damage Conference*, 13-14 May, The Hague, Netherlands: Society of Petroleum Engineers.

NASR-EL-DIN, H. A., AL-OTHMAN, A. M., TAYLOR, K. C. & AL-GHAMDI, A. H. 2004. Surface Tension of HCl-Based Stimulation Fluids at High Temperatures. *Journal of Petroleum Science and Engineering,* 43, 57-73.

NASR-EL-DIN, H. A., CHESSON, J. B., CAWIEZEL, K. E. & DE VINE, C. S. 2006 Published. Lessons Learned and Guidelines for Matrix Acidizing with Viscoelastic Surfactant Diversion in Carbonate Formations. *SPE Annual Technical Conference and Exhibition*, 24-27 Sep, San Antonio, Texas, USA: Society of Petroleum Engineers.

NASR-EL-DIN, H. A., LYNN, J. D. & AL-DOSSARY, K. A. 2002 Published. Formation Damage Caused by a Water Blockage Chemical: Prevention through Operator Supported Test Programs. *International Symposium and Exhibition on Formation Damage Control*, 20-21 Feb, Lafayette, Louisiana, USA: Society of Petroleum Engineers.

NEGAHBAN, S., WILLHITE, G. P., WALAS, S. M. & MICHNICK, M. J. 1986. 3-Liquid-Phase Equilibria of Ternary and Quaternary Mixtures, Water N-Decane 2-Butyloxyethanol and Water N-Octane 1-Propanol Sodium-Chloride Experimental Measurements and Their Correlation with the Uniquac Model. *Fluid Phase Equilibria*, 32, 49-61.

NEGIN, C., ALI, S. & XIE, Q. 2017. Most Common Surfactants Employed in Chemical Enhanced Oil Recovery. *Petroleum*, 3, 197-211.

NIST. 2017. *Nist Chemistry Webbook: Nist Standard Reference Database Number 69* [Online]. Available: https://webbook.nist.gov/chemistry/ [Accessed April 2018].

NOWACK, B. & STONE, A. T. 2006. Competitive Adsorption of Phosphate and Phosphonates onto Goethite. *Water Res*, 40, 2201-2209.

OECD 1995. Test No. 107: Partition Coefficient (N-Octanol/Water): Shake Flask Method. *OECD Guidelines for the Testing of Chemicals, Section 1: Physical-Chemical properties.* Paris, France: OECD Publishing.

OECD 2004. Test No. 117: Partition Coefficient (N-Octanol/Water), HPLC Method. *OECD Guidelines for the Testing of Chemicals, Section 1: Physical-Chemical properties.* Paris, France: OECD Publishing.

OECD 2006. Test No. 123: Partition Coefficient (1-Octanol/Water): Slow-Stirring Method. *OECD Guidelines for the Testing of Chemicals, Section 1: Physical-Chemical properties.* Paris, France: OECD Publishing.

PARDUE, J. E. 1991 Published. A New Inhibitor for Scale Squeeze Applications. *SPE International Symposium on Oilfield Chemistry*, 20-22 Feb, Anaheim, California, USA: Society of Petroleum Engineers.

PAYNE, G. E. 1987 Published. A History of Downhole Scale Inhibition by Squeeze Treatments on the Murchison Platform. *Offshore Europe*, 8-11 Sep, Aberdeen, Scotland, UK: Society of Petroleum Engineers.

PEARSON, R. G. 1968a. Hard and Soft Acids and Bases HSAB .1. Fundamental Principles. *Journal of Chemical Education*, 45, 581-587.

PEARSON, R. G. 1968b. Hard and Soft Acids and Bases HSAB .2. Underlying Theories. *Journal of Chemical Education*, 45, 643-648.

PERKINELMER. 2010. *Clarus 500/580 GC User's Guide* [Online]. Available: https://www.perkinelmer.com/lab-solutions/resources/docs/GDE_Clarus500-580UserGuide.pdf [Accessed April 2018].

POYNTON, N., TIDSWELL, R., STEELE, J., WOOD, J. & EARLY, R. 2000 Published. Squeezing Aqueous Based Scale Inhibitors into a Water Sensitive Reservoir - Development of a Squeeze Strategy.

International Symposium on Oilfield Scale, 26-27 Jan, Aberdeen, Scotland, UK: Society of Petroleum Engineers.

PRZYBYLINSKI, J. L., RUGGERI, J. W., WINFIELD, M. S. & WAKLEY, W. D. 1996 Published. Optimization of Scale Inhibitor Squeeze Treatments in the Cedar Lake Unit. *CORROSION 96*, 24-29 Mar, Denver, Colorado, USA: NACE International.

RAO, C. N. R. 1975. *Ultraviolet and Visible Spectroscopy: Chemical Applications,* London, England, UK, Butterworth.

RAO, Y. V. C. 2013. *Chemical Engineering Thermodynamics,* Hyderabad, India, Universities Press (India) Private Limited.

REACHCENTRUM. 2012. *Glycol Ethers Reach Consortium* [Online]. Available: https://www.reachcentrum.eu/consortium/glycol-ethers-reach-consortium-50.html [Accessed April 2018].

REDDY, P. S. & RANI, K. Y. 2012. A Simple Algorithm for Vapor-Liquid-Liquid Equilibrium Computation. *Industrial & Engineering Chemistry Research,* 51, 10719-10730.

RENON, H. & PRAUSNITZ, J. M. 1968. Local Compositions in Thermodynamic Excess Functions for Liquid Mixtures. *Aiche Journal,* 14, 135-144.

RODEBUSH, W. H. & FELDMAN, I. 1946. Ultraviolet Absorption Spectra of Organic Molecules. III. Mechanical Interference of Substituent Groups with Resonance Configurations. *Journal of the American Chemical Society,* 68, 896-899.

SASSEN, C. L., FILEMON, L. M., DELOOS, T. W. & ARONS, J. D. 1989. Influence of Pressure and Electrolyte on the Phase-Behavior of Water + Oil + Nonionic Surfactant Systems. *Journal of Physical Chemistry,* 93, 6511-6516.

SCHOLZ, E. 1984. *Karl Fischer Titration*, Springer.

SCHULTZ, H., BAUER, G., SCHACHL, E., HAGEDORN, F. & SCHMITTINGER, P. 2006. *Potassium Compounds*.

SCOTT, G. C. & LITTLEWOOD, M. J. 2000 Published. Development of a Downhole Scale Management Philosophy for Water Sensitive Reservoirs. *SPE International Symposium on Formation Damage Control*, 23-24 Feb, Lafayette, Louisiana, USA: Society of Petroleum Engineers.

SHAW, S. S., SORBIE, K. S. & BOAK, L. S. 2010 Published. The Effects of Barium Sulphate Supersaturation, Calcium and Magnesium on the Inhibition Efficiency: 2. Polymeric Scale Inhibitors. *SPE International Conference on Oilfield Scale*, 26-27 May, Aberdeen, Scotland, UK: Society of Petroleum Engineers.

SHEN, J. & CROSBY, C. C. 1983. Insight into Strontium and Calcium-Sulfate Scaling Mechanisms in a Wet Producer. *Journal of Petroleum Technology,* 35, 1249-1255.

SHULER, P. J., LU, Z., MA, Q. & TANG, Y. 2016 Published. Surfactant Huff-N-Puff Application Potentials for Unconventional Reservoirs. *SPE Improved Oil Recovery Conference*, 11-13 Apr, Tulsa, Oklahoma, USA: Society of Petroleum Engineers.

SIGMA-ALDRICH. 2018. *Gas Chromatography: Capillary GC Columns* [Online]. Available: https://www.sigmaaldrich.com/analytical-chromatography/gas-chromatography/columns.html [Accessed April 2018].

SKOOG, D. A. 2007. *Principles of Instrumental Analysis / by Douglas A. Skoog, F. James Holler, and Stanley R. Crouch,* Belmond, Calif., Belmond, Calif.: Brooks/Cole.

SORBIE, K. S., JIANG, P., YUAN, M. D., CHEN, P., JORDAN, M. M. & TODD, A. C. 1993 Published. The Effect of pH, Calcium, and Temperature on the Adsorption of Phosphonate Inhibitor onto Consolidated and Crushed Sandstone. *SPE Annual Technical Conference and Exhibition*, 03-06 Oct, Houston, Texas, USA: Society of Petroleum Engineers.

SORBIE, K. S. & LAING, N. 2004 Published. How Scale Inhibitors Work: Mechanisms of Selected Barium Sulphate Scale Inhibitors across a Wide Temperature Range. *SPE International Symposium on Oilfield Scale*, 26-27 May, Aberdeen, Scotland, UK: Society of Petroleum Engineers.

SORBIE, K. S., YUAN, M. & JORDAN, M. M. 1994 Published. Application of a Scale Inhibitor Squeeze Model to Improve Field Squeeze Treatment Design. *European Petroleum Conference*, 25-27 Oct, London, England, UK: Society of Petroleum Engineers.

SØRENSEN, J. M. & ARLT, W., 1980. Liquid–Liquid Equilibrium Data Collection: Ternary and Quaternary Systems Dechema Chemistry Data Series. V, 3, DECHEMA (Deutsche Gesellschaft für Chemisches Apparatweren).

SUTHERLAND, L. & JORDAN, M. 2016 Published. Enhancing Scale Inhibitor Squeeze Retention with Additives. *SPE International Oilfield Scale Conference and Exhibition*, 11-12 May, Aberdeen, Scotland, UK: Society of Petroleum Engineers.

SUZUKI, H. 1960. The Ultraviolet Absorption Spectra of Stilbene and Some Related Compounds in the Solid State Measured by the Pressed Kcl Disk Technique. *Bulletin of the Chemical Society of Japan,* 33, 944-952.

TANNER, R. N. & WITTINGHAM, K. P. 1986 Published. Scale Control During Waterflooding Operations: A Field Appraisal of Inhibitor Requirements and Performance. *International Meeting on Petroleum Engineering*, 17-20 Mar, Beijing, China: Society of Petroleum Engineers.

TAYLOR, K. C., AL-GHAMDI, A. H. & NASR-EL-DIN, H. A. 2003 Published. Effect of Rock Type and Acidizing Additives on Acid Reaction Rates Using the Rotating Disk Instrument. *International*

Symposium on Oilfield Chemistry, 05-07 Feb, Houston, Texas, USA: Society of Petroleum Engineers.

TAYLOR, K. C., AL-GHAMDI, A. H. & NASR-EL-DIN, H. A. 2004. Effect of Additives on the Acid Dissolution Rates of Calcium and Magnesium Carbonates. *SPE Production & Facilities,* 19, 122-127.

TETKO, I. V. & TANCHUK, V. Y. 2002. Application of Associative Neural Networks for Prediction of Lipophilicity in Alogps 2.1 Program. *J Chem Inf Comput Sci,* 42, 1136-1145.

THE-AMERICAN-CHEMISTRY-COUNCIL. 2000. *Commonly Used Names for the Largest Production Volume Ethylene Glycol Ethers* [Online]. Available: https://drive.google.com/open?id=1xH-m-D35ZHEONL8oyzCcEbod5ADANkya [Accessed April 2018].

TJOMSLAND, T., SÆTEN, J. O., VIKANE, O., ZETTLITZER, M. & CHEN, P. 2008 Published. Veslefrikk Scale Control Strategy and Economic Implications: Revisited 7 Years Later - Did We Improve? *SPE International Oilfield Scale Conference*, 28-29 May, Aberdeen, Scotland, UK: Society of Petroleum Engineers.

TSUBOKA, T. & KATAYAMA, T. 1975. Modified Wilson Equation for Vapor-Liquid and Liquid-Liquid Equilibria. *Journal of Chemical Engineering of Japan,* 8, 181-187.

VAZQUEZ, O., FURSOV, I. & MACKAY, E. 2016. Automatic Optimization of Oilfield Scale Inhibitor Squeeze Treatment Designs. *Journal of Petroleum Science and Engineering,* 147, 302-307.

VAZQUEZ, O., MACKAY, E. J., AL SHUAILI, K. H., SORBIE, K. S. & JORDAN, M. M. 2008 Published. Modelling a Surfactant Preflush with Non-Aqueous and Aqueous Scale Inhibitor Squeeze Treatments. *Europec/EAGE Conference and Exhibition*, 09-12 Jun, Rome, Italy: Society of Petroleum Engineers.

VAZQUEZ, O., MACKAY, E. J., JORDAN, M. M. & SORBIE, K. S. 2009 Published. Impact of Mutual Solvent Preflushes on Scale Squeeze Treatments: Extended Squeeze Lifetime and Improved Well Clean-up Time. *8th European Formation Damage Conference*, 27-29 May, Scheveningen, The Netherlands: Society of Petroleum Engineers.

VAZQUEZ, O., THANASUTIVES, P., ELIASSON, C., FLEMING, N. & MACKAY, E. 2011. Modeling the Application of Scale-Inhibitor-Squeeze-Retention-Enhancing Additives. *SPE Production & Operations*, 26, 270-277.

VETTER, O. 1977 Published. Scale Prediction in Geothermal Operations-State of the Art. *SPE International Oilfield and Geothermal Chemistry Symposium*, 27-29 Jun, San Diego, California, USA: Society of Petroleum Engineers.

VETTER, O. J. 1973. The Chemical Squeeze Process Some New Information on Some Old Misconceptions. *Journal of Petroleum Technology,* 25, 339-353.

VETTER, O. J. 1976. Oilfield Scale---Can We Handle It? *Journal of Petroleum Technology,* 28, 1402-1408.

VETTER, O. J. & CRICHLOW, H. B. 1979. *Injection, Injectivity and Injectability in Geothermal Operations: Problems and Possible Solutions,* Washington, USA, Vetter Research.

VETTER, O. J. G. 1975. How Barium Sulfate Is Formed: An Interpretation. *Journal of Petroleum Technology,* 27, 1515-1524.

VETTER, O. J. G. & PHILLIPS, R. C. 1970. Prediction of Deposition of Calcium Sulfate Scale under Down-Hole Conditions. *Journal of Petroleum Technology,* 22, 1299-1308.

VU, V. K., HURTEVENT, C. & DAVIS, R. A. 2000 Published. Eliminating the Need for Scale Inhibition Treatments for Elf Exploration Angola's Girassol Field. *International Symposium on Oilfield Scale*, 26-27 Jan, Aberdeen, Scotland, UK: Society of Petroleum Engineers.

WALAS, S. M. 1985. *Phase Equilibria in Chemical Engineering,* Boston, USA, Butterworth.

WALTON, W. B. 1989. *Method for Removal of Paraffin from Producing Oil Wells*. USA patent application US4813482A. 21/03/1989.

WALTZ, R. A., MORALES, J. L., NOCEDAL, J. & ORBAN, D. 2006. An Interior Algorithm for Nonlinear Optimization That Combines Line Search and Trust Region Steps. *Mathematical Programming,* 107, 391-408.

WANG, Y., BAI, B., GAO, H., HE, L. & ZHAO, F. 2008 Published. Enhanced Oil Production through a Combined Application of Gel Treatment and Surfactant Huff'n'puff Technology. *SPE International Symposium and Exhibition on Formation Damage Control*, 13-15 Feb, Lafayette, Louisiana, USA: Society of Petroleum Engineers.

WAT, R. M. S., SORBIE, K. S., TODD, A. C., PING, C. & PING, J. 1992 Published. Kinetics of $BaSO_4$ Crystal Growth and Effect in Formation Damage. *SPE Formation Damage Control Symposium*, 26-27 Feb, Lafayette, Louisiana, USA: Society of Petroleum Engineers.

WEINTRITT, D. J. & COWAN, J. C. 1967. Unique Characteristics of Barium Sulfate Scale Deposition. *Journal of Petroleum Technology,* 19, 1381-1394.

WILLIAMS, G. D., COLLINS, I. R. & WADE, S. R. 1999 Published. Enhancing Mineral Scale Dissolution in the near-Wellbore Region. *SPE Annual Technical Conference and Exhibition*, 03-06 Oct, Houston, Texas, USA: Society of Petroleum Engineers.

WILSON, G. M. 1964. Vapor-Liquid Equilibrium. Xi. A New Expression for the Excess Free Energy of Mixing. *Journal of the American Chemical Society,* 86, 127-130.

WILSON, G. M. & DEAL, C. H. 1962. Activity Coefficients and Molecular Structure - Activity Coefficients in Changing Environments - Solutions of Groups. *Industrial & Engineering Chemistry Fundamentals,* 1, 20-23.

WU, H. Y., XU, Y. M., DABROS, T. & HAMZA, H. 2004. Development of a Method for Measurement of Relative Solubility of Nonionic Surfactants. *Colloids and Surfaces A: Physicochemical and Engineering Aspects*, 232, 229-237.